



**An Innovative Approach to Dynamic Driving  
Simulations for Vehicle Thermal Management  
Processes**

A thesis submitted in fulfilment of the requirements for the degree of Doctorate of Philosophy

Kristian Haehndel

B.Eng.

School of Aerospace Mechanical and Manufacturing Engineering

College of Science Engineering and Health

RMIT University

U&A 2011

## **Declaration**

I certify that except where due acknowledgement has been made, the work is that of the author alone; the work has not been submitted previously, in whole or in part, to qualify for any other academic award; the content of the thesis/project is the result of work which has been carried out since the official commencement date of the approved research program; any editorial work, paid or unpaid, carried out by a third party is acknowledged; and, ethics procedures and guidelines have been followed.

Kristian Haehndel

February 2015

# Acknowledgements

The following research was conducted during my employment within the BMW Group in Munich, Germany. This collaborative project with RMIT University represents a new dimension to the RIIERP (RMIT International Industry Experience and Research Program). *BMW Research an Australian First*. I would like to express my sincere gratitude to the BMW Group for their employment, research facilities and funding, RIIERP for the initial career opportunities at the BMW Group and finally the unspoken and hero/founder of the program, Professor Abanteriba, from whom thousands of students internationally owe their successes to. Additionally Professor Abanteriba's supervision and direction to the research project was invaluable in which I am deeply grateful.

I have been fortunate throughout the various stages of my life to have special mentors who have believed in my potential, who had guided me through the darkness of a lonely road and who wanted nothing in return other than my happiness and friendship. I would like to recognize each of these individuals from whom I dedicate this work to:

Dr. Torsten Frank, my industrial supervisor, whose genius is only matched with the depths of his patience and compassion. He is the dream maker, who is responsible for the success in my career, and the consequent careers of many RMIT students within the BMW Group. We are all eternally grateful for your countless contributions. Mr. Frieder Christel and Dr. Mahmoud Reza Maneshkarimi, my consultants, who introduced me to the world of vehicle simulation and adopted me amongst their elite team of engineers. Dr. Anthony Jefferies, whose time, consultation and review had shaped the form of following document. Dr. Andreas Bauknecht, with his career training, life lessons, management philosophy and friendship, which has forged my leadership style. Outside of work, Dr. Kai Morganti, who taught me that academic excellence has more to do with discipline, dedication and consistent improvement, than one's natural abilities. Mr. Jason Bloomfield, who taught me the true meaning of personal power, the importance of purpose and responsibility which can fuel man's determination to achieve impossible feats. Mr. Ashwin Nambia, Mr. Hasantha Jayaweera and Mr. Daniel Kovacs who initialised the seed of this journey before my undergraduate education, and who shared the dream of pursuing greatness through sacrifice.

I would like to thank the students and colleagues who supported me throughout this research project who are: Mr. Steve Devos, Mr. Angus Pere, Mr. Amrinder Dhinsa, Dr. Boris Mazar, Dr. Martin Maier and Dr. Andreas Eder. I am grateful for your support, belief and commitment to myself and this project.

I would also like to express my gratitude to my family, who supported me throughout my life, with the journey into the unknown and the pursuit of happiness, which took me across the world. I will never forget the tough times, the lessons, and the sacrifices of my parents, to educate me, to teach me, to guide me and ultimately to let me go. It is through the commitment of my parents that I feel

grounded, driven and passionate to seize every opportunity life presents, to cherish every moment and to never be ungrateful or complacent.

A special note must be said about my extended family, uncles, aunts and cousins, who all supported the dreams of a child, the confusion of a teenager and the determination of a young man. I like to especially thank my Uncle and Godfather, Mr. Anthony Walpola, who generously donated time and resources in exposing me to positive aspects of life and till today is a strong example of all round success.

I would like recognize my two brothers, who surprisingly consist of contradicting personalities. My eldest brother Devinda, who quietly shines as a bright light of success within my family, whose dedication and selflessness is a benchmark to follow. His wonderful wife (Madhu) and daughter (Chantel) are a pure representation of love. Devinda is the vehicle of my success whilst my other brother (Prasanna) is the fuel. Prasanna's loud, passionate and never give up fighting spirit has become an integral part of my personality. And through the embodiment of his energy I have overcome many challenges in my life including his own unfortunate death in 2002. May my life be a continual manifestation of his hard-work and a dedication to him and the opportunities he never had.

Finally I like to thank Katharina Huber, for her consistent and never ending perseverance during the last 5 years of our life together. Her determination to support me, through my failures and successes is a credit to her character. Without her love and support this thesis, and my current success would not have materialised.

*Whatever the mind of a man can conceive and believe, the hand of a man can achieve!*

- *Napoleon Hill, Think and Grow Rich*

# Abstract

Extending from steady state simulation cases allows engineers to investigate the "real" on road conditions that are typically associated with transient characteristics. The ability to predict time dependent thermal behavior of vehicle environments leads to improved product development (with optimised modification potential) and an inherent reduction in experimental dependency and cost. Additionally many of the critical thermal cases experimentally validated are coupled to non-equilibrium boundary conditions, resulting either in an over-prediction through steady state 3-D CFD modeling or an inaccurate prediction through 1-D modeling.

Today's current industrial standard for virtual vehicle thermal management is mainly limited to steady-state conditions with some semi dynamic cases. Previous attempts have been proposed in the literature by industrial experts, to simulate unsteady thermal behavior of these time dependent vehicle conditions (e.g. thermal soak and hill climb). However, some of these proposals require a dependency on strong computing power, complete 3-D exhaust flow simulations, and complex multi-model coupling arrangements. Even though these methods incorporate realistic modeling approaches (due to the envisioned availability in computational resources), they lack the potential to accommodate complex boundary conditions, and to date no methodology has been able to simulate dynamic driving scenarios. Which brings up the question, why?

The research proposes that the vehicle simulation field has overlooked the possibility to attempt highly transient cases, such as dynamic driving, due to the extreme volatility existing within vehicle boundary conditions, coupled to the traditional approaches which attempt to simulate these conditions. Therefore for numerical stability the simulation time scales have to be drastically reduced in order to resolve the high boundary condition fluctuations. This naturally exaggerates the calculation time for reasonable results and consequently compromises the application of the methodology for industry (considering the vehicle development time constraints). Therefore due to the simulation paradigm, "that original boundary conditions need to be modeled", dynamic driving scenarios for full vehicle configurations is considered unfeasible.

Simulation simplification is typically made on the geometrical modelling side, the implementation of physics or the assumptions of certain sub-system parameters, but significant alteration has never been made to the fundamental vehicle boundary conditions. However it is clear that the mass of the component can dampen the speed of its surface averaged thermal response to a given set of boundary conditions. Therefore the component essentially reacts at a different time scale to that of the exposed energy flux. Through this understanding it is evident that there is a potential to simplify the boundary conditions (therefore accelerating the calculation) based on the response nature of components. The following research aims at challenging the current simulation paradigm by introducing a methodology which simplifies the vehicle boundary conditions.

The research goal is firstly the proof that dynamic driving profiles are possible to simulate with the current computational resources for full vehicle configurations. And secondly, the simplification of boundary conditions coupled to a new methodology to simulate these conditions,

can replicate the time dependent component temperature behaviors, without significant depreciation in simulation accuracy.

In the following research, a technique is presented which simplifies the high frequency changes within vehicle boundary conditions through the utilisation of wavelet transform based signal decomposition. Through identifying the thermally relevant frequency ranges (which correspond to component temperature change) a simplified boundary condition signal is derived. This simplified signal is then utilised in a quasi-transient approach to simulate the time dependent thermal behavior of the vehicle under highly dynamic loading conditions (e.g. Race-Track).

A sensitivity study was also conducted to identify the propagation of error corresponding to the utilisation of simplified boundary conditions compared to the original input signals. Then a quasi-transient approach was compared to a fully transient approach in order to identify the error associated with the utilisation of multiple steady state CFD solutions. Additionally several investigations were conducted on the type of CFD solution necessary to achieve appropriate convection conditions for a quasi-transient approach. Ultimately the optimal parameters from these prior sensitivity studies corresponding to the least introduced error were implemented on a full vehicle configuration. Here profile independence was explored by transferring the proposed methodology to alternative dynamic driving profiles.

Simulation results on multiple profiles were validated through experimental climatic wind tunnel tests, where a strong correlation was attained. These results were achieved with very little penalty on resources, whereby the methodology yielded a fraction of the calculation times (using 1/5<sup>th</sup> of the computing capacity) published in literature by alternative methods on simpler driving profiles. Additionally it was found that the simulation accuracy achieved was independent of driving profile, with discrepancies corresponding to modeling limitations on the vehicle. These results further confirmed the transferability capacity of the proposed methodology and the potential for wide scale application beyond the focus of this investigation.

# Contents

	<b>Nomenclature</b>	<b>V</b>
<b>1.0</b>	<b>Introduction</b>	<b>1</b>
1.1	Background.....	1
1.2	Motivation.....	2
1.2.1	Final Frontier for VTM.....	3
1.2.2	Further Applications for Dynamic Driving.....	3
1.2.3	Academic Motivation.....	4
1.3	Methods of Investigation.....	4
1.3.1	Theoretical Methods.....	4
1.3.2	Numerical Methods.....	5
1.3.3	Experimental Methods.....	6
1.4	Current Body of Knowledge.....	6
1.4.1	Vehicle Aerodynamics Using CFD.....	6
1.4.2	Steady State Vehicle Thermal Management.....	7
1.4.3	Transient Vehicle Thermal Management.....	9
1.4.4	Boundary Condition Simplification.....	10
1.5	Objectives of Thesis.....	11
1.6	Outline of thesis.....	12
<b>2.0</b>	<b>Numerical Fundamentals</b>	<b>13</b>
2.1	Computational Fluid Dynamics.....	13
2.1.1	CFD Software.....	13
2.1.2	Governing Equations.....	13
2.1.3	Applied Models of Investigation.....	15
2.1.4	Discretisation & Solver.....	17
2.2	Computational Thermodynamics.....	18
2.2.1	Thermal Software.....	18
2.2.2	Modes of Heat Transfer.....	18
2.2.3	Applied Models for Investigation.....	21



2.3	Techniques of Simulation.....	23
2.3.1	Coupling Software.....	23
2.3.2	Thermal-Fluid Coupled Approach.....	24
<b>3.0</b>	<b>Simplifying Vehicle Boundary Conditions</b>	<b>26</b>
3.1	Motivation and Background.....	26
3.2	Transient Boundary Conditions.....	28
3.2.1	Race-Track Profile.....	28
3.2.2	Handling Profile.....	29
3.2.3	Highway Profile.....	29
3.2.4	Street Profile.....	30
3.2.5	Summary of Profiles.....	31
3.3	Signal Simplification.....	31
3.3.1	Standard Averaging Schemes.....	31
	<i>3.3.1.1 Simple Moving Average</i> .....	31
	<i>3.3.1.2 Weighted Moving Average</i> .....	32
3.3.2	Signal Processing.....	33
	<i>3.3.2.1 Fourier Transform</i> .....	33
	<i>3.3.2.2 Wavelet Transform</i> .....	34
	<i>3.3.2.3 Wavelet Decomposition</i> .....	35
3.4	Thermal Response Characterisation.....	37
3.4.1	Flat Plate Analogy.....	38
	<i>3.4.1.1 Example 1</i> .....	39
	<i>3.4.1.2 Example 2</i> .....	41
	<i>3.4.1.3 Example 3</i> .....	42
3.4.2	Thermal Criteria for Critical Frequency.....	43
3.4.3	Critical Frequency & Decomposition Level.....	44
3.4.4	Thermal Response Matrix.....	45

<b>4.0</b>	<b>Development of Methodology</b>	<b>47</b>
4.1	Stage 1 - Modeling Exhaust Conditions.....	47
4.1.1	Exhaust system Configuration.....	47
4.1.1.1	<i>Former Methods</i> .....	48
4.1.1.2	<i>Proposed 1-D Method</i> .....	49
4.1.2	Exhaust Gas Dynamics.....	50
4.1.2.1	<i>Convective Augmentation Factor</i> .....	50
4.1.2.2	<i>Entrance Effect</i> .....	51
4.1.2.3	<i>Engine Induced Pulsation</i> .....	52
4.1.2.4	<i>Surface Condition</i> .....	54
4.1.2.5	<i>Geometrical Influences</i> .....	55
4.1.2.6	<i>Total CAF</i> .....	57
4.1.3	Exhaust Heat Transfer Coefficient Prediction Tool.....	57
4.2	Stage 2 - Sub-Module Investigation.....	59
4.2.1	Full Transient Scheme.....	60
4.2.2	Quasi-Transient Scheme.....	61
4.2.3	CFD Quantity Investigation.....	63
4.2.4	CFD Type Investigation.....	65
4.3	Stage 3 - Full Vehicle Investigation.....	67
4.3.1	Modeling & Physics.....	67
4.3.1.1	<i>Engine</i> .....	67
4.3.1.2	<i>Exhaust System</i> .....	68
4.3.1.3	<i>Heat Exchanges</i> .....	69
4.3.1.4	<i>Rotating Parts</i> .....	69
4.3.2	Cell Reduction Techniques.....	70
4.3.3	Full Vehicle Quasi-Transient Approach.....	71
4.3.3.1	<i>Simplified Profiles</i> .....	73
<b>5.0</b>	<b>Results and Validation</b>	<b>77</b>
5.1	Stage 2 - Sub-Module Results.....	77
5.1.1	Weighted Moving Average Results.....	78

5.1.2	Wavelet Derived Profile - Exhaust Results.....	80
5.1.3	Wavelet Derived Profile - Heat Shield Results.....	82
5.1.4	Wavelet Derived Profile – Under-Body Results.....	84
5.1.5	Effect of False Initial Temperature Results.....	85
5.1.6	CFD Type Investigation Results.....	87
5.1.7	CFD Quantity Investigation Results.....	89
5.2	Stage 3 - Full Vehicle Results.....	91
5.2.1	Race Track Profile.....	92
5.2.2	Handling Course Profile.....	96
5.2.3	Highway Driving Profile.....	99
5.2.4	Street Driving Profile.....	101
<b>6.0</b>	<b>Discussion and Analysis</b>	<b>105</b>
6.1	Stage 2 - Sub-Module Discussion.....	105
6.1.1	Boundary Condition Simplification Using WMA Schemes.....	105
6.1.2	Boundary Condition Simplification Using Wavelet Transformation.....	108
6.1.3	Effects of False Initial Temperature Discussion.....	109
6.1.4	Sensitivity of CFD Type.....	109
6.1.5	Sensitivity of CFD Point Quantities.....	111
6.1.6	Summary of Stage 2 Findings & Errors.....	112
6.2	Stage 3 - Full Vehicle Discussion.....	113
6.2.1	Profile Analysis.....	113
6.2.2	Solution Recycling.....	116
6.2.3	Turn-Over Time.....	116
6.2.4	Additional Errors.....	118
	<b>Conclusions and Future Recommendations</b>	<b>120</b>
	<b>References</b>	<b>123</b>
	<b>Appendix 1</b>	<b>128</b>
	<b>Appendix 2</b>	<b>135</b>
	<b>Appendix 3</b>	<b>140</b>
	<b>Appendix 4</b>	<b>143</b>

## Nomenclature

### Symbols

Symbol	Dimension	Definition
$\lambda$	[W/m.K]	Thermal Conductivity
$u_i$	[m/s]	Velocity of Flow
$\delta_{ij}$	[-]	Kronecker Delta
$f_i$	[N]	Body Forces
$h$	[J/kg]	Specific Enthalpy
$q_i$	[W/m <sup>2</sup> ]	Diffusion Heat Flux Vector
$S_R^h$	[W/m <sup>3</sup> ]	Energy Source Term
$t$	[s]	Time
$\emptyset$	[Variable Dependent]	General Variable
$\mu$	[Pa.s]	Dynamic Viscosity
$\mu_{\text{bulk}}$	[Pa.s]	Bulk Fluid Viscosity
$\mu_{\text{skin}}$	[Pa.s]	Surface Viscosity
$\mu_t$	[Pa.s]	Turbulent Viscosity
$A$	[m <sup>2</sup> ]	Area
$A^*$	[m <sup>2</sup> ]	Effective Area
$A_1$	[-]	Approximated Information at Decomposition 1
$A_1$	[m <sup>2</sup> ]	Surface area of Element 1
$A_{1-2}$	[m <sup>2</sup> ]	Contact area between element 1 and 2

$A_2$	[-]	Approximated Information at Decomposition 2
$A_n$	[-]	Approximated Information at Decomposition n
$A_s$	[m <sup>2</sup> ]	Exposed Surface Area
CAF	[-]	Convection Augmentation Factor
$C_p$	[J/kg.K]	Specific Heat
D	[m]	Diameter of Pipe
$D_1$	[-]	Detail Information at Decomposition 1
$D_2$	[-]	Detail Information at Decomposition 2
$D_{Bend}$	[m]	Bend Diameter
$D_h$	[m]	Hydraulic Diameter
$D_n$	[-]	Detail Information at Decomposition n
$E^*$	[J]	Characteristic Energy
$E_{In}$	[W]	Energy In
$E_{Out}$	[W]	Energy Out
$F$	[-]	Frictional Factor
$F_{1-1}$	[-]	View Factor of Element 1 to 1
$F_{1-2}$	[-]	View Factor of Element 1 to 2
$f_{critical}$	[Hz]	Critical Frequency
$f_{max}$	[Hz]	Maximum Frequency
h	[W/m <sup>2</sup> .°C]	Heat transfer coefficient
$h_1$	[W/m <sup>2</sup> .°C]	Heat Transfer Coefficient for element 1
k	[W/m.°C]	Thermal conductivity
$k_{1-2}$	[W/m.°K]	Conductivity from element 1 to 2
$L_c$	[m]	Characteristic Length
M	[kg/kmol]	Molecular Weight
$M$	[kg]	Mass
$M^*$	[kg]	Effective Mass

P	[m]	Perimeter
Pr	[-]	Prandlt Number
R	[J/mol.K]	Universal Constant
$r_{\text{Bend}}$	[m]	Bending Radius
Re	[-]	Reynolds Number
$Re_{\text{pul}}$	[-]	Reynolds Number from Pulsation
$S_0$	[-]	Original Signal
T	[K]	Absolute Temperature
$T_1$	[°C]	Temperature of Element 1
$T_2$	[°C]	Temperature of Element 2
$T_{\infty}$	[°C]	Air Temperature
$T_f$	[°C]	Fluid Temperature
$T_s$	[°C]	Surface Temperature
$T_{\text{Surr}}$	[°C]	Surrounding Temperature
$v_{\text{Mean}}$	[m/s]	Mean Velocity
Wo	[-]	Womersley Number
x	[m]	Length of Pipe
$\alpha$	[m <sup>2</sup> /s]	Thermal Diffusivity
$\Delta x=L$	[m]	Length
$\varepsilon$	[-]	Body Emissivity
$\varepsilon_1$	[-]	Emissivity of Element 1
$\varepsilon_2$	[-]	Emissivity of Element 2
$\nu$	[m <sup>2</sup> /s]	Kinematic Viscosity
$\rho$	[m <sup>3</sup> /kg]	Density of Fluid
$\sigma$	[W/m <sup>2</sup> .K <sup>4</sup> ]	Stefan-Boltzmann Constant
$\omega$	[Hz]	Angular Frequency
$\alpha$	[-]	Coupling Strength

## Operators

Symbol	Definition
$\overline{(\cdot)}$	Reynolds Averaging
$(\cdot)'$	Reynolds Fluctuation
$\underline{(\cdot)}$	Averaged Properties

## Subscripts

Symbol	Definition
$\infty$	Fluid Far From Surface
<i>Air</i>	Standard Air at Atmospheric Pressure
<i>Bend</i>	Bend
<i>Cond</i>	Conduction
<i>Conv</i>	Convection
<i>Critical</i>	Critical
<i>Depend</i>	Dependent
<i>Ent</i>	Entrance
<i>Geom</i>	Geometry
<i>Imp</i>	Imposed
<i>In</i>	In
<i>Max</i>	Maximum
<i>Mean</i>	Mean
<i>Out</i>	Out
<i>Pul</i>	Pulsation
<i>Rad</i>	Radiation
<i>Real</i>	Real
<i>s</i>	Surface
<i>Solid</i>	Solid
<i>Surf</i>	Surface
<i>surr</i>	Surroundings
<i>Total</i>	Total

## Superscripts

Symbol	Definition
--------	------------

---

*	Characteristic Properties
---	---------------------------

## Abbreviations

Abbreviation	Definition
--------------	------------

---

CAD	Computational Aided Design
CAE	Computational Aided Engineering
CAF	Convective Augmentation Factor
CAT	Catalytic Converter
CFD	Computational Fluid Dynamics
CFD_N	Number of Steady State CFD Points
CS	Cold Solutions (Uncoupled Steady State CFD Solutions)
cvgIT_[N]	Convergence of Initial Temperature Error at N degrees
CWT	Continuous Wavelet Transform
devCold	Deviation Between Original Signal and One with Cold Solutions
devIO[N]	Deviation of Interpolated Points of N Quantity
devW/C	Deviation Between Original Signal and One with Mixed Solutions
devWarm	Deviation Between Original Signal and One with Warm Solutions
devWavelet	Deviation Between Original Signal and Wavelet Form
devWMA	Deviation Between Original Signal and WMA Form
DWT	Discrete Wavelet Transform
EAS	End Acoustic Silencer
FEM	Finite Element Method
FT	Fourier Transform
FT	Fully Transient Approach
FVM	Finite Volume Method
IO[N]	Interpolated Points of N Quantity
IT_[N]	Initial Temperature State at N degrees
MAS	Middle Acoustic Silencer
MFR	Moving Frames of Reference
OEM	Original Engineering Manufacturer
Pre-CAT	Exhaust Pipe Prior To Catalytic Converter



QT	Quasi Transient Approach
RANS	Reynolds Averaging Numerical Simulations
RTS	Race Track Simulation
SMA	Simple Moving Average
STFT	Short Time Fourier Transform
VS	Volume-Control Shape
VTM	Vehicle Thermal Management
WCSM	Warm-Cold Solution Mixing (Mixed Steady State CFD Solutions)
WMA	Weighted Moving Average
WS	Warm Solutions (Coupled Steady State CFD Solutions)
WT	Wavelet Transform

## Classifications

Classification	Definition
<i>Cold Solutions</i>	Uncoupled Steady State CFD Solutions to a Thermal Solver
<i>Dampening</i>	Processes of Removing Irrelevant Frequencies from Boundary Conditions
<i>Decomposition</i>	Processes of Removing Irrelevant Frequencies from Boundary Conditions
<i>De-Noised Signal</i>	Simplified Velocity Boundary Conditions
<i>Information</i>	Boundary Conditions
<i>ISO-Surface</i>	3-D Surface generated from CFD Velocity Field
<i>Mapping</i>	Processes of Projecting 3-D Information onto corresponding 3-D geometry based on coordinate position.
<i>Noise</i>	Thermally Irrelevant Frequencies existing within Boundary Conditions
<i>Temperature Fixing</i>	Enforcing Constant Temperature
<i>Thermal Footprint</i>	Simplified Velocity Boundary Conditions
<i>Warm Solutions</i>	Coupled Steady State CFD Solutions to a Thermal Solver
<i>Warm-Cold Solutions</i>	Mixing between Steady State Solutions (both warm and cold) to Create New Solutions

# Chapter 1

## Introduction

### 1.1 Background

Since the emergence of shared memory systems and parallel computing, Computational Aided Engineering (CAE) has been used to support vehicle development [Sri05]. The numerical evaluation either through finite element methods (FEM) or finite volume methods (FVM) of concept vehicle designs has promoted the acceleration of the overall vehicle development process. Since the 90's vehicle development times have experienced substantial reductions [Fra11]. The evident advantages of shortened development times have been exploited by the industry to further improve vehicle concepts or implement new technology in earlier phases. This is called “front loading” vehicle designs within the development process. Additionally, cost advantages can be realised when concepts can be quickly evaluated numerically rather than through experimental methods; all of which require a physical prototype, a substantial financial investment, and a large amount of testing time. This virtual alternative provides engineers with a means of evaluating multiple design options quickly during the pre-development phase, whilst providing the optimal design configuration to compliment the final experimental validation.

Computational fluid dynamics (CFD) has played a significant role in front loading early vehicle designs. This is due to the time and cost efficiencies of software compared to full scale hardware validation. Today within the automotive industry CFD has become an integral engineering tool in nearly all vehicle design disciplines. Traditionally CFD was used to evaluate vehicle aerodynamics [Ahm84]. However over time its applications have broadened to internal combustion [Haw05, Mes06], brake cooling [Her05], engine cooling and lubrication [Dis13],

intake modelling [Dep02], exhaust modelling [Far06, Hae13, Dep02, Cha99, Ban08, Kan99, Wan05] , inner cabin comfort [Cur09], environmental effects [Rug07], battery modelling [Rei07], full vehicle under-body heat protection [Rei12] and a range of smaller applications in pre-development projects.

One of the primary focuses in the automotive industry is the total vehicle integration of all major sub-systems and the evaluation of the thermal load experienced within the vehicle under-body environments. This is called vehicle thermal management (VTM), and the tools of investigation are commonly a combination of experimental (climatic wind tunnels) and numerical methods (CFD).

## 1.2 Motivation

Current industrial standard for numerical VTM is mainly limited to steady-state conditions. This is due to the time constraints of productive pre-development processes, the available industrial computing power and the complexities surrounding full vehicle computational models. The resulting affect requires a turn-around (calculation) time of 1 week [Chr10] in order evaluate alternative designs consecutively and remain within the assigned vehicle development schedule. The standard VTM process uses a numerical model with steady state boundary conditions in order to evaluate the thermal distribution and high thermal localisation (Hot-Spots) on under-body components [Hae10]. These components may then be altered to improve the vehicle design, material allocation or to implement heat protection techniques such as thermal shielding. The steady-state conditions are usually known to the engineer through experimental experience and are normally selected due to their tendency to produce thermal specific conditions. It is clear that the exponential rise in parallel computing power in the near future may facilitate faster turn-around times and provide an opportunity for engineers to evaluate non-steady driving conditions supporting the current industrial development time schedules. Vehicles are becoming more complex with the integration of thermal management systems, through monitoring, controlling and changing the performance of the engine or cooling mechanisms to further improve the fuel efficiency. Therefore transient phenomena must be incorporated within production simulations in order to accurately represent the time dependent heat fluctuation throughout the vehicle. Hence strong emphasis has been placed on research engineers to develop methodologies for the near future that can efficiently utilise the potential resources to simulate transient vehicle conditions.

Extending from steady state cases allows engineers to investigate the "real" on road conditions of vehicle driving cycles. The ability to predict time dependent thermal characteristics of vehicle environments leads to improved product development (with rapid modification) and a reduction in the number of experiments and subsequent cost. Additionally, many of the critical thermal cases experimentally validated have non-equilibrium boundary conditions, resulting either in an over-prediction through steady state 3-Dimensional modeling or an inaccurate prediction through 1-Dimensional modeling.

Some previous attempts have been proposed in literature by industrial experts, to simulate time dependent behavior of semi-dynamic vehicle conditions (particularly in the case of thermal soak and dynamic hill climbing) [Rei08, Dis13]. Some of these proposals require strong

computing power, complete 3-Dimensional exhaust flow simulations, and complex fluid-solid coupling arrangements between two or more CFD models. Even though these methods incorporate realistic modeling approaches (due to the expected future availability in computational resources), they lack the potential to accommodate complex boundary conditions (for highly dynamic profiles) without the inherent dependency on continually increasing the computational power. The usage of excessive resources (including time) ultimately compromises the speed of a vehicle's development phase, which at times has a dependency on frequent design changes. Hence a new methodology must be explored to meet the needs of industry whilst optimising the use of current resources to accommodate future vehicle complexities. The advantage in pursuing an efficient methodology which intelligently incorporates the flow complexities of a vehicle simulation allows OEMs to redistribute resources back into the engineering teams for the development of new vehicle technologies. Any minor inaccuracies introduced within the front loading phase are considered insignificant and outweighed by the benefits of early prediction. This strategy thereby increases the volume of pre-development projects due to the speed advantages of the simulation and accelerates the maturity of early concept designs, therefore reducing the need for unnecessary prototype experiments.

### 1.2.1 Final Frontier for VTM

The Race Track Simulation (RTS) can be considered the final frontier for VTM numerical techniques as it is one of the most highly dynamic transient cases. In order numerically to resolve RTS conditions using current industrial methods (as well as those proposed in literature), the required time scales for both the high-gradient velocity profiles and the high-frequency changes of heat sources must be extremely small. This results in extravagant and costly simulation process which becomes dependent on large amounts of computing hardware to reduce the overall turn-around period. Simpler examples have already been observed in literature, such as the dynamic hill climb resulting in over 30 days of calculation time utilising 500% more computing power per simulation (512 cores) to that commonly available in industry [Dis13]. These results are not only time inefficient, but also the implementation of such methodologies for RTS would require a massive investment in computing hardware, manpower and software licensing, which ultimately compromises the advantages of CAE (in comparison to the traditional experimental methods). The following investigation aims at producing a robust RTS methodology which utilises the conventional resources (up to 96 cores) efficiently for direct implementation to the productive pre-development processes.

### 1.2.2 Further Applications for Dynamic Driving

A further advantage of developing a methodology which resolves RTS conditions is the transferability to less dynamic alternative driving profiles. Even though the primary focus of the investigation is the highly volatile conditions experienced on the race-track, a universal methodology is the overall academic aspiration. Hence alternative driving profiles will also be evaluated with the proposed methodology, in order to ascertain the broader application potential.

These profiles include the following:

1. Handling Course Profile
2. Highway Driving Profile
3. Street Driving Profile

### 1.2.3 Academic Motivation

The relationship between input variables and output data can classify the thermal response of a complex vehicle system containing a wide variety of independent components with differentiating masses directly or indirectly connected through conductivity and radiation. The fact that component characteristics<sup>1</sup> can influence its thermal behaviour has inspired the current investigation to exploit the response nature of these characteristics. Through the identification of the thermally relevant information<sup>2</sup> within the exposed boundary conditions alteration or simplification can be made to accelerate the calculation time. To date, normal simulation practices involve the utilisation of the original boundary conditions (without alteration) and pursue simplification on the modelling side, either through geometrical reductions or 1-D modelling. If the boundary conditions can be optimally altered and simplified without incurring significant errors that may change the thermodynamic behaviours of components, this may reveal an overlooked region within simulation sciences. The inherent advantages and application potential to further develop such a simulation approach goes well beyond the current automotive investigation. The methodology may provide the means of understanding and predicting even more complex thermodynamic problems which currently are not possible due to the dynamic nature of the boundary conditions coupled to the standard approach of simulating these highly volatile conditions. On the premise that the approach adopted in this research leads to results of acceptable level of accuracy then it would achieve its twin goals of significantly contributing to the body of knowledge and challenging the tradition paradigm<sup>3</sup> in simulation sciences.

## 1.3 Methods of Investigation

Theoretical, numerical and experimental means of investigation are the primary techniques utilised to develop the dynamic driving methodology.

### 1.3.1 Theoretical Methods

The mathematical component of the research is to investigate the potential methods in smoothing, filtering, simplifying or decomposing dynamic input conditions for use in vehicle simulations. These techniques may include a range of statistical and de-noising methods available in literature. The aim is to study a set of potential options available, and to investigate the application of these techniques to the thermal numerical simulation.

<sup>1</sup>Material Properties, Thermal Mass, Position and Relative Connectivity within the Vehicle.

<sup>2</sup>The Frequency range which induces thermal change above a pre-defined tolerance.

<sup>3</sup>That the original boundary conditions must be simulated to achieve the outcomes of the investigation

Additionally the investigation aims at establishing a theoretical relationship between heating and cooling sources, to the component characteristics and the resultant thermal response to input parameters.

1. Investigation of the potential signal simplification techniques and their application to input boundary conditions. Each technique is evaluated by its potential to replicate the real thermal conditions either through comparison to numerical or experimental data.
2. The determination of the thermal footprint signal<sup>4</sup> via theoretical analogies linking frequency to temperature change based on component properties. The development of a thermal response characterisation algorithm which is used to identify relevant and irrelevant frequency ranges within input boundary conditions.

### 1.3.2 Numerical Methods

The numerical investigations will encompass a two phase evaluation process. The first phase aims at identifying potential simplification techniques and corresponding modelling approaches for transient boundary conditions. Due to the size and complexity of full vehicle numerical models, an initial sub-module is constructed in order to evaluate efficiently the alternative simplification techniques compared to a traditional full transient simulation. The boundary conditions are derived from real vehicle data obtained from an experimental test. The influences of time-step acceleration, simplified profiles, coupling techniques, alternative CFD solution types and time interpolation will be investigated within the sub-module. The propagation of error including the alternative sources of error will be evaluated in order to further minimize these discrepancies within a full vehicle model. Out of the potential options an optimal candidate will be selected to be further utilised on full vehicle geometry. Hence the second phase of the numerical investigation revolves around the adaption of previously investigation with the inclusion of complex physics conditions experienced within real vehicle models. These conditions may include the modelling techniques for rotating objects, heat exchangers, engine cooling fan, and the full exhaust system. The two phase numerical investigation is as follows:

#### *Phase 1: Sub-Module*

1. Evaluation of alternative simplified profiles to substitute the real dynamic boundary conditions.
2. The identification of error sources, error propagation and their consequent effect on thermal resolution.
3. Assessment of alternative coupling techniques of steady-state CFD solutions types. The influences of quantity and location of mapped CFD data on thermal resolution.
4. Selection of the optimal combination<sup>5</sup> of simulation parameters based on previous sensitivity study for utilisation in a full vehicle configuration.

<sup>4</sup>The simplified versions of the input boundary conditions

<sup>5</sup>With the minimum induced error on CFD solution quantities and types

## *Phase 2: Full Vehicle Configuration*

1. Assessment of full vehicle thermal response to simplified input conditions.
2. Evaluation of thermal modelling techniques of real components.
3. Evaluation of method transferability to alternative driving profiles.

### 1.3.3 Experimental Methods

Initially experimental data will be analysed to identify the potential influences and trends between input boundary conditions and output temperature profiles. Once the experimental analysis is completed the data will be further utilized to validate simulation techniques explored within this investigation. Experimental resources include the use of climatic wind tunnels, which allow vehicle configurations to experience highly dynamic driving conditions in a contained environment. Climatic wind tunnels have the advantage of repeatability and data consistency compared to the large uncertainty inherent with on-road testing. This uncertainty in on-road testing is due to the unpredictability of environmental/driver conditions. Therefore control testing within tunnels increases the confidence in both the experimental data and proposed simulation methodology.

## **1.4 Current body of knowledge**

The following section presents a concise literature summary commencing with the origins of CFD in the automotive world. Once this is established a review of the prior work published in the field of vehicle thermal management simulations is presented, specifically focusing on the current body of knowledge which directly pertains to the research field.

### 1.4.1 Vehicle Aerodynamics Using CFD

Even though numerical VTM is a relatively new technology, the automotive industry has been an early user of simulation practices utilising CFD since attention was generated through the publication by Ahmed in 1984 [Ahm84]. Ahmed proposed a simple geometrical configuration of a bluff body with a potential adjustable slant in the rear of the geometry. The Ahmed model itself could induce particular flow fields which replicated those of traditional vehicles. Unlike the Ahmed body, a full vehicle computational model is a complex assembly of sub-systems each interacting with each other. Hence early adoption for vehicle aerodynamic simulation only focused on the outer body. Cogotti & Berneburg investigated the flow characteristics through an engine compartment utilising an experimental wind tunnel [Cog91]. They emphasised the role CFD could play in future for visualisation of highly turbulent flow phenomena within the engine bay. Kobayashi & Kitoh shared the opinion of Cogotti and Berneburg whilst reiterating the benefits of CFD and its consequent potential to reduce costs and dependency on experimental wind tunnel testing [Kob92]. However Kobayashi & Kitoh did also indicate the difficulty in simulating vehicle configurations including the immense numerical options available to model such flow phenomena which at that time was not extensively validated in vehicle applications. Summa released a publication detailing the process of calculating the aerodynamic properties of a corvette ZR1 outer body for steady and unsteady conditions

[Sum92]. It was found that the CFD code accurately predicted the pressure distribution along the hood of vehicle in comparison to experimental results. From this date numerous publications begun to appear indicating the growing adoption of CFD within the industry. Today vehicle aerodynamic performance is measured through a combination of experimental and numerical techniques [Ben11, Nat14]. However the emphasis of simulation has moved extensively into the realm of implementing unsteady conditions. An example of this is the work of Oettle et.al, who measured the time dependent surface pressure against the front glass when fluctuating the vehicle yaw angle [Oet12]. Similar work has also been published by Wojciak et.al, who investigated the effect on drag and lift of transient model motion using sliding meshes [Woj12]. The aim of that investigation was to accurately validate the unsteady wake formation and pressure distributions over the vehicle surface. Transient vehicle aerodynamic simulations now encompass weather conditions such as snow and rain, overtaking manoeuvres, the effect of steering and drifting situations and the effect of particle impact and consequent damage to outer body [Chr14].

#### 1.4.2 Steady State Vehicle Thermal Management

CFD was not only of interest for vehicle aerodynamics but also indicated a potential to simulate the thermal state of the vehicle. Unlike basic aerodynamic calculations; which could simplify the models to the outer body, thermal simulations required a tremendous amount of geometrical and multi-physics detail in order to appropriately establish the complex heat transport mechanisms. Hence, to build a vehicle for thermal consideration all major thermally contributing sub-systems and their mechanisms needed to be incorporated.

##### *Heat Exchanger*

Reister was the first to publish a detailed methodology in simulating flow through an engine compartment [Rei94]. From this it was found that the heat exchangers played a critical role in adding thermal energy to the convective fluid flow. Pervaiz et.al, published material on determining air and coolant temperatures within the heat exchangers and condenser of a vehicle in order to simulate the effect of adding heat to the airflow [Per97]. The publication presented a computational model in which the phase change of the refrigerant was implemented without the need to model the complex internal geometry of the heat exchanger. Binner also investigated the vehicle heat exchangers and developed a detailed numerical model of the internal geometry [Bin00]. Additionally his PhD investigated the impact of geometrically simplifying the heat exchanges by using only the outer geometry (box) and applying heat transfer correlations to replicate the heat transportation process. The artificial heat exchanger boxes could then be assigned directional porosity in order to simulate the pressure differential normally experience when air is forced through the vehicle heat exchanger. To date, this methodology is used for vehicle heat exchanges to generate the proper thermal field within the engine compartment [Hae13].

##### *Engine Fan*

Once the proper thermal field was achieved then the momentum effects of the engine fan needed to be incorporated to rotate the temperature field during the simulation. This can be difficult to incorporate as traditionally moving parts need to be simulated transiently and with a sliding



mesh or adaptive meshing arrangement based on time-step. Spindler investigated the effects of fan rotation within the engine compartment and through the vehicle's under-body environment [Spi05]. The methodology utilised a moving reference frame (MRF) which assumes symmetrical properties about the perpendicular axis in the center of the boundary. Spindler proposed this methodology for steady state calculations to mimic the momentum given to the fluid by providing a rotational speed to the fan. This proved to be very successful and is also currently the standard simulation practice for the vehicle fan, wheels, drive shafts and axles [Hae13].

### *Engine*

The engine itself is a complicated system consisting of direct liquid cooling to the block, oil circuits and internal combustion. Disch proposed a methodology which aimed to resolve the thermal behaviour of the engine [Dis13]. The methodology attempted to assemble a series of sub-system simulations together into a single model. The combusted gas convective data was mapped directly on the inner side of the cylinder, and head. Coolant heat transfer coefficients were extracted from a coupled 3D simulation and mapped onto exposed coolant jacket area of the engine. Additionally the oil circulation was modelled in order to incorporate the convective behaviour of the flow paths which followed through the oil heat exchanger, around the oil filter, into the intake/exhaust gallery to the cylinder head and turbocharger. Disch stated that the modelling of these conditions were necessary to incorporate the thermo-mechanical effects within a vehicle. For VTM purposes the engine is one of the simplest systems to simulate due to its thermally regulated nature. Therefore the outer thermal conditions of the engine can be predicted and implemented as boundary conditions for the simulation without the consideration of internal mechanisms. This implementation is usually done by a 1-D model to set the outer component temperatures of the engine within a particular operating range. The thermo-mechanical effects requiring high thermal resolution on the engine and its inner components as proposed by Disch are not the focus of this current research project.

### *Exhaust*

The exhaust system is the primary heat source within the vehicle under-body environment and is the central cause for many thermally related issues within the vehicle. Hence in order to accurately predict the thermal behaviour of the vehicle the exhaust system must also be appropriately represented within a computational model; whereby its active participation in the conjugate heat transfer process is felt. Traditionally for VTM simulations the exhaust systems are temperature fixed to constant value derived from experimental data [Fra09]. 3-D simulations for the internal exhaust system tend to be costly and time inefficient especially with the introduction of turbochargers and catalytic converters, making steady state exhaust simulations nearly unfeasible for industry but not impossible. Enriquez-Geppert proposed a methodology to simulate the entire exhaust system in 3-D taking into account the interaction to the surrounding vehicle geometry [Enr11]. This was focused on steady state conditions and coupling techniques between the full vehicle model and exhaust sub-model. This method showed promising results however did not improve the inherent disadvantages of large turn-around times required to solve the problem. Haehndel proposed a methodology of segregating the exhaust system into a series of connecting pipes, where heat transfer coefficients were

applied to the inner surfaces of the components [Hae09]. In order to achieve the appropriate heat transfer coefficients for steady state conditions, 1-D Nusselt number correlations were used to represent the gas dynamic phenomena experienced by the each individual component. Then within the exhaust system a series of fluid nodes were created and linked to form a 1-D fluid stream, whereby the gas temperatures and mass flow rates could be associated to the stream [Hae10 & Hae13]. Heinemann adapted the philosophy from Haehndel to incorporate the exothermic reaction in the catalytic converter [Hei09]. Based on experimental data Heinemann derived a correlation to represent the required energy enhancement to the gas due to the reaction properties of the catalytic converter. Schlipf further adapted the 1-D fluid stream method for the application to acoustic silencers within the exhaust system [Sch11]. The internal geometry of the silencer systems were modelled and altered the heat transfer coefficients to compensate flow phenomena due to wall impingement, insulation, hollow chambers and internal pipe perforations. This drastically improved the local thermal resolution on the surfaces of the acoustics silencer systems [Hae14a]. Finally, Devos developed a process to enhance the heat rates induced within the turbocharger by implementing Dean and Nusselt number correlations for centripetal flow vortices [Dev14]. The internal heat rates of the turbocharger could be simulated and connected through the exhaust fluid stream piping network. Good agreement was achieved with experimental results.

#### 1.4.3 Transient Vehicle Thermal Management

The process of simulating full vehicle geometry for thermal management processes requires the interaction between two domains; firstly the fluid region which encompassed the convective flow parameters, and secondly the solid region which associates the thermal aspects to components. In order to achieve this there are two alternative approaches predominately found within literature. The “all in one” approach, attempts to cluster the simulation into a single CFD solver [Rei12]. The “Segregated approach” aims at coupling results between two or more solvers hence sharing the work load [Wei05]. Both these approaches have inherent advantages and disadvantages, and for transient simulations these conditions tend to further exaggerate due to the complexity of the problem.

##### *Fully-Transient “All in One” Approach*

Weidmann et.al, published an approach for simulating the vehicle thermal soak scenario within a single CFD solver [Wei08]. It was proposed that avoiding segregation could accelerate the simulation turn-around time as transportation of data between two different solvers could be avoided. In order to do this the vehicle model within the CFD solver would need to be constructed using solid elements. Unlike the segregated approach which uses specialised thermal software to represent component thicknesses artificially through shell elements. Additionally the boundary conditions for both thermal and fluid phenomena were transient. Hence the simulation would need to incorporate the smallest time scale necessary to resolve the fluid phenomena and apply that same time scale also to the thermal phenomena. This approach was also later utilised by Reister and Bauer on full vehicle models for steady unsteady vehicle simulations [Rei12]. The methodology introduced the inner-cabin aspects of the vehicle whilst using automisation to accelerate the assignment of interfaces between solid parts. Disch (2013)

then further extended the technique to increase the realism of the models by introducing full exhaust and engine for the transient condition of a vehicle towing a trailer up a hill [Dis13].

#### *Quasi-Transient “Segregated” Approach*

Weidmann proposed a methodology for an under hood analysis for the natural convection phenomena utilising a quasi-transient coupling approach [Wei05]. The fluid domain (in CFD) was segregated from the thermal domain for a simplified engine compartment. The resulting surface temperatures from the thermal domain was mapped into a steady state CFD model; while the fluid temperatures and heat transfer coefficients were introduced into a transient thermal domain. Between the individual CFD points time interpolation was conducted by the thermal solver to produce heat transfer coefficients and fluid temperatures on the surfaces of components for each time-step. This style of approach was also adopted by Kaushik whereby he used several steady state CFD points to represent the time dependent convection experienced within the vehicle [Kau07]. Schuetz et.al, released a segregated approach to brake cooling, coupled to the thermo-mechanical application [Sch08]. He used again the stand-alone thermal model mapping several steady state CFD results to be time interpolated. Franchetta et.al, & Pryor et.al, addressed the thermal soak scenario utilising the segregated approach coupled to the effects of natural convection within the engine bay [Fra06 & Pry11]. The results from both of these investigation proved very successful and indicated potential for further development in the transient field.

#### 1.4.4 Boundary Condition Simplification

In order to address complexities within vehicle models, VTM simulations generally have a degree of controlled simplification. This type of simplification is primarily conducted on the vehicle geometry itself, removing small components (e.g. clips or bolts) from the numerical model [Chr12]. These components naturally are less critical and due to their small masses often don't contribute significantly to the thermal state of the vehicle. Additionally the CFD model is prone to a series of assumptions, from near wall treatments (to represent the development of the thermal/velocity boundary layer), ideal fluid conditions, rotating and moving parts, the energy exchange through the heat exchangers and finally even using the numerical estimation of Navier-Stokes to represent the fluid field [Ten04, Sri05]. All of the above examples, address simplification conducted through the pre-processing stage of modelling full vehicle conditions utilising commercial software. They attempt either to reduce the complexity of the geometry or simplify the physics of the simulation. However none of these examples attempt to simplify the fundamental boundary conditions of vehicle as that is counterintuitive for the engineer. Why should the engineer change the vehicles boundary conditions? It is the one unexplored region in simulation sciences (primarily in CFD) which challenges the old paradigm; that one must simulate the exact boundary conditions the vehicle is experiencing, in order to achieve the appropriate prediction.

Through experimental investigation it can be clearly demonstrated that in dynamic cases there is no direct correlation between the component temperature responses to that of the highly volatile boundary conditions [Hae13b]. This suggests that the time scales between thermal and fluid phenomena are not equal (due to the temperature inertia generated by a component's

mass). Hence there is an opportunity to exploit this phenomena by simplifying the vehicle boundary conditions to suit the time scales of the thermal model, in turn accelerate the calculation time. This can be considered as the removal of “thermal noise” from the boundary conditions as the noise itself doesn’t contribute to temperature change. There are many signal processing techniques in achieving this type of removal, from moving average schemes, to Fourier analysis or even Wavelet transformations.

A running average (or moving average) has been a commonly attributed tool for statistical analysis in a variety of applications, ranging from GPS signal processing [Shm02], stock analysis [Rob02] and forecasting sales [Joh99]. It can consist of a simple formation, where series range is unbiased, or alternatively can be regressed to favour particular conditions such as the weighted moving average [Shm02].

When considering more sophisticated signal processing methods, Fourier analysis has been used in a wide spread of applications. Frequency analysis has been conducted for many years in the automotive industry on NVH (noise, vibration and harshness) in attempt to remove unwanted noise from non-stationary signals and better understand the core performance of the vehicle [Hua08]. Another example is the analysis of knock occurrence and intensity in spark ignition engines, via high frequency signal analysis [Ger09] or identify and control the fuel dynamics in port injection [Sha08]. Here short time Fourier transforms and Wavelet transforms can be used to firstly understand the performance of an engine and then to optimise the calibration to maintain safe conditions of the engine. For multi-resolution signal processing wavelet transformations become more attractive, as they can project the signal onto a set of scales. Therefore one can identify and visualise the non-contributing information. This can be particularly useful for non-periodic signals, for example in multi-phase flow regimes [Fu11], image processing [Fis01] or fault detection [Tsa09, Zhe06, Che12]. In Shannon’s theory of communication, he attempts to identify the noise characteristics in a signal by expressing it as *entropy* (or meaningless information) [Sha48]. This is quantified by the statistical uncertainty (or randomness) within a signal containing information and the likelihood of a signal to proceed from a given position to the next. A similar methodology can be pursued for the vehicle boundary conditions, as identifying the noise (thermally irrelevant information) and removing it prior to the simulation naturally accelerates the calculation time, and in turn can make dynamic driving scenarios feasible to simulate. This is the core research contribution in the following investigation.

## **1.5 Objectives of Thesis**

The research aims to develop a novel methodology for full vehicle transient thermal simulations under dynamic boundary conditions. The core contribution of the research is the process of simplifying the high frequency inputs via signal processing techniques whilst maintaining the core phenomena which affects the time dependent component temperature behaviour. In order to achieve this, identification of the necessary frequency bandwidth within boundary conditions must be theoretically derived. The goal of the investigation is to improve turn-around times for dynamic driving cases without significantly compromising the simulation accuracy. The following research questions are to be addressed:

1. Is it feasible to integrate complete vehicle architecture into a 3-D computational environment in an efficient manner encompassing all relevant thermal characteristics for dynamic boundary conditions?
2. Can the time dependent boundary conditions be simplified without compromising the resultant transient thermal behaviour of underbody components?
3. Can Quasi-Transient simulation techniques provide accurate thermal resolution for the dynamic changes in vehicle boundary conditions?
4. What are the corresponding sensitivities to the proposed methodology? Can the error be quantified with its influences over time?
5. Can the methodology be transferred to alternative driving profiles?

## **1.6 Outline of the Thesis**

The fundamentals of CFD and computational thermodynamics are addressed in chapter 2. The governing equations are described including the modes of heat transfer. Additionally chapter 2 details the different software packages used in combination with the coupling methods between 1-D and 3-D tools. Chapter 3 introduces the first core focus of the research; the simplification techniques of transient boundary conditions. This includes the several mathematical approaches to remove non-thermally contributing information from input conditions for the simulation. Additionally the alternative driving profiles are explored for this investigation. Chapter 4 describes the second core focus of the research; the development of the simulation methodology. Three stages of development are explored, each building the fundamental blocks necessary to achieve full vehicle transient simulations. The selected boundary condition signal processing method is presented for each individual driving profile with corresponding quasi-transient data. Chapter 5 compiles the simulation results of the individual stages of the methodology development and presents the sensitivities associated with the proposed modelling strategies. Chapter 6 analyses these results and quantifies the associated errors with the methodology. The sensitivities are further explored and the propagation of error is justified for proposed approach. Finally the concluding remarks and future work are given in chapter 7.

# Chapter 2

## Numerical Fundamentals

As discussed within chapter 1, a segregated methodology may be useful for accelerated turn-around times for transient simulations. Considering the following investigation attempts to simulate the most extreme driving conditions, which to date, has never been achieved, a segregated methodology in combination with a quasi-transient approach can be advantageous. The following section provides a summary of the numerical fundamentals of both computational fluid dynamics and thermodynamics. Since the focus of the research is on the development of a methodology for transient vehicle thermal simulations of dynamic driving scenarios, the standard industrial numerical approaches will be used. These include the models used to solve the fluid flow field and the thermal phenomenon.

### 2.1 Computational Fluid Dynamics

#### 2.1.1 CFD Software

The fluid dynamics software utilised in this investigation is *Star-CCM+* (version 7.1), a software provided by CD-Adapco. *Star-CCM+* provides the means of numerically predicting external convection characteristics of under-body flow dynamics at variable vehicle velocities. *Star-CCM+* is a complete 3-D CFD prediction software package. The applications of the software package range from basic fluid flow scenarios to complicated multi-phase situations. The software provides the durability, robustness and stability to tackle a wide range of industrially demanded problems. Therefore it is one of the most commonly used software's in the Automotive and Aerospace industries.

#### 2.1.2 Governing Equations

The governing equations for fluid dynamics represent the conservation laws of physics. These include the conservation of mass, Newton's second law, and the first law of thermodynamics [Tu08]. All CFD is based upon the solution of these transport equations for the application to fluid flow scenarios.

##### *Conservation of Mass*

The conservation of mass is the fundamental physical law that matter is neither created nor destroyed within a closed system. Mass conservation then dictates that rate of change within a system is equivalent to the mass flux crossing its boundaries. This can be mathematically represented in Equation 2.1, where  $t$  is time,  $\rho$  is the density and  $u_i$  is the velocity of the flow.

$$\frac{\partial \rho}{\partial t} + \frac{\partial (\rho u_i)}{\partial x_i} = 0 \quad (2.1)$$

### The Momentum Equation

According to Newton's second law of motion, the rate of change of momentum can be described as the summation of forces acting on the corresponding fluid, which must equal the combination of its mass and acceleration. Hence the momentum equation can be defined below in Equation 2.2, whereby  $\tau_{ij}$  represents the stress tensor and  $f_i$  the body forces on the fluid.

$$\frac{\partial(\rho u_i)}{\partial t} + \frac{\partial(\rho u_i u_j)}{\partial x_j} = -\frac{\partial p}{\partial x_i} + \frac{\partial \tau_{ij}}{\partial x_j} + \rho f_i \quad (2.2)$$

### Conservation of Energy

Similar to the conservation of mass, the first law of thermodynamics dictates that energy cannot be created or destroyed, but only can change form. The physical interpretation of the law can be described in three components as the local acceleration of the fluid, the advection and its corresponding diffusion. Adding the energy source term  $S_R^h$  as a means of introducing external effects, Equation 2.3 is formulated, where  $h$  represents the specific enthalpy of the fluid and  $q_i$  the corresponding heat flux.

$$\frac{\partial(\rho h)}{\partial t} + \frac{\partial(\rho h u_i)}{\partial x_i} = -\frac{\partial q_i}{\partial x_i} + \frac{dp}{dt} + \tau_{ij} \frac{\partial u_j}{\partial x_i} + S_R^h \quad (2.3)$$

The following investigation assumes ideal gas properties due to the high temperature state of the fluid in vehicle underbody flow regimes. At high temperatures the inter-molecular forces are less effective in a real gas, therefore an ideal gas assumption can be introduced. Equation 2.4 represents the fundamental ideal gas law.

$$\rho = \frac{pM}{RT} \quad (2.4)$$

The stress tensor ( $\tau_{ij}$ ) can be determined using the Stokes law for Newtonian fluid, thus producing Equation 2.5 whereby  $\mu$  represents the dynamic viscosity and  $\delta_{ij}$  the Kronecker delta.

$$\tau_{ij} = \mu \left( \frac{\partial u_i}{\partial x_j} + \frac{\partial u_j}{\partial x_i} \right) - \frac{2}{3} \mu \frac{\partial u_k}{\partial x_k} \delta_{ij} \quad (2.5)$$

The energy equation can be further simplified by removing the frictional heat source term (third term on the right hand side) from Equation 2.3. The heat flux derived from Fourier's conduction and energy transportation law is presented in Equation 2.6, where  $\lambda$  represents the thermal conductivity of the fluid.

$$q_i = -\lambda \frac{\partial T}{\partial x_i} + h \quad (2.5)$$

Enthalpy is represented by Equation 2.6, where  $c_p$  corresponds to the specific heat capacity of the fluid.

$$h = h_0 + \int_{T_0}^T c_p(T) dT \quad (2.6)$$

Since enthalpy is a function of temperature the following Equations 2.7 and 2.8 can be considered.

$$\frac{\partial h}{\partial x_i} = \frac{\partial h}{\partial T} \frac{\partial T}{\partial x_i} \quad (2.7)$$

$$\frac{\partial h}{\partial x_i} = c_p \frac{\partial T}{\partial x_i} \quad (2.8)$$

From the above stated simplification the energy formulation take the new form presented in Equation 2.9

$$\frac{\partial(\rho h)}{\partial t} + \frac{\partial(\rho u_i h)}{\partial x_i} = -\frac{\partial}{\partial x_i} \left( -\frac{\mu}{Pr} \frac{\partial h}{\partial x_i} \right) + S_R^h \quad (2.9)$$

### 2.1.3 Applied Models for Investigation

As previously stated the following research aims at utilising standard industrial models and commercial software to develop and verify a novel methodology for high dynamic thermal vehicle simulations. Therefore the following section aims at addressing the most robust, widely validated and commonly accepted models used in CFD for vehicle simulations.

#### *Reynolds Number*

Reynolds Number (Re) is a dimensionless parameter representing the ratio of the inertial forces to the viscous forces within fluid flow regime derived from the investigation of Osborne Reynolds (1883) [Rey83]. It is commonly utilised as a means of flow regime classification: laminar, transitional or turbulent. The Reynolds number can be classified by Equation 2.10, whereby U represents the flow velocity, L the corresponding length scale and  $\nu$  the kinematic viscosity of the fluid.

$$Re = \frac{\text{Inertial Forces}}{\text{Viscous Forces}} = \frac{UL}{\nu} \quad (2.10)$$



## Reynolds Averaged Numerical Simulations (RANS)

RANS is the most commonly used model for fluid flow within engineering application and is primarily used for scenarios consisting of turbulent fluid flow. Turbulent processes naturally consist of fluctuating flow conditions whereby the RANS model aims at time-averaging these conditions to achieve mean flow velocity. This can be advantageous for engineering applications which focus on resolving mean conditions. For example, the steady state vehicle simulations where time-localised fluctuations of velocity are not of primary importance for the overall vehicle thermal management. The simplification of these fluctuations through time-averaging techniques results in a low computational cost with good near wall resolution. Hence the RANS method is used in the following investigation. Equation 2.11, 2.12 and 2.13 describe the time averaged transport equations for mass, momentum and energy.

$$\frac{\partial \rho}{\partial t} + \frac{\partial(\rho \bar{u}_i)}{\partial x_i} = 0 \quad (2.11)$$

$$\frac{\partial(\rho \bar{u}_i)}{\partial t} + \frac{\partial(\rho \bar{u}_i \bar{u}_j)}{\partial x_j} = -\frac{\partial \bar{p}}{\partial x_i} + \frac{\partial \bar{\tau}_{ij}}{\partial x_j} - \frac{\partial(\rho \overline{u'_i u'_j})}{\partial x_j} + \rho \bar{f}_i \quad (2.12)$$

$$\frac{\partial(\rho \bar{h})}{\partial t} + \frac{\partial(\rho \bar{u}_i \bar{h})}{\partial x_i} = -\frac{\partial}{\partial x_i} \left( -\frac{\mu}{\text{Pr}} \frac{\partial \bar{h}}{\partial x_i} \right) - \frac{\partial(\rho \overline{u'_i h'})}{\partial x_i} \quad (2.13)$$

The transport equations presented above are similar to those for laminar flows except for the addition of the turbulence terms ( $\rho \overline{u'_i u'_j}$  and  $\rho \overline{u'_i h'}$ ). These terms are unknown and are commonly classified as the Reynolds stresses.

### *k-ε Two Equation Turbulence Model*

In order to solve the unknown terms within the RANS method a relationship between mean velocity and heat sources needed to be established. In 1868, Boussinesq proposed a methodology to solve the Reynold stresses by introducing a relationship between the mean rates of deformation and turbulent viscosity [Bou68]. Launder and Spalding (1974) later developed transport equations to compensate the turbulent quantities [Lau74], which today is the most commonly used and validated turbulence model within industry, the two equation k-ε turbulence model [Tu08]. The local turbulence viscosity ( $\mu_t$ ) is addressed in Equation 2.14, where  $C_\mu$  is an empirical constant, k is the turbulent kinetic energy and ε is rate of turbulent energy dissipation.

$$\mu_t = \rho C_\mu \frac{k^2}{\varepsilon} \quad (2.14)$$

#### 2.1.4 Discretisation & Solver

In order to solve the transport equations for any given flow problem, the partial differential equations must be converted into a discrete system of algebraic equations. Therefore the domain containing the given flow scenario must be divided into a set of non-overlapping control volumes (or 3-D grids) in which the algebraic equations can be solved. There are several numerical techniques to solve these algebraic equations from finite element method (FEM), finite difference method (FDM) or finite volume method (FVM). For the following investigation, FVM will be utilised due to its flexibility to deal with unstructured control volumes within a complex domains [Chu02]. This is particularly useful for sophisticated geometries such as that of a vehicle, which generally consists of an arrangement of non-uniform surfaces, sharp bends and intricate contours.

##### *Finite Volume Method*

In 3-D fluid flow problems the system of partial differential equations cannot be simplified and is difficult to solve analytically, therefore numerical methods are utilised to estimate the values of the dependent variables. This is conducted after the domain is discretised into finite-control volumes containing a series of centralised and boundary nodes. Using cylindrical coordinate system  $(r, \theta, x)$  as an example, the differential equations can be expressed with respect to the general variables,  $\phi$  (the distance between nodes),  $\Gamma$  (the diffusion coefficient), and  $S$  (the source term), as the following (Equation 2.15) :

$$\int_V \frac{\partial}{\partial x} (\rho u \phi) dV + \int_V \frac{1}{r} \frac{\partial}{\partial r} (\rho r v \phi) dV = \int_V \frac{\partial}{\partial x} \left( \Gamma \frac{\partial \phi}{\partial x} \right) dV + \int_V \frac{1}{r} \frac{\partial}{\partial r} \left( r \Gamma \frac{\partial \phi}{\partial r} \right) dV + \int_V S dV \quad (2.15)$$

The integration can be performed by calculating the surface area and in turn the volume of the control element.

##### *Mesh Type*

The division of the computational domain for the discretisation of the transport equations is classified as the mesh. There are many strategies used to generate meshes, whether that would be structure or unstructured mesh, conformal or non-conformal mesh between regions and propagating or uniform mesh density. Each aim at creating the cells (control volumes) within the simulation domain in the most efficient and effective way, considering the calculation time and accuracy. Here mesh independence studies are conducted to find the optimal mesh densities and cell orientation for the simulation. Cell types can either be tetrahedral, hexahedral or polyhedral. For this investigation, a combination of hexahedral and polyhedral cells are utilised due to the distinct advantage in solution speed, memory and increased time to convergence

compared to the tetrahedral counterpart [Cda14]. The meshing strategy for full vehicle configurations is discussed later in chapter 4, with the development of the methodology.

### *Segregated Flow Solver*

In order to solve the transport equations for the discretised cells an additional algorithm is required for the iterative process. Here a segregated solver is utilised for the velocity and pressure in combination with the SIMPLE (Semi-Implicit Method for Pressure-Linkage Equations) algorithm for incompressible fluid flow. The SIMPLE scheme is one of the most popular iterative methods for pressure-velocity coupling within many commercial codes used for industrial applications [Tu02]. Introduced by Patankar and Spalding (1972), the scheme aims at iteratively guessing the pressure field and calculating the discretised momentum equations, therefore updating the velocity field until convergence is achieved [Pat72]. This scheme is particularly suited for hexahedral structured and staggered meshing types, whereby the velocity components can be evaluated at the cell faces, whilst the pressure, temperature and turbulent quantities can be stored at the cell centroid [Tu02]. These techniques can accelerate the solution to convergence and promote faster calculation times, hence it is utilised within the following investigation.

## **2.2 Computational Thermodynamics**

### 2.2.1 Thermal Software

The thermodynamics software utilised in this investigation is *Radtherm*, a Thermo-Analytics software package. *Radtherm* possesses a useful feature for vehicle modelling; 3D surface geometrical shells in which elements are thermally linked through the integration of 1D thermal/fluid nodes. The convection, conduction and radiation calculations are performed through an energy balance equation, whereby environmental effects can additionally be integrated within the numerical computation. *Radtherm* is constructed by a modern C++ code and the program allows for “cross-platform functionality” which facilitates the in-house coupling of cyclic computations between software packages [Tai09]. The solver has an integrated library of common routines, and supports the construction for conditionally specific thermal properties. The temperature and heat transfer characteristics can be defined through user input as a function of boundary constraints.

### 2.2.2 Modes of Heat Transfer

Heat transfer analysis is the study of the amount or type of thermal energy being transported from one system to another due to the temperature differential. The three means by which heat transfer occurs are conduction, convection and radiation. Below is a brief description of the three distinct means of heat transfer.

### Conduction

Conduction is the transportation of highly excited particles within a material to the neighbouring less energetic ones through means of inter-molecular interactions [Cen05]. It is the propagation of phonons (through vibrations) in a solid body which allow for energy exchange between particles. Figure 2.1 graphically describes the transfer of heat energy through a material from a higher ( $T_1$ ) to a lower ( $T_2$ ) temperature.

Equation 2.16 presents the energy rate produced from conduction through a material exposed to a temperature differential, where  $k$  corresponds to the conductivity of a material.

$$\dot{Q}_{Conduction} = kA \frac{T_1 - T_2}{\Delta x} \text{ (W)} \quad (2.16)$$

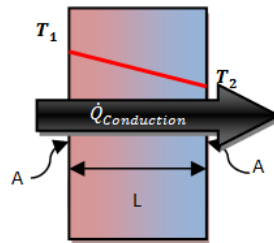


Figure 2.1: Conduction Theory, (adapted from [Cen05])

### Convection

There are two forms of convection: either “Natural” or “Forced”, and both are experienced within the vehicle under-body environments. Within normal driving conditions forced and natural convection are present, however the influences of natural convection are assumed to be negligible compared to the impact of forced convection. Forced convection can be considered as a fluid being forced to flow over a body by means independent of the body itself. A common example can be the air flow induced by vehicle movement, which in turn exposes under-body components to a major form of cooling.

Natural convection occurs due to the buoyancy effects of air flow movement generated through density variations of a fluid surrounding a body. These variations are a direct result of the temperature differential between the body and the surrounding environment [Cen05]. When a vehicle is motionless (and the cooling fan is off) the primary convection mechanism is natural convection.

$$\dot{Q}_{Convection} = hA_s(T_s - T_\infty) \text{ (W)} \quad (2.17)$$

Equation 2.17 (derived from Newton's Law of Cooling) demonstrates that convection has strong dependence on temperature difference, where  $A_s$  is the exposed area,  $T_s$  the surface temperature and  $T_\infty$  the temperature of the fluid. Therefore component temperatures need to be accurately calculated within a CFD calculation in order to improve the estimation of the heat transfer rate based on vehicle speed.

### *Conjugate Heat Transfer*

Conjugate Heat Transfer (CHT) is the combined mechanism of conduction and fluid flow, and occurs when thermal energy is transferred to or from a solid surface to an adjacent fluid or gas [Cen05]. The interactions between conducting surfaces and surrounding fluid, influences the heat transfer within the specific component. With respect to exhaust system heat transfer, there is a cooling effect from the external convection experienced along the outside surface of a component and in addition, there are also the heating influences of the hot combusted gasses to the internal surface of a pipe. Hence CHT is experienced through the direct transportation of heat from the exhaust gas, through the component material, to the air flowing over the component. This air then transports the thermal energy through movement to another location of the vehicle, or away from the vehicle.

### *Radiation*

Radiation is the transfer of electromagnetic energy as a result of electronic configuration changes within the atoms or molecules. Energy transfer through thermal radiation does not require the presence of a medium and is the fastest means of energy transportation of all heat transfer modes [Cen05]. All bodies whether solid, liquid or gas emit absorb or transmit radiation energy. The two main properties of this interaction are the emissivity ( $\epsilon$ ) and absorptivity ( $\alpha$ ) of the surface condition of a body (as shown in Equation. 2.18).  $T_s$  is the surface temperature of the body,  $T_{Surroundings}$  represents the temperature of the environment and  $A_s$  is exposed areas of the body.

$$\dot{Q}_{Radiation} = \epsilon\sigma A_s(T_s^4 - T_{Surroundings}^4) \quad (2.18)$$

Within a vehicle's environment the primary heat sources (combustion chamber and exhaust system) expose surrounding components to a high degree of thermal radiation. Figure 2.2 provides a visual representation of a simplified system. Hot-end components such as the turbo-charger tend to emit higher magnitudes of radiation than absorbed. Therefore hot-end exhaust components are normally covered (or wrapped) by high reflectivity material to shield surrounding sensitive vehicle components and to avoid these parts exceeding their operating temperature ranges.

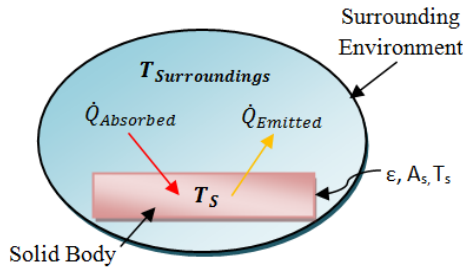


Figure 2.2: Radiation Theory, (adapted from [Cen05])

### 2.2.3 Applied Models for Investigation

Within a shell based thermal model, the geometry is meshed into a network of individual elements. The elements themselves consist of a front and back surfaces, separated by a user defined thickness. The heat transfer calculation is conducted on each side of an element considering the conduction transfer between elements, the incident and reflected radiation, and the exposed convection on the element surface. Additionally when an element requires an energy augmentation an imposed heat flux is also integrated within the energy balance computation [Tai09]. This augmentation feature is useful when modelling exothermal energy increase within the catalytic converter and its chemical kinetics. Figure 2-3 provides a graphical representation of the multilayered numerical element (left) and its corresponding *Radtherm* visualisation (Right).

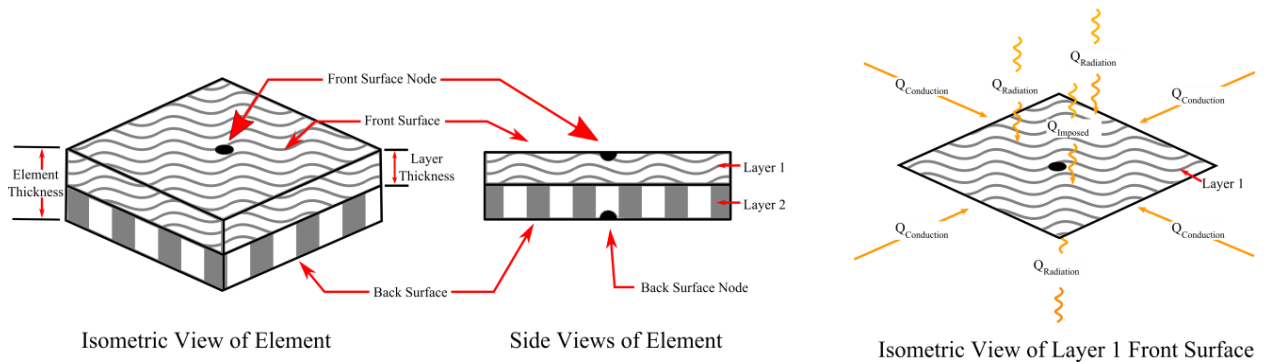


Figure 2.3: Heat Transfer Models of Individual Element

Each element consists of an energy balance in the form of Equation 2.19 and 2.20. The combination of convection, conduction, radiation and imposed heat fluxes are used to derive the time dependent nature of heat transfer for each element. It can be seen that the individual elements specific thermal capacity,  $C_p$ , and mass,  $m$ , have a direct influence on its energy behaviour over time. This is particularly important under transient conditions when accurate thermal tendency are pursued. Hence the modelling and integration of material property and weight are critical for the simulation.

$$\frac{\partial E}{\partial t} = \Sigma \dot{Q} \quad (2.19)$$

$$mC_p \frac{\partial E}{\partial t} = \dot{Q}_{\text{Convection}} + \dot{Q}_{\text{Conduction}} + \dot{Q}_{\text{Radiation}} + \dot{Q}_{\text{Imposed}} \quad (2.20)$$

For example, we can consider a set of elements linked together (Figure 2.4) whereby the individual influences of heat transfer can be mathematically described as convection, conduction and radiation.

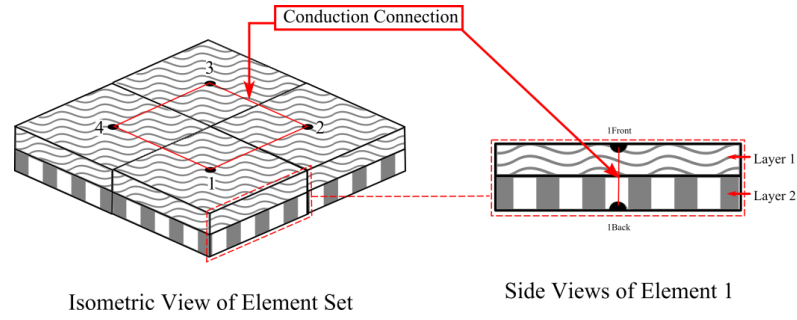


Figure 2.4: Set of elements

If these elements correspond to an under body vehicle component then heat transfer coefficients ( $h$ ), fluid temperatures are extracted through the CFD solver and are mapped onto the surface of these two elements. Equation 2.21 provides the convection equation executed with thermal solver derived from Newtons law of cooling, where  $T_f$  is the fluid temperature extracted from the CFD solver,  $T_1$  is the surface temperature of the element 1 within the thermal solver.

$$\dot{Q}_{\text{Convection}} = h_1 A_1 (T_f - T_1) \quad (2.21)$$

The conduction (Equation 2.22) is based on the user-defined material properties which are density, thermal conductivity and specific heat, where  $T_j$  and  $k_j$ , refer to the second element in direct contact to the first.

$$\dot{Q}_{\text{Conduction}} = \sum_{j=1}^{N_{\text{conduction}}} \frac{k_{1-j} A_{1-j}}{L_{1-j}} (T_1 - T_j) \quad (2.22)$$

In the case where the thickness between elements is not identical the contact surfaces are re-calculated using an imaginary node to act as a junction between the two elements. Figure 2.4 describes the conduction through an elemental thickness from  $1_{\text{front}}$  to  $1_{\text{back}}$ , representing the front and back surfaces of an element.

The radiation equation 2.23 utilises user defined surface properties (emissivity and absorptivity) within its computation of individual heat transmissions. These surface properties are also dependent on the type of component and condition of that component.

$$\dot{Q}_{Radiation} = \frac{\varepsilon_1 A_1}{1 - F_{1-1}(1 - \varepsilon_1)} \left[ \sum_1^N \sigma F_{1-j} (T_1^2 + T_j^2) (T_1 - T_j) (T_{1k} - T_j) + \sum_1^N \left( (1 - \delta_{1-j}) F_{1-j} \frac{1 - \varepsilon_j}{\varepsilon_j} \right) \frac{Q_j}{A_j} \right] \quad (2.23)$$

Prior to an iteration process within thermal solver a view factor calculation takes place, using the voxel-based ray tracer method. This method places a unit hemisphere over the centroid of each element surface, which then is spatially subdivided based on the user-specified accuracy conditions [Tai09]. The volume between elements is also subdivided into voxels. As the ray is cast (from the centroid of an element) voxels are visited in sequence whereby tracking of the ray can be performed. This also applies to rays which are reflected from one element to another [Tai09]. Once the ray tracing is conducted the view factors are calculated and used to compute the radiation variables within the governing equations.

Compiling these governing equations into the below Equation 2.24 yields:

$$h_1 A_1 (T_f - T_1) + \sum_1^{N_{conduction}} \frac{k_{1-j} A_{1-j}}{L_{1-j}} (T_j - T_1) + \dot{Q}_{Imposed} = \frac{\varepsilon_1 A_1}{1 - F_{1-1}(1 - \varepsilon_1)} \left[ \sum_1^N \sigma F_{1-1} (T_1^2 + T_j^2) (T_1 - T_j) (T_1 - T_j) + \sum_1^N \left( (1 - \delta_{1-j}) F_{1-j} \frac{1 - \varepsilon_j}{\varepsilon_j} \right) \frac{Q_j}{A_j} \right] \quad (2.24)$$

Imposed heat flux terms integrated to simulate energy release/gain are auxiliary functions with the governing code.

## 2.3 Techniques of Simulation

As previously described a segregated methodology is pursued therefore the following investigation will utilise two software packages to resolve the fluid-thermal phenomenon under transient conditions. The following section aims at providing a brief overview on the techniques utilised to achieve this objective.

### 2.3.1 Coupling Software

There are two methods commonly explored within the literature to couple a fluid solver to a thermal counterpart; firstly the utilization of commercial software or alternatively the development of in-house scripts. Both methods attempt to exchange the relevant boundary conditions between the software packages. For steady-state vehicle conditions, the commercial software packaged called *MpCCI* developed by Fraunhofer SCAI is used. For transient



conditions, personalised scripts developed by Thermo-Analytics are used to map the alternative steady-state CFD points to a transient thermal solver.

### 2.3.2 Thermal-Fluid Coupled Approach

#### *Steady-State Coupling*

The process of coupling a full vehicle model for steady state conditions requires the continuous exchange of surface boundary conditions between both thermal and fluid solvers. This cycling process proceeds until both solvers achieve a state of numerical convergence. Figure 2.5, shows the coupling process between the fluid solver (Star-CCM+) and the thermal solver (Radtherm). Firstly the component surface temperatures are exported out of the thermal solver as element based tables. Each element corresponding to a coordinate location within the 3-D domain. These tables are then used to map part temperatures directly onto the corresponding geometry within the fluid solver. This sets the boundary condition part temperatures within the fluid solver which then proceeds to calculate the corresponding near wall heat transfer coefficients and air fluid temperatures. Once the numerical CFD convergence has occurred, these parameters are mapped back into the thermal solver on the corresponding parts, hence allowing the thermal solver to proceed with its conjugate heat transfer calculation. Again this is done utilising coordinate based tables. The entire coupling loop requires a series style procedure, freezing one solver until the other solver has completed the calculation and has exchanged the relevant boundary conditions.

The coupling process generally results in 8 to 10 exchange loops for steady-state calculations until convergence is achieved for component temperatures. This can naturally vary depending on vehicle type, load condition and quality of the numerical model. Quality of the numerical model refers to the mesh and the appropriate assignment of boundary conditions which accurately represent the physical phenomena. The method of ensuring simulation convergence is through the monitoring of changes in a series of component surface temperatures in addition to probing  $h$  and  $T_{fluid}$  data at alternative locations within the fluid domain. When the changes are less than the user specified tolerance, simulation convergence is achieved.

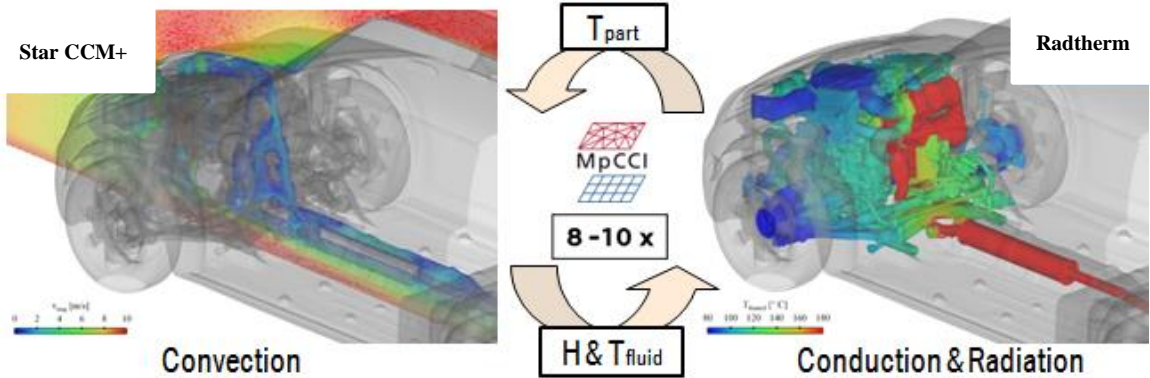


Figure 2.5: Steady State Coupling Arrangement for Full Vehicle

## Quasi-Transient Coupling

Adopting a similar coupling approach as [Wei05, Kau07, Pry11], quasi-transient methodologies are investigated for high dynamic driving profiles Figure 2.6 graphically provides an example of a “loosely” coupled approach. A series of steady state CFD points (denoted as red circles) are calculated and stored prior to the thermal simulation. These points are coupled in the traditional way previously described. The thermal solver is then assigned to run a transient driving profile (denoted in black). The CFD derived  $h$  and  $T_{\text{fluid}}$  data are mapped onto corresponding surfaces of the thermal solver at specific time locations along the driving profile. The thermal solver then conducts a linear time interpolation between these CFD points (denoted the blue line) based on the user defined time-step. I04 refers to the time interpolation between 4 CFD points within the given driving profile. The velocity value difference between the linear interpolated data and that of the real driving profile is denoted as devI04. This visually explores the deviation of the quasi-transient approach and is represented as the blue areas at the bottom of Figure 2.6. This is particularly useful when analysing simulation accuracy and identifying or locating the potential misrepresentations of convection within the methodology.

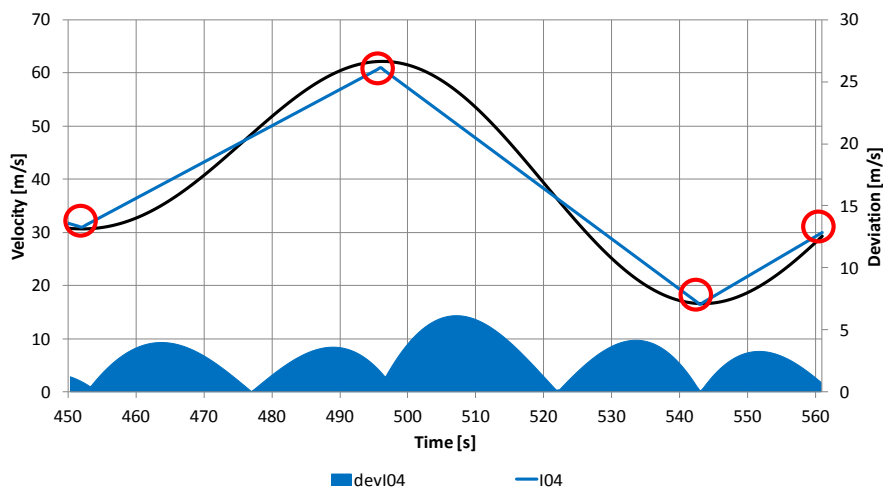


Figure 2.6: Quasi-Transient Coupling Arrangement Example

One of the main features of this method is that the coupled simulations are assigned to specific times throughout the transient thermal simulation rather than coupled continuously at each time-step, allowing for further improvement in turnaround time. Therefore the thermal solver functions as a standalone process, without the waiting periods of a traditional coupled transient segregated approach. Additionally the potential to recycled CFD solutions within the thermal simulation can also be exploited.

The methodology of altering the boundary conditions is further discussed within chapter 3, whereby several approaches are investigated. The selection of CFD solution quantities and types for a particular driving profile are derived from a sensitivity study described in chapter 4 and later discussed in chapter 5 & 6.

# Chapter 3

## Simplifying Vehicle Boundary Conditions

### 3.1 Motivation and Background

As previously discussed in chapter 1, transient VTM simulations have been predominately focused on semi dynamic conditions such as the thermal soak or hill climb. Whereas highly dynamic conditions such as the race-track or customer driving profiles have not been address within the literature. This is due to a variety of reasons some of which are explored within the following chapter. Additionally highly dynamic driving scenarios introduce a certain degree of simulation uncertainty to researchers. These uncertainties can be described as the following:

1. The proper modelling of the vehicle for time dependent simulations

The integration of the full vehicle geometry requires a certain degree of simplification even for steady-state simulations. When addressing transient behaviour the thermal masses within the vehicle must be accurately modelled in order to resolve the time dependent thermal behaviours of the corresponding components of interest. Two approaches are available to implement proper representation of component mass.

- *Solid component modelling*: This is the process of creating real representations of components with solid elements to represent the respective component thickness. For full vehicle configurations this methodology results in the time consuming process of meshing each individual system with real thickness and joining components through contact interfaces. Additionally there is an exponential increase in cell quantities (and calculation time) due to the inherent dependency of each component (regardless of thickness) requiring a minimum of three cells through its cross-section to numerically resolve the thermal distribution. This is a critical aspect as connecting parts must be interface through the contact area, in order for conduction to occur. In exhaust systems this is normally the cross-sectional area. This approach is unfeasible for a full vehicle configuration based on the amount of components (over 500), the increase in cell quantities, the difficulty to interface between parts and maintain mesh conformity, the increase in calculation time to resolve the thermal behaviour requiring even more computational power and the application to transient dynamic driving, which would multiple the effect of all of the above disadvantages.
- *Shell component modelling*: This process allows the external 3-D body of a component to be modelled and its thickness be artificially introduced into the calculation via the governing thermodynamic equations, as shown in chapter 2. Additionally without geometrical representation the thicknesses can be altered in both size and material (such as a multilayer configuration). This can be advantageous on the modelling side, due to ease of construction and substantially reduced cell quantities. It is also useful in the development phase as multiple heat protection designs can be quickly evaluated (by altering the thicknesses or materials) without the need to remodel or reconstruct the vehicle numerically. However, careful attention must be paid to representing the

thickness correctly as not all components have a uniform thickness which can drastically alter the mass of the component and its time dependent thermal behaviour. Hence one important task is to extract the weight of the component from CAD and apply a corresponding 1-D thickness that represents that weight or alternatively associate a 0-D lumped capacitance to the component itself. The following investigation will utilise the shell modelling approach due to the advantages with preparation cost, calculation speed, and potential to address the complex transient conditions of dynamic driving.

## 2. The resources required to solve the time dependent physics within the vehicle

- The resources required to attempt such a dynamic simulation is entirely dependent on the methodology pursued. Two alternative approaches are available in literature, “all in one” or a “segregated” approach. These have been previously discussed within chapter 1. Neither approach has been previously applied to highly volatile conditions such as dynamic driving profiles. Hence the resources to resolve these conditions are not entirely known. However, certain extrapolations can be made from known published material on both approaches. For the “all in one” approach, Disch, published a methodology for a 740 second dynamic hill climb, resulting in 38 days of calculation time on 120 processes [Dis13]. Alternatively, Pryor, published a “segregated” approach for a thermal soak of 20 minutes on a truck. The methodology utilised 6 CFD solutions in a quasi-transient scheme with an estimated turn-over time of 2 weeks [Pry11]. When comparing approaches the “all in one” resulted in approximately 19.5 simulated seconds per 24 hours of calculation, with the “segregated” approach resulting in approximately 86 simulated seconds within 24 hours. This is equivalent to 4.5x speed increase when utilising a “segregated” approach in combination with a quasi-transient scheme. Therefore, due to the time interpolation potential of the “segregated” approach, and the potential reduction in calculation times, the following investigation will utilise the segregated methodology.

## 3. The cost to accuracy ratio of potential approaches and their corresponding benefits

- As mentioned previously, the costs (manpower/time/computing hardware) are known for all potential approaches except for the dynamic driving application. Additionally all approaches can achieve a degree of acceptable accuracy for industrial standards [Dis13, Pry11]. Therefore penalty in accuracy should not be a driving justification for not furthering the development of simulation methodologies. Rather the approaches should search for the optimum combination between resources and accuracy to extend CAE functionality and its advancement over traditional experimental methods. This is the primary driver for the following investigation.

## 4. The nature of the vehicle boundary conditions

- Out of all uncertainties, the dynamic nature of the vehicle boundary conditions make it considerably difficult for researchers to attempt a VTM like simulation. This is due to the simulation paradigm that the original boundary conditions need to be simulated and must not be altered. Therefore to do so, the time-step sizes for high frequency changes need to be extremely small in order to avoid numerical instability. Simplification can be

made either on the modelling side, the implementation of physics or the assumptions of certain subsystem parameters, but never has it been made to the fundamental vehicle boundary conditions. If however, the boundary conditions were simplified (without compromising the accuracy of component temperature behaviour) the potential to increase the time-step sizes and accelerate the calculation time would justify a feasible attempt at the simulation. Hence the core academic contribution within the following chapter aims to address the simplification methods of the fundamental vehicle boundary conditions. In order to do so the original vehicle boundary conditions will be explored in combination with a review of potential mathematical simplification techniques.

## **3.2 Transient Vehicle Boundary Conditions**

The following section introduces the standard alternative driving profiles commonly validated on road and within climatic wind tunnels for productive vehicle development processes. Each profile consists of unique characteristics derived from the customer driving behaviour. The importance to validate these profiles is to ensure that the thermal limits of the vehicle's components are not exceeded during operation of the vehicle. The current investigation of these profiles through experimental methods allows engineers to improve product design and heat protection mechanisms. If it is possible to simulate with CFD tools, the consequent effect on the development process would be of substantial value, not only in the cost savings associated with experimental validation but also with the time advantages within development schedules.

### **3.2.1 Race-Track Profile**

The race-track profile is the most extreme driving condition a vehicle could potentially experience during its operational life time. For this investigation the most volatile track derived conditions were selected in order to evaluate the methodology. One famous track with large velocity amplitudes and high corresponding frequencies is the Nuerburgring race track.

The Nuerburgring is classified as the most difficult and dangerous race track on earth [REF]. Its profile consists of consists of 20.8 km long track with approximately 300m of elevation change. The track is located near the town of Nuerburg, Germany. The track has been used for many events ranging from the grand prix to the 24 hour endurance race for touring car competitions. Figure 3.1 provides a generalised velocity profile derived from experimental data for 3 laps around the track (left) and a frequency spectrum of using Fourier transform of the profile characteristics.

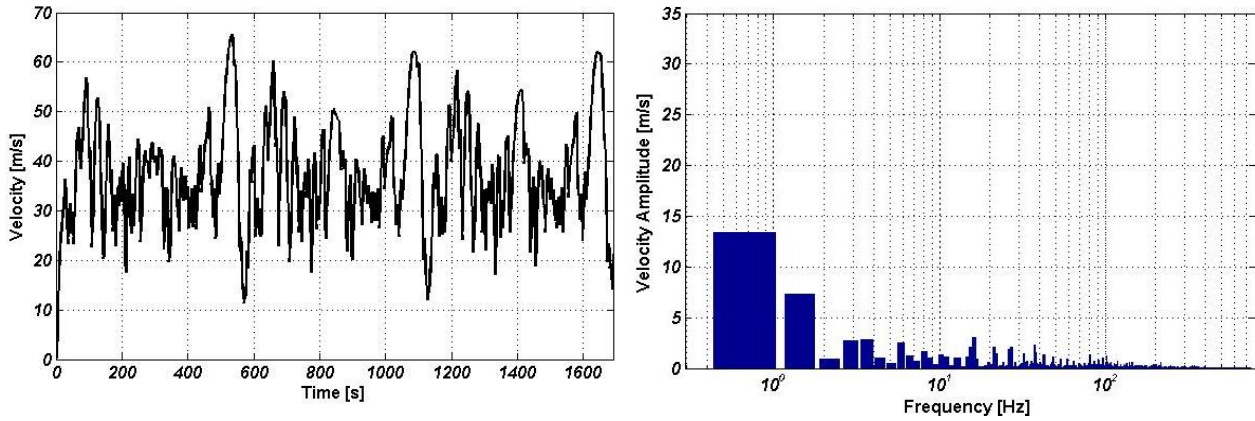


Figure 3.1: Velocity of Race-Track Profile (left) with Frequency Spectrum (right)

### 3.2.2 Handling Profile

The handling profile represents a classic mid-range speed race course, whereby the vehicle is exposed to a range of complex manoeuvres in order to evaluate the vehicle's handling and feel. The handling profile has a vehicle speed ranging from 150km/h to 30 km/h combined with the hard braking, cornering and acceleration causing demanding thermal conditions. Additionally, due to the heavy fluctuation load on the engine and the lower levels of vehicle induced convection (compared to the Nuerburgring) sensitive components are exposed to higher than normal temperature ranges. Figure 3.2 shows a velocity profile of the handling course with corresponding Fourier derived frequency spectrum.

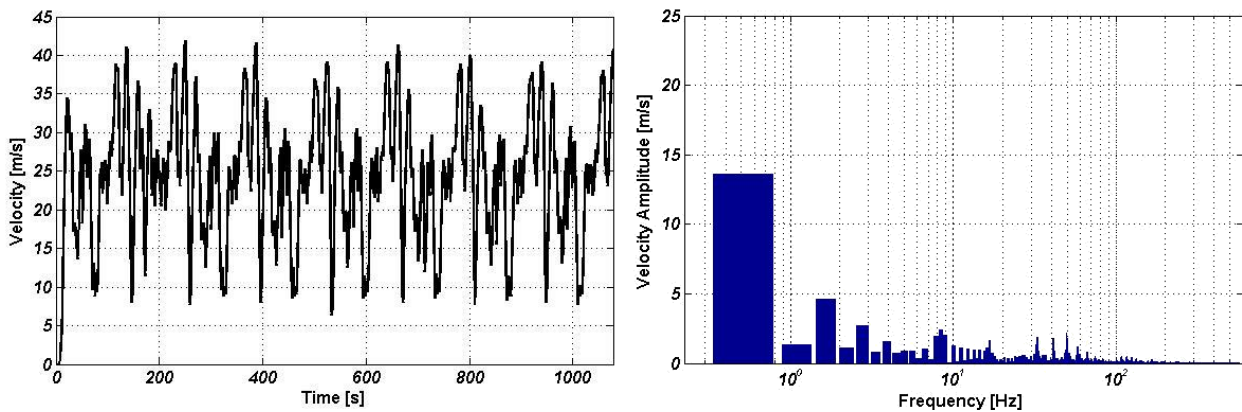


Figure 3.2: Velocity of Handling Profile (left) with Frequency Spectrum (right)

### 3.2.3 Highway Profile

A common driving profile within Europe and especially within Germany is the highway driving (Autobahn) scenario. The profile represents the driving behaviour of a high speed enthusiast who enters the highway and gradually increases his speed. Then after a short period of time he/she attempts to rapidly increase the vehicle speed to its maximum limits before he/she is

slowed down drastically due to traffic. This repeats several times until the driver follows a less aggressive acceleration profile. This phase of the profile is a thermally critical one, as the engine is pushed to its limits on successive rounds whilst the convection is limited due to the sharp deceleration phases. After this phase the highway profile resembles a more traditional high speed drive, it includes overtaking manoeuvres, cruising and emergency braking. Figure 3.3 describes the highway profile for an 850 second drive time with its corresponding Fourier derived frequency spectrum.

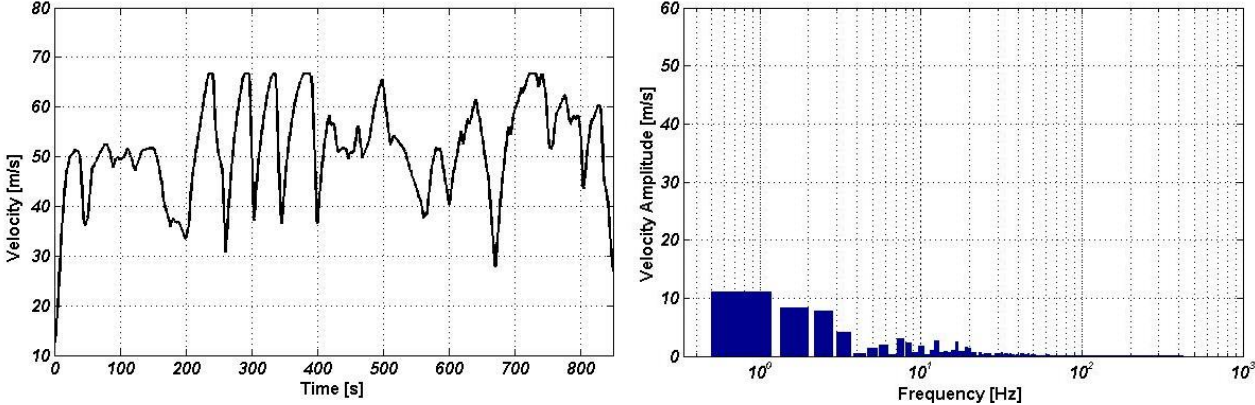


Figure 3.3: Velocity of Highway Profile (left) with Frequency Spectrum (right)

### 3.2.4 Street Profile

The street profile is an example of a vehicle along a country road. The street profile represents a sharp increase in vehicle velocity till the speed limit is reached (130km/h) and then maintains a relatively constant speed for a given period of time, slowly decelerating when approaching a residential area. The deceleration is gradual and somewhat less aggressive as the previous profiles. Ultimately the vehicle enters a residential area with a speed of 80 km/h. This popular profile exhibits less velocity volatility and is thermally interesting for less sensitive components which respond to long term influences. Figure 3.4 exhibits the velocity for the street profile for an 858 second period with corresponding Fourier derived frequency spectrum.

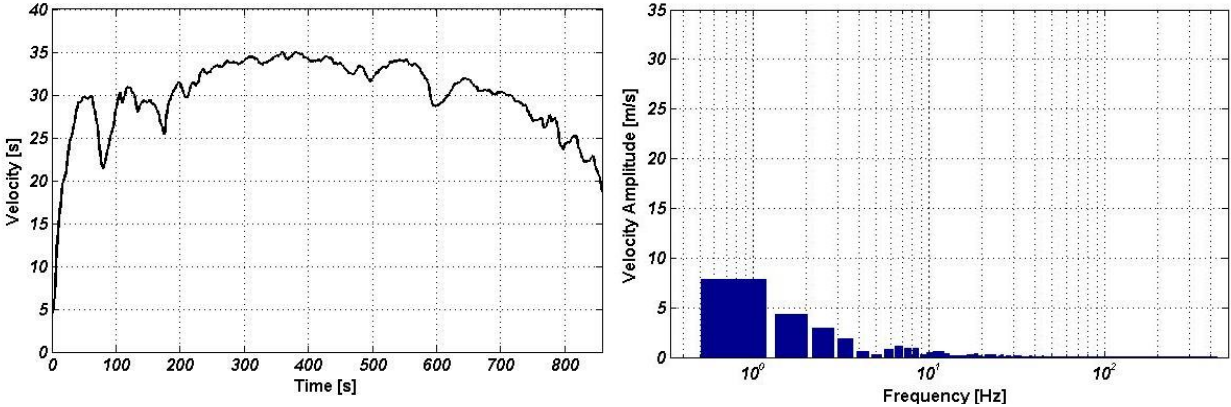


Figure 3.4: Velocity of Street Profile (left) with Frequency Spectrum (right)

### 3.2.5 Summary of Profiles

From the race-track profile to the street profile, it can be seen that the high velocity-frequency component is gradually decreasing. Hence even though the proposed methodology attempts to resolve the most dynamic and volatile conditions, the secondary objective of the investigation is to ascertain the applicability of the methodology to alternative profiles and where the limits of the philosophy are.

## 3.3 Signal Simplification

The observation of experimental data indicates that the high frequency changes in vehicle velocity do not necessarily cause high frequency temperature changes of under-body components [Hae13b]. Component temperature tendencies correspond to their specific masses and the fundamental nature of the driving profile, with the variations of temperature following longer term time scales than short transient boundary condition changes. This rationale challenges the old simulation paradigm whether it is necessary to simulate the high frequency components in boundary conditions, or whether simulation of a simplified version of the boundary conditions would achieve the same temperature behavioural patterns in components. The following section covers a range of simplification techniques which could be used to remove irrelevant information from boundary conditions. All the following techniques have been evaluated on a sub-module prior to the final development of the methodology. This sub-module will be addressed in chapter 4 with the final simplification theory for vehicle simulations discussed within the following chapter.

### 3.3.1 Standard Averaging Schemes

As previously discussed in chapter 1, averaging schemes have been used in a variety of industrial applications. The goal of a moving average is to dampen high frequency inputs or data fluctuations to describe the average profile or trend of a series consisting of time dependent data. Initial investigations were conducted utilising averaging schemes, as an attempt to quickly evaluate the rationale of the research. However the core of the research contribution is in the utilisation of a sophisticated frequency based simplification technique, therefore only a brief description on averaging schemes and their outcomes to the research is warranted in the following section.

#### 3.3.1.1 Simple Moving Average

A simple moving average (SMA) is the most commonly utilised statistical scheme for simplifying highly volatile time dependent data [Joh99]. The formulation for a SMA is given in Equation 3.1, where  $v_n$  denotes the vehicle velocity and a given integer  $n$  (number of data points).



$$SMA = \frac{1}{n} \sum_{i=1}^n v_i = \frac{v_n + v_{n-1} + \dots + v_2 + v_1}{n} \quad (3.1)$$

The total value of vehicle speed is then divided by the summation of sampling points  $\sum n$ . The advantages of the SMA is its ease and simplicity of implementation. An initial investigation attempted to utilise randomly selected ranges for an SMA type for profile simplification. Here the race-track profile boundary conditions were selected for a single lap in order to evaluate the potential of the simplification technique. The total profile period was 561 seconds, with time steps of 0.5 seconds. The evaluated SMA sampling ranges were 50%, 30%, 15% and 7.5 % of the data series. From this initial investigation two outcomes were achieved. Firstly the SMA type profiles could not effectively represent the high velocity peaks (which were seen to be a major influence on convection rates) without the inherent reduction of the sampling range [Per13b]. Secondly when reducing the sampling range to accommodate for the high velocity peaks, an introduction of unwanted information (high frequency components) in other regions of the SMA derived profile occurred. Additionally, due to the simple nature of the SMA, the derived profiles tended to lag slightly behind the original data. This lag or time shift is due to the dependency of the averaging scheme sampling past data information. In order to accommodate this offset a forward-backward sampling scheme was implemented. To improve the velocity peak representation a weighted moving average (WMA) scheme was evaluated.

### 3.3.1.2 Weighted Moving Average

The WMA approach is achieved through biasing the sampling rate using a linear-pyramid weighting scheme, as seen in Equation 3.2. This can be performed using the same ranges of the SMA.

$$WMA = \sum_{i=1}^n \frac{nv_i}{i_n} = \frac{nv_n + (n-1)v_{n-1} + \dots + 2v_2 + v_1}{i_1 + i_2 \dots i_n} \quad (3.2)$$

The improvements from the SMA were evident in areas of high velocity peaks and rapid velocity changes. Here the same sampling ranges (to the SMA) were selected (50%, 30%, 15% & 7.5%) of a 561 seconds of the race-track profile. It was found that the WMA of 15% series range was the best at emulating the component behaviours compared to the other averaging schemes. The WMA proved so successful in test models, that a full vehicle model was used to further evaluate its potential. The results of the full vehicle investigation formed the first publication on race-track simulation for VTM [Hae13b]. A good agreement was achieved between simulation and experimental data further supporting the claims for boundary condition simplification.

One of the biggest disadvantages of the SMA and WMA is its inability to support profile independence. Even though the WMA was very successful for the race-track profile, its

percentage range for alternative profiles produce poor results. The simplification either over simplified critical regions or was too volatile in irrelevant thermal frequency ranges.

The above investigation concluded that the boundary conditions could be simplified with appropriate accuracy [Hae13b] however the transferability of that simplification method must be dependent on the frequency ranges of the profile. Hence the next logical step was to explore signal processing techniques in order to extract the frequency spectrums of input signals and remove the information which did not contribute component temperature changes.

### 3.3.2 Signal Processing

Signal processing is a common practice within many industries dealing with stationary to non-stationary data series types [Iee13]. As presented in section 3.2 a frequency spectrum was conducted on the boundary conditions of all investigated driving profiles, hence the relevant and irrelevant frequency ranges for the race-track profile based on the simulation results of the former investigation were known. However the impact of frequency ranges for alternative profiles was not yet validated. Therefore the search for a universal methodology directed the research towards more sophisticated signal processing techniques.

#### 3.3.2.1 Fourier Transform

The well-known Fourier Transform (after Joseph Fourier) is a mathematical transformation to convert information within the time domain to the frequency domain. The continuous FT is defined in Equation 3.3, where  $\omega$  represents the angular rate equal to  $2\pi f$ , where  $f$  is the frequency. The FT is commonly represented as the square of its modulus, creating what is known as a power spectrum [Bar92].

$$\hat{f}(\omega) = \int_{-\infty}^{\infty} f(t)e^{-i\omega t} dt \quad (3.3)$$

The continuous FT is very well suited for the application of signals that repeat themselves, however for non-repeating signals (such as those within vehicle boundary conditions) a Short Time Fourier Transform (STFT) can be advantageous as it utilises a pre-defined time window to analyse the signal. The STFT is defined in equation 3.4, where  $g$  is the windowing function derived from Gaussian and  $\tau$  is the centred time.

$$\hat{f}(\omega, \tau) = \int_{-\infty}^{\infty} f(t)g(t - \tau)e^{-i\omega t} dt \quad (3.4)$$

The windowing function of the STFT is very good at capturing high frequencies; however it struggles with localised changes in time due to the constant window width [Rio91]. Additionally information out of the window of observation window is not represented within the derived STFT. This is called spectral leakage. A solution to this problem can be to narrow the window of inspection, however this compromises the low frequency components of the signal requiring normally a larger time window to be also incorporated [Bar92]. In order to

realise the high and low frequency ranges as well as the localised transients, representation in both frequency and time was necessary. A promising method of producing dilation in both time and frequency is the wavelet transform.

### 3.3.2.2 Wavelet Transform

The Wavelet Transform (WT) has the ability to decompose a signal into a set of scales, and project this information onto a set of base functions. These base functions are classified as the mother wavelet, whilst each of the scales are dilated in both time and frequency domains. The set of scales constituted the wavelet coefficients and the summation of these coefficients reassembles scales into its original signal. The Continuous Wavelet Transfer (CWT) is defined in Equation 3.5, where  $\Psi$  represents the mother wavelet, and  $a$  and  $b$  are the dilation and translation factors.

$$CWT_{\Psi}f(a, b) = W_f(b, a) = \frac{1}{\sqrt{a}} \int_{-\infty}^{\infty} \Psi\left(\frac{t-b}{a}\right) x(t) dt \quad (3.5)$$

Similar to the FT, the CWT is limited to stationary repeating signals; therefore a discrete wavelet transform (DWT) is presented in Equation 3.6, where  $\Psi_{m,n}$  is the mother wavelet translated and dilated by factors  $m$  and  $n$ .

$$DWT_{\Psi}f(m, n) = \int_{-\infty}^{\infty} f(t) \Psi_{m,n}(t) dt \quad (3.6)$$

$$\Psi_{m,n}(t) = 2^{-m} \Psi(2^m t - n) \quad (3.7)$$

Due to the mother wavelet orthonormal nature and the ability of the wavelet to dilate in both time and frequency domain, no signal information is lost in DWT [Vid91]. However the high frequency information correlated to the noise within a signal can be removed forming a simplified version of the signal. The multi-resolution analysis through wavelet decomposition can be particularly useful when searching for a universal methodology to simplify multiple vehicle driving profiles. Figure 3.5 provides an example comparison between a STFT, (which is dilated only in the time domain) and a DWT (which dilated in both time and frequency domains). It is clear that DWT is far superior in incorporating localised changes in the signal and more appropriate in dealing with the non-repeating nature of the investigated driving profiles.



Figure 3.5: Comparison between STFT (left) and DWT (right) (adapted from [Bar92])

### 3.3.2.3 Wavelet Decomposition

The wavelet decomposition is a multi-resolution process of projecting frequency information onto a set of base functions, called scales. There are two sets of information which are projected, the low frequency range (or low pass) information and the high frequency range (or high pass) information. This produces two groups of scales consisting of the different layers of information dependent on the decomposition level. Figure 3.6 provides an example of a decomposition process up to a level  $n$ . This can also be considered as a low pass, high pass filtering system for frequency information. Here the original signal ( $S_0$ ) is split into two scales of information,  $A_1$  (approximated coefficients) and  $D_1$  (detail coefficients), corresponding to the decomposition of level 1. The coefficients are used to scale and dilate the base wave functions with a net zero area.  $A_1$  consists of the projected frequency range between 0 and  $f_{max}/2$ , whereas  $D_1$  consists of the projected frequency range between  $f_{max}/2$  and  $f_{max}$ . These are denoted in blue and red respectively. The maximum frequency is identified from a Fourier type analysis of the original input signal. As the level of decomposition increases the project frequency range (or inspection window) of both high pass and low pass scales are shortened in combination with using the approximate coefficients from the previous level. Therefore this process progressively simplifies the signal via the removal of high pass information ( $D_n$ ) at each individual level, as seen in Figure 3.6. In this investigation the complete detail coefficients are removed from the approximated signal. However this can also be tailored to include a percentage of information per detail coefficient at each decomposition level. This is a typical signal processing technique and is available in many commercial software packages such as *Matlab* via a tool box [Mat14].

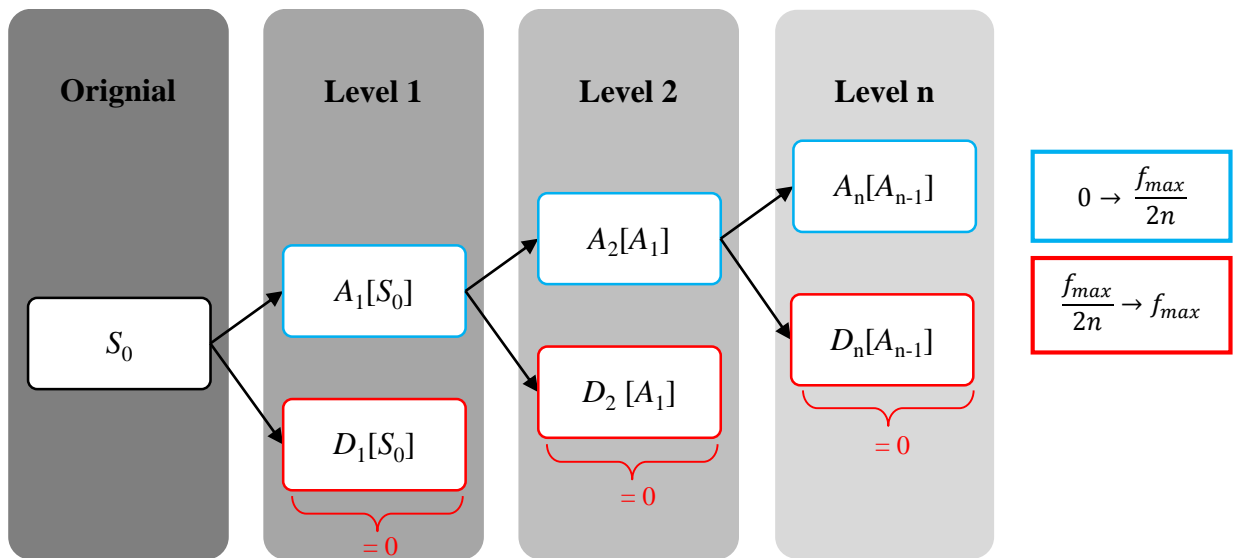


Figure 3.6: Signal Decomposition Theory using Wavelet Transform

Mathematically the operation can be described in equation 3.8, where the original signal at  $n=0$  can be reassembled back by adding the summation of the series  $D$  to the current approximated signal at  $n$ .

$$S_0 = A_n + \sum_{i=0}^n D \quad (3.8)$$

### Mother Wavelet

There are many available mother wavelet functions which could be utilised within the investigation. Some of the most commonly used wavelets functions are Haar, Gaussian, Daubechies and Dmeyer. Each function contains a unique location and scale which gives the wavelet its shape and form. All wavelet functions have the ability to be dilated and scaled, corresponding to the frequency projected onto the wavelet at its window of inspection. Since the mother wavelet function has a zero area it can be decomposed into scales as previously described and summated to form the original signal. Since the methodology is not dependent on the mother wavelet type rather on the removal of unwanted high frequency components, all smooth type wavelet function could be utilised. For this investigation the Dmeyer wavelet function is utilised as it is an orthogonal wavelet with infinite levels of decomposition defined in the frequency domain.

### Example

In order to demonstrate the decomposition process an example is presented in Figure 3.7, where  $S$  is the original signal (here a race-track velocity profile),  $a_6$  corresponds to the approximated signal (or simplified signal) at the 6<sup>th</sup> level of decomposition and  $d_{1,2,3,4,5,6}$  represent the individual detail coefficients removed from the original signal to form  $a_6$ . It can also be seen that the detail coefficient correspond to a zero net area due to the base function (or mother wavelet) form. As shown previously in equation 3.8, this allows the signal to be reassembled back into its original form via the summation of all detail coefficients.

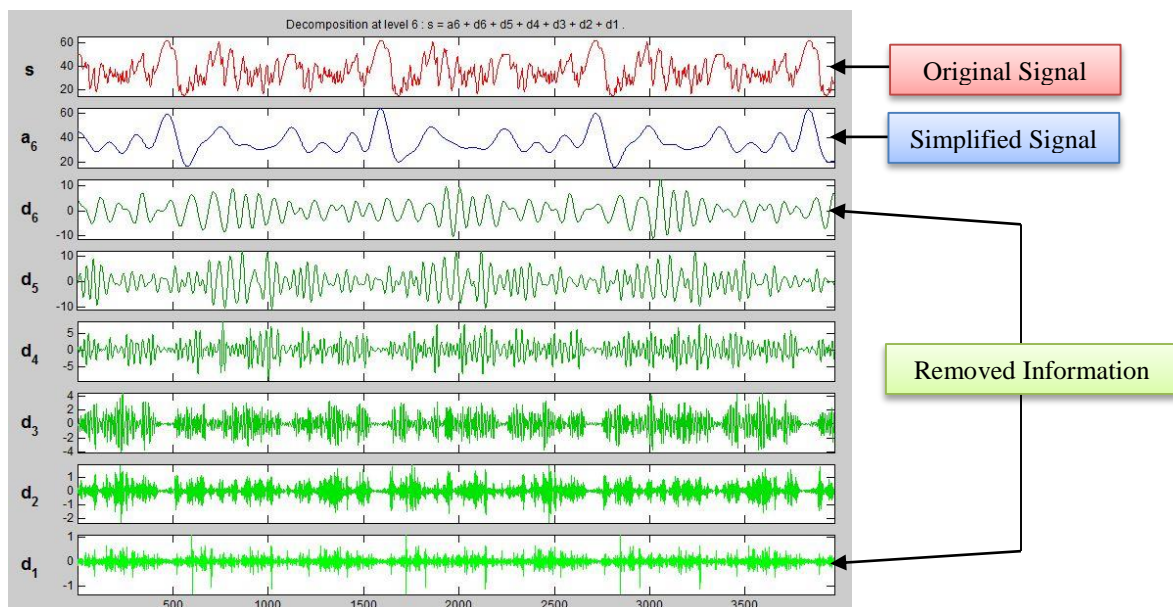


Figure 3.7: Signal Decomposition Example using Wavelet Transform

Even though the wavelet transform provides a solution to the problem of transferability and signal simplification through the process of information removal, it still leaves certain

decomposition criteria to be defined. The decomposition criteria is then dependent on the current application, therefore certain questions need to be answered in order to determine what thresholds should be implemented. Firstly, what degree of decomposition (how many levels of scales) is necessary to adequately represent the time dependent convection boundary conditions? Can all profiles be decomposed and simplified to the same levels? It is clear that not all profiles consist of the same frequency distribution, some with higher maximum frequencies than others. An additional factor is the influence of thermal mass (high sensitivity to low sensitivity) and the response relationship to input frequencies. Hence an investigation into the characterisation of a vehicle was necessary to determine the decomposition thresholds within the wavelet transformation approach.

### **3.4 Thermal Response Characterisation**

The thermal response characterisation was a study into the influences of convection frequencies (derived from velocity) to component temperature change. Establishing a critical frequency point which irrelevant information could be removed from original input boundary conditions was essential in the employment of the wavelet transform signal simplification methodology.

If we consider the vehicle as a system, the inputs as the vehicle speed, exhaust mass flow rate, temperature, and the outputs as component surface temperature, we notice that the specific heat capacity coupled with a components weight can drastically alter the temperature fluctuation of a component. Additionally it can be observed that the components proximity and corresponding connection to its surroundings affects its thermal behaviour. Naturally components closer to the exhaust system are exposed to higher level of radiation, whereas components away from the heat source rarely react to its presence. The location of a component also plays an important role on its surface temperature due to its exposure to convection. Some components may be tucked away from direct exposure to under-body airflow, resulting in high concentration of temperatures (or hot spots), others seem to expose larger contact areas to airflow (such as under-body panels) whose response is tightly coupled to the velocity profile. The location and proximity of the component is only one side in understanding the thermal problem. The material properties of components and their specific heat capacities influence their time dependent temperature behaviour. Some components are highly conductive (such as heat shields) while others seem to resist heat conduction (absorption material). The connectivity of a component to its surrounding also influences the amount of thermal energy which can be stored in the component as well as transported to other components through contact.

#### *Vehicle Component Groups*

A vehicle can be considered to consist of over 500 components each with differentiating masses, positional identities and unique connectivity to surrounding parts. Therefore particular groups need to be defined to simplify the system. Grouping components not only reduces the complexity of the problem but allows researchers to quickly identify the potential problem regions within the vehicle. As convection is the heat transfer mechanism which is to be simplified within this investigation the components were grouped based on their geometric position within the vehicle and corresponding masses. Three groups within the following

investigation were categorised, high sensitivity, medium sensitivity and low sensitivity. High sensitive components referred to those with small masses positioned within the vehicles underbody, where the convection heat rates would theoretically be the strongest. Medium sensitivity components were those in the engine bay, where masses were bigger in combination with the lower convection rates. Low sensitivity components corresponded to those with larger masses (such as internal heat shields) where contact area to convection was the lowest.

Highly sensitive components tend to respond very quickly to boundary condition changes, whereas less sensitive components require longer period of exposure to thermally react. The fundamental research philosophy revolves around the fact that the thermal mass, as well as its contact to its surroundings (either through conduction or convection) alter the degree of temperature variation. However, in order to evaluate what frequency range is necessary to stimulate temperature change within a component, system, or group, a characterisation study of the vehicle must be conducted with simple analogies to represent the heat transfer phenomena being experienced by components within the above described groups.

### 3.4.1 Flat Plate Analogy

The following section aims at identifying the frequency threshold for the wavelet decomposition process by introducing a flat plate analogy. The conditions of the vehicle are simplified to an energy frequency being applied to the flat plate over time. The area ( $A$ ) and contact to surroundings ( $k$ ) can be seen in Figure 3.8.

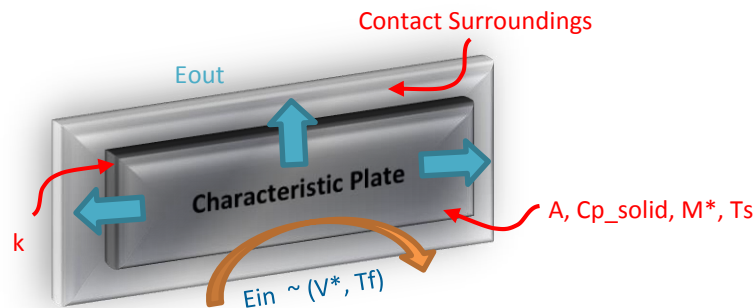


Figure 3.8: Characteristic Flat Plate.

The material properties ( $C_{p\_solid}$ ) and exposed fluid temperatures ( $T_s$ ) can be altered to resemble a vehicle component or group. This can be advantageous to simulate close proximity components to heat sources. The energy exposed to the plate ( $E_{in}$ ) is oscillating based on a specific frequency,  $f$  (Equation 3.9). Additionally the characteristic energy flux ( $E^*$ ) described in Equation 3.10, represents the vehicle induced driving conditions. These can be classified through the multiplication of the local fluid temperatures, characteristic velocity ( $v^*$ ), exposed area to convection ( $A^*$ ), density of the air ( $\rho_{Air}$ ) and thermal capacity based on the air temperature ( $C_p$ ).

$$E_{In} = \frac{2 \cdot E^*}{f} \quad (3.9)$$

$$E^* = T_{f\_Air} \cdot v^* \cdot A^* \cdot \rho_{Air}(T_{Air}) \cdot C_p(T_{Air}) \quad (3.10)$$

The effective area (Equation 3.11) introduces a dimensionless parameter called the coupling strength ( $\alpha$ ) which represents the percentage of area exposed to the convection. To accommodate the near wall velocity conditions due to flow passing over the plate a correction factor of 1% is used to represent the development of the boundary layer [Cen05]. This results in a characteristic velocity ( $v^*$ ). For a transient profile, the maximum velocity within the entire profile ( $v_{max}$ ) is used to represent the worst case vehicle speed as seen in Equation 3.12.

$$A^* = \alpha \cdot A \quad (3.11)$$

$$v^* = 0.01 \cdot v_{Max} \quad (3.12)$$

To determine the surface temperatures on the flat plate Equation 3.13 is utilised, whereby an effective mass ( $M^*$ ) is applied in combination to the thermal capacity of the plate material ( $C_{p\_Solid}$ ).

$$\Delta T_s = \frac{E_{IN}}{C_{p\_Solid} \cdot M^*} \quad (3.13)$$

The effective mass is derived to represent the conduction properties of components to surrounding geometries. The energy received and transported through the plate can then represent the conduction characteristics of surrounding geometry connected to the part of interest. This can also be considered as the percentage of energy that the part holds, with the remaining percent being transported to surrounding geometry. When a part is connected to highly conductive surrounding, much of its thermal energy is lost to the surrounding. On the contrary, if a part is connected to low conductive or no surroundings, much of its thermal energy is contain within the part. This can be expressed as the following:

$$M^* = \frac{E_{In}}{E_{In} - E_{Out}} \cdot M \quad (3.14)$$

The allowable temperature change was derived from current experimental error ranges. This was equivalent to 3K variation [Nat14]. To demonstrate this analogy and how a threshold frequency can be derived from analytical methods, some examples are provided in the following section. Each example corresponds to an alternative approach dependent on the engineer's objectives for the simulation. This is further discussed in section 3.4.2.

### 3.4.1.1 Example 1 - Supporting Arm – High Sensitivity Group

Within the following example a single component is selected as the basis to derive the threshold frequency for the full dynamic driving vehicle simulation. It is assumed that this component consists of the smallest mass within the vehicle, hence the engineer could achieve a very accurate estimation on the whole vehicle thermal state. The component of choice is the supporting arm within the front left hand side of the vehicle. This can be seen within Figure



3.8, where a flat plate representation of the component can be derived. The area of the can be extracted from CAD, whereby the material properties can then be used to determine the weight of the component. Within this example it is assumed that 80% of the area is making contact to the fluid, hence a coupling strength ( $\alpha$ ) of 0.8 is defined. The fluid temperature is 400 K, resulting in an air specific heat of approximately 1010 J/kg.K and a density of 0.88 kg/m<sup>3</sup>. The maximum velocity in the profile can be defined as 30 m/s with the remaining parameters denoted in Figure 3.8.

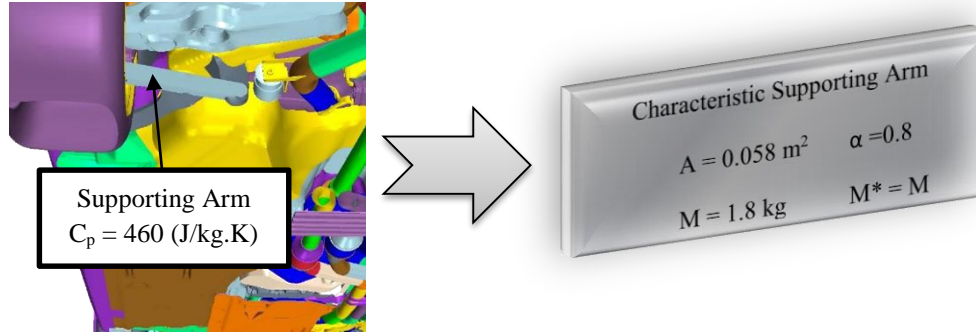


Figure 3.8: Example 1 – Supporting Arm.

In order to solve for  $f$  the maximum allowable temperature change ( $\Delta T_s$ ) needs to be defined. Here a 3K tolerance is implemented. Note that altering the temperature change will alter the frequency threshold derived. Once the temperature tolerance is defined the previously discussed equations can be re-organised into the following form:

$$f = f_{critical} = \frac{2 \cdot E_{In}}{C_{p\_Solid} \cdot M^* \cdot \Delta T_s} = \frac{2 \cdot [T_{f\_Air} \cdot v^* \cdot A^* \cdot \rho_{Air} \cdot C_{p\_Air}]}{C_{p\_Solid} \cdot M^* \cdot \Delta T_s} \quad (3.15)$$

Where,

$$A^* = \alpha \cdot A = 0.8 \cdot 0.058 = 0.046 \text{ m}^2 \quad (3.16)$$

$$v^* = 0.01 \cdot v_{Max} = 0.01 \cdot 30 = 0.3 \text{ m/s} \quad (3.17)$$

Therefore,

$$E^* = T_{f\_Air} \cdot v^* \cdot A^* \cdot \rho_{Air} \cdot C_{p\_Air} = 400 \cdot 0.3 \cdot 0.046 \cdot 0.88 \cdot 1010 = 4.9 \text{ kW} \quad (3.18)$$

Assuming that the connectivity of the component does not result in energy losses, the effective mass becomes equivalent to the mass of the component, as shown below in Equation 3.19

$$M^* = \frac{E_{In}}{E_{In} - E_{Out}} \cdot M = \left[ \frac{4948.8}{4948.8 - 0} \right] \cdot 1.8 = 1.8 \text{ kg} \quad (3.19)$$

Hence the critical threshold frequency can be derived as,

$$f_{critical} = \frac{2 \cdot E^*}{C_{p\_Solid} \cdot M^* \cdot \Delta T_s} = \frac{98000}{460 \cdot 1.8 \cdot 3} \approx 4.0 \text{ Hz} \quad (3.20)$$

### 3.4.1.2 Example 2 – Under-Body – Medium Sensitivity Group

In the second example, a group of parts are selected within the medium sensitivity group, in order to display a multi-component approach. For this example an under-body panel, heat shield and tunnel panel are used to derive the base frequency threshold as seen in Figure 3.9. This method attempts to group the components together and average their parameters in order to convert them into generalised features for the flat plate analogy. It should be noted that this type of approach would normally consider all components within the under-body. Similarly to example 1, the maximum velocity in the profile is 30 m/s with a fluid temperature of 400 K. The tunnel panel has a weight of 5kg, with an area of 0.29 m<sup>2</sup>. The heat shield consists of a multi-layer arrangement with air insulation and has a consequent weight of 1kg, with an area of 0.16 m<sup>2</sup>. Finally the under-body panel has the largest area of 0.85 m<sup>2</sup> with a weight of 7kg.

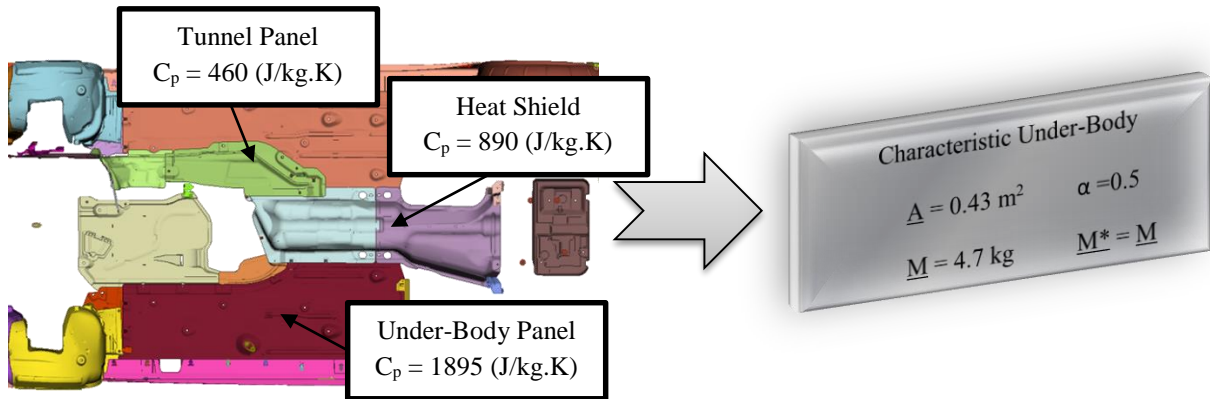


Figure 3.9: Example 2 – Under-Body.

Again the maximum allowable temperature change has been defined as 3K. Unlike example 1, in order to solve for  $f$  the component parameters need to be averaged. Therefore small alterations need to be made to Equation 3.14 to accommodate the averaged parameters. This can be seen below in Equation 3.19, where  $\bar{A}$  refers to the average area,  $\bar{M}$  corresponds to the average mass and  $C_{p\_Solid}$  represents the averaged specific heat over the three components.

$$f_{critical} = \frac{2 \cdot [T_{f\_Air} \cdot v^* \cdot \bar{A} \cdot \rho_{Air} \cdot C_{p\_Air}]}{C_{p\_Solid} \cdot \bar{M}^* \cdot \Delta T_s} \quad (3.21)$$

Where,

$$\underline{A} = \frac{0.29+0.16+0.85}{3} = 0.43 \text{ m}^2, \quad \underline{M} = \frac{5+1+7}{3} = 4.7 \text{ kg}, \quad C_{p\_Solid} = \frac{460+890+1895}{3} = 1088 \frac{\text{J}}{\text{kg} \cdot \text{K}} \quad (3.20)$$

Assuming again that all components experience a coupling strength of 50%,  $A^*$  and  $v^*$  are the following,

$$\underline{A}^* = \alpha \cdot \underline{A} = 0.5 \cdot 0.43 = 0.215 \text{ m}^2 \quad (3.21)$$

$$v^* = 0.01 \cdot v_{Max} = 0.01 \cdot 30 = 0.3 \text{ m/s} \quad (3.22)$$

Therefore

$$E^* = T_{f\_Air} \cdot v^* \cdot \underline{A}^* \cdot \rho_{Air} \cdot C_{p\_Air} = 400 \cdot 0.3 \cdot 0.215 \cdot 0.88 \cdot 1010 = 23 \text{ kW} \quad (3.23)$$

Hence the critical threshold frequency can be derived as,

$$f_{critical} = \frac{2 \cdot E^*}{C_{p\_Solid} \cdot \underline{M}^* \cdot \Delta T_s} = \frac{46000}{1088 \cdot 4.7 \cdot 3} \approx 3 \text{ Hz} \quad (3.24)$$

### 3.4.1.3 Example 3 – Gearbox Housing – Low Sensitivity Group

In the final example a Gearbox housing component is select as the only component of interest within the vehicle simulation. This is called a problem driven approach. Here the engineer identifies prior to the simulation that only a single component is of interest. Therefore he can tailor the threshold frequency to his given problem and potential remove further information from the signal. In Figure 3.10, a representation of the gearbox housing is presented, whereby the identical flow conditions of example 1 & 2 are utilised. However in this case, it is assumed that 25% of the energy is lost via conduction paths within the gearbox housing (essentially doubling is characteristic mass). Additionally due to the location of the component only 20% of the component (bottom part) is coupled to the convection, therefore resulting in a coupling strength of 0.2.

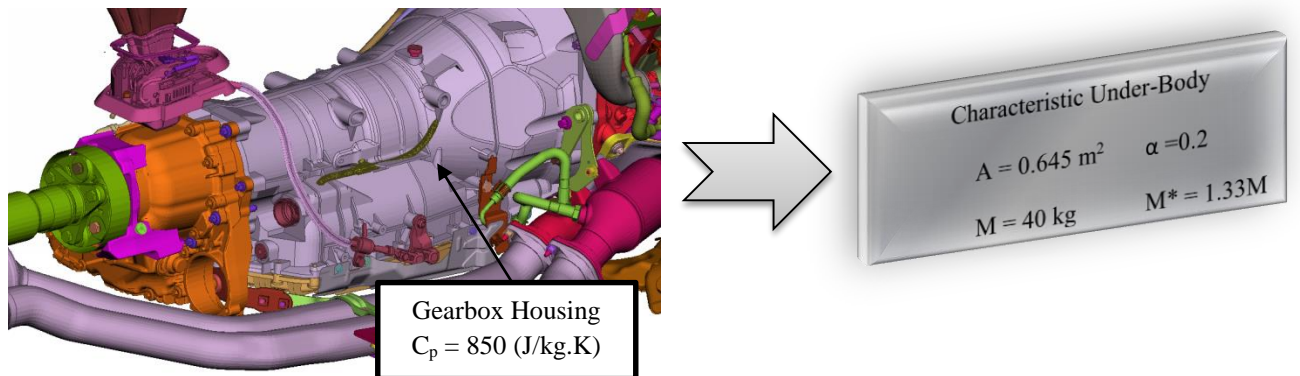


Figure 3.10: Example 3 – Gearbox Housing.

Similar to example 1, the following equation is utilised.

$$f_{critical} = \frac{2 \cdot E_{In}}{C_{p\_Solid} \cdot M^* \cdot \Delta T_s} = \frac{2 \cdot [T_{f\_Air} \cdot v^* \cdot A^* \cdot \rho_{Air} \cdot C_{p\_Air}]}{C_{p\_Solid} \cdot M^* \cdot \Delta T_s} \quad (3.25)$$

Where,

$$A^* = \alpha \cdot A = 0.2 \cdot 0.645 = 0.129 \text{ m}^2 \quad (3.26)$$

$$v^* = 0.01 \cdot v_{Max} = 0.01 \cdot 30 = 0.3 \text{ m/s} \quad (3.27)$$

Therefore,

$$E^* = T_{f\_Air} \cdot v^* \cdot A^* \cdot \rho_{Air} \cdot C_{p\_Air} = 400 \cdot 0.3 \cdot 0.129 \cdot 0.88 \cdot 1010 \approx 14 \text{ kW} \quad (3.28)$$

Considering the 25% energy loss to internal conduction paths, Equation 3.27 can be used, where  $E_{Out} = 0.25E_{In}$

$$M^* = \frac{E_{In}}{E_{In} - E_{Out}} \cdot M = \left[ \frac{13758.6}{13758.6 - 3439.7} \right] \cdot 40 = 53 \text{ kg} \quad (3.29)$$

Hence the critical threshold frequency can be derived as,

$$f_{critical} = \frac{2 \cdot E^*}{C_{p\_Solid} \cdot M^* \cdot \Delta T_s} = \frac{28000}{850 \cdot 53 \cdot 3} \approx 0.2 \text{ Hz} \quad (3.30)$$

### 3.4.2 Thermal Criteria for Determination of Critical Frequency

The critical frequency can be analytically derived based on the previously discussed analogy; however the definition of the plate itself and corresponding parameters remains dependent on the engineer's interpretations of the problem. This can be problematic and confusing in a number of ways as the frequency range which is removed from the signal can be highly sensitive to parameters inserted into the analytical analogy. Hence a standard must be formulated in the selection of these parameters based on the motivations for the simulation. There are three approaches in solving this problem, which are the following:

- Detailed approach → the engineer selects the smallest characteristic thermal mass with the highest coupling strength to determine the corresponding critical frequency based on the mean vehicle velocity of the driving profile. This is the most computationally expensive approach as a large majority of irrelevant frequency ranges for surrounding components are maintained within the signal. This approach can be seen within example

1, where the engineer selects the supporting arm as a basis to calculate the critical frequency. In that case up to 4 Hz of information is retained within the original signal.

- **Balanced approach** → the engineer identifies the three major categories (high to low sensitivity) within the vehicle and averages the corresponding parameters between these categories. This approach is the most efficient and broadly applicable for the entire vehicle. It additionally provides good representation of all major sub-systems within the vehicle. In example 2, a similar approach was seen where components in the under-body were average to attain the critical frequency. Therefore resulting in a lower critical frequency of 3Hz compared to example 1.
- **Problem driven approach** → the engineer identifies the regions of simulation interest (in advance) and calculates the average characteristic parameters specifically for those regions. In return he neglects the remaining components within the vehicle. This approach is one of the most useful for industry as many of the critical thermal regions are known to the engineer before the simulation is conducted, either through experience or experimental data on a predecessor vehicle configuration. Example 3 provides an indication of such an approach, where the gearbox housing was the focus of the simulation. Due to its mass and location, a critical frequency of 0.1 Hz was achieved. This theoretically indicates that a substantial amount of information can be removed from the signal without affecting its thermal response (with the 3K tolerance range).

Within the following investigation the “balanced approach” has been selected to validate the proposed methodology for a wide range vehicle components.

### 3.4.3 Thermal Critical Frequency & Decomposition level

The critical frequency is the threshold point whereby a component does not thermally react to the exposed frequency conditions based on a pre-defined temperature delta. The allowable temperature change is normally derived from standard experimental error. Hence any frequency above this decomposition threshold can be removed from the original boundary condition frequency scales (defined by the wavelet transform) forming a new simplified profile. The critical frequency is used to stop the wavelet decomposition by altering the frequency window. This can be seen in Equation 3.31, where  $n$  represents the decomposition level,  $f_{max}$  the maximum frequency inherent in the boundary condition signal and  $f_{critical}$  the critical frequency derived from the previously discussed methods.

$$f_{critical} > \frac{f_{max}}{|2n|} \quad (3.31)$$

The identification of the number of decompositions can then be fed back as boundary conditions within the wavelet transform methodology. The decomposition will then be dependent on the profile (through the maximum frequency) and the derived critical thermal frequency. It is clear that not all frequencies will produce a whole number for decomposition purpose, therefore the produced  $n$  will be rounded up to the next integer.

### 3.4.4 Thermal Response Matrix

From the flat plate analytical investigation a thermal response matrix was formed, covering all potential combinations of variables within the given vehicle categories, whilst providing the critical frequency for the plate to react to a temperature change of 3K. Figure 3.11 provides an example of the response characteristics of the plate with respect to the relative thermal mass (left) and the coupling strength (right). It can be observed that there is an inverse relationship between the critical frequency and increasing mass, this relationship is shifted towards the frequency direction when increasing the fluid temperatures exposed to the flat plate. This can also suggest that the closer coupled a component is to the heat source the stronger the temperature response is. In order to further investigate this, the coupling strength was varied with mass (right of Figure 3.11). The exponential rise in critical frequency based on coupling strength validates the positional significance of components in the under-body. Increasing the mass of the component indicates a dampened response which validates the importance of modelling the components with representative weight.

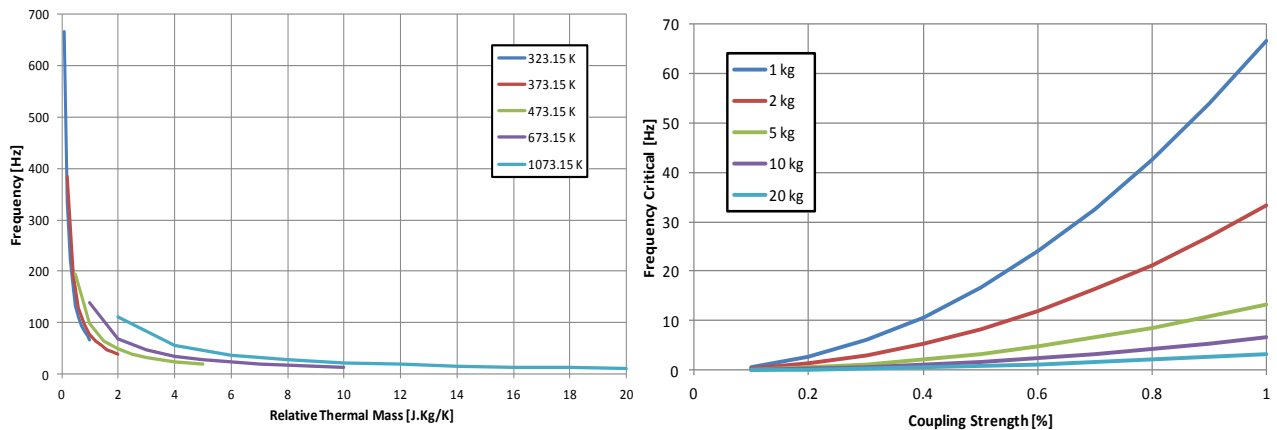


Figure 3.8: Thermal Response Example

By merging the accumulated data together a 3-D thermal response map can be derived. From this map an engineer may provide the parameters of interest to identify the critical frequency which in turn can be used in the wavelet transformation and signal simplification technique. It is also to be noted that within real dynamic driving condition the maximum frequency is usually far beyond the point of physical or thermal realisation. This can be seen within the boundary condition frequency spectrums (Figures 3.1-3.4). The reason for this is due to the inherent measurement noise within instruments. Therefore even though these high frequencies are used to denote the maximum frequency and therefore the decomposition level, they have no impact on thermal response of components.

## *Summary*

Within chapter 3, boundary condition simplification was explored through a variety of methods. The boundary conditions themselves were examined and the simplification technique for this investigation was discussed. It was found that the wavelet transformation due its flexibility in time and frequency scaling was the optimal simplification methodology for the following investigation. However the determination of decomposition levels needed to be addressed. In order to establish the decomposition level necessary for the boundary conditions an analytical flat plate approach was introduced. Here based on the vehicle conditions, component mass and location a threshold frequency could be derived. This critical frequency then could be used to stop the wavelet decomposition at a given level. In the next chapter, the development of the overall dynamic driving methodology is described. Three dependent stages are explored, where stage 1 aims at addressing the primary heat source within the vehicle; the exhaust system. Stage 2 aims at evaluating the signal processing techniques described within this chapter on a sub-module. And finally stage 3 provides the full vehicle investigation using the exhaust modelling techniques addressed in stage 1 and the optimal simulating conditions derived from the sensitivity study of stage 2.

# Chapter 4

## Development of Methodology

The development of the methodology for full vehicle dynamic driving simulation requires 3 stages of investigation. Stage 1 corresponds to the representation of the primary heat source within the vehicle. Here 1-D correlations are used to introduce the corresponding time-dependent heat rates within the exhaust system. In chapter 4, the theory behind these heat rates are explored for steady state conditions, where they are later extrapolated for the transient investigation. The results of stage 1 for steady state conditions can be found in appendix 2, with corresponding transient results presented in chapter 5 and later discussed in chapter 6. Stage 2 explores the simplification techniques previously discussed in chapter 3 on test case which consists of simplified geometry of a vehicle. In addition to altering the boundary conditions, a sensitivity study is outlined in investigating the influences of the quasi-transient approach in combination with steady state CFD solution types and consequent effect on thermal resolution. Stage 3 represents the final methodology for full vehicle configurations under dynamic boundary conditions. This phase of the investigation embodies and utilises the research findings of the previous stages and assembles the optimal modelling parameters for the transient thermal simulation. Chapter 4 aims at outlining the theory, investigation objectives and the research approach of the individual stages, where chapter 5 presents the results of the individual stages and chapter 6 discusses the relationship between the stages.

### 4.1 Stage 1 - Modelling Exhaust Conditions

The exhaust system is the major heat source within the vehicle's under-body environment. Its influence on the thermal time dependent response of under-body components is critical to incorporate within simulation techniques in order to resolve the conjugate heat transfer phenomena. The technology of modelling exhaust systems under steady state conditions was developed in prior years to this research investigation, where the results and analysis can be found in a series of publications [Hae10, Hae13a, Hae14a, Dev14]. However the success of the following investigation is dependent on the theory and techniques previously developed for steady state conditions. Here, these fundamental concepts are to be extrapolated for transient conditions. Therefore it is warranted to provide an overview of the technology previously developed addressing its potential to be applied for the current investigation.

#### 4.1.1 Exhaust System Configurations

The exhaust components are divided into two categories, namely the "hot end" and "cold end." The former comprises all components within the engine bay; in the latter the remaining components downstream from catalytic converter exit. The main purpose of this separation is to group components with similar thermal characteristics (external convection and internal gas dynamic phenomena). The hot end components tend to experience a third of the external convection exposed to downstream parts (Cold-End). Additionally the engine bay consists of a higher thermal concentration due to high temperature component proximity.



A schematic of an example BMW in-line 6 cylinder turbo-charged upstream catalytic converter exhaust configuration (here referred to as Model 1) is given in Figure 4.1. Common to many BMW exhaust configurations, Model 1 features two muffler systems; a Middle Acoustic Silencer (MAS) and the traditional End Acoustic Silencer (EAS). The MAS and EAS are used to dampen and alter the resonance sound generated from internal combusted gas flow. Both contain complex internal structures including air and fibreglass insulation configurations. The upstream positioning of the catalyst is advantageous for reduced cold start emissions of hydrocarbons (HC) and carbon monoxide (CO), due to reduced ‘light off’ time.

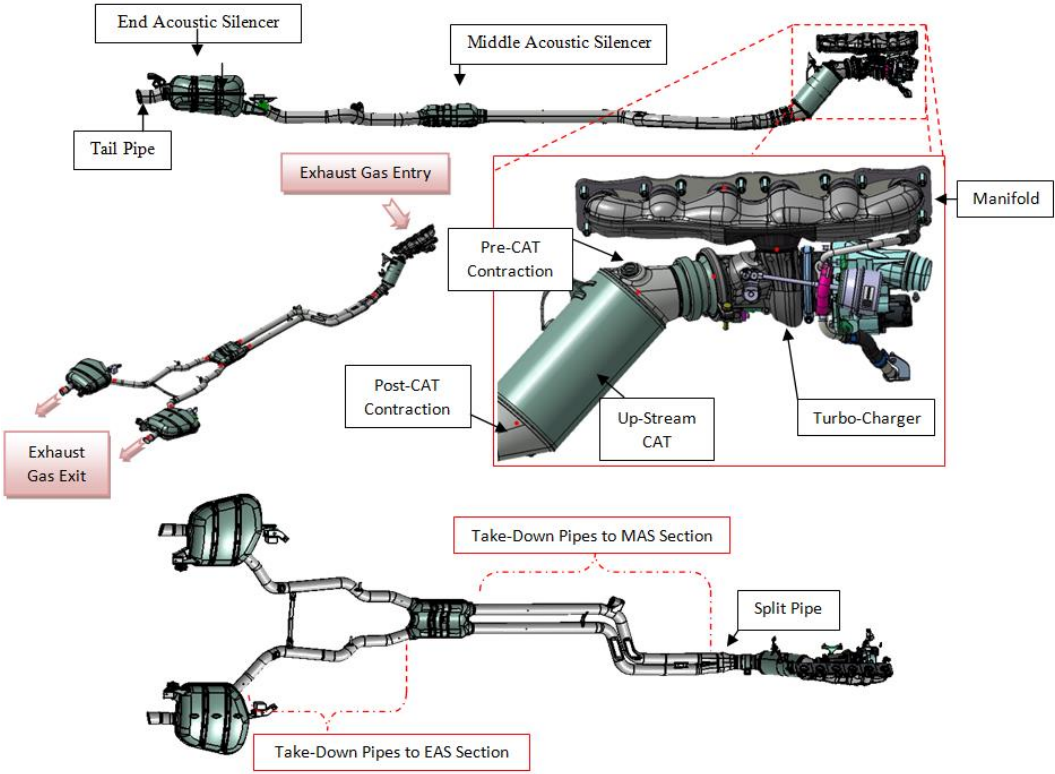


Figure 4.1: Example CAD representation of BMW (Model 1) Exhaust Configuration.

Model 1 also contains what is known as a ‘split pipe’ which separates the flow into two segments. Alternative internal flow conditions are evident for individual take down sections. Model 1 is to be used as example in the following chapter to describe an assortment of modelling techniques for different components in the exhaust system.

4.1.1.1 Former Methods

The former practices (prior to 2009) within BMW to computationally establish under-body heat transfer involve surface fixing of exhaust component temperatures which have been either derived from experience or empirically [Hae10, Hae13a]. This method allows for the conjugate heat transfer calculation to be performed. However this process inherently contains several disadvantages which fail to encompass the proper thermal distribution along exhaust components (especially in time dependent scenarios). Temperature fixing compromises the overall thermal behaviour of the vehicle’s under-body and consequently introduces a large source of error for transient cases.

The following disadvantages of temperature fixing exhaust components are as follows:

1. The dependency of know surface temperature data, either derived from experimental testing or professional experience. For transient cases this is further exaggerated.
2. Inaccurate representation of the temperature distribution along the surface of a component (Figure 4.2).
3. Inaccurate calculation of conjugate heat transfer.

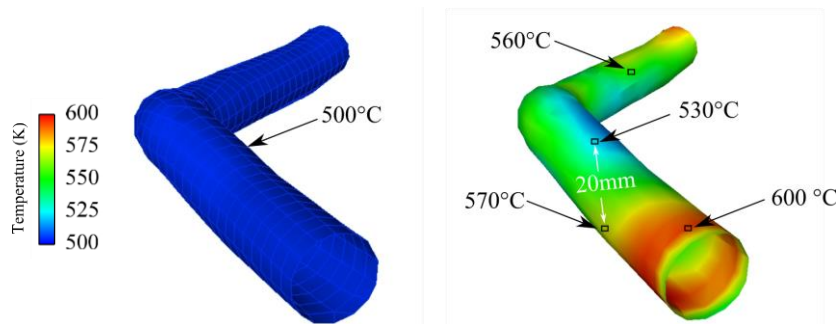


Figure 4.2: Comparison between a temperature fixed surface (left) and a temperature differential along the surface of an exhaust take down pipe.

Many exhaust components experience time dependent temperature variations which influence the entire under-body heat transfer process (Figure 4.2). Temperature fixing a surface incorrectly assumes that the component experiences a constant surface temperature over time and also that the surrounding under-body parts (including the exposed convective air flow) is exposed to an inaccurate conjugate heat transfer source. It is evident within Figure 4.2 that the temperature difference along the surface of a component can vary significantly with position. This variation additionally influences the magnitude of emitted radiation (as radiation has a power dependence on temperature). The temperature fixing of a surface assumes that the radiation is uniformly exposed with a constant magnitude to surrounding components, and introduces an additional source of error.

Additionally temperature fixing the exhaust system for transient cases can be not only physically incorrect but pose as significant modelling problem. The temperature would have to be selected based on experimental data and carefully implemented at selected times during the unsteady simulation to capture the behaviour of the exhaust.

#### 4.1.1.2 Proposed 1-D Methodology

As the exhaust system is one of the highest temperature components in the vehicle under body environment, it is important to represent the internal heat transfer within the exhaust to ensure that an accurate surface temperature distribution is formulated. The proposed method introduces a 1-D fluid stream within the exhaust system (Figure 4.3), where the combination of estimated internal heat transfer coefficients and alternative modelling techniques allow for the integration of 3-D gas dynamic influences. The initial boundary conditions (gas temperature and mass flow rate) for fluid flow are extracted from experimental data.

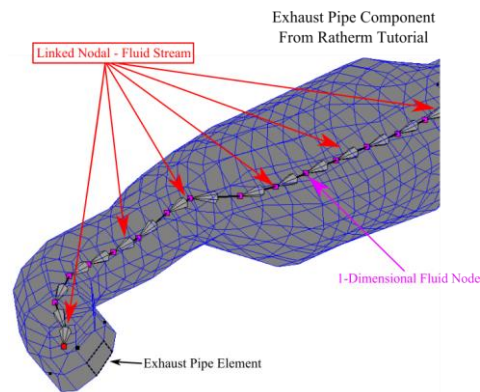


Figure 4.3: Internal fluid stream within exhaust component example (Adapted from ThermoAnalytics, 2009).

This method provides a step forward towards the independence of experimental data, being used within a computational environment (through surface fixing). The advantages include:

- Allows for the development of higher accuracy computational models.
- Provides a means of predicting exhaust component surface temperatures on the underbody of a virtual vehicle, for time dependent exhaust gas mass flow rate and temperature.
- Dependencies remain on the outer convection whilst inner exhaust heat transfer rates are partially resolved.
- Improves overall simulation quality and thermal resolution within the exhaust system.

#### 4.1.2 Exhaust Gas Dynamics

A survey of the open literature identified four primary exhaust system heat transfer phenomenon as the main influences on thermal behaviour: entrance effects, engine induced pulsation, surface condition and geometry.

##### 4.1.2.1 Convective Augmentation Factor

Due to the complexities of multi-variable influences on exhaust heat transfer, many literature developed Nusselt number correlations are constructed from experimentally specific testing conditions [Kan99]. These models become limited in their application to alternative exhaust configurations or variable engine characteristics. In industry it is common practise to use a convective augmentation factor (CAF) to compensate an inaccurate heat transfer simulation for flow phenomena not incorporated within a theoretical Nu model [Hae13a]. This method avoids the dependency on empirically assigning surface temperatures, whereby the means of Nusselt number generation is based upon fundamental correlations published within literature. The following investigation searches to understand the augmentation influence of each phenomenon based on its individual CAF value with standard theoretical Nusselt relations for straight pipes.

The CAF can be difference between what is experienced in reality to the theoretical estimation ( $Nu_{Ideal}$ ) utilised within the computational domain. Hence the  $Nu_{Real}$  can be described below in Equation 4.1.

$$Nu_{Real} = Nu_{Ideal} \cdot CAF \quad (4.1)$$

Utilising Sieder-Tate model as an initial base Nu number correlation [Cen05] the formulation becomes:

$$Nu_{Real} = 0.027Re^{0.8}Pr^{1/3} \cdot CAF \quad (4.2)$$

It can be seen that the  $Nu_{Real}$  (Equation 4.2) is simply the mathematical enhancement of the  $Nu_{ideal}$  to match the experienced experimental heat transfer within a component. The constitution of the CAF for each exhaust component is assumed to be the combination of the four phenomena discussed in the next section.

#### 4.1.2.2 Entrance Effect

When a combusted gas enters an exhaust component it experiences what is called an entrance effect. The boundary layer development of a fluid is dependent on the no-slip condition. This condition influences the growth of the boundary layer and hence the heat transfer at the surrounding walls of an exhaust pipe.

It is logical that the boundary layer thickness grows with increasing distance along a tube; until it reaches the centre of the pipe due to the effects of viscosity. The distance to this point is known as the velocity/thermodynamic entrance length and the fluid characteristics within this region are classified as “developing”, as the maximum temperature or respective velocity is yet to be reached. Understanding this boundary layer development can assist engineers in the selection of heat transfer correlations which encompass the phenomena. Figure 4.4 provides a comparison between the development of the velocity boundary layer and the corresponding thermal boundary layer.

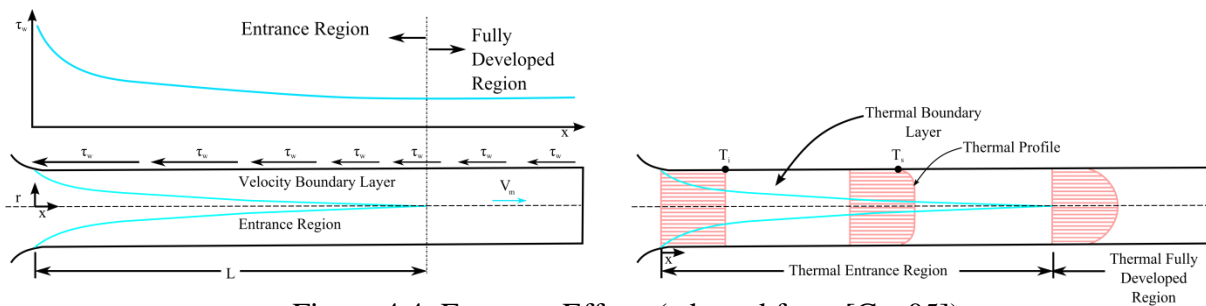


Figure 4.4: Entrance Effect, (adapted from [Cen05]).

Farrugia et.al (2006) investigated the influence of entrance phenomena on the entire heat transfer process within straight pipe extension from an exhaust port of a 1.9 litre, four cylinder 1992 Saturn spark-ignition test bench engine [Far06]. Using cycled average heat flux measurements he was able to adapt the Boelter et.al (1948) entrance formulation [Boe48] to derive the following CAF correlation (Equation 2.3). The CAF model aims to compensate a base heat transfer correlation (Sieder-Tate) **only** for the effects of entrance, hence enabling engineers to distinguish between possible phenomena influence. These effects can be described

purely as a function of distance (x) and pipe diameter (D), indicating that the entrance augmentation is dominated by geometrical constraints and internal flow characteristics. Similar to the Sieder-Tate correlation the effects of differential viscosity characteristics within the combusted gas are assumed to be uniform.

$$CAF_{Entrance} = \left\{ \left( \frac{28}{Re^{0.36}} \right) + \left( \frac{2.1}{\left( \frac{x}{D} \right) * Re^{0.11}} \right) \right\} * \left\{ \frac{1}{\sqrt[3]{Pr}} \left[ \frac{\mu_{skin}}{\mu_{bulk}} \right]^{0.14} \right\} \quad (4.3)$$

The expected trend of this CAF formulation is negative whereby with increasing Reynolds numbers and distances from the point of initial entry, there is a decreasing tendency for numerical augmentation.

Figure 4.5 provides a description of the effects of accumulated parameters on heat transfer and the contributing effects of the entrance phenomena on the total augmentation influence. Farrugia et.al indicates that in a standard case (x/D =100), between 5000 to 15000 Reynolds, the effects of entrance phenomena are negligible as the thermal boundary layers have become fully developed [Far06]. At a Reynolds Number of 15000, the heat transfer characteristics do not require any further augmentation to accurately be represented.

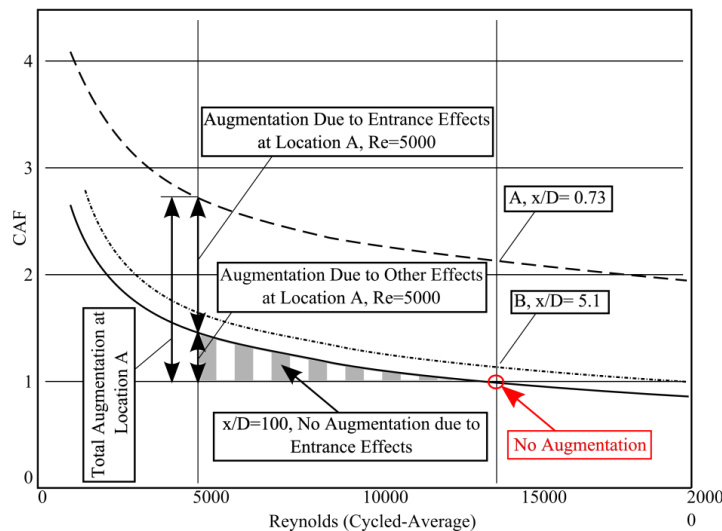


Figure 4.5: Heat Transfer Augmentation Due to Entrance (adapted from [Far06])

When distance 'x' along the pipe is equal to twenty times the diameter, the internal pipe flow is characterised as fully developed [Cen05]. However the above correlations do not encompass the effects of consequent geometrical influence such as sudden contractions, bends and diffusions. It is to be assumed that with a significant geometrical change within a piping network, there is an equal possibility for flow re-development and entrance re-initiation.

#### 4.1.2.3 Engine Induced Pulsation

In a four stroke engine the exhaust gases are produced only once per cycle (every 720° rotation of the crankshaft). In the case of multi-cylinder engines these exhaust gas strokes occur at varying times due to differing positions of individual pistons. The combination of exhaust valve

timing and the geometrical constraints of exhaust ports results in engine induced exhaust pulsation.

The published literature on pulsation enhance heat augmentation indicate conflicting results [Guo06]. Recent studies have shown that the combination of pulsation amplitude, frequency and oscillation have confusing influences, whereby in some instances heat transfer is enhanced and in others it is decreased due to pulsation [Wan05]. A method of understanding the problem of pulsation enhancement is the integration of a dimensionless parameter called the Womersley number ( $Wo$ ) within the analytical computation.

The Womersley number (Equation 4.4) provides a means of distinguishing which components (at which engine speeds and operating loads) may be vulnerable to pulsation heat transfer enhancement based on the current research progress.

$$Wo = R * \left(\frac{\omega}{\nu}\right)^{0.5} \quad (4.4)$$

According to Wang et al (2005), the optimal range of the Womersley number whereby heat transfer enhancement is at a maximum around 40 [Wan05].

In Figure 4.6 it can be seen that higher Womersley numbers (above 50) only have an influence in the entrance region (approx.  $x=60\text{mm}$ ) of the tested data. Additionally it was found that heat transfer had strong dependency on Reynolds number up to 25,000 (whereby effects after this point remain relatively constant). This point may be classified as the critical Reynolds number of Pulsation ( $Re_{pul}$ ). As most internal flow condition of exhaust pipes are above the  $Re_{pul}$  it can be assumed that the influence of Reynolds on pulsation results in a CAF of approximately 1.7.

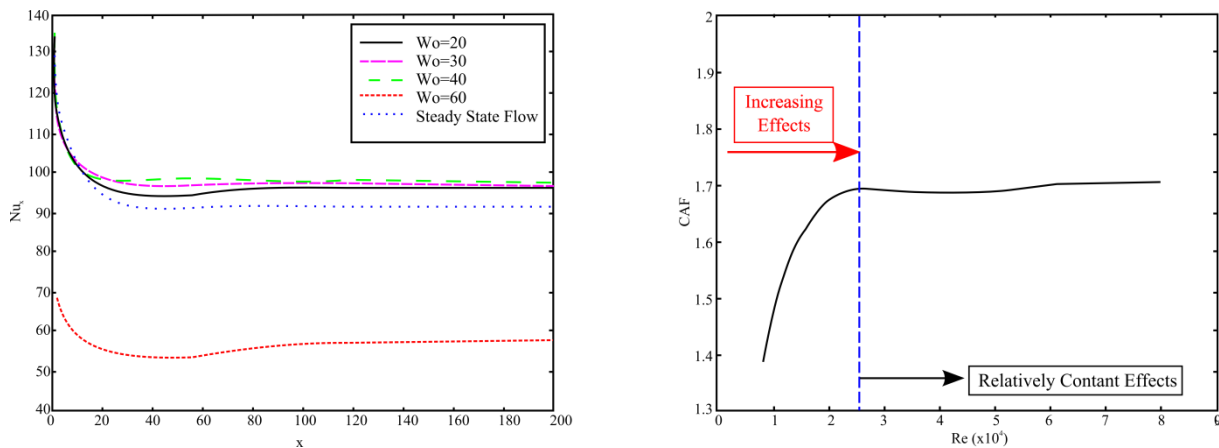


Figure 4.6: Heat Transfer Enhancement Due to Womersley and Reynolds numbers (adapted from [Wan05]).

The velocity amplitude also has a significant influence on the heat transfer enhancement of a system (shown in Figure 4.7). Experimental results by Wang et al (2005) indicate that when the velocity amplitudes exceed a factor of 1.5 the corresponding heat transfer enhancement is dramatically increased in an exponential manner [Wan05]. Wang et al (2005) defines the velocity amplitude as the variance from the mean velocity within an exhaust component.

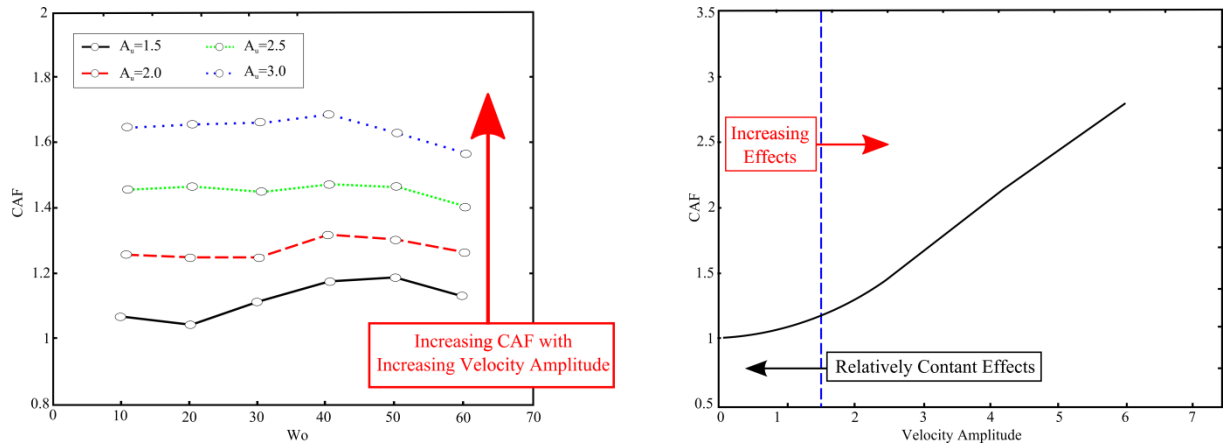


Figure 4.7: Heat Transfer Enhancement due to Velocity Amplitude, (adapted from [Wan05]).

Based upon the diametric constraints of general exhaust pipe configurations it is to be assumed that the velocity amplitude does not exceed a value 1.5 and remains relatively constant throughout the variable component configurations of the simulated exhaust systems.

#### 4.1.2.4 Surface Conditions

The internal surface condition of an exhaust pipe may vary considerably with respect to position, hence making the prediction of surface friction difficult. Friction can significantly enhance the free stream turbulence within a pipe, resulting in higher heat transfer coefficients [Cha99]. Hence a more elaborate heat transfer model which encompasses friction characteristics of pipe surfaces (Figure 4.8) is necessary for improved results.

One approach is to model the system with a specific frictional profile; however results are often not representative of mass production component manufacturing tolerances and changes in the surface condition over the lifetime of the component. Additionally the condensation of water along pipe bends and the accumulation of combusted material along a pipe wall can lower heat transfer coefficients within an exhaust configuration. Such phenomena are difficult to incorporate into a numerical environment as the influences and determination of these conditions is not fully understood.

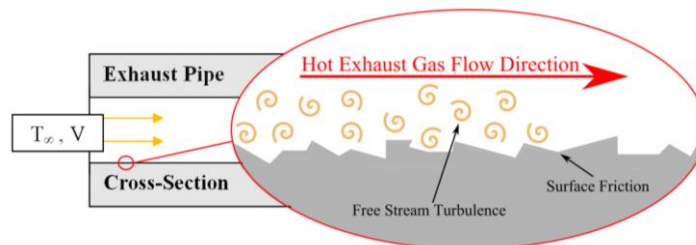


Figure 4.8: Surface Friction Description with an Exhaust Pipe.

Alternatively, one may introduce an enhanced base Nusselt number model which encompasses the broad frictional phenomena throughout the operating positions of an engine. Correlations for rough-walled pipes include the Gnielinski [4-5] (for hydraulically smooth conditions), the Petukhov and Popov [4-6] (for transitionally rough conditions) and the Bhatti and Shah [4-7]

formulation (for fully rough conditions) [Cen06]. Each correlation requires a frictional factor ( $F$ ) to be assigned, where  $\varepsilon$  is the surface roughness and  $D$  is the pipe diameter.

$$Nu = \frac{\left(\frac{F}{8}\right)Re - 1000Pr}{1 + 12.7\left(\frac{F}{8}\right)^{0.5}*(Pr^{2/3} - 1)} \quad F = \frac{1}{\left[1.8 \log_{10} \left\{ \frac{6.9}{Re} + \left(\frac{\varepsilon/D}{3.7}\right)^{1.11} \right\}\right]^2} \quad (4.5)$$

$$Nu = \frac{(F/2)RePr}{1 + 13.6f + \left[ \left( 11.7 + 1.8Pr^{-\frac{1}{3}} \right) * \left( \frac{f}{2} \right)^{0.5} * (Pr^{\frac{2}{3}} - 1) \right]} \quad F = \frac{1}{[3.64 \log(Re) - 3.82]^2} \quad (4.6)$$

$$Nu = \frac{(F/8)RePr}{1 + (F/8)^{0.5} * [(4.5Re^{0.2}Pr^{0.5}) - 8.48]} \quad F = \frac{1}{\left[1.8 \log_{10} \left\{ \frac{6.9}{Re} + \left(\frac{\varepsilon/D}{3.7}\right)^{1.11} \right\}\right]^2} \quad (4.7)$$

The selection of a component specific frictional model is dependent on the known tested data of the components individual surface conditions. For example when an exhaust system is experimentally tested for endurance the simulation methodology incorporates a higher frictional model to compensate for ageing. When the surface condition is completely unknown a default frictional model is employed (hydraulically smooth). Even though these models do not incorporate the effects of particle build-up, they provide a higher accuracy base model (compared to Sieder-Tate), whereby correctional factors can be implemented to encompass the remaining experienced flow phenomena.

#### 4.1.2.5 Geometrical Influences

The influence of geometrical constraints on exhaust pipe heat transfer is a phenomenon which is yet to be fully characterised in literature. This is mainly due to the complication involved in simulating three-dimensional behaviour of fluid flow, pulsations combined with the turbulent nature of internal gas flow and the composition of the exhaust gas. Additionally many exhaust systems are not purely of a circular tube type and may contain complicated configurations including internal structures EAS.

As the thermal simulation environment is *Radtherm*, in combination with the shell modelling approach discussed in chapter 3, it is not feasible to include internal exhaust configurations. However a multilayer surface can be integrated within the computation to compensate for component insulation or internal pipe bends. The method of this integration will be discussed later in the chapter.

Chan et al (1999) investigated modelling techniques in exhaust pipe heat transfer at engine cold start [Cha99]. To adapt Nusselt number correlations to complicated bend configurations (Figure 4.8), Equation 4.8 was utilised where,  $D_{bend} = 2 \cdot r_{bend}$ . The radius of the bend ( $r_{bend}$ ) can be determined from the length of the pipe and the bending angle.



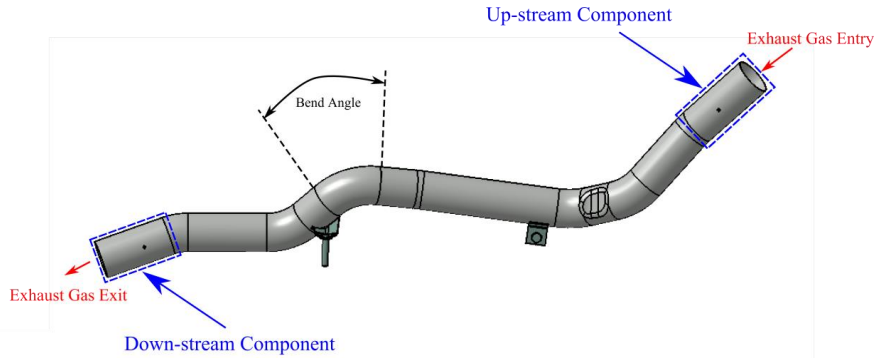


Figure 4.8: BMW Model 1 Takedown Piping Network (BMW Group).

$$CAF_{bend} = 1 + \frac{21D}{D_{bend} * Re^{0.14}} \quad (4.8)$$

The correctional factor (Equation 4.8) may be applied to individual bending components allowing heat transfer coefficients to be independent from other exhaust components

It is important to note that many exhaust components (especially within the cold end section) contain non-circular diametric piping configurations, which alter significantly from the ideal circular type. When analysing an exhaust component it is critical to understand that the diameter of a pipe has a great influence on the calculation of Reynolds number, which in turn affects the prediction of internal base Nusselt number values. In order to avoid an incorrect prediction such non-circular pipe arrangements can be integrated into the Reynolds number calculation using hydraulic diameters (Figure 4.9)

In situations of pipe diffusions or contractions (most common with pipes before and after Catalytic Converter/Turbo components) the average diameter is selected between inlet and outlet cross-sections, as described in Figure 5.9.

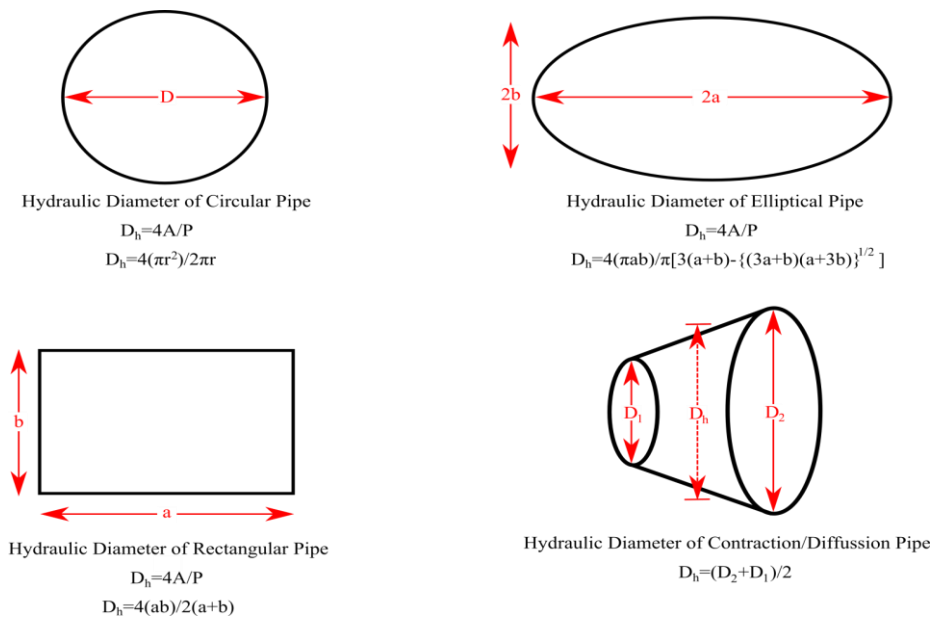


Figure 4.9: Variations in Hydraulic Diameter within Exhaust Configurations

#### 4.1.2.6 Total CAF

As mentioned previously the experienced Nusselt number within a simulated exhaust component is the multiplication of an ideal (text-book) correlation with a correction factor (CAF). This factor either enhances or reduces the ideal Nusselt number value to encompass the internal flow phenomena experienced within the component.

As many exhaust components not only consist of a single phenomenon (such as entrance) but multiple phenomena in combination, a Total CAF (Equation 4.9) must be striven for. The total CAF consists of individual phenomena correctional effects multiplied with each other in order to provide a unique numerical value used to augment a text book Nusselt number correlation as seen in Equation 4.10.

$$CAF_{Total} = CAF_{Entrance} * CAF_{Pulsation} * CAF_{Surface} * CAF_{Geometry} \quad (4.9)$$

$$Nu_{Real} = Nu_{Ideal} * CAF_{Total} \quad (4.10)$$

This method of CAF multiplication is used through the investigation and implemented within the exhaust system to represent the internal gas dynamic phenomena.

#### 4.1.3 Exhaust Heat Transfer Coefficient Prediction Tool

Post 2009, the methodology described above has become an integral component in modelling steady-state simulation cases at BMW. In 2010, an excel based tool was developed encompassing the previously discussed correlations for components within an exhaust piping network [Hae10, Hae13a]. The tool aimed at assembling the correlations for the engineer in a user friendly interface, where the primary inputs were, exhaust mass flow rate, inlet gas temperature and rpm. Here the engineer assigned the geometrical parameters (diameters, lengths and bending angles) and constructed the piping network visually on the interface. The tool then estimated the heat transfer coefficient (HTC) of each individual component within the piping network. Then engineer then exported these HTC's and assigned them to the inside surface of the each component within the exhaust system. In addition to standard exhaust pipe functionality of the tool, work was conducted by Heineman (2010) which aimed at predicting the augmentations to the gas temperature through the catalytic converter [Hei10]. Therefore a heat rate was applied directly to the gas 1-D fluid node to replicate the increase in gas temperature. In 2011, a methodology for predicting the internal heat transfer phenomena in acoustic silencer was introduced into the exhaust tool [Sch11, Hae14a]. In this methodology the EAS was segregated into individual chambers consisting of internal pipe geometry, whereby heat rates were generated to represent chamber dependent flow phenomena (e.g. impingement and pipe perforation). This work lead to a further improvement in the predictability of surface temperatures along acoustic silencers. To accommodate the complex flow pattern in turbo-chargers, Devos (2013) developed a methodology of improving the internal heat rates within the turbo-charger introducing a new Nu number formulation based on dean vortices [Dev14]. Here the turbo-charger was segregated into 3 parts, whereby the volute section utilised the dean vortices based Nu number correlation, the turbine a standard seider-tate formulation and the

turbine-shroud, a combination of entrance and pulsation CAF's. In Appendix 3a, an illustration of the exhaust HTC tool is provided with a description of the different software features.

*Steady State to Transient Functionality*

In order to accommodate the time-dependent nature of the primary heat source under dynamic driving conditions, the previously discussed exhaust tool needed to be modified. The primary change was adapting the steady-state functionality for transient input conditions. This was achieved by assuming that every time-step in the transient boundary conditions could be represented as an independent steady state condition. Therefore the tool could still utilise the previously discussed correlations on a time-step basis, essentially producing a new HTC value at each new time interval. This assumption removes the need for historical data (e.g. what was the state of the gas in the previously time-step), however can introduces the potential misrepresentation of time dependent flow influences. Due to the 1-D nature of the approach as well as the application of surface averaging the HTC values to the inside of exhaust components, it was assumed that these discrepancies would be over-compensated and could be neglected. Therefore the tool was altered to accommodate time dependent boundary conditions and predict a transient HTC profile (as shown in Figure 4.10). This time-dependent HTC profile was then generated for each exhaust component (in the identical fashion to the steady state methodology) via the utilisation of macros within excel in order to calculate the multiple time steps. The process of modelling the exhaust piping network within the tool remained unaltered, where the MFR and gas temperatures for the inlet could be directly imported into the tool. This is shown within Figure 4.10, where it can be seen that the time dependent HTC (denoted in yellow) has a strong relationship to the MFR of the gas (denoted in blue). This corresponds to the Nu Number dependency on the Reynolds number. In Appendix 3b, an illustration is provided of the new transient functionality of the tool.

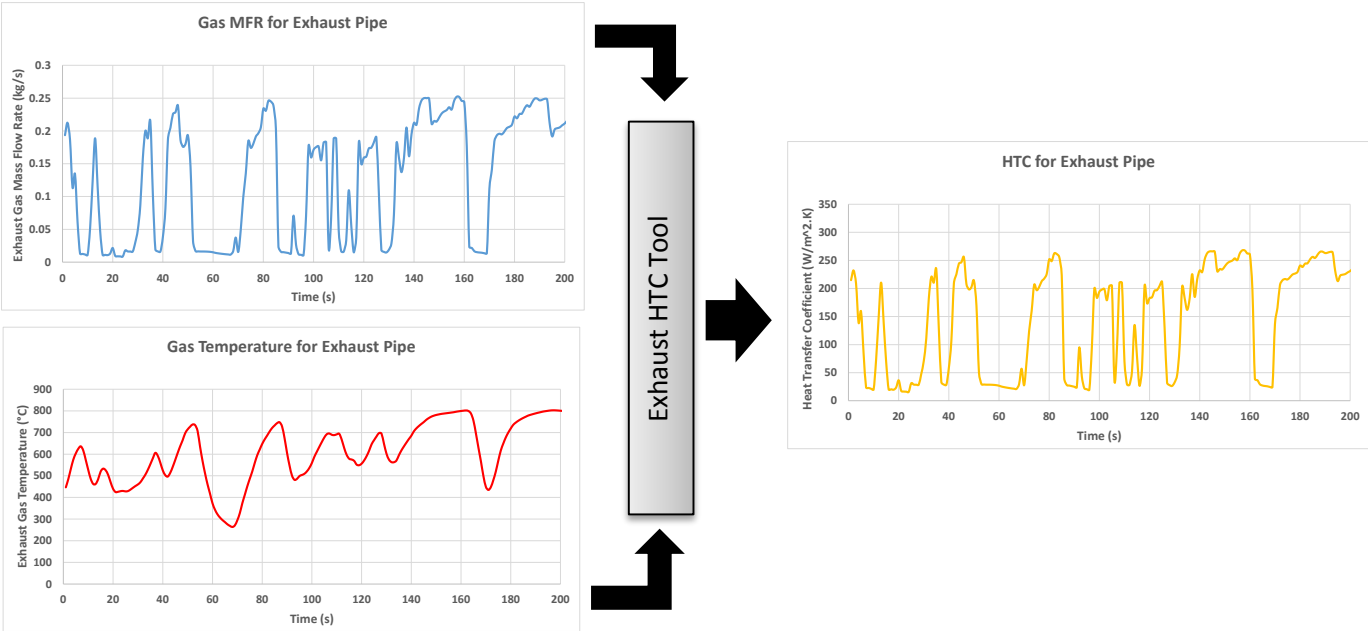


Figure 4.10: Exhaust Heat Transfer Coefficient Prediction Process

## 4.2 Stage2 - Sub-Module Investigation

The following section outlines the initial investigation of utilising signal processing techniques to simplify the boundary conditions of dynamic driving profiles. The module was derived from a full vehicle geometry and was selected for this investigation due to its geometrical simplicity. Due to its size and number of components the module can facilitate quicker turn-around times and provide the means to calculate dynamic profiles under traditional full transient techniques. The full transient simulations will be then used as a reference for comparison to simplified boundary conditions simulations and quasi-transient approaches. Additionally due to the numerical nature of the investigation the error of utilising simplified boundary conditions can be isolated in combination with the propagation of compounding errors due to the quasi-transient approach. The results from this investigation have been featured in SAE publication [Hae14b] and will be addressed in chapter 5.

The sub-module was designed to emulate the thermal relationship of components of a full vehicle during unsteady flow conditions. Therefore the module consists of a generalised component layout representing the basic under-body configuration of most vehicles (Figure 4.11). This model was utilised due to its robustness, resulting from the relatively simple geometry; and its compact file size, allowing for a larger number of simulations to be conducted. This is advantageous when a sensitivity study is necessary. Additionally the module facilitated the ability to conduct full transient simulations and compare the error induced through quasi-transient approaches.

The basic structure of this module consists of a simplified section of a vehicles under-body, complete with multiple heat shields and floor panels, a section of the drive shaft and various components of an exhaust system. The exhaust system, containing an acoustic silencer and two sections of exhaust pipe (one upstream of the silencer, one downstream), is particularly important in this study as it is the heat source of the system, impacting the thermal behaviour of surrounding components.

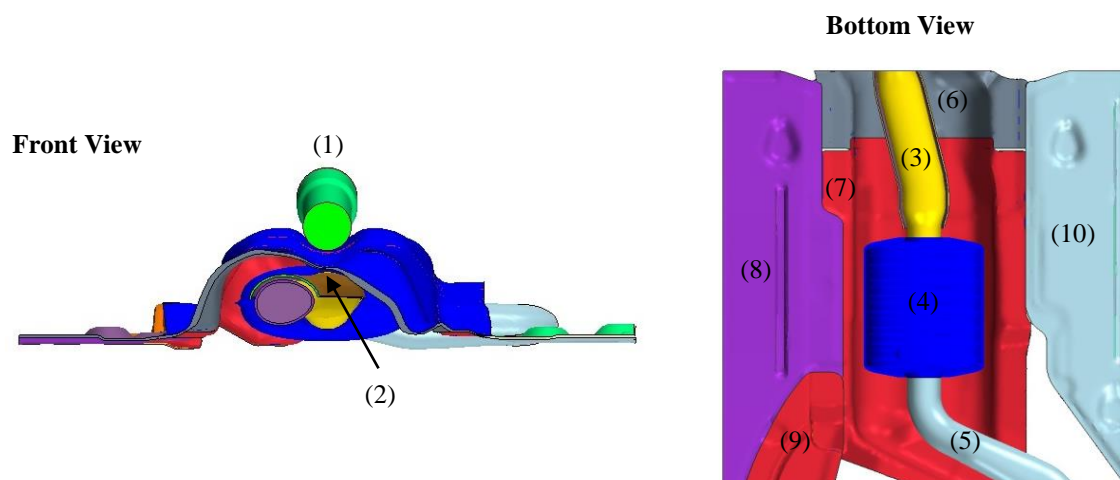


Figure 4.11: Test Module (Front and Bottom View)

Experimental data from the Nuerburgring test track was selected due to the highly dynamic lap profile, containing areas of prolonged high velocity along with multiple velocity changes over short periods of time. The Nuerburgring race track itself possesses the largest frequency spectrum of all evaluated profiles within the investigation, hence it was advantageous to utilise this profile to evaluate the compounding effect of errors, the influence on calculation speed and potential quasi-transient coupling methodologies. The results from the test module will be utilised to define the optimal methodology for full vehicle integration in stage 3.

Table 4.1 presents the component list for the sub-module corresponding with the number allocation in Figure 4.11. The table consisting of the materials for each component and their specific heat capacities, where component 3 and 5 possess temperature dependent properties. Component consist of a multi-layer arrange hence the thermal properties are calculated via the individual layers. There are 3 layers within the acoustic silencer, the first and third are steel with the second being air.

#	Name	Material	Specific Heat Capacity (J/kg-K)
1	Driveshaft	Steel	460.967
2	Exhaust Heat Shield	Aluminium	893
3	Exhaust Pipe 1	Steel	650 ( $T_{operation}$ )
4	Acoustic Silencer	Multi-layer	-
5	Exhaust Pipe 2	Steel	650 ( $T_{operation}$ )
6	Heat Shield 1	Aluminium	893
7	Heat Shield 2	Aluminium	893
8	Under-body Panel R1	Absorber	1895
9	Under-body Panel R2	Absorber	1895
10	Under-body Panel L	Absorber	1895

Table 4.1: Component Data for Test Module

#### 4.2.1 Full Transient Scheme

In order to allow for comparison of the various simplification schemes researched, a transient simulation needs to be conducted using the experimental boundary conditions obtained from the Nuerburgring test track data. It is important to investigate all aspects of the simulation, from the warm-up phase all the way through to component operating conditions.

For this simulation multiple solvers were used in tandem, each with its assigned task and necessary boundary conditions. *Star-CCM+* was implemented to calculate the fluid flow properties around the test module, with the input velocity shown in Figure 4.13-4.14. The thermal simulation was performed by *Radtherm*, using the exhaust gas mass flow rate and temperature as input data for the heat source. A coupling program, *MpCCI*, is used to allow for data exchanges between the solvers at specified intervals which for this simulation was every time-step (0.5 seconds). The wall temperature is exported from *Radtherm* whilst the wall heat transfer coefficient and film temperature are exported from *Star-CCM+*, each being surface mapped onto geometry in the opposing solver (Figure 4.12) at each time-step.

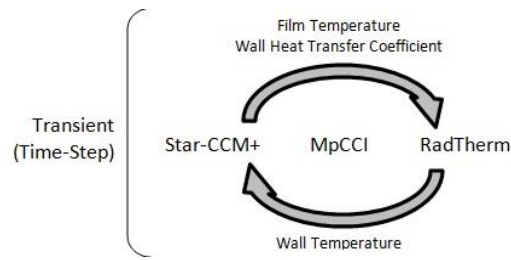


Figure 4.12: Full Transient Coupling Process

To reduce the computational cost of the simulation, a 1-D fluid stream was applied to the exhaust system in lieu of a full 3-D CFD approach. This was to be done with the help of a 1-D exhaust modelling tool previously discussed, calculating the heat transfer coefficients experienced in each section of the exhaust system at each time-step. All transient simulations were initialised with a steady-state *Radtherm* model at “room” temperature, similar to that found in a vehicle upon ignition.

#### 4.2.2 Quasi-Transient Scheme

Although the fully transient approach to simulating a driving profile is considered the most realistic representation of component behaviour under varied loading, it does require an extravagant amount of time to complete the simulation (as discussed in chapter 1) and yet it has never been attempted for highly dynamic driving profiles. Quasi-transient methods have shown promising potential in industry and as previously discussed with chapter 1 & 2 could provide a method of achieving highly dynamic vehicle conditions.

Similar to the full transient approach, the quasi-transient approach requires the use of coupled steady state simulations to solve the external fluid properties. This however is only calculated for the individual steady state points. One of the main features of this method is that the coupled simulations are assigned to specific times throughout the transient thermal simulation rather than coupled continuously at each time-step. An example profile is presented in Figure 4.13, whereby in grey the real profile is denoted, the green line denotes a simplified version of the profile and the red circles indicate the steady state points. Between each steady-state point the convection information is time interpolated.

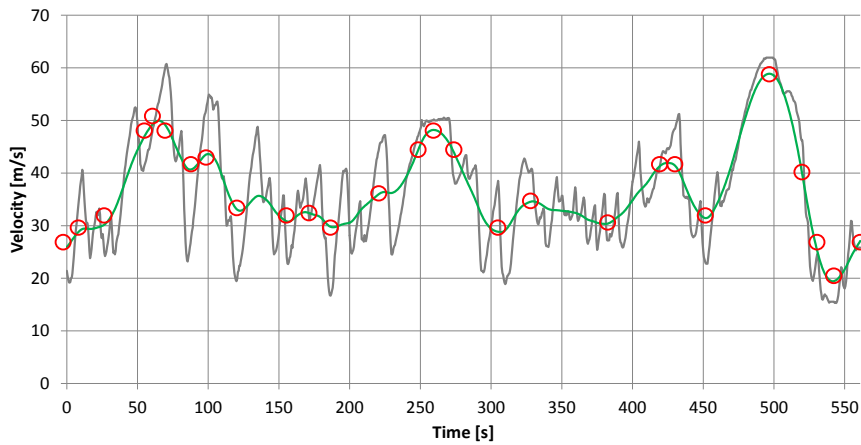


Figure 4.13: Comparison between transient and a WMA velocity profile with Steady-State CFD solution points

The simplified profile in Figure 4.13 is of a WMA with a 15% sampling range over a 561 second lap period (with 0.5 seconds integers). Another example simplification type is presented in Figure 4.14. This is a wavelet derived profile (denoted in black) with corresponding steady state points denoted in red. The wavelet profile was derived from the methodology previously discussed in chapter 3. Here a “balance approach” was selected, averaging the components masses and coupling strengths in order to predict the critical frequency of the sub-module.

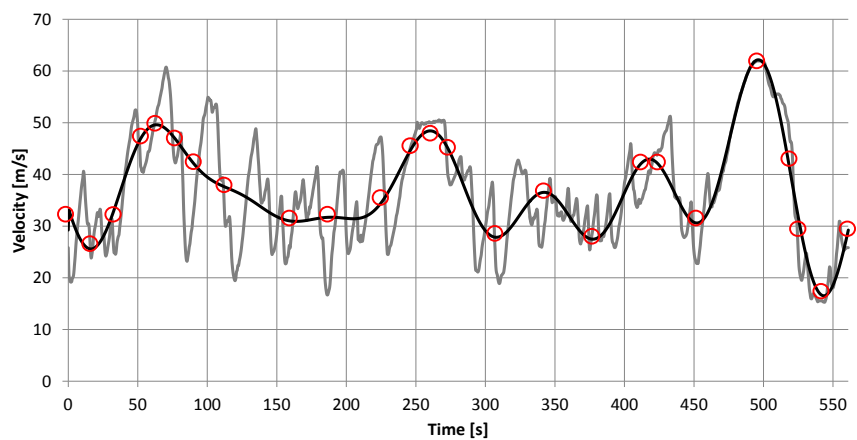


Figure 4.14: Comparison between transient and a Wavelet velocity profile with Steady-State CFD solution points

Clear differences can be seen between both the wavelet and the WMA derived profiles. Firstly the WMA tends to experience more frequency changes during the times between 50-160 seconds. This is removed by the wavelet transform to produce a smooth transition period. Additionally the wavelet reaches peak velocity conditions at time 495 seconds which correlate well with the real conditions of the vehicle, whilst the WMA under predicts these conditions due to its inherent averaging nature.

Both simplified profiles are not representative of the time-interpolated convection profile experienced within the thermal solver, rather a guideline for the selection of steady state CFD

points. Since the interpolation is of a linear type the simulated profile would consist of linear connections between steady state CFD points through time.

### Velocity Fluctuation Simplification

As seen in Figure 4.13 the WMA profile carries additional velocity fluctuations between times 50 to 160 seconds. This however is removed from the Wavelet transform and initial investigations suggested that there is a relatively low change in temperature in this phase [Hae13b]. In order to validate its relevance within the system a detailed investigation into this part of the profile was conducted. On the left of Figure 4.15 the original signal compared to the WMA time interpolated profile is presented. The deviation (devWMA) between the original signal and its corresponding simplified signal is denoted as a blue area. On the right hand side of Figure 4.15 is a randomly selected range of simplified time interpolated profiles. Here a series of simplified interpolation profiles were developed that reduced the number of CFD points in the section from six to a mere two, with the second point held constant whilst the first is varied between 50-61m/s, with the import time also varied to match the transient profile. Again the deviation can be witnessed as a coloured area underneath the profile denoted as devV61 (corresponding the V61 interpolation) to devV50 (corresponding to V50 interpolation). It is clear that the WMA derived interpolation profile produces the least amount of deviation, whilst each removed fluctuation profiles increases the deviation, with the V61 having the largest overall difference and the V50 having the least.

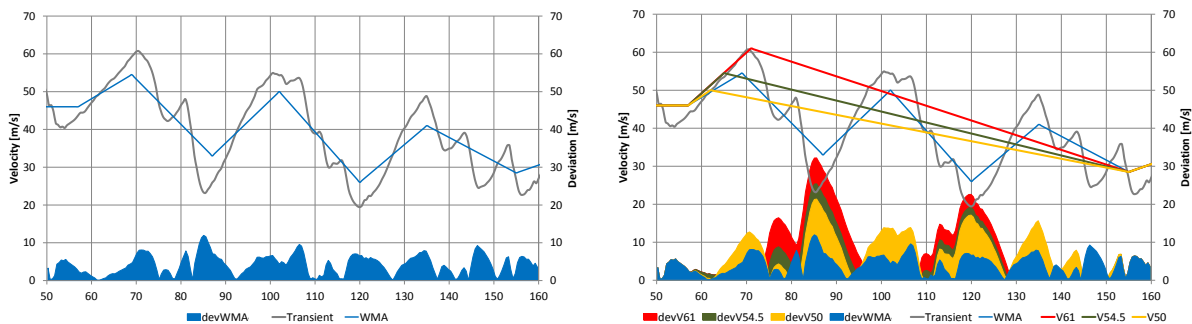


Figure 4.15: Velocity Simplification

### 4.2.3 CFD Quantity Investigation

To ensure a level of standardisation throughout the investigation, each simplified profile is modelled using only 12 coupled CFD solutions mapped 30 times per lap. As the range of selected data is decreased and the lap becomes more dynamic, the time interpolation by the thermal solver can be introducing error compared to the transient data. An increase in deviation due to selected CFD points can reduce the effectiveness of the external convection especially in areas of a large change in velocity over an extended time period. With this in mind, a WMA simplified profile was selected from 450 to 561 seconds that contains two relatively large changes in velocity over a long time period.



Figure 4.16 displays how the initial time-interpolation profile deviates from the selected WMA data due to only the amount of CFD points utilised. To investigate what effect this deviation from the averaging approach has on the resulting component behaviours, alternate profiles are constructed that contain an increased set of data points within this section of the lap, each gradually smoothing the profile until it conforms closely to that of the WMA scheme. This can be seen in Figure 4.16, where I04 to I06 refer to the quantities of steady state CFD solutions interpolation over the profile.

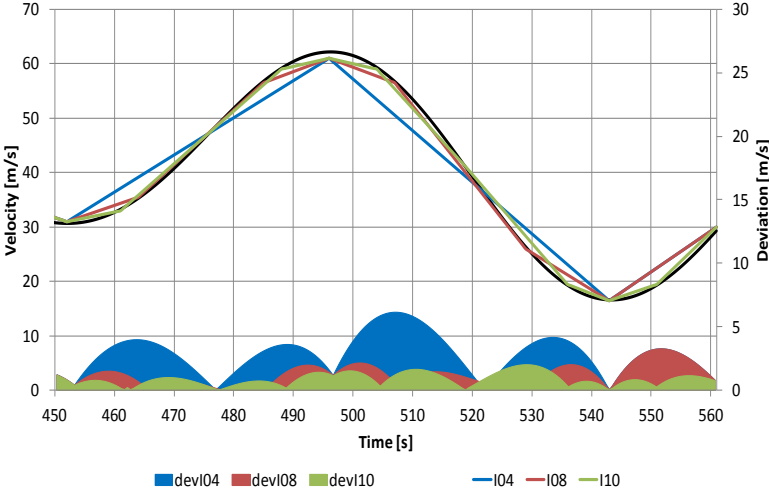


Figure 4.16: CFD Point Quantity Investigation

The range of steady state CFD points investigated in this section was from the minimum 4 to the maximum 24. The differences between the original profile and the amount of steady state CFD points which are linearly interpolated through time can be further seen in Figure 4.17, where the transient data is denoted in black with the corresponding quantities of steady state CFD points displayed on the top right hand corner of each graph. The results from this investigation are presented in chapter 5, with corresponding discussion of findings in chapter 6. The optimal steady state CFD quantities for a quasi-transient dynamic driving profile are later utilised for the full vehicle simulation based on this investigation.

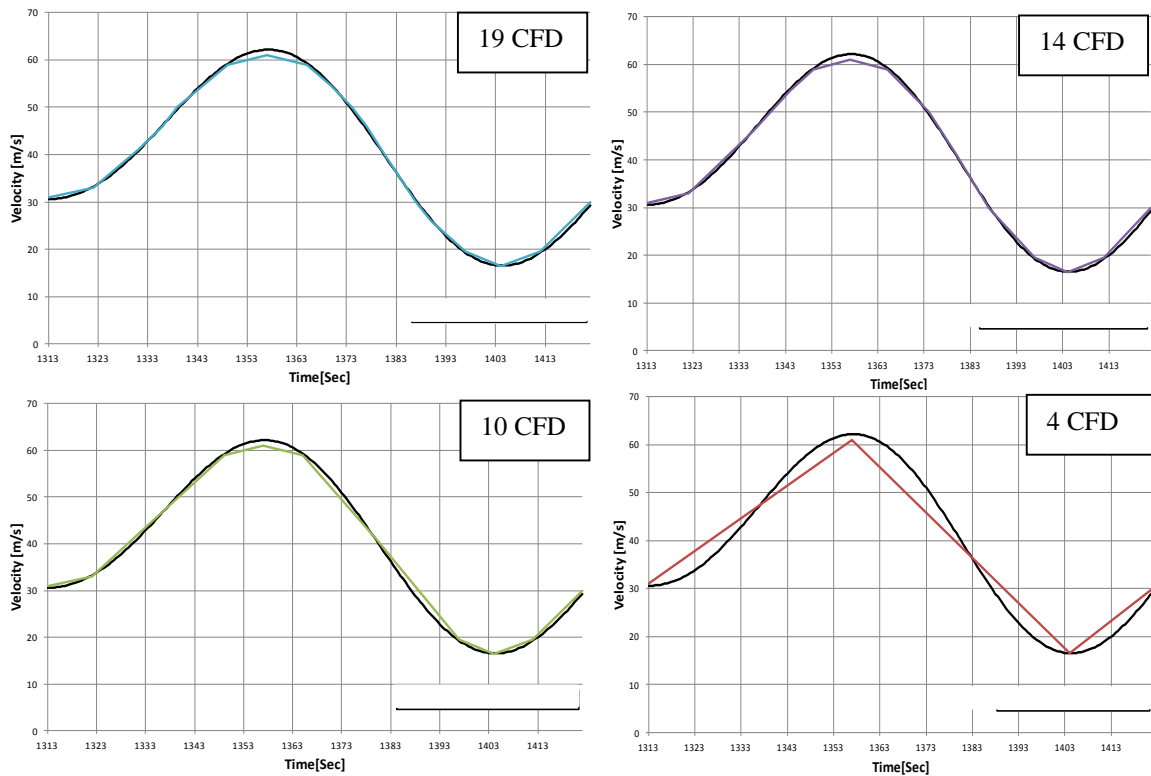


Figure 4.17: CFD Point Quantity Variation

#### 4.2.5 CFD Type Investigation

As stated previously, the quasi-transient approach uses coupled steady-state CFD solutions to calculate the convection conditions for each of the selected velocities. This allows for generation of external heat transfer coefficients comparable to those experienced during the transient approach. As coupled solutions are quite computationally expensive, the feasibility of this heat transfer coefficient generation is investigated through the implementation of non-coupled solutions or cold solution (CS), where the fluid simulation is solved without thermal input.

Alternatively, an engineer may implement warm-solutions (WS), (those coupled between a thermal and fluid solver) for each steady case corresponding to the loading conditions simulated. The expectation being that the WS create a thermal profile similar to that experienced during transient simulation whilst the CS produce an alternative profile at an increased rate of cooling. This could be advantageous during the warm-up phase of the module as the component temperatures are cooler (to that of the normal operating temperature) therefore the surrounding fluid temperatures in contact with the components would share attributes to the CS.

An additional investigation is conducted to test the viability of mixing the CS and WS to model the transient. This method involves the use of both the warm and cold coupled solutions in what can be called the Warm-Cold Solution Mixing (WCSM) approach. A WCSM approach consists of various areas of the profile containing thermally different steady-state solutions. On the left of Figure 4.18 the basic principles of the WCSM scheme are displayed. In areas of acceleration

in the driving profile WS are implemented (denoted in red), whilst during deceleration CS are used (denoted in blue). During the brief periods where the CFD solution is held constant the same thermal CFD solution is used. Interpolation is conducted between the CFD solutions as in normal cases.

Another potential mixing scheme is presented on the right hand side of Figure 4.18, where WS<sub>1</sub>, represents a solution coupled at the minimum engine load, WS<sub>2</sub>, is a solution coupled at the maximum engine load, and CS<sub>1</sub> and CS<sub>2</sub> are the corresponding uncoupled solutions at both load positions. This method analyses the type of load condition a vehicle could be experiencing (for example, heavy deceleration) and utilises a combination of solutions to mix the appropriate percentages (based on vehicle conditions) of fluid temperatures and heat transfer coefficients. This can be seen with the crossover of WS<sub>2</sub> to CS<sub>1</sub>, representing a deceleration. An alternatively an acceleration can be observed between CS @ 1to WS @ 2. This methodology has shown promising results however has been utilised for the current investigation. It is to be noted that the methodology may be addressed a potential region for future work.

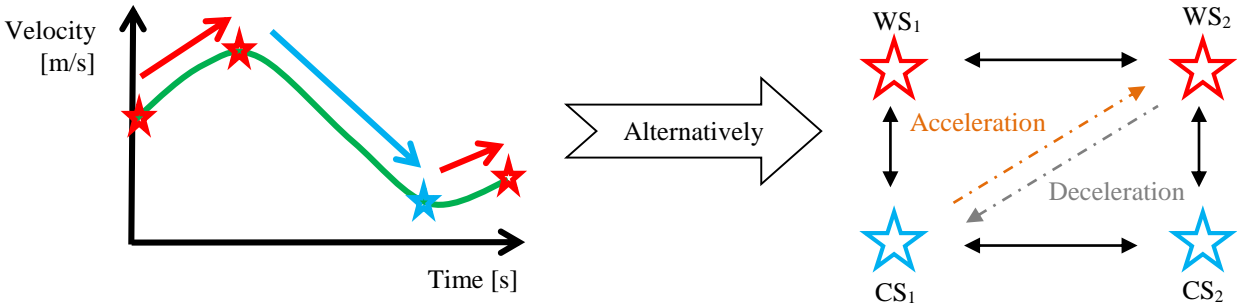


Figure 4.18: Warm-Cold Solution Mixing example.

The determination of the particular solution type layout is important in emulating the specific convection conditions. It is clear that during the acceleration phases the power-plant of the vehicle is experiencing heavy loading in terms of temperature and convection. This suggests that WS are better suited to acceleration phases due to inherent heat in the system. On the other hand, during periods of deceleration the mass flow rate through the exhaust is drastically reduced in combination with engine loading, suggesting that CS during these phases may be advantageous in over-compensating the cooling effects and increase temperature stabilisation of components. Within the current investigation a simple WCSM method has been utilised with warm solutions during acceleration and cold solution for low velocity conditions. The percentage mixing between both solutions has not been addressed.

*Effects of False Initial Temperature*

The initial part temperature of the system has a substantial influence on the warm-up characteristics of component temperatures. The investigation aims at understanding these influences and quantifying them by purposely introducing an initial temperature error within

the simulation. For example, when the initial temperature of a component is 20°C, to introduce error an engineer may initialise the component at a temperature of 25°C, hence the initial error of the component is 5K. The impact of the 5K on component behaviour is to be understood through this investigation. Once an error is placed within the simulation the time length required for the component to return to its original time dependent behaviour pattern (based on simulations without initial temperature error) can be measure. From this a correlation based on time can be determined in order to further identify potential errors within the full vehicle configuration. The results from this investigation are displayed in chapter 5.

### **4.3 Stage 3 - Full Vehicle Investigation**

Stage 3 embodies the entire research philosophy discussed within this investigation. It attempts to utilise the findings and techniques from the prior stages on a full vehicle geometry. Therefore the prediction of internal heat transfer coefficients discussed in stage 1 are implemented within the exhaust system. The signal simplification philosophy derived in chapter 3 is used on the time dependent boundary conditions of the vehicle. The findings from the sensitivity analysis of stage 2 are exploited within the full vehicle simulation to minimise potential error. And finally the location, quantities and types of CFD points necessary for the quasi-transient simulation are formulated within a tool developed for dynamic driving profiles. The following section aims at addressing a final complete methodology for multiple dynamic driving profiles accompanied with experimentally validated data via climatic wind tunnel. The following section provides details of the modelling considerations coupled to the implemented physics within full vehicle CFD conditions.

#### **4.3.1 Modelling and Physics**

The vehicle consists of a variety of sub-systems operating together and contributing to the overall thermal behaviour. Each individual sub-system employs certain physics and modelling considerations which allow it to properly interact within the total vehicle geometry. Therefore the following section aims at describing each of the sub-systems and how they are modelled. The standard RANS model is used for ideal gas, where the k- $\epsilon$  two layer turbulence equation is implemented within the simulation. An all  $Y^+$  correction factor is utilised to adjust the near wall phenomena with the primary fluid for the simulation as standard air.

##### *4.3.1.1 Engine*

As the engine is a thermally regulated system, with water and oil cooling mechanisms, the outside surface temperature (which is a contributing factor in VTM) of the motor remains relatively constant [Rau14]. The maximum temperature gradient occurs along the vertical direction, from the top cover to the oil pan. This temperature distribution can be easily modeled and for transient conditions and can be implemented with a 1-D model. The 1-D model exposes the surface of the engine to a rate of temperature change commonly experience within reported data.

#### 4.3.1.2 Exhaust System

The exhaust system within the investigation is a double manifold, twin turbo-charger, upstream and downstream catalyst configuration, consisting of a MAS and two EAS systems. The exhaust itself has been further segregated in 82 individual parts to suit the 1-D fluid stream methodology described in the prior stage. This segregation is conducted in the pre-processing phase of the simulation prior to the calculation. Additionally each component is segregated based on the characteristic internal gas dynamics. For example, if there is a bend within the exhaust pipe, the bend itself is segregated in order to apply the bending CAF (Equation 4.8). Segregation is also conducted for pipe contractions or diffusions, when the pipe diameter changes, for the energy augmenting components (turbo-charger and catalytic converter) and finally for the MAS/EAS based on chamber and internals. Each segregation is carefully implemented to be compatible with the corresponding CAF's implemented in the exhaust gas dynamics theory. An isometric view of the exhaust system with individual parts (denoted in colour) can be seen in Figure 4.19. A zoom on the hot-end of the exhaust system further displays the details of the segregation.

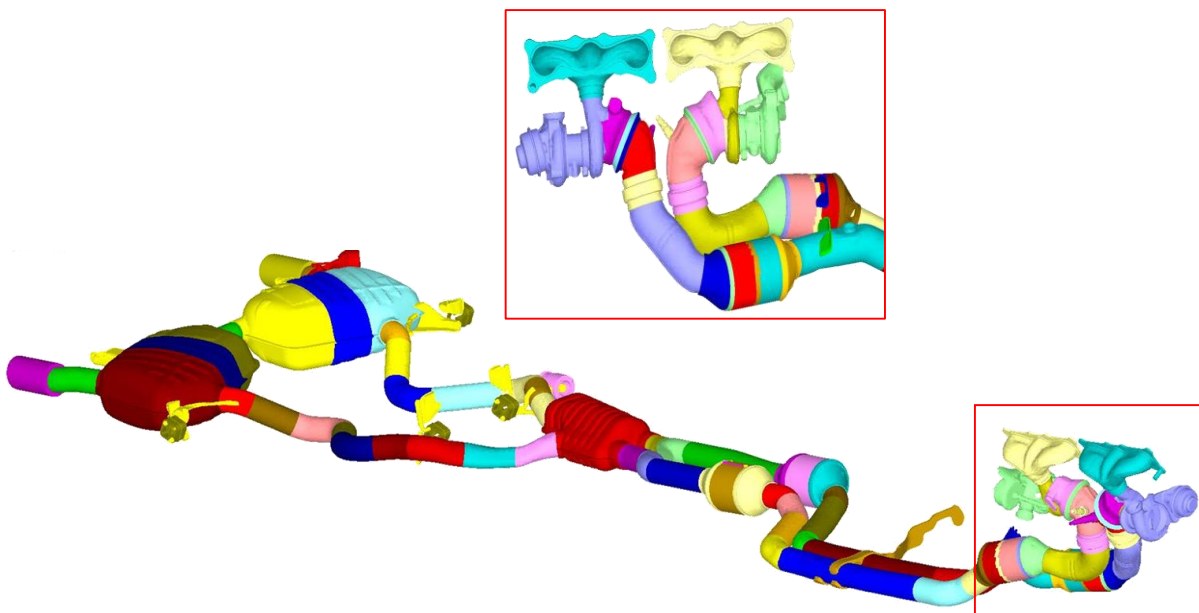


Figure 4.19: Vehicle Exhaust System

#### *Multi-Layer Components*

With the exhaust system, many components have internal structures contributing to the thermal mass of the component. A typical component with an internal structure is the EAS described below in Figure 4.20. The methodology adapted within this investigation to model such components is through the utilisation of a multilayer configuration within the thermal solver. The average thickness of each layer is modelled for each corresponding chamber of the EAS, with the inside pipe being exposed to the exhaust heat transfer coefficient and outside surface

exposed to the convection. This is depicted (in Figure 4.20) below with a cross-section view of the component.

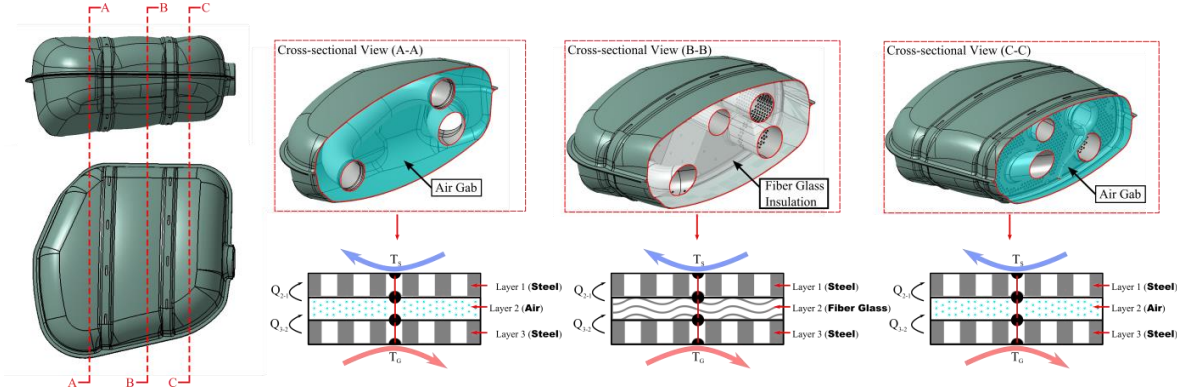


Figure 4.20: EAS Multi-Layer Example

Not only EAS/MAS configuration have internal structures that need to be compensated within the simulation. Another series of components within the under-body containing multiple materials are heat shields, absorption panels and carbon-fibre components. These components are model with the same multi-layer philosophy as that in the EAS. It is to be noted that all components are modelled based on the available CAD data. Therefore the masses, internal configurations and geometrical properties are derived from the raw CAD data, not the final numerical model (which may at times be a simplified version of the vehicle).

4.3.1.3 Heat Exchangers

Within the integrated cooling systems of a vehicle heat exchangers are used in converting and transporting thermal energy from the motor to the surrounding airflow. Within the CFD model a basic dual stream heat exchange is defined between two identical porous regions; One representing the airflow through the heat exchanger, the other representing the coolant flow through the heat exchanger. An energy exchange option is activated with *starccm+* whereby a cold stream table is provided consisting of mass flow and heat transfer rates. The heat exchange rate (energy given to the fluid) is set to the maximum performance of the heat exchange for each steady state CFD solution. This is to replicate the behavior of the heat exchangers when the vehicle is experiencing extreme load conditions. Additionally the data relevant to the boundary conditions (cooling fluid mass flow rate) of the heat exchangers are derived from experimental data.

4.3.1.4 Rotating Parts

The majority of rotational parts within the vehicle are treated using the moving frame of reference (MFR) methodology, rotating about a predefined axis. As well as the engine fan, the rotating parts are the wheels, drive shaft, fan belt pulleys and the axles. All these components are artificially rotated either through the utilisation of MFR, or through local surface tangential

velocity specifications. The data for the rotational speeds are derived from vehicle velocity for the wheels, axles and drive shaft depending on the gear ratio of transmission. The fan and engine belt pulley rotational speed is extracted from experimental data.

### 4.3.2 Cell Reduction Techniques

A volume control shape (VS) is a geometrical based 3-D constraint, which enables the volume meshing tool (within the CFD solver) to specify unique cell characteristics within the region. It is used to improve resolution (through increased cell density) within critical areas of the vehicle such as vehicle body architecture, motor, intakes, and gearbox. In turn other areas of less interest such as the wind tunnel can be meshed more coarsely. Hence an economic procedure for cell delegation is performed. In the past these volume control shapes tended to be of basic geometrical configurations, such as cubes, spheres and rectangular boxes. However when applying such a scheme to a complete vehicle in order to economise cell densities around the critical regions (such as body architecture as seen in Figure 4.21, in the 2012 benchmark), clear inefficiencies can be seen. The entire rectangular volume shape consumes high amounts of cell quantities. In order to further increase resolution, whilst promoting efficiency and new volume control shape is implemented as a geometrical offset of surface geometry present in the actual vehicle model (Figure 4.21, 2013 improvements). This offset surface is then repaired, merged, and closed to achieve a sealed volume. Further improvements can be realised by extracting and Iso-surface from the vehicles velocity field. This Iso-surface is then also offset and closed to create a larger volume denoted in pink in Figure 4.21. The iso-surface is created through coupling the 2013 Benchmark model with a thermal model in order to generate the appropriate velocity field. A third coupling loop is then achieved through the mesh generation for the vehicle as displayed in Figure 4.21.

	<b>2012 Benchmark</b>	<b>2013 Benchmark</b>	<b>2014 Benchmark</b>
<b>Total Cell Quantities</b>	45 Million Cells	22 Million Cells	18 Million Cells
<b>% Reduction</b>	n/a	51 %	18 %

Table 4.2: Cell Reduction Statistics

Table 4.2 details the reductions achieved in the evolution of the vehicle meshing standards. These reductions have facilitated higher turn-around times for individual steady state CFD points and have further increase the efficiency of the proposed methodology. A mesh independency study was conducted in order to ascertain the quality of convective heat transfer coefficients and fluid temperatures. Due to the cell densities retained within the control volumes, very small to no difference were experienced with these parameters. Further details can be found in Appendix 5.

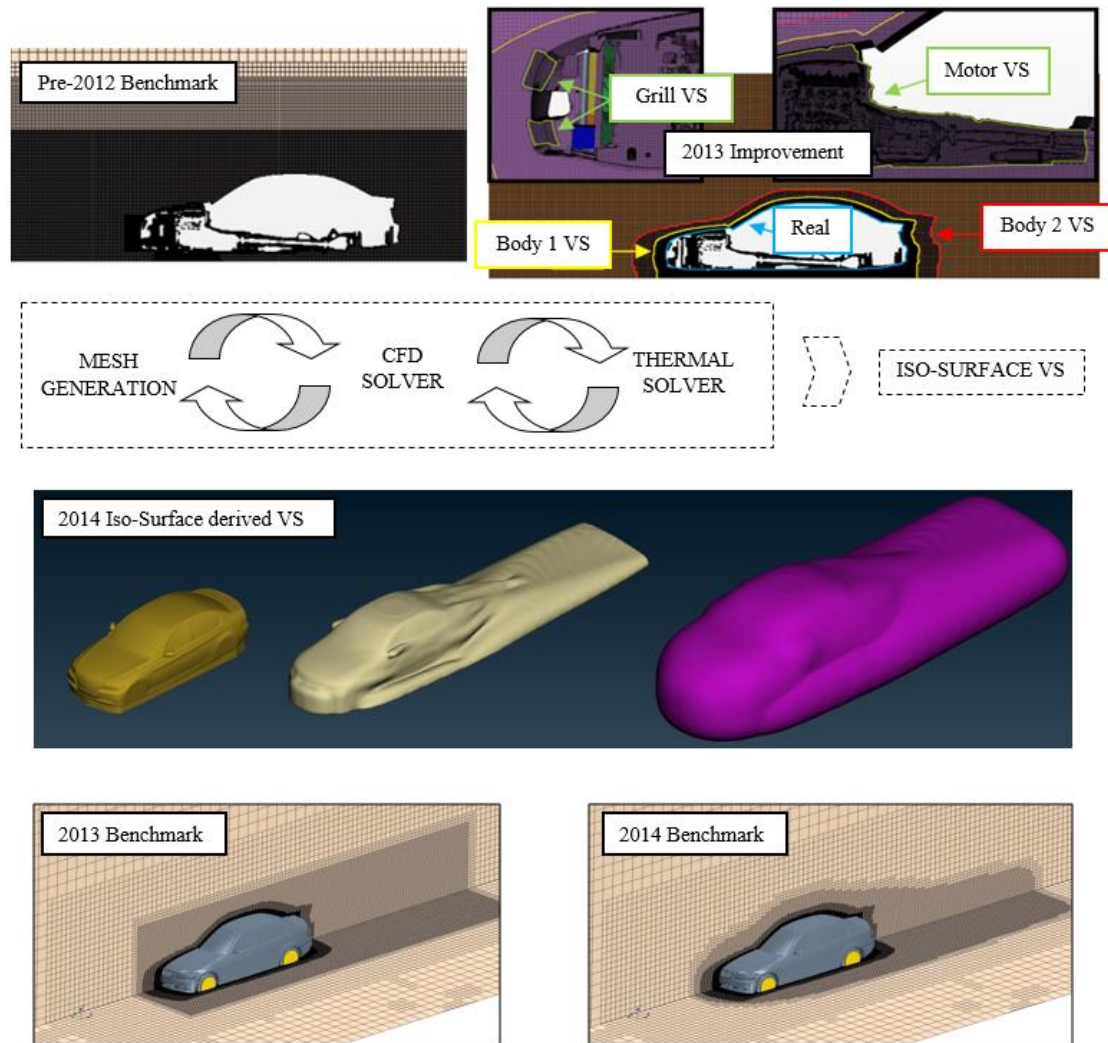


Figure 4.21: Evolution of Vehicle Meshing Techniques

#### 4.3.3 Full Vehicle Quasi-Transient Approach

The following section provides the summary of the derived simplified profiles for the investigated driving conditions. Additionally the method of CFD point allocation is described referring to the results of stage 2, in chapter 5. All unique steady-state CFD points are thermally initialised with the maximum temperature condition experienced within the vehicle. This allows for CFD point recycling within individual profiles as well as transferring data to alternative profiles. The ability to recycle CFD points has a significant impact on the overall turn-around time of the methodology, as it reduces the quantities of new CFD points which need to be calculated. The recycling philosophy is described in the subsequent section.

##### *Thermal Threshold Conditions for Vehicle Boundary Condition Simplification*

The identification of the critical frequency or response threshold describing the bounding limits of thermally relevant to irrelevant information was addressed via the flat plate analogy described within chapter 3. The “balanced approach” was selected for the full vehicle



configuration. Similar to example 2 in chapter 3, the major components of interest within the vehicle with the 3 thermally sensitive groups were identified. Here sub-groups were generated in order to produce a series of flat plate representations for each of the individual sub-systems. Once all major components within the vehicle were grouped, parameters determining the average masses, the average coupling strengths and average material properties could be summed into a single formulation to derive a critical frequency per sub-system. Then based on the importance of the sub-system weighted averaging was used to derive a global frequency threshold for the entire vehicle. The method of achieving this is described in Appendix 4, where the list of components and flat plate parameters are presented. With this single analytical representation of the entire vehicle the critical frequency was established and the decomposition level was identified for each dynamic driving profile within this investigation. Considering that each dynamic driving profile is conducted with the identical vehicle, the critical frequency remained unaltered. However due to the maximum frequency inherent within the boundary conditions, the levels of the decomposition varied between each dynamic driving profile.

### *CFD Point Allocation*

The time location of the steady state CFD points is a critical aspect in reproducing the proper convectional characteristics of the desired driving profile. This can be released as the methodology exploits the CFD time interpolation algorithm within the thermal solver. In stage 2, a sensitivity analysis was conducted in investigating the influences of the steady state CFD point locations including the corresponding errors induced with quantities. This is presented within Chapter 5 and discussed in Chapter 6. The findings of stage 2 study were correlated towards approximating the acceptable deviation of time interpolated data to that of the desired profile. It was found that a 1.8% deviation produced the optimal compromise between accuracy and quantities of solutions. Therefore as a signal is simplified a series of points are assigned based on this deviation. Starting from the time 0, the first point is assigned; the second point is denoted to the next time step, where a linear line is artificially draw between points. This line is then compared to the desired driving profile (here the simplified signal) whereby a difference is generated based on area. This difference is then equated to a percentage. Only when the data violates the 1.8% deviation another CFD point is assigned to the profile. Therefore when the deviation is below 1.8%, the next time step is selected, again drawing an artificial line between points and comparing areas to derive the deviation percentage. This process continues from one time step to another until a new CFD point is assigned. When this occurs the starting point becomes the new CFD point location, whereby the next time step is probed for the deviation. Once the profile is completely analysed and the points are assigned, a phase of consolidation occurs. The consolidation phase searches for points that are near another (from a velocity perspective), averaging between them and assigning a new unique CFD point for all time regions consisting of that particular vehicle speed. This allows the profile to consist of unique CFD points which defer from each other significantly and facilitates a further reduction on the quantities of CFD points and the consequent overall turn-around time of the methodology.

### 4.3.3.1 Simplified Profiles

The following section presents the developed signal simplification tool utilised for all simulated profiles within the scope of the research investigation. The original signal is denoted in blue, with the corresponding removal of thermally irrelevant information denoted in black. Denoted in red, is the simplified profile derived from using the wavelet transformation techniques previously discussed in chapter 3. The last section of the graph is the quasi-transient profile (the profile used for the simulation) denoted in green, with corresponding steady state CFD points denoted as red boxes. As previously discussed the allocation of CFD points was based on a 1.8% deviation algorithm, where points were consolidated and recycled throughout the profile at identical vehicle speeds. The quantities of unique CFD points and the number of times these points were recycled are addressed within the tables 4.3 to 4.6. From the highest frequency case (the race-track) to the semi-steady state case (street driving) it can be seen that the wavelet transform signal estimation becomes less representative when the original boundary conditions becomes less dynamic. This provides a clear indication of the advantages of the signal simplification approach for dynamic cases and the potential limits of the methodology for less dynamic vehicle conditions. Additionally the critical frequency for the vehicle (in appendix 4) remains unaltered for each profile, therefore only the decomposition levels changed based on the maximum frequency within the original boundary conditions.

#### *Race Track Profile*

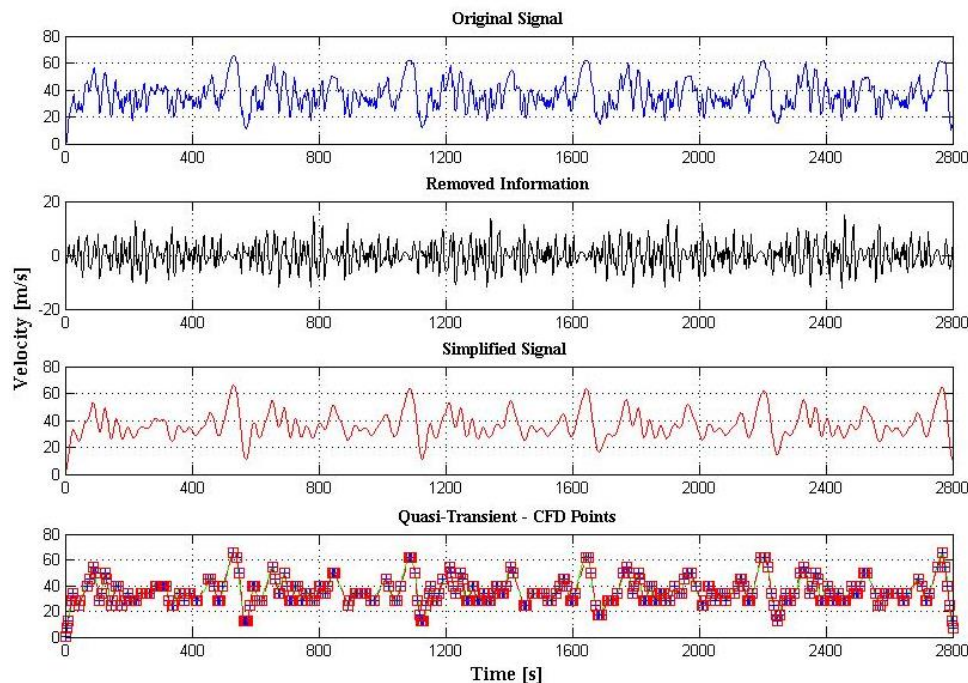


Figure 4.19: Race Track Profile Simulation Approach

<b>Amount of Unique CFD Points</b>	13 Steady State CFD Solutions
<b>Total Amount of CFD Locations</b>	405 Mapped Time Locations

Table 4.3: Race Track Profile Simulation Approach Statistics

### Handling Course Profile

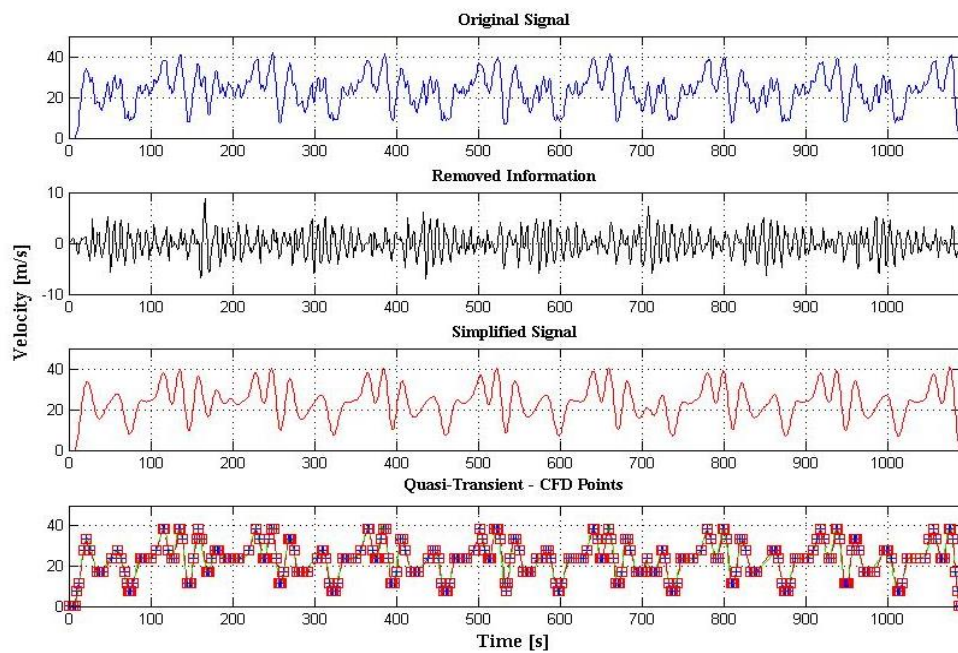


Figure 4.20: Handling Course Profile Simulation Approach

<b>Amount of Unique CFD Points</b>	8 Steady State CFD Solutions
<b>Total Amount of CFD Locations</b>	343 Mapped Time Locations

Table 4.4: Handling Course Profile Simulation Approach Statistics

### Highway Driving Profile

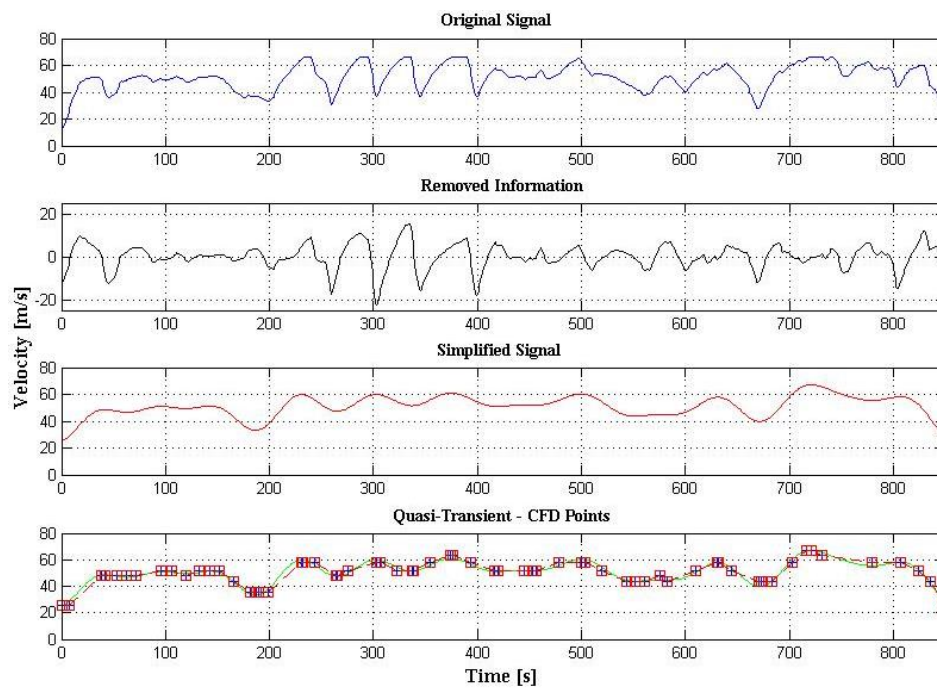


Figure 4.21: Highway Profile Simulation Approach

<b>Amount of Unique CFD Points</b>	8 Steady State CFD Solutions
<b>Total Amount of CFD Locations</b>	68 Mapped Time Locations

Table 4.5: Highway Driving Profile Simulation Approach Statistics

### Street Driving Profile

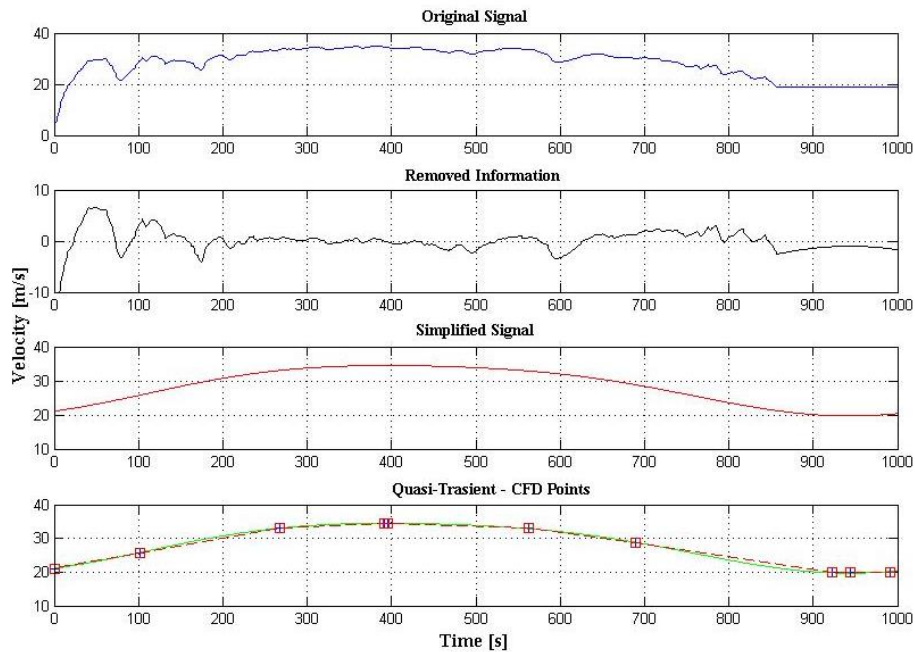


Figure 4.22: Street Profile Simulation Approach

<b>Amount of Unique CFD Points</b>	6 Steady State CFD Solutions
<b>Total Amount of CFD Locations</b>	12 Mapped Time Locations

Table 4.6: Street Driving Profile Simulation Approach Statistics

### Summary

Chapter 4 has outlined the individual stages of development process for a full vehicle configuration to be numerically modelled under dynamic driving conditions. The results of each individual stage are presented within chapter 5 and discussed in chapter 6. Stage 1 represented the implementation of 1-D correlations to represent the primary heat source within the vehicle. The results of this stage are presented within appendix 2 as the investigation was conducted prior to this research topic. These correlations were adapted via a developed exhaust tool for transient conditions. Stage 2 aimed at identifying the potential errors when simplifying boundary conditions in combination with a quasi-transient approach. Here sensitivity studies were conducted on the type and quantity of CFD solutions necessary to represent the convection conditions of a dynamic profile. The findings from this investigation were then directly implemented within the stage 3 for full vehicle configurations. A developed signal processing

tool was presented, which summates the philosophy and the findings of the entire research project. The tool was used to simplify a series of dynamic driving profiles, indicated the time locations of CFD points within the transient thermal model. In the next chapter the results of stage 2 and stage 3 are explored. The connection between stages 2 and 3 are discussed in chapter 6. Additionally the approach for the exhaust system modelling can be validated via the full vehicle configuration where experimental data is accompanied with the simulation results.

# Chapter 5

## Results and Validation

As discussed in chapter 4, the development methodology was dependent on 3 stages of investigation. The first stage consisted of predicting the heat transfer rates through the exhaust system via the implementation of 1-D fluid nodes in the thermal solver. The results of this investigation are attached in appendix 2 as they were achieved prior to this research investigation. However the transient implementation of the 1-D heat transfer correlations are discussed within stage 3 of this chapter. Stage 2 sub-module investigations and corresponding sensitivity studies are presented within the following chapter. Chapter 5 additionally presents the results from the full vehicle investigation of stage 3 on 4 dynamic driving profiles. This data is accompanied by experimental validation utilising the dynamic thermal wind tunnels of BMW.

### 5.1 Stage 2 - Sub-Module Results

As discussed in chapter 4, a sub-module investigation was conducted to evaluate the effects of altering the boundary conditions on the simulation accuracy. In order to do this the race-track profile was chosen as a benchmark due to its inherent high velocity fluctuations within the boundary conditions. The sub-module was then calculated under transient conditions utilising the current traditional methods available in literature. The data from this investigation was used to validate the influences of simplifying the boundary conditions in conjunction with quasi-transient methods. Additionally several sensitivity studies were conducted in order to further optimise the quasi-transient approach and accelerate the overall calculation times.

The initial approaches employed to simplify the boundary conditions were classical averaging schemes, which produced promising results [Hae13b, Hae14b]. In the early investigations a simple moving average scheme was found to be not suitable due to the inherent lag effects altering the time-location of convection on corresponding parts. This is because traditional SMA schemes utilise historical data (sampling from the past points) there due to the non-biased nature of the averaging equation (discussed in chapter 3) the produced simplified profile is time shifted behind the original data. This results in component temperature behavioural delays, in comparison to full transient data. In order to avoid this problem weighted moving averages (WMA) were selected. The WMA neutralised the delay affects due to the linear weighting system in combination with sampling 50% of the data in front of the given time step. Figure 5.1 provides a spider plot of the deviation of alternative simplification methods investigated, where dev refers to the average percentage deviation between the simplified profile and the original boundary conditions. This is achieved through subtracting the area underneath the profile from that of the original per time-step and averaging the magnitude of these values over the total time.

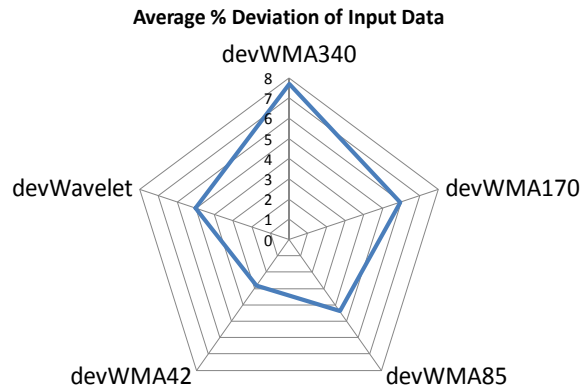


Figure 5.1: Average Deviation of Simplified Approaches

The numerical value after the WMA (for example WMA42) represents the size of the sampling range used. The time-step size is 0.5 seconds with a profile length of 561 seconds. It can be clearly observed that with increasing the series range of a WMA equally resulted in higher deviations to the original boundary conditions. Therefore it could be expected that the corresponding accuracies improved as the weighted scheme reduced its sampling series (hence resembling more of the original input data more closely).

### 5.1.1 Weighted Moving Average Results

Figure 5.2 to Figure 5.4 provide an example of the average surface temperature results of all WMA schemes with corresponding error displayed as the secondary axis on each plot. One major observation that can be made is the magnitude of temperature fluctuation depreciating with distance away from the major heat source. The exhaust pipe (Figure 5.2) consists of the highest magnitude of temperature fluctuation whilst the heat shield (Figure 5.4) produces the least. This has significant impacts on the accuracy of each individual WMA scheme.

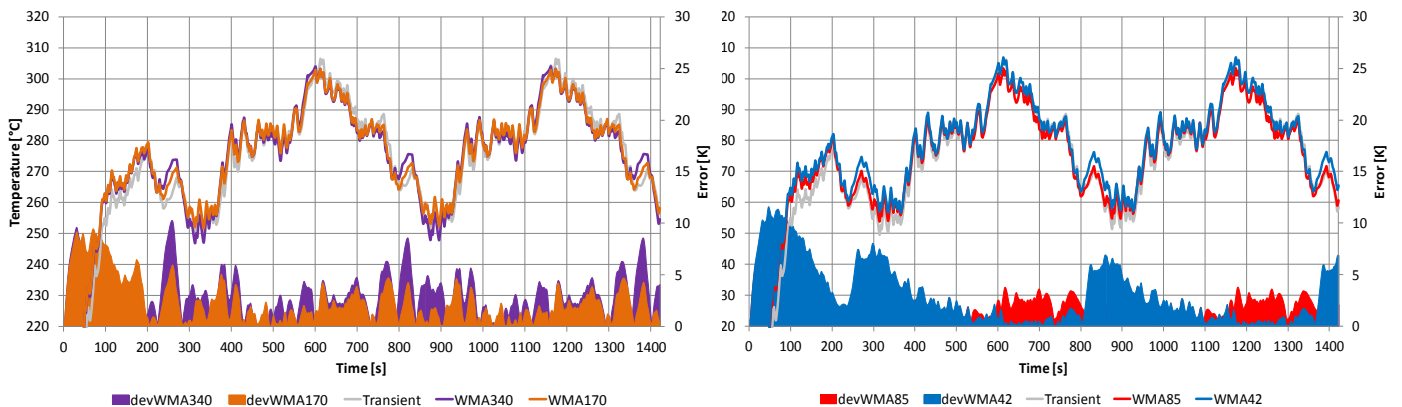


Figure 5.2: Exhaust Pipe Comparison of WMA schemes to Full Transient (Time 0 – 1420)

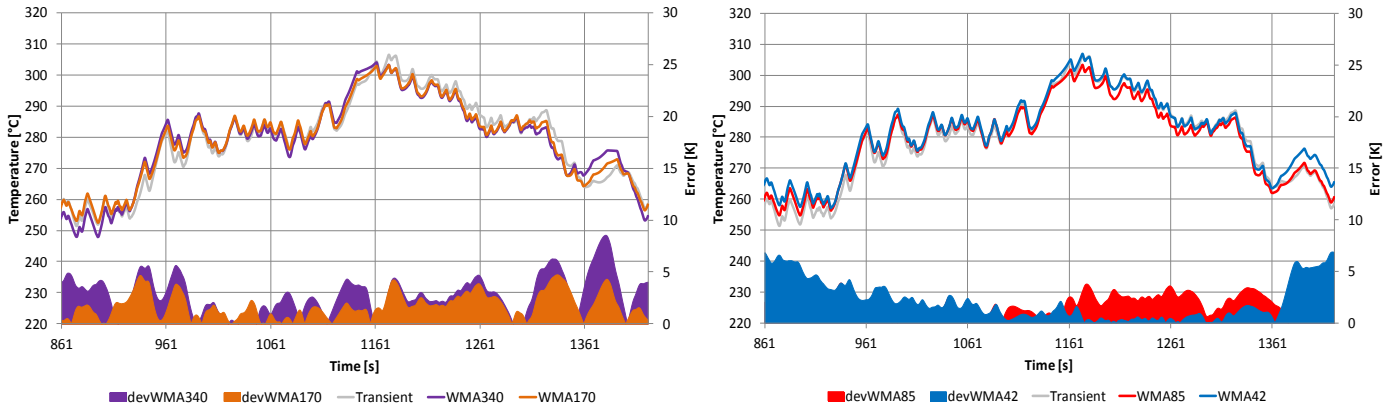


Figure 5.3: Exhaust Pipe Comparison of WMA schemes to Full Transient (Time 861 – 1420)

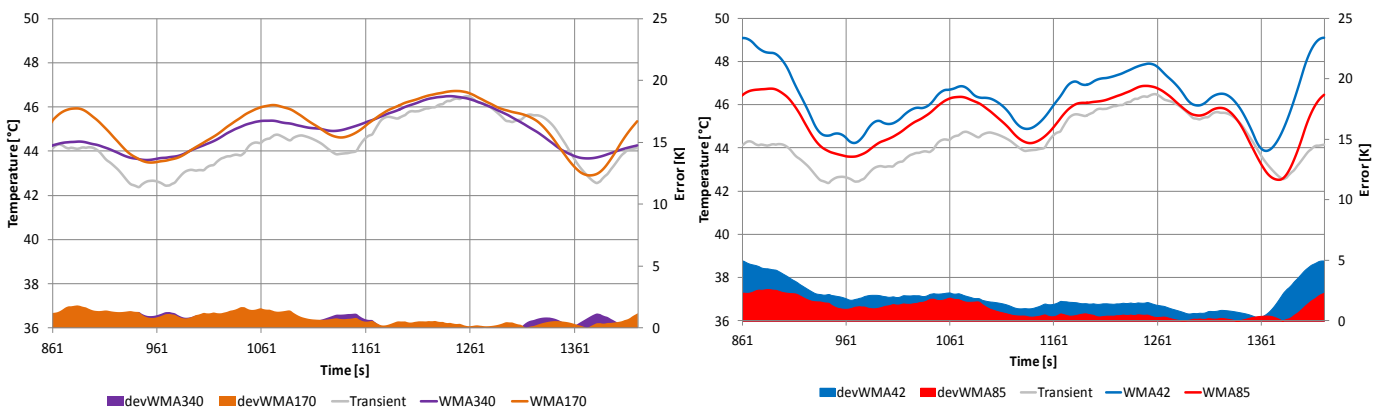


Figure 5.4: Heat Shield Comparison of WMA schemes to Full Transient (Time 861 – 1420)

The average deviation of the 4 investigated components within the sub-module based on each WMA scheme is presented in Figure 5.5. Here it can be seen that two contradicting patterns of accuracy are experienced within the system simulation. The exhaust component and corresponding exhaust heat shield tend to improve in accuracy with smaller sampling ranges of the WMA, whilst the predictions for the underbody heat shields and under-body panel deteriorate. This can also be seen within Figure 5.4 where the larger sampling ranges of the WMA have improved the temperature behaviour of the heat shield in comparison to the smaller WMA ranges. There are three possible reasons for this discrepancy, firstly the larger range WMA schemes suit the small fluctuation temperature behaviour of both the heat shield and under-body panel. Secondly, the introduction of more CFD solutions within the smaller range WMA schemes has resulted in an increase of error associated with the steady-state assumptions of each individual CFD solution. Finally since there are more CFD solutions within the smaller range WMA schemes the probability for interpolation errors between solutions (due to the mapping algorithm) also increases. However this decrease of accuracy is very small compared to the improvements of predictability on the exhaust system and close proximity exhaust heat shield.



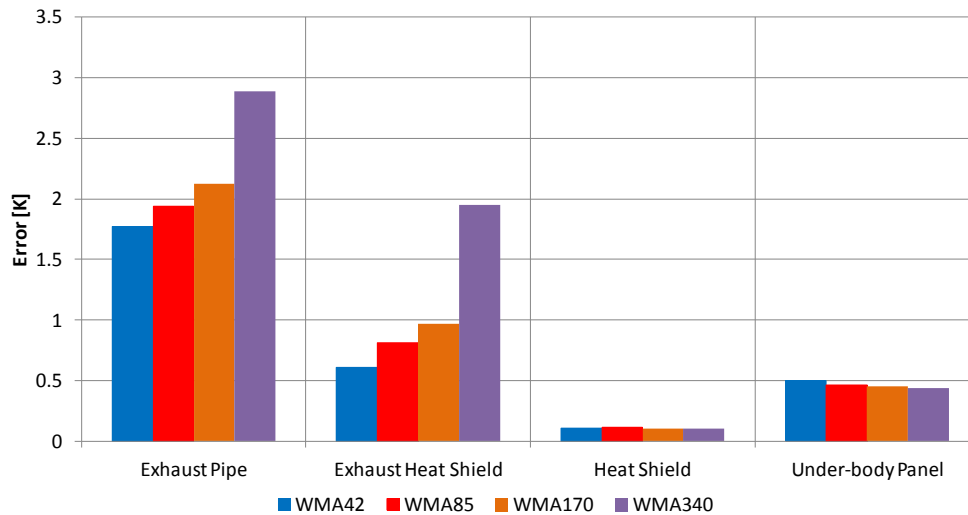


Figure 5.5: Error of WMA schemes to Full Transient for all parts

### 5.1.2 Derived Wavelet Profile - Exhaust Results

As described in chapter 4, the wavelet transform methodology produces a unique representation of the alternative frequency components inherent within the original boundary conditions. Identifying the critical frequency allows the engineer to establish what ranges of frequency are thermally irrelevant and can be discarded from the original boundary conditions to produce the simplified profile. This signal is then utilised to replace the original boundary conditions in order to accelerate the simulation via the potential application of larger time steps. Additionally one can employ the quasi-transient methodology in order to further accelerate the calculation time through the utilisation of steady state CFD points. Within the sub-module investigation the derived wavelet profile for the race-track conditions was explored. Unlike the WMA investigation component of stage 2, the simplified signal was evaluated via both transient and quasi-transient methodologies. This was to establish the error associated purely from the wavelet profile and identifying the portion of the total error associated with quasi-transient techniques.

Figure 5.6 exhibits the differences in component temperature between the real boundary conditions (here as a reference) and those resulting from the wavelet profile run in transient and quasi-transient. The percentage error for both simulations to the reference conditions are presented on the right hand side of Figure 5.6. One immediate observation that can be seen in Figure 5.6 is that the quasi-transient approach accelerates the warm-up phase of the exhaust component and therefore has a larger discrepancy to the reference data (denoted in blue). This is primarily due to the one way coupling of the quasi-transient methodology. Each individual steady state CFD solution is coupled to a steady state thermal model. Here fluid temperatures and heat transfer coefficients are mapped onto a transient thermal model at particular times, where the data is interpolated between points. Due to the CFD steady state solution being coupled to a particular thermal state the fluid temperatures are higher than what would be experienced in the warm up (with cold component conditions). This is not present under

transient modelling conditions (denoted in red in Figure 5.6) as temperature dependent information is cycled between solvers per time-step.

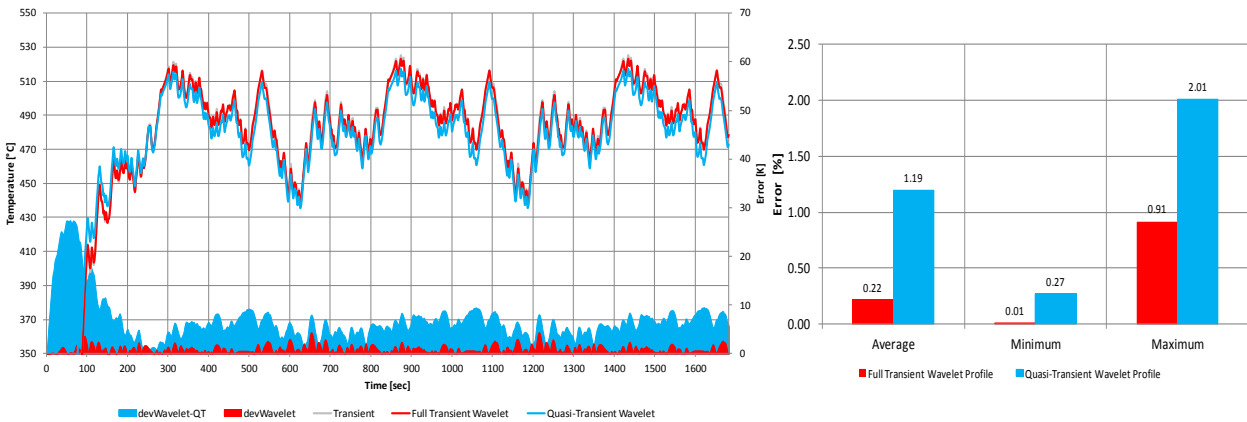


Figure 5.6: Exhaust Pipe Comparison of Wavelet Approach Full Transient to Quasi-Transient (left) and Error Comparison (Right)

An isolated section of temperature tendency can be seen within Figure 5.7. Here the influences of the wavelet profile in transient compared to quasi-transient can be realised. The quasi-transient solution continually under predicts the temperature behaviour of the exhaust component, exaggerating this in higher vehicle speeds (between 1600 – 1640 seconds). This can only be the result of the steady state nature of the individual CFD solutions traditionally representing the theoretical conditions if the vehicle remained at a constant speed for an infinite amount of time. Therefore it overestimates the convection (or cooling) under transient conditions.

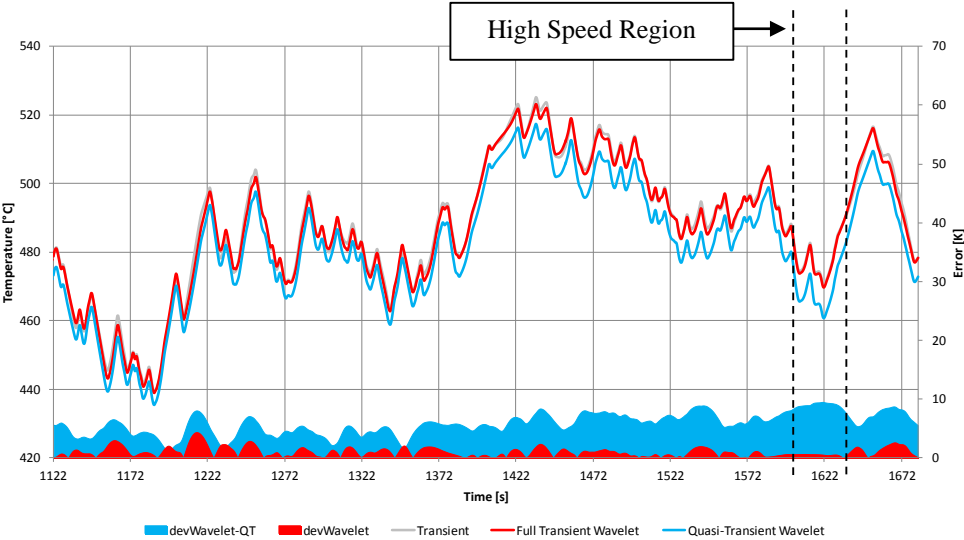


Figure 5.7: Exhaust Pipe Temperature Comparison of Wavelet Approach Full Transient to Quasi-Transient (Time 1122 – 1680)

A further look into the convective characteristic of the exhaust pipe (Figure 5.8) reveals that during the same period of high vehicle speed the convection rate introduced via the quasi-transient approach is substantially higher than the transient or reference conditions. This results

in the component experiencing lower temperatures. Again this can only indicate that that steady state assumptions over-estimate the vehicles convection due to the nature of the solution. Under maximum velocity conditions this over-estimation is exaggerated whereas for lower velocity conditions the error is substantially less (as seen in Figure 5.8).

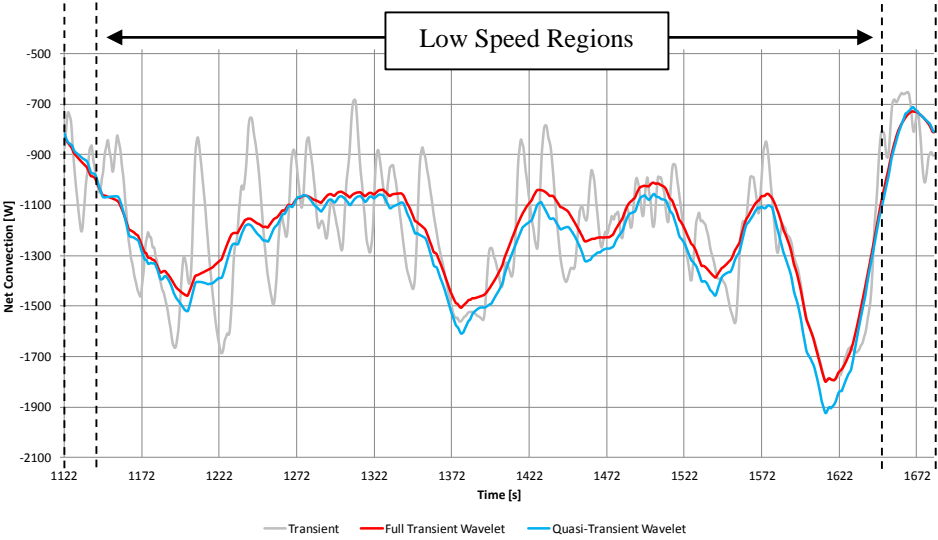


Figure 5.8: Exhaust Pipe Convection Comparison of Wavelet Approach Full Transient to Quasi-Transient (Time 1122 – 1680)

### 5.1.3 Derived Wavelet Profile - Heat Shield Results

Similarly to the WMA investigation the heat shield had higher discrepancies utilising a quasi-transient approach compared to that of reference conditions. Figure 5.9 provides the temperature behaviour of the component over time with respect to the reference conditions compared to the transient and quasi-transient wavelet approaches. On the right hand side of Figure 5.9 the average percentage error of the component can be analysed. Unlike the exhaust pipe the maximum percentage error introduced via the altering of the boundary conditions was between 2% - 3%.

This was further exaggerated with the quasi-transient approach resulting in a total maximum average error around 7 %. Therefore the influence of the steady state CFD points was approximately 5%. Considering the temperature conditions of the heat shield are substantially lower than that of the exhaust pipe these percentages correlate to an approximate error of 5K. This is an acceptable compromise for productive simulations within industry considering the time-resource advantages of the methodology. Again like the exhaust pipe the quasi-transient approach resulted in an accelerated warm-up phase constituting the largest error period of the total simulation (denoted in blue).

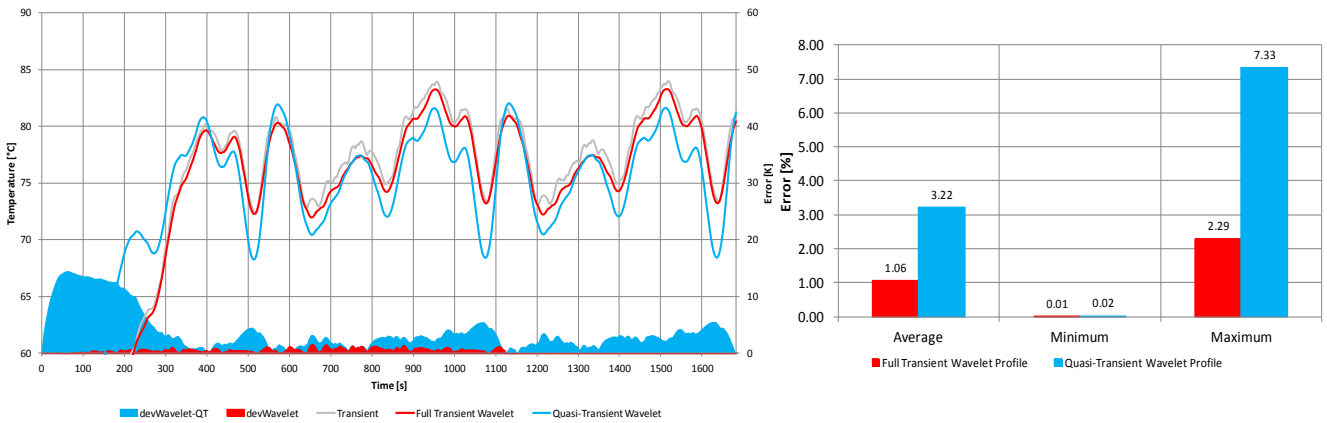


Figure 5.9: Heat Shield Comparison of Wavelet Approach Full Transient to Quasi-Transient (left) and Error Comparison (Right)

Additionally the minimum error is presented in Figure 5.9. This corresponding to the cross-over when the temperature behavior moves from under-prediction to over prediction or vice versa.

Time isolation of the temperature behaviours can be seen in Figure 5.10, whereby similarly to the exhaust component the quasi-transient solution continuously under-predicted the temperature behaviour. This correlates the enhanced cooling rates exposed to the component (Figure 5.11) in areas of higher vehicle speeds (1600-1640 seconds). Unlike the exhaust pipe convection rates the heat shield experiences an under-prediction in convection crossing over to a positive integer between the time periods of 1640 to 1680 seconds. This can be a result of an over compensation of the thermal part temperatures within the CFD solution, which in-turn over heat the contact fluid within the CFD model. The higher temperature fluid is then introduced to the transient thermal model, where it adds thermal energy to the component through convection rather than cooling the component.

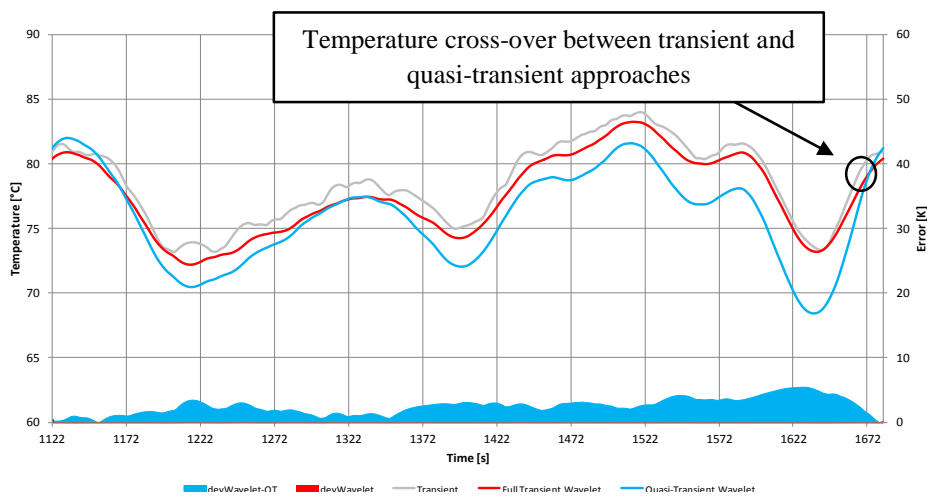


Figure 5.10: Heat Shield Temperature Comparison of Wavelet Approach Full Transient to Quasi-Transient (Time 1122 – 1680)

The cross-over of temperature behavior can be also seen in convection rates, where the quasi-transient begins to add energy to the components surface. This confirms that the thermal component state within the individual CFD solution is at a higher temperature than in the transient phase after 1640 seconds (Figure 5.11).

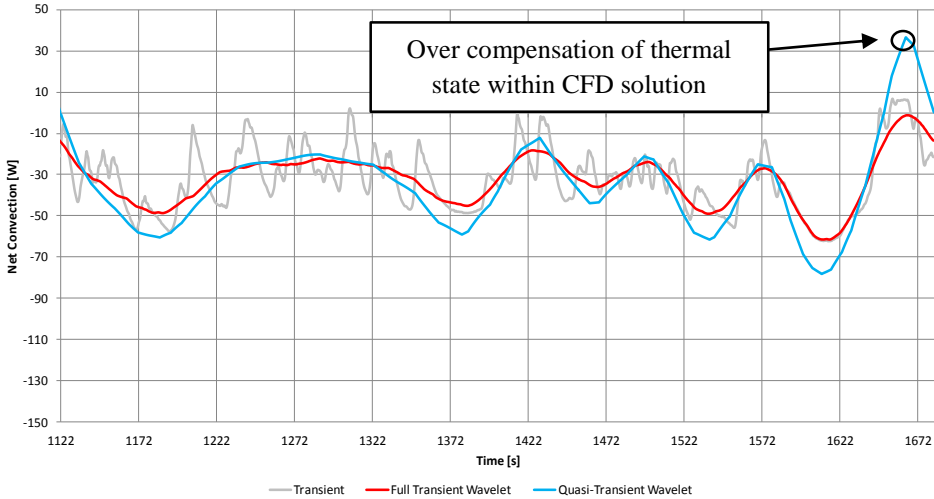


Figure 5.11: Heat Shield Convection Comparison of Wavelet Approach Full Transient to Quasi-Transient (Time 1122 – 1680)

5.1.4 Derived Wavelet Profile – Under-Body Panel Results

The under-body panel had the highest maximum error percentage in the quasi transient wavelet approach. This can be seen in Figure 5.12, where the component experiences an alternative temperature tendency to that of the reference and transient wavelet conditions. It is also important to note that the maximum discrepancy experienced within the quasi-transient wavelet approach was approximately 3K. Again this is satisfactory for the goals of this investigation.

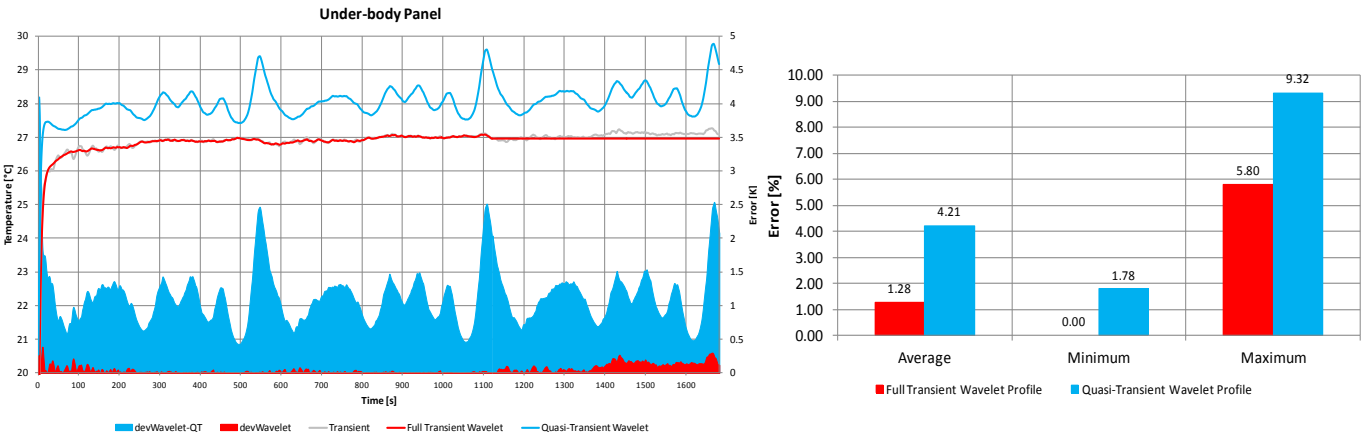


Figure 5.12: Under-Body Panel Comparison of Wavelet Approach Full Transient to Quasi-Transient (left) and Error Comparison (Right)

An isolated time range can be seen within Figure 5.13 whereby the temperature error of the quasi-transient wavelet approach is denoted in blue. Alternatively to the exhaust pipe and heat shield the under-body panel over-predicts in temperature behaviour.

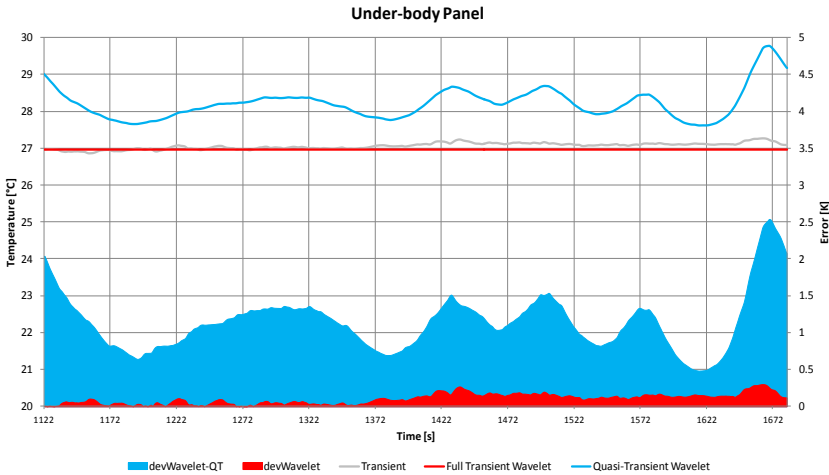


Figure 5.13: Under-Body Panel Temperature Comparison of Wavelet Approach Full Transient to Quasi-Transient (Time 1122 – 1680)

However its convection profile (Figure 5.14) clearly indicates an over extraction of energy compared to the reference convection and transient wavelet conditions. This can only mean that the core discrepancies apparent in the temperature behaviour are a result of interpolation errors along the large surface of the panel. This can engender both time interpolation problems as well as geometrical interpolation errors associated with the data mapping of CFD points. Due to the size of the discrepancy and the randomised behaviour patterns of this component it can be concluded that a systematic error is the likely cause.

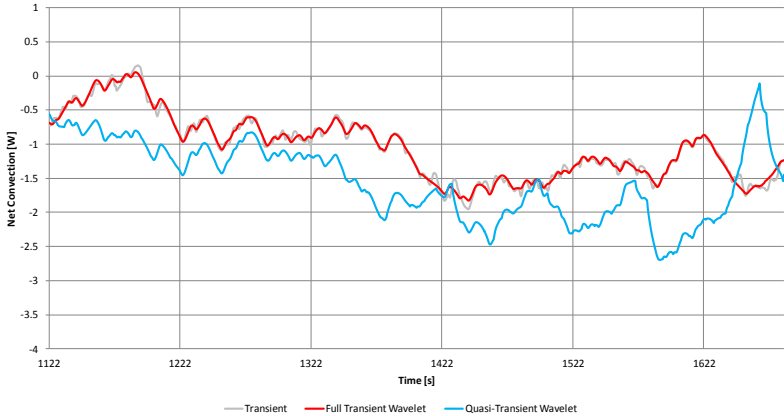


Figure 5.14: Under-Body Convection Comparison of Wavelet Approach Full Transient to Quasi-Transient (Time 1122 – 1680)

5.1.5 Effect of False Initial Temperature Results

One major influence which affects the overall simulation convergence of a profile (irrelevant to its simplification approach) is the initial temperatures of components. This is not only

important in the warm-up phase of a simulation but is crucial in alternative dynamic profiles where it is not necessary to start from ambient conditions. For full vehicle geometry this can introduce an additional complexity to the simulation, since not all components are the same temperature for the case of non-ambient start-ups. In order to understand further the consequences of false temperature initialisation the sub-module components, alternative starting temperatures were investigated. These temperatures were selected from 0°C to 50°C with 5K intervals in combination with a WMA simplification scheme. This allows for an investigation of the relationship between the simplifications errors coupled to the false initialisation temperature. The duration of the temperature error was monitored until it was converged to its natural solution tendency for that particular WMA scheme. Figure 5.15 provides an example of a component exposed to alternative initial temperature conditions (denoted by colour) compared to that of the transient reference behaviour (denoted in grey), where the number after IT refers to the initial temperature. IT\_20 corresponding to the original WMA produced temperature behaviour.

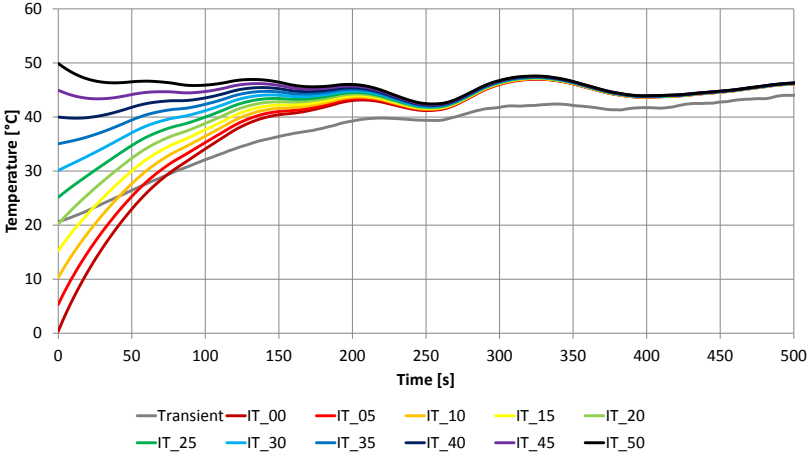


Figure 5.15: Effects of False Initialization Temperature on Exhaust Heat Shield

The thermal deviation is presented in Figure 5.16. It is clear that the simplification schemes also influences the time taken to reach thermal stabilisation (TS) for a given false initial temperature state. Additionally a cross-over pattern can be seen during the early time phase of the simulation, where devIT\_25 (the real component temperature state) commences at a 0 deviation. Additionally higher initialised temperature values (over 25°C) result in no cross-over. This indicates that the WMA scheme continually over-predicts the component temperatures.

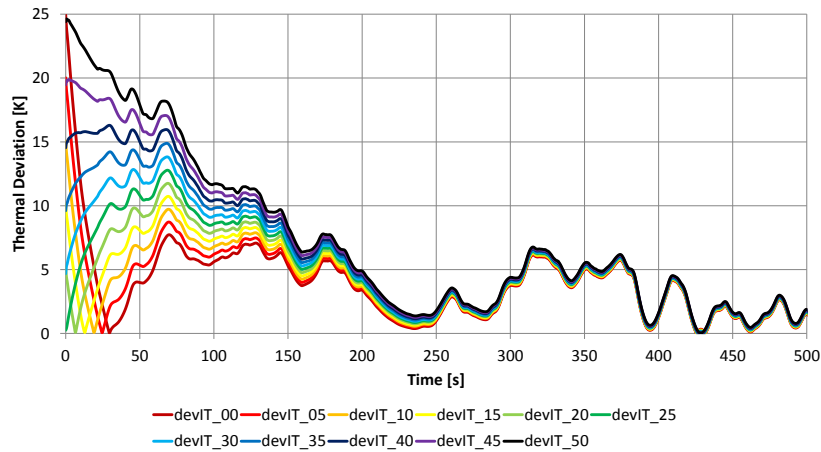


Figure 5.16: Deviation Associated with False Initialization Temperature on Exhaust Heat Shield

In order to isolate the error associated with simplification technique, the profile laps are subtracted from one another, leaving only the error associated with falsely initialising the component temperatures in combination with the quasi-transient approach. This can be observed in Figure 5.17 whereby nearly all components take over 400 seconds to reach TS. Thermal convergence refers to the deviation between temperatures of subsequent laps, where cvg represents the data labels of the alternative initialised temperatures. Additionally the component initialised with the correct temperature (cvgIT\_25) consist of a maximum error of 7 K. This correlated well with the previous investigation (Section 5.1.1) where the maximum error induced via the quasi-transient approach was of approximately 7K.

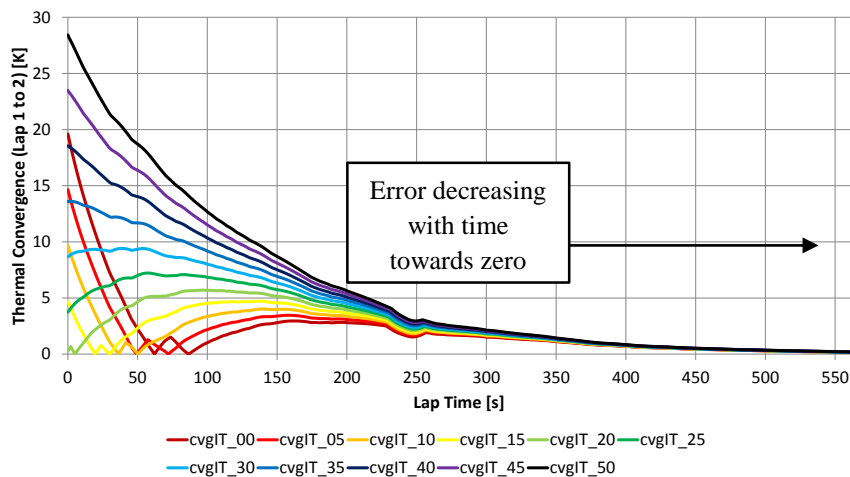


Figure 5.17: Thermal Convergence of False Initialization Temperature on Exhaust Heat Shield

### 5.1.6 CFD Type Investigation Results

The type of steady state solution selected for the quasi-transient approach is critical in representing the time-dependent convective characteristics (heat transfer coefficient and fluid temperature) of the dynamic driving profile. Therefore an investigation on three alternative solution types was conducted in combination with a WMA simplification scheme. As discussed



in chapter 4, the three alternative solution types consisted of a warm (steady state coupled solution), a cold (steady state uncoupled solution) and an initial attempt at a mixing regime between solution types (here classified as warm/cold). The basic mixing strategy implemented within this investigation consisted of WS for acceleration phases and cold solutions for deceleration phases.

Figure 5.18 indicates the temperature behaviour (of the exhaust pipe) for alternative solution types based on the WMA to that of the reference transient solution. Here error is calculated based on temperature difference between the approach and the transient. This error is then average over the profile to create a percentage format. It can be observed that the cold solutions (those not coupled to a thermal solver) tend to improve the predictability of the warm-up phase (based on the error displayed on the left of Figure 5.18)

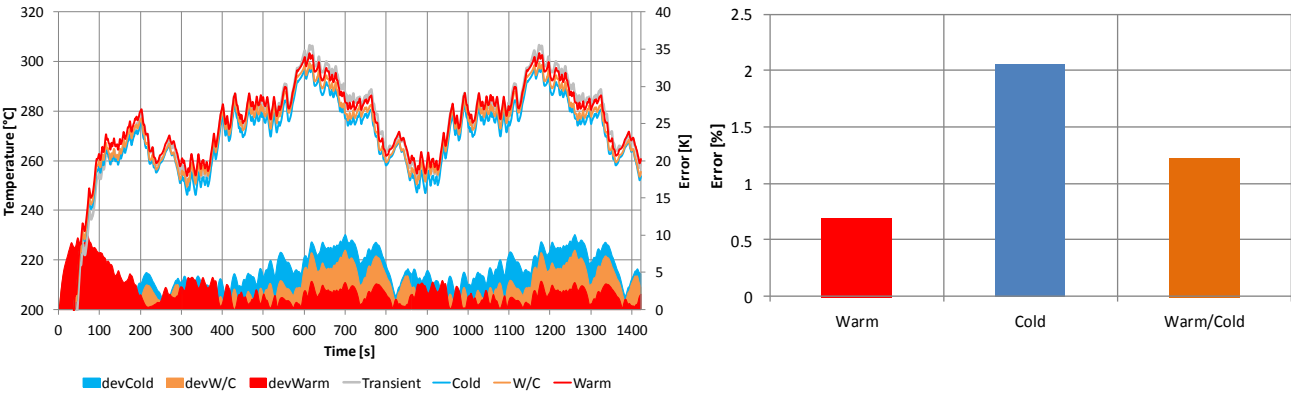


Figure 5.18: Exhaust Solution Type Temperature Comparison (left) with Error Comparison (Right)

This a result of the fluid temperatures within the steady state solutions better representing the convection during the cold start-up. Again the warm solutions tend to over-predict this phase similarly to the previous investigations of the WMA. The mixing between cold and warm solutions produces an error percentage between that of warm and cold (right hand side of Figure 5.18). This is a result of the mixing between both solutions types, where the error inherent in fluid temperatures for the WS are compensating with the CS.

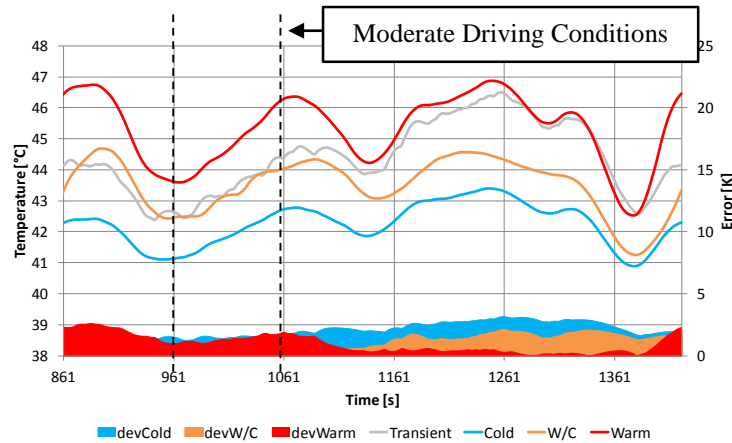


Figure 5.19: Heat Shield Solution Type Temperature Comparison

Figure 5.19 provides time isolation (during a moderate driving phase) temperature behaviour of the heat shield with corresponding solution types. It is clear that for this component the warm solutions are closely tied to the reference temperature behaviour. However the mixing of solution types better performs during the early phases of the profiles. This is due to the gradual fluctuation of velocity conditions between 961 and 1061 seconds, which consist of neither heavy acceleration nor deceleration. This example demonstrates that mixing can potentially accommodate circumstances where moderate driving conditions are experienced.

#### 5.1.7 CFD Quantity Investigation Results

Not only is the solution type important in establishing the proper heat transfer coefficients and fluid temperatures within the quasi-transient methodology, but also the number of steady state solution necessary to represent the convection conditions play an vital role in the overall thermal resolution. This is due to the interpolation aspects of the quasi-transient methodology. Therefore an investigation on the sub-module was conducted to evaluate the acceptable deviation of multiple solutions which are linearly interpolated to be used instead of the original boundary condition curve. The range of alternative solution quantities evaluated has been previously described in chapter 4. A section of the race-track profile was selected as due to significant component temperature change seen within experimental data during this phase [Hae13b]. The phase corresponds to the gradual acceleration (final straight) and deceleration of the race-track profile.

Table 5.1 provides the deviation of the linear interpolated solution quantities to the reference velocity conditions. With increasing number of solutions the percentage deviation varies from 8.9% with 4 CFD solutions to 1.62% with 24 solutions. Additionally the deviation tails off to a constant range about 1.5 % due to the linear interpolated nature of the quasi-transient methodology. The deviation is calculated based on the area difference of the linear interpolated profile to the original. The number of CFD points and their consequent locations within the profile are randomised in order to avoid biased results.

Number of CFD Solutions	% Deviation to Original Profile
4	8.95
10	2.65
14	1.83
19	1.63
24	1.62

Table 5.1: CFD Solution Quantity to Percentage Deviation of Original Profile

On the left hand side of Figures 5.20 to 5.22, an average error plot is provided corresponding to the three major components within the sub-module. Here it can be clearly seen that a tail off in accuracy is experienced past 14 steady state CFD points, after which no further thermal improvement is observed by increasing the number of solutions.

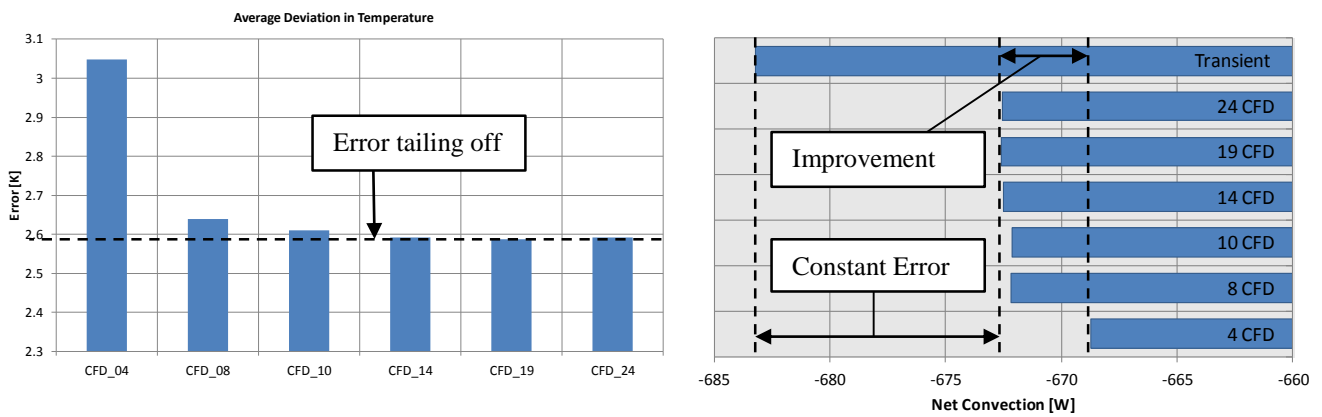


Figure 5.20: Exhaust Pipe Error Distribution on Solution Quantity (Left) with Net Convection (Right)

This can be compared to the convection rates (right hand side of Figure 5.20 to 5.22) per solution quantity type. Again a tail off tendency is experienced with convective energy past 14 CFD solutions. This clearly isolates the error induced via the quasi-transient approach independent of solution quantities. Additionally the errors experienced correlate very closely to the errors of the simplification approach addressed in the previous section. Therefore it can be stated that the potential of convection representation with CFD quantities has been reached past 14 CFD points on this particular profile. It is important to note that the location influences of the CFD points in all studies were not investigated, rather selected arbitrarily. This was done to neutralize the likelihood of positional based errors.

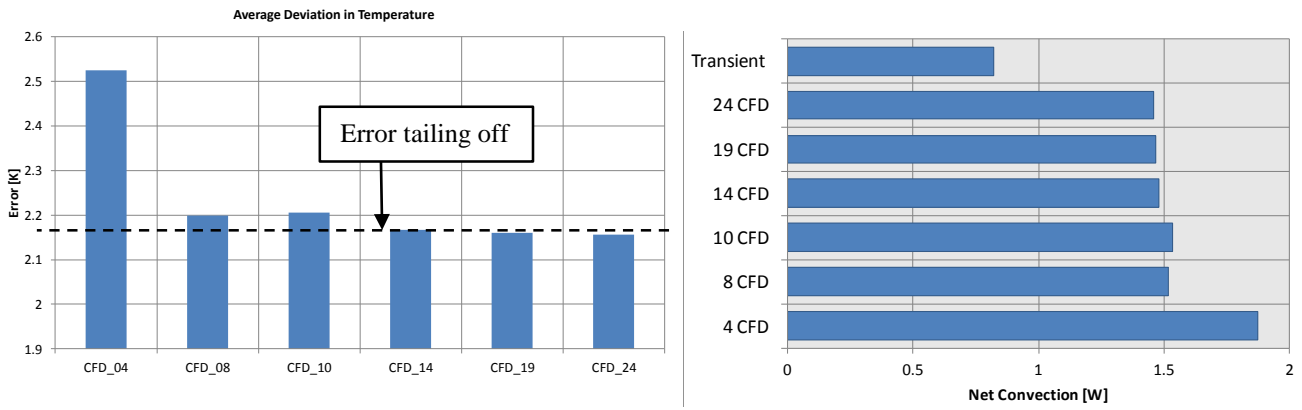


Figure 5.21: Heat Shield Error Distribution on Solution Quantity (Left) with Net Convection (Right)

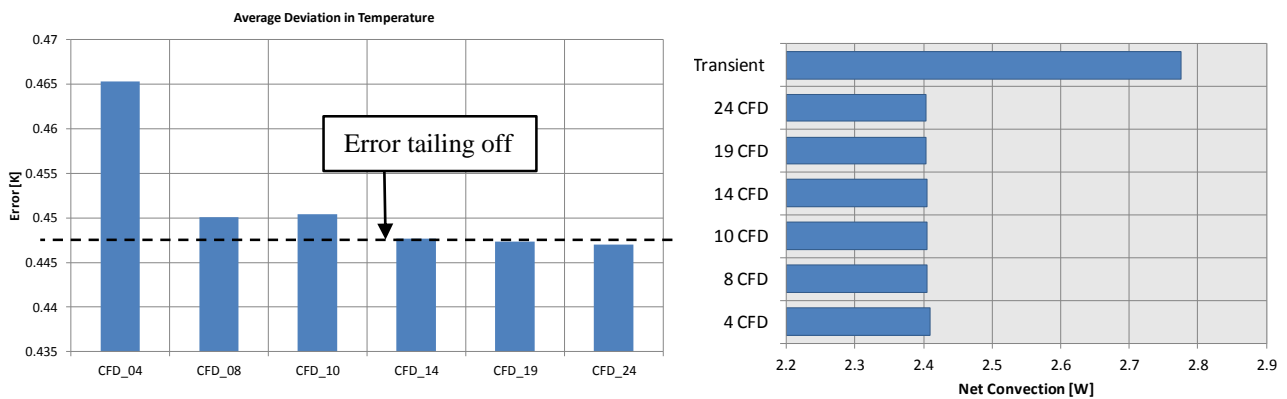


Figure 5.22: Under-Body Panel Error Distribution on Solution Quantity (Left) with Net Convection (Right)

## 5.2 Full Vehicle Configuration

In chapter 4, a methodology was explored to remove the high frequency components within the vehicle boundary conditions based on a critical frequency threshold derived from analytical analysis of the vehicle. This critical frequency was implemented to determine the amount of information that can be removed from the boundary conditions. Through the wavelet transformation methodology a simplified signal was derived based upon the decomposition level governed by the critical frequency. This footprint was the basis of the convection conditions simulated for the entire vehicle configuration. A quasi-transient approach was opted to represent the footprint signal by assigning a series of steady state CFD solutions and time interpolating between these solutions via a transient thermal solver. Four alternative dynamic driving profiles were investigated on a full vehicle numerical model in order to evaluate the potential transferability of the methodology. For this investigation 10 thermal sensor positions were selected based upon relevance (heat source), distribution along the entire vehicle (under-body panels) and alternative material conditions (heat shields). Additionally the same sensors were probed for each dynamic driving profile in order to establish a comparative analysis. It is important to note that not all experiments were conducted with the identical vehicle however with the same vehicle type. Each experiment was conducted in climatic wind tunnels whereby the vehicle was placed on a rolling dyno-meter. The dyno-meter replicated the resistance of the road, where the engine followed the load conditions of profile. The wind tunnel produced the

time dependent wind conditions which replicated the velocity of the dynamic driving profile. The tests were conducted multiple times per dynamic driving profile in order to ascertain confidence in the experimental data. This also ensures the integrity of the proposed methodology and its potential transferability. In the following section the experimental data is denoted in red, with corresponding simulation data denoted in black. Additionally the original boundary conditions are compared to the simplified signal (here defined as the footprint signal) for each investigated profile, accompanied with statistical information.

### 5.2.1 Race Track Profile

As previously discussed in chapter 3, the race-track profile can be considered the most thermally extreme driving conditions experienced by a vehicle during its operational life time. Therefore the profile naturally contains a large quantity of high frequency components associated with rapid velocity changes. This profile then becomes an optimal candidate (and first place to start) for this type of investigation. On the left of Figure 5.23, a comparison between the derived footprint signal and original driving conditions is displayed. A statistical overview is shown on the right hand side of Figure 5.23.

It is clear that the footprint signal has neglected a substantial amount of high frequency information (approximately 15%). The decomposition level for this particular profile was 7 levels with the original boundary conditions consisting of a 748 Hz maximum frequency.

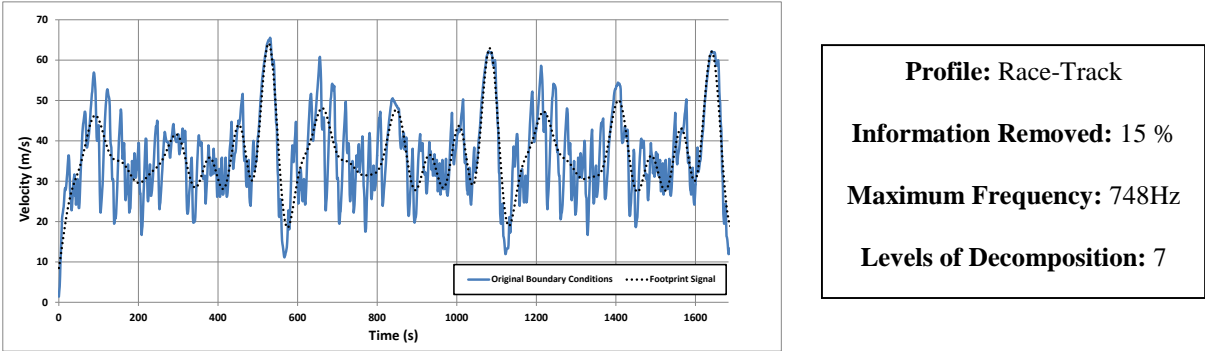


Figure 5.23: Race-Track Profile with Simplified Signal

Figure 5.24 shows two of the highest temperature components within the vehicle, the manifold and turbo-charger. Both components achieve very good prediction tendencies compared to the time dependent experimental data. One major observation which can be made is the immediate thermal discrepancies during the warm up phase (0 to 500 seconds).

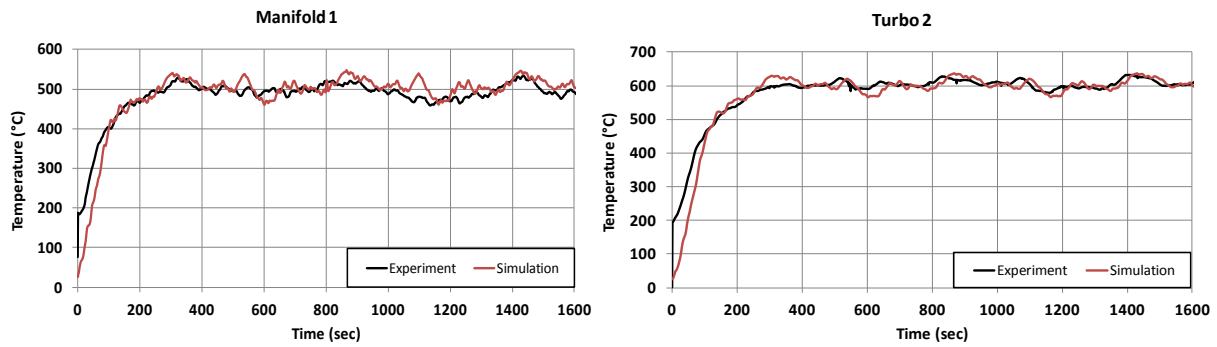


Figure 5.24: Manifold (left) and Turbo-charger (Right) Comparison

The simulation data on both components under-predict the time dependent temperature behaviour during this phase. This is contradictory to what was found in stage 2 of the research where the sub-module had the tendency to over-predict the warm up phase due to the thermal nature of the steady state solutions utilised. One reason for this discrepancy is the 1-D exhaust heat rate assumption made on both these components. Additionally the heat transfer coefficient is constant at every time step over the component surface. Both pulsation and entrance effects are strongly dominating the internal heat fluxes within these components. Therefore due to the cold nature of the component coupled to the acceleration phase of the vehicle (starting for 0 km/h) the 1-D steady state assumptions (per time step) of the internal heat rates are naturally compromised. Past the catalytic converter the effects of pulsation and entrance effect are neutralised. Therefore the underestimation of thermal behaviour during the warm-up phase is a result of miss-representation of internal heat rates coupled to the 1-D assumptions associated with their production. This can be clearly seen in consequent component temperature comparison (Figure 5.25 to Figure 5.28), whereby all subsequent probe regions result in the standard steady state induced over-prediction recognised in the prior investigation of stage 2.

In Figure 5.25 the catalytic converter and upstream connecting pipe are examined. Again a strong relationship between simulation and experimental data is formed. On the right of Figure 5.25 the catalytic converter (here denoted as CAT) surface temperature is displayed. The thermal distribution over the catalytic converter is also significant due to its upstream position in the exhaust tunnel. Therefore it is critical to probe the appropriate thermal location which corresponds to the thermo-couple position. This is further discussed in section 6.2.3. The major discrepancies occur during time periods 200 to 424 seconds and 575 to 800 seconds. Here the error range is approximately 25K, which is satisfactory for heat sources of such high temperature. It is to be noted that the convection rates (derived from CFD) mapped over the surface of the hot-end components can vary significantly with position. Introducing time interpolation between steady state points may increase the chance of misrepresentation of time-dependent phenomena such as turbulence.

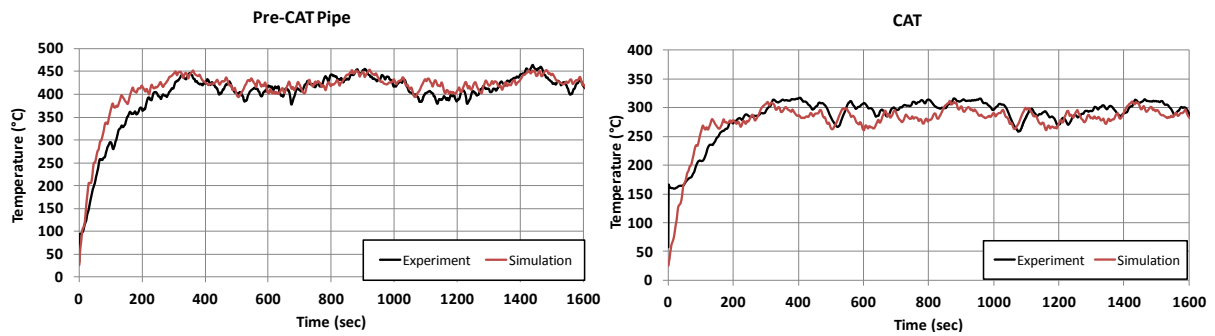


Figure 5.25: Pre-CAT Pipe (left) and CAT (Right) Comparison

One the take-down pipe (left of Figure 5.26), discrepancies seem to be an exaggeration of the component temperature behaviour. This can be seen around 1100 seconds, where the rise in temperature is approximately 25K more than the experimental behaviour. This particular error location is shared on the Pre-CAT Pipe (left of Figure 5.25), the manifold (left of Figure 5.24) and the under-body panel (left of Figure 5.28). Because of its occurrence on multiple components this may indicate that the source of error is strongly linked to the steady state CFD solutions utilised in this time frame. One conclusion that can be made is the over-prediction of fluid temperatures on the exhaust components (resulting in an exaggerated component temperatures rise) and therefore a consequent under-prediction of fluid temperatures on the under-body panel (resulting in lower component temperatures). The thermal energy balance between the exhaust component and the transportation of heat to the under-body panel has been misrepresented during this time period.

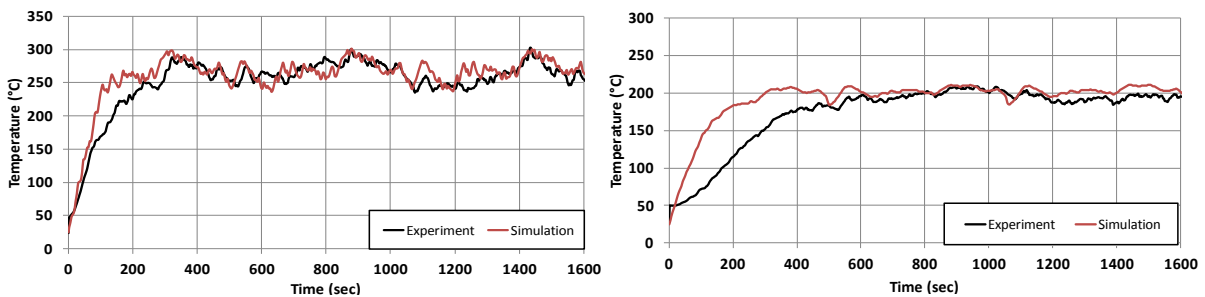


Figure 5.26: Take-Down Pipe (left) and Middle Acoustic Silencer (Right) Comparison

The acoustic silencers both middle (right of Figure 5.26) and end (left of Figure 5.27) produce substantially shorter warm-up behaviours compare to experimental data. Not only is the silencer system geometry simplified within the simulation (internal components, chambers, and perforations are not modelled), the 1-D internal heat transfer coefficients are averaged based on the chamber delegation. This methodology has proved successful under steady state conditions [Hae14a], however was never validated for transient boundary conditions, particularly chambers consisting of high amounts of porous medium and insulation. Additionally during the warm-up phase, gasses have not completely passed through these mediums from one chamber to another; therefore some chambers can be left without the presence of the hot gas until the pressures are high enough to force the gases through the porous medium. This can be seen with the experimental data whereby the temperature tendencies indicate that the only thermal transport mechanisms (which are contributing to the temperature change) are radiation and

conduction. One method to improve the estimation is to conduct a full 3-D simulation purely for the acoustic silencers in order to represent the time dependent flow conditions. However this is an expensive solution and the coupling arrangement becomes very difficult between sub-models and a full vehicle configuration. An additional error that is also contributing to the sharp rises in simulation tendencies on the acoustic silencer systems is the miss-representation of thermal mass. The systems are model as shells with artificial thickness and multi-layer arrangements to incorporate insulation. However the thickness and layers are dependent on uniform conditions. Therefore the assumption that is made is that the overall thickness is uniform around the component chamber. This is not always correct and can inherently alter the mass of the component. This can be also contributing to the accelerated warm-up conditions of the acoustic silencers. Once warm-up is achieved both acoustic silencers converge to the temperature conditions experienced within the experiment.

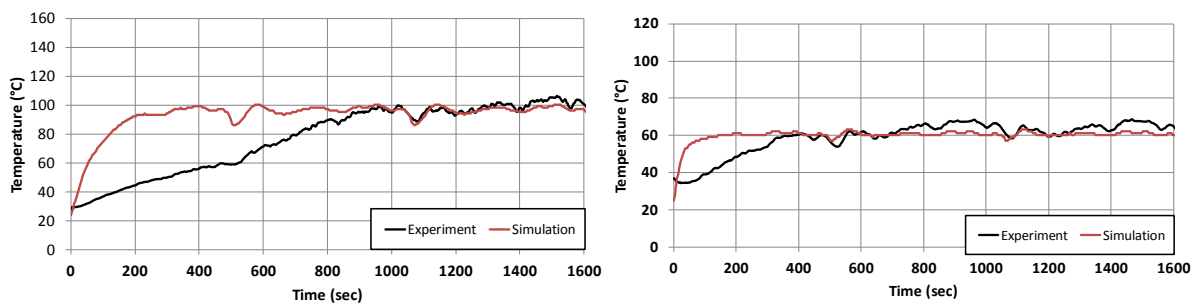


Figure 5.27: End Acoustic Silencer (left) and Underbody Heat Shield (Right) Comparison

The non-exhaust components investigated were of alternative type, material properties and geometrical configurations. The under-body heat shield (right of Figure 5.27) consists of an aluminium outer shell with porous insulation material, positioned in front of the under-body catalytic converter. Therefore the component was exposed to a substantial amount of radiation. The panels are generally larger area components consisting of a hard foam type material. The simulation tendencies for all three components proved to follow experimental data. Due to the location of the heat shield and its material properties only one conclusion can be made from the observed warm-up discrepancy. The uniform thickness implemented within the simulation has under-estimated the thermal mass of the component. Therefore similar to the engine floor panel (right of Figure 5.28) the temperatures rise prematurely and tail off to the standard temperature range experienced within the experiment. Even though the errors are small in comparison to the exhaust system further optimisation on the component representation needs to be conducted. This however it is not an easy task due to the unclear nature of the thermal properties of many of these types of components.



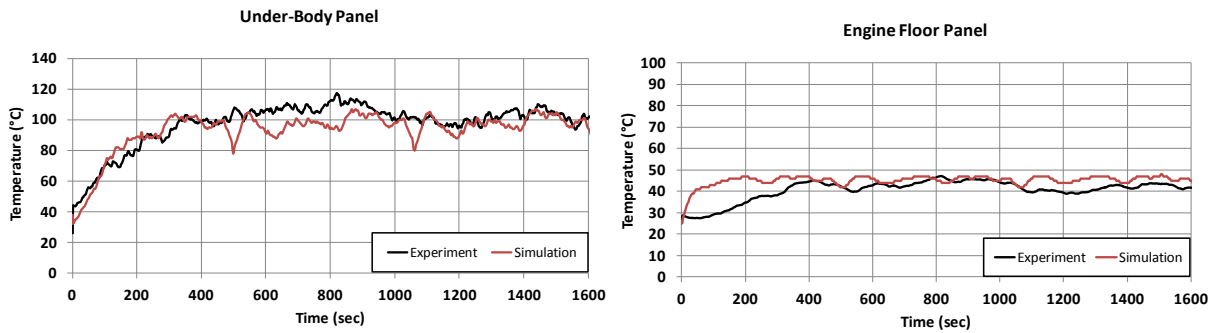


Figure 5.28: Under-Body Panel (left) and Engine Floor Panel (Right) Comparison

### 5.2.2 Handling Course Profile

The first step in evaluating the transferability goals was conducted on a similar high frequency profile, the handling course. The major difference between the handling course and the race-track profile was the magnitude of velocity fluctuations. Here, the handling course primarily consisted of vehicles speeds under 150 km/h. This was a good starting point to evaluate the process of eliminating high frequency information at lower vehicle load conditions. The comparison between the derived footprint signal and original boundary conditions are displayed on the left of Figure 5.29. Here similarly to the race-track profile a substantial amount of high frequency information removed. This was approximately 9.7% of the total boundary condition information within the experiment. The maximum frequency within the original signal was 570 Hz, which is over 150 Hz less than that of the race-track profile. For the handling course a decomposition of 6 levels was conducted.

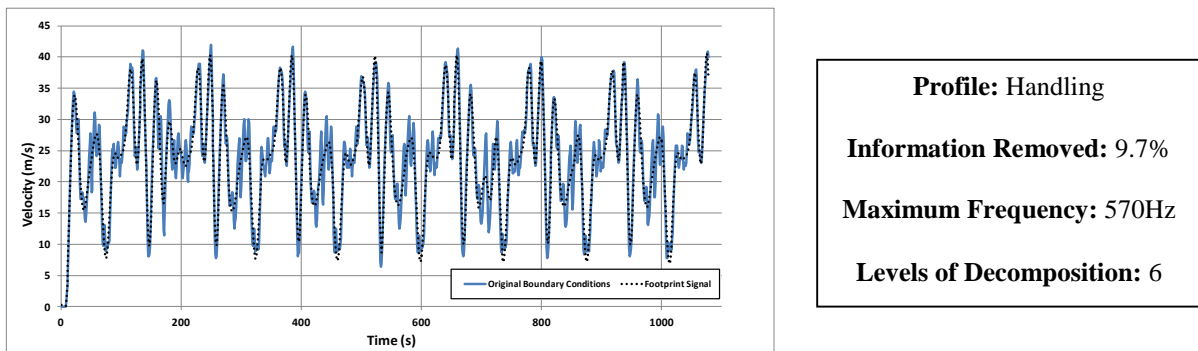


Figure 5.29: Handling Course Profile with Simplified Signal

The two high temperature exhaust components (seen in Figure 5.30) produced a strong tendency compared to the experimental temperature behaviours. Similarly to the race-track profile the turbo-charger performed extremely well with a slight under prediction during warm-up conditions. On the other hand the manifold produced a relatively constant temperature tendency fluctuating about 475 °C. The maximum deviation experienced by the manifold was approximately 25°C. This is acceptable considering the high temperature range of the upstream exhaust component.

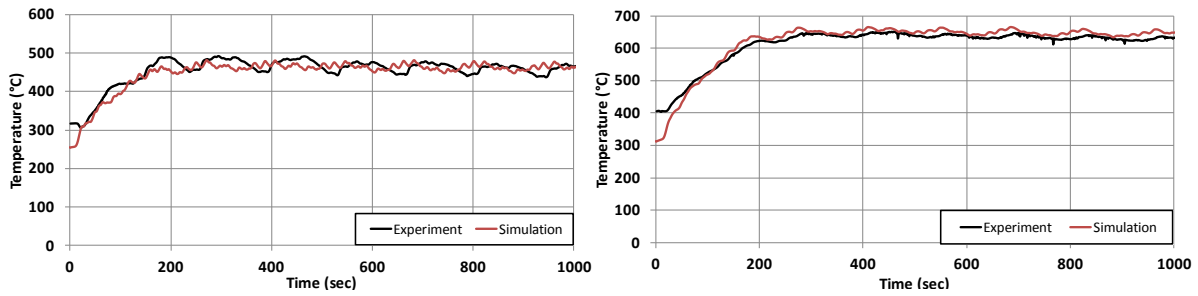


Figure 5.30: Manifold (left) and Turbo-charger (Right) Comparison

The same phenomenon is experienced on the pre-cat pipe as well as the catalytic converter (Figure 5.31). These components also fluctuate about a constant temperature unlike the race-track simulation. A factor contributing to this discrepancy was the frequency at which CFD solutions were mapped onto the thermal solver. This was on average every 31 seconds compared to the race-track profile of an average of 46 seconds. The nature of the handling profile also consist of highly rapid counteracting conditions, which in the quasi-transient approach results in extreme opposing CFD points selections. This has inherently neutralised the convection conditions over time resulting in relatively constant temperature behaviour of the component. One method to improve the solution quality on the manifold is to increase the amount of information removed from the boundary conditions, therefore smoothing out the footprint signal and reducing the frequency of CFD mapping periods.

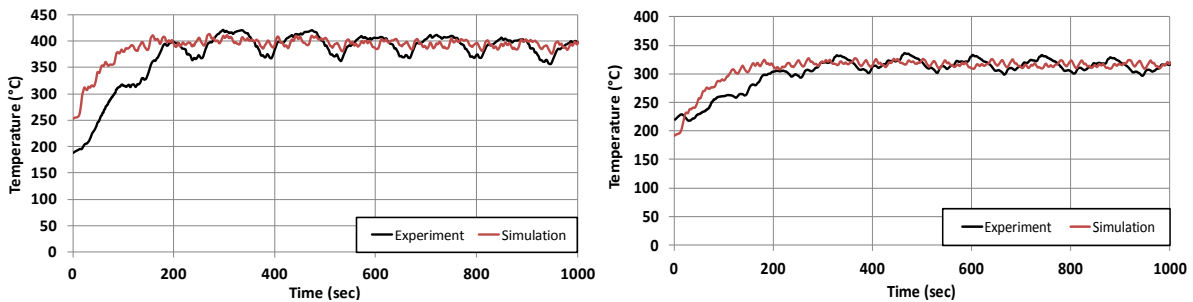


Figure 5.31: Pre-CAT Pipe (left) and CAT (Right) Comparison

As suggested in stage 2 of the investigation the quasi-transient method has resulted in a premature warm-up condition on the remaining component of the vehicle (Figure 5.32 to Figure 5.34). This is due to the excess thermal energy existing within the fluid temperatures of the steady-state CFD solutions. In order to minimise this error, the utilisation of cold solutions (or alternatively mixing solutions) could be incorporated in the warm-up phase. As the vehicle in this test was thermally pre-conditioned the initial temperatures on components are not of the ambient. Therefore it is clear that the initial temperature used in the simulation have introduced a carry on error which prolongs the component to reach thermal convergence to that of the experimental data.

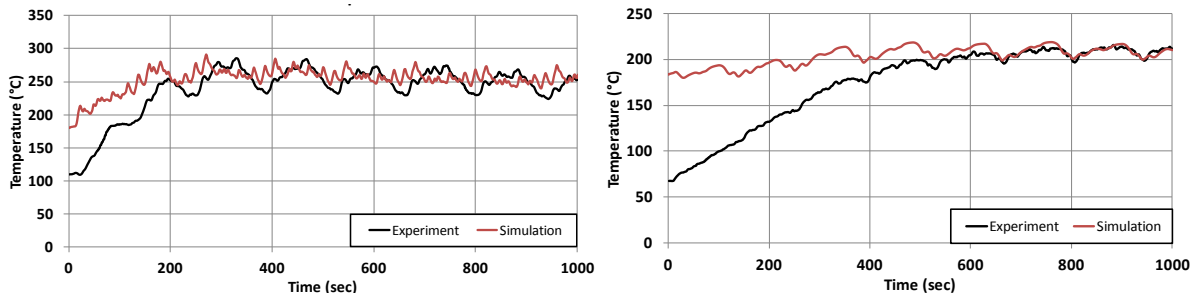


Figure 5.32: Take-Down Pipe (left) and Middle Acoustic Silencer (Right) Comparison

The acoustic silencers exhibit again a slow warm-up phase during the experiment, validating the conclusions of the race-track simulation. The delay periods themselves correlate very closely to that experienced on the race-track conditions. The middle acoustic silencer requires approximately 500 seconds reaching warm-up, whereas the end acoustic silencer requires approximately 800 seconds. This indicates that the chambers themselves independent of the dynamic driving profile require a certain time frame to reach thermal fluctuating conditions. The discrepancies seen in both race-track and the handling course on the silencer systems can be a result of the characteristic thermal masses within these components in combination with chamber stagnation of gases and component initial temperatures.

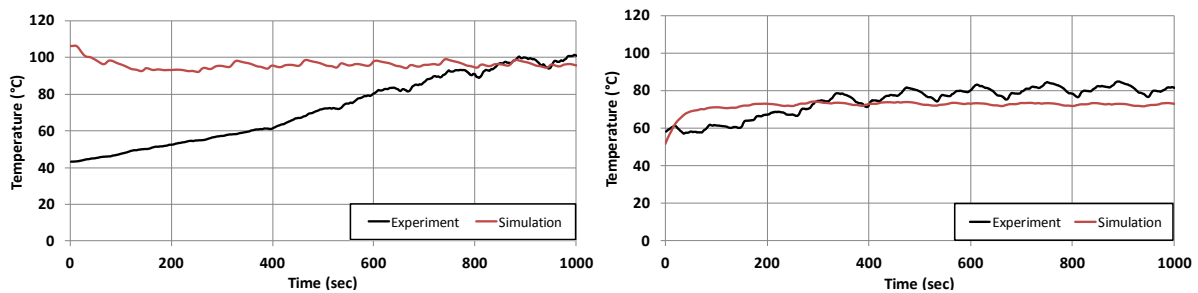


Figure 5.33: End Acoustic Silencer (left) and Underbody Heat Shield (Right) Comparison

The heat shield (right of Figure 5.33) and engine floor panel (right of Figure 5.34) both tail off to a constant temperature. The heat shield has an average error of 10 K whereas the engine floor panel displays an error of 5K. Both these predictions are satisfactory based on the goals of the investigation. Even though the under-body panel (left of Figure 5.33) is within temperature range of the experiment its localised tendencies are contradictory. It can be seen that this is a result of a particular CFD solution recycled multiple times during the simulation. The error due to the steady state CFD point was localised to two independent locations in the race-track profile. However in the handling course this is much more frequent.

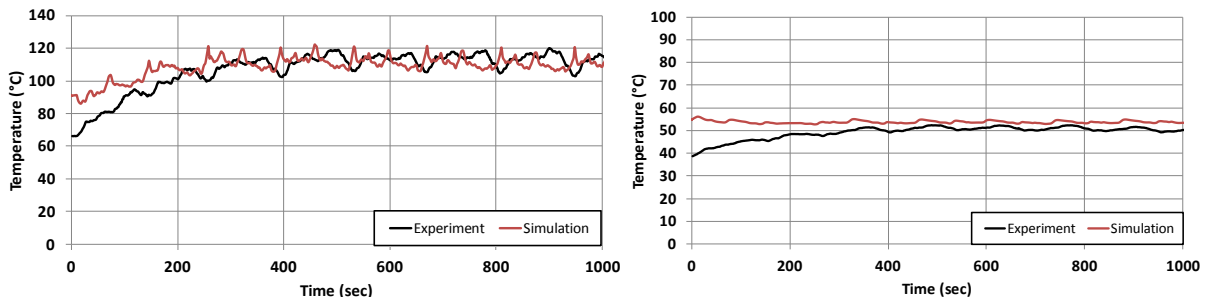


Figure 5.34: Under-Body Panel (left) and Engine Floor Panel (Right) Comparison

### 5.2.3 Highway Driving Profile

Proceeding away from the high frequency conditions of the previous driving conditions, the highway profile provides a hybrid case which is commonly explored within vehicle thermal management processes. As seen in Figure 5.35 the highway profile consists of a range of alternative driving characteristics such as a rapid acceleration/deceleration phase (200 to 400 seconds). The derived footprint signal can be seen as a dotted black line in Figure 5.35 whereby 8.89% of information has been removed from the original boundary condition signal. The maximum frequency within the original boundary conditions for this particular profile is 427 Hz again lower than the race-track and handling course profile. This has ultimately resulted in fewer levels of decomposition (in this case 5).

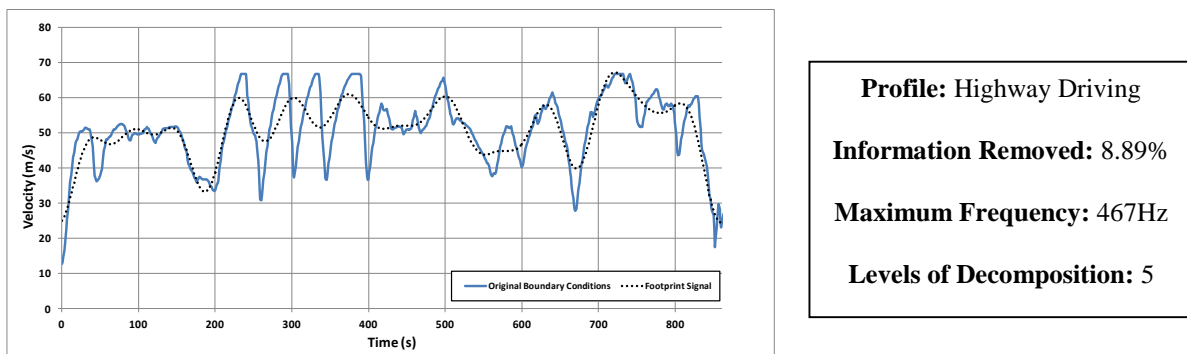


Figure 5.35: Highway Driving Profile with Simplified Signal

The manifold and turbo-charger (Figure 5.36) exhibit high accuracy prediction characteristics with a maximum deviation of approximately 25K. Unlike the previously profiles the pre-conditioning of the vehicle coupled to the quasi-transient warm solutions utilised, has resulted in minimal temperature initialisation errors.

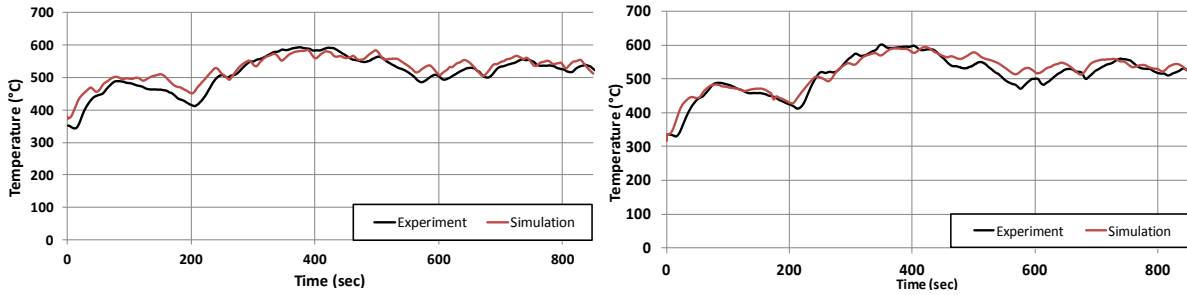


Figure 5.36: Manifold (left) and Turbo-charger (Right) Comparison

Due to this pre-conditioning no warm-up is observed. Figure 5.37 displays the relationship between the pre-cat pipe and cat to experimental information. Here it can be seen that pre-cat pipe consists of a temperature error in initialisation of approximately 75 K. Even though the temperature behaviour of the simulation resembles that of the experiment the initial error has consequently altered the total behaviour of the profile, reducing the amount of overall fluctuation. The catalytic converter exhibits similar tendencies, bouncing about the experimental conditions with a maximum deviation of 50K in the initial time frames.

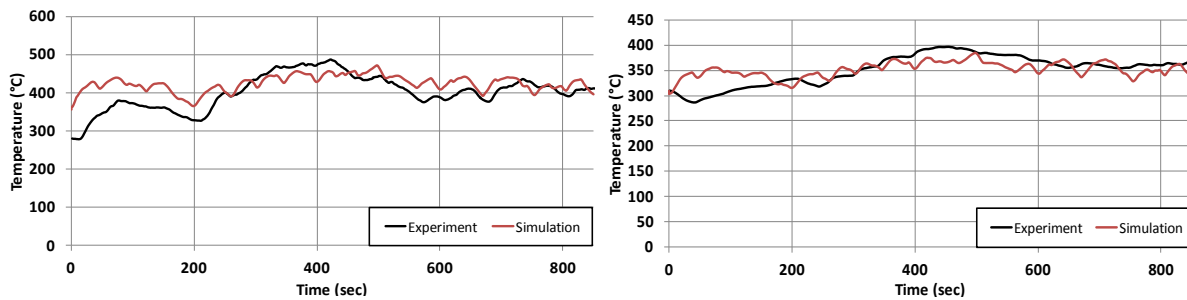


Figure 5.37: Pre-CAT Pipe (left) and CAT (Right) Comparison

One major observation that can be made is that the simulated results (independent of profile) of the pre-cat pipe, cat and take-down pipe (left of Figure 5.38) consist of slightly higher temperature fluctuations than that of the experiment. This can be an indicator the 1-D heat rates within these parts are over-estimating the surface temperatures.

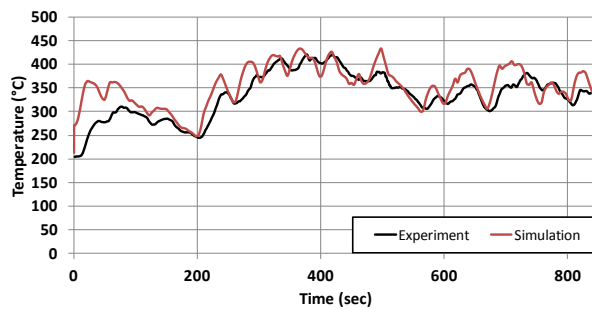


Figure 5.38: Take-Down Pipe

The end acoustic silencer (left of Figure 5.39) results in nearly perfect temperature behaviour with a maximum deviation of 10 K. This again validates the assumption that during the warm-up phase internal gas stagnation occurs within particular chambers creating a prolonged temperature behaviour. As the highway profile is pre-conditioned the gas chambers are

completely filled upon the experimental start. Therefore temperature conditions match those to the simulation very well due to the inherent warm solutions utilised.

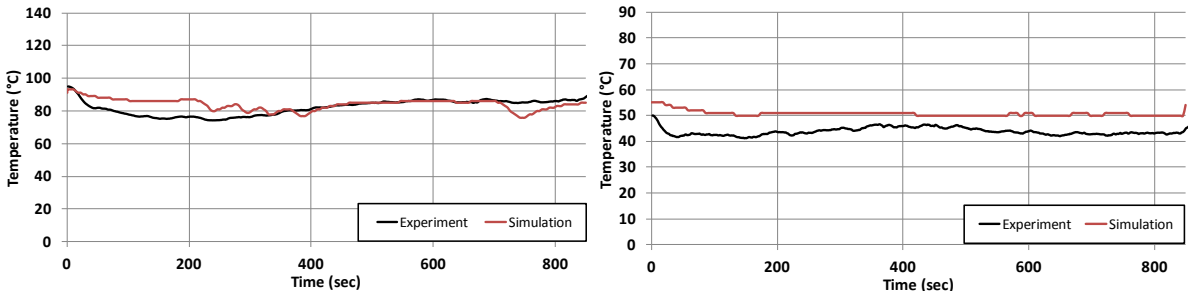


Figure 5.39: End Acoustic Silencer (left) and Underbody Heat Shield (Right) Comparison

Similarly to the previous simulated cases the under-body heat shield (right of Figure 5.39) consists of relatively constant temperature conditions with an average deviation of approximately 7K. On the other hand this discrepancy is substantially reduced on the engine floor panel (right of Figure 5.40). This indicates that the simplified signal is very well suited for thermally larger mass components under less dynamic conditions. On the left of Figure 5.40, the under-body panel temperature behaviour is displayed. Here a maximum temperature variation of 20 K is achieved. The area of primary error coincides between the time period of 350 and 450 seconds. This is identical to the error regions of the pre-cat and cat components. Considering that the under-body panel is in close proximity to the pre-cat pipe and catalytic converter itself, the convection conditions during that period can be at variance with real conditions. Examining the original profile one can observe that at the 350 second mark, the end phase of a rapid acceleration/deceleration is present, where entry to relatively constant speed condition occurs. Whereas the simplified signal (denoted as a dotted line) removes the rapid deceleration component and smooths out the volatility. This could result in lower (and smoother) temperature conditions. The primary cause of the discrepancy is a result of the interpolated steady state solutions to match the simplified signal which naturally has increased the rate of convection during that period compared to the experimental data.

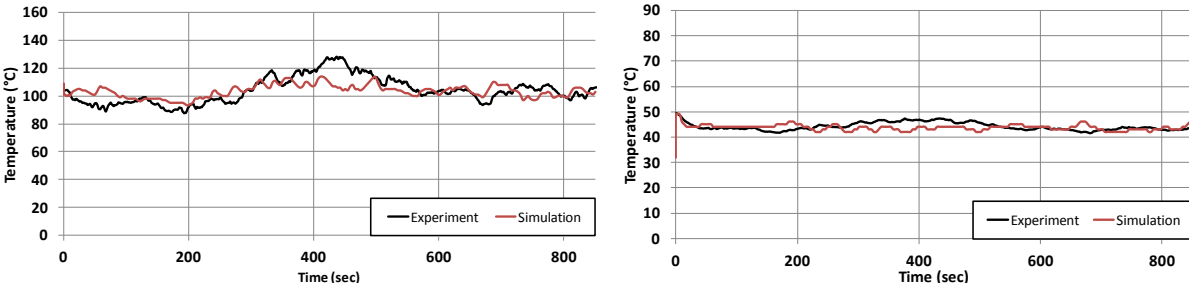


Figure 5.40: Under-Body Panel (left) and Engine Floor Panel (Right) Comparison

### 5.2.4 Street Driving Profile

The street profile is the final dynamic case evaluated in this investigation and consists of the lowest frequency within the original boundary conditions (maximum frequency of 392 Hz). Therefore it is an interesting case to evaluate the ultimate reaches of the methodology. Figure

5.41 displays the vehicle boundary conditions compared to the simplified signal. The amount of decomposition levels necessary for this profile was 4 with approximately 6.9% information removed. One immediate observation that can be made is the gradual decay of decomposition levels and information removed with the respective frequency conditions of the investigated profiles.

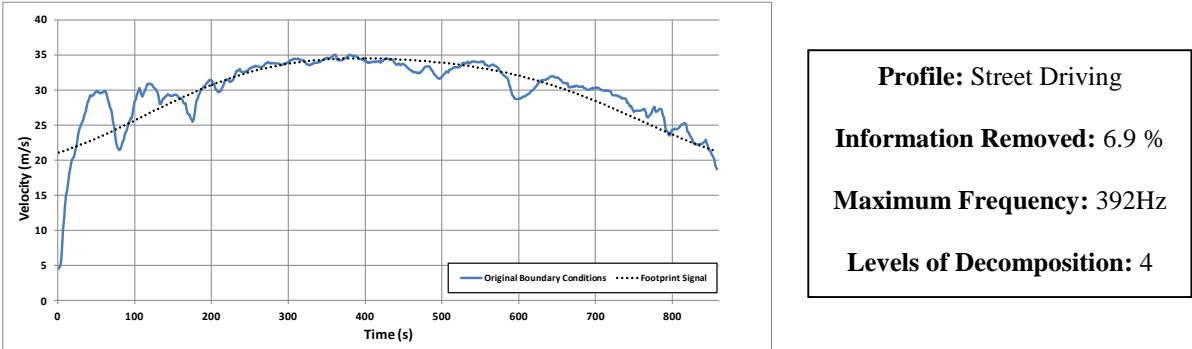


Figure 5.41: Street Driving Profile with Simplified Signal

The two upstream exhaust components can be seen in Figure 5.42 to exhibit overall very good temperature profile tendencies. This is also due to the lower dynamic conditions resembling the steady state nature of the utilised CFD solutions. Slight under predicts are observed in the turbo-charger during initial time periods. This is similar to that of the race-track and handling course, however substantially less in magnitude. This indicates the origin of the error to be fundamentally tied to the false initial temperature conditions. It also indicates the error within the 1-D exhaust heat transfer rate prediction.

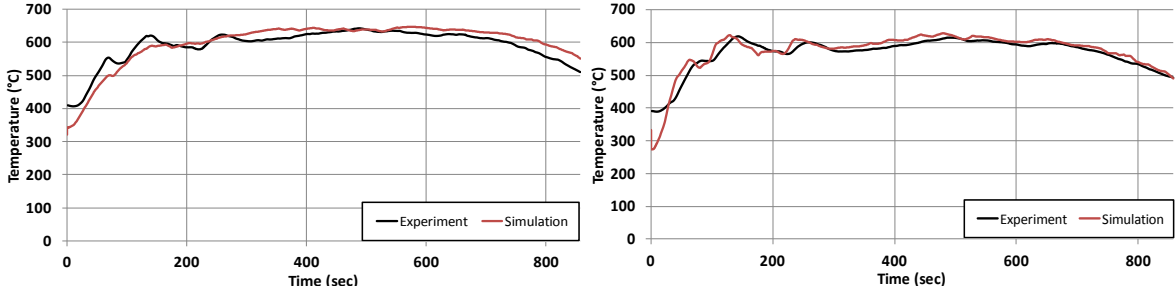


Figure 5.42: Manifold (left) and Turbo-charger (Right) Comparison

A smooth temperature tendency can be seen within the pre-cat pipe and catalytic converter components (Figure 5.43) which is comparable to the manifold and turbo-charger. The pre-cat pipe experiences a sharp temperature rise at time 780 seconds. This error is due to the 1-D estimated internal heat transfer rates which switch between one Nu number correlations to another. The error can be minimised by altering the switch or by smoothing out the transition between internal heat transfer coefficients.

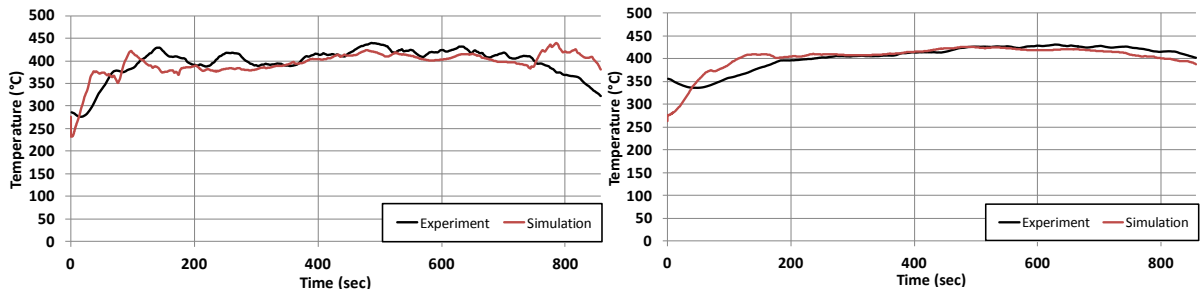


Figure 5.43: Pre-CAT Pipe (left) and CAT (Right) Comparison

In Figure 5.44 the temperature behaviour of the take-down pipe and middle acoustic silencer can be observed. Here the maximum deviation between both parts is 25K and falls within the pre-defined investigation tolerance.

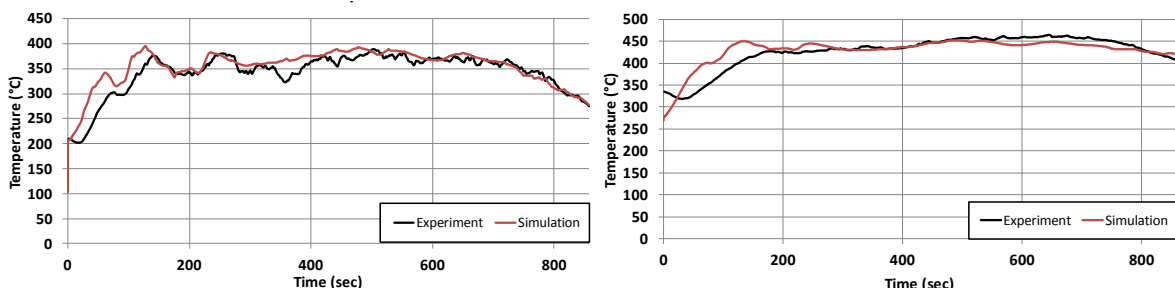


Figure 5.44: Take-Down Pipe (left) and Middle Acoustic Silencer (Right) Comparison

The end acoustic silencer (left of Figure 5.45) exhibits similar temperature trends as the experiment however a consistent under-prediction with a temperature offset of 12K is experienced. As mentioned previously the location of the temperature sensor is critical in sustaining the integrity of the comparison. However as many vehicles were experimentally validated there is a small uncertainty regarding the position of the sensor and whether it is in the identical location compared to the previous profiles. Therefore the consistent discrepancy indicates that the sensor has been slightly moved from the position.

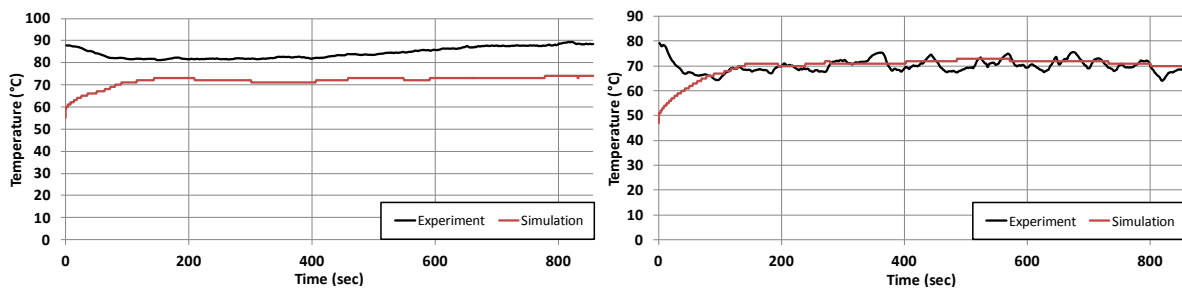


Figure 5.45: End Acoustic Silencer (left) and Underbody Heat Shield (Right) Comparison

The under-body heat shield (right of Figure 5.45) performs consistent with previous investigations. A constant temperature path is witnessed within the experimental data. The only error contained within the profile is the initialisation of temperatures. This is again due to the vehicles pre-conditioning aspects. These initial temperature errors can also be seen in Figure



5.46 with the under-body panel and engine floor panel. However both components stabilise at the temperature of the experiment. The temperature tails off to a constant value as previously experienced in the highway profile. However within the street driving profile the constant temperature behaviour of both components is exaggerated. This correlates well to the quasi-dynamic nature of the profile and the utilisation of steady state convection conditions for the transient thermal model.

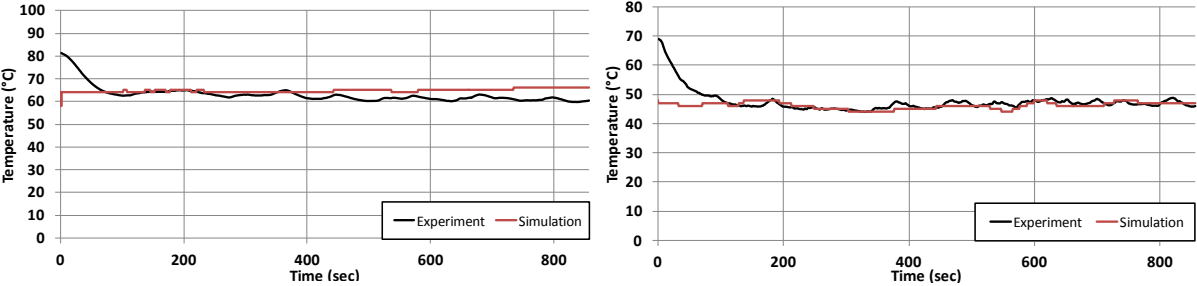


Figure 5.46: Under-Body Panel (left) and Engine Floor Panel (Right) Comparison

*Summary*

In chapter 5 results from several investigations corresponding to the development dynamic driving methodology are presented. The sub-module investigation provided a means of establishing the quantity of error related to the simplification of the boundary conditions. Additionally the error associated with the quasi-transient approach was also identified. A sensitivity analysis revealed error corresponding to the number of steady state CFD points utilised within the quasi-transient approach. The results from the full vehicle configuration were explored where common errors were seen between alternative driving profiles. These errors were identified as the 1-D assumptions made on the exhaust system, the initialisation temperatures of particular profiles, the utilisation of steady state CFD solutions and the representation of masses within the system. Within the next chapter, comparisons are made between multiple stages and individual investigation to derive conclusions from the results obtained within the current research project. Chapter 6 provides a deeper analysis of the results whilst justifying the proposed methodology based on accuracy, turn-around time and wider applicability.

# Chapter 6

## Discussion

In the previous chapter the results of several research investigations pertaining to the development of a methodology for dynamic driving were presented. The research philosophy of simplifying boundary conditions was discussed in chapter 3, where a series of sensitivity studies outlined in chapter 4 were conducted in order to evaluate the potential errors of a quasi-transient approach. The following chapter aims at discussing the results achieved from chapter 5 through analysing the relationship between several studies and their consequent outcomes.

### 6.1 Stage 2 - Sub-Module Discussion

The sub-module was utilised as a means of evaluating early simplification techniques. Here an assortment of alternative simplification approaches were explored, ranging from WMA schemes to wavelet transformation methods. Figure 5.1, in Chapter 5, provides a general comparison of the percentage deviation of each simplification technique to the original boundary conditions. Here it can be observed that the highest boundary condition deviation of approximately 7.5% was associated with a WMA sampling 60% of its series. This scheme produced an average overall component temperature error of 1.25%. Alternatively the smallest boundary condition deviation of 3% was experienced by a WMA sampling 7.5% of the series range. The average component temperature error of this scheme was 0.725%. The Wavelet transformation consisted of 5% boundary condition deviation however resulted in the best approximation of the component temperature tendencies. The temperature error associated with the usage of a wavelet transformation method was approximately 0.64%. Considering that the WMA sampling 7.5% series range consisted of more individual steady state CFD points than the wavelet transformation, the additional accuracy coupled to the economic nature of the wavelet transformation indicated promising potential for full vehicle calculations in Stage 3.

One additional aspect that was considered was the transferability potential of the wavelet methodology to alternative driving profiles compared to the WMA schemes which were inherently dependent of series range. The ability to determine the critical frequency allowed the wavelet transformation to be applied to all dynamic driving signals to produce the simplified version of the signal without the need to adjust the series range under standard averaging schemes. This drastically accelerated the pre-processing time in stage 3, reduced the number of steady state CFD solutions for the quasi-transient approach and ultimately resulted in faster turn-around times for the full vehicle transient thermal simulations.

#### 6.1.1 Boundary Condition Simplification Using WMA Schemes

When evaluating the simplification influences of a WMA on the boundary conditions of the sub-module it is very important to understand the influences of the quasi-transient method on the convective energy changes over time. Ultimately the error associated with the utilisation of quasi-transient approach to represent the time dependent convection characteristics of a dynamic profile is directly related to the number of the CFD points implemented as well as the employed boundary condition simplification scheme. The implementation of a smaller

sampling WMA scheme (and therefore more CFD points) does not always improve the quality of the solution and within particular parts may compromise its accuracy. This is due to the steady nature of the individual CFD points which are coupled to a steady state thermal solution. One way to analyse this phenomena is to extract the convection rates on individual components and compare them to their transient counterpart (here classified as the reference behaviour). Figure 6.1 (left) provides an example of the exhaust pipe convection behaviour under transient conditions (denoted in grey) and quasi-transient conditions for alternative WMA schemes (denoted as colour). It can be observed that larger WMA ranges dampen the high frequency fluctuations of convection whereas the smaller WMA's encompass these conditions. One useful technique is comparing the area underneath each of the convection profiles to that of the transient in order to ascertain the convection energy flux on the component. The time average error of each of these WMA'S compared to the transient can be seen on the right hand side of Figure 6.1. Here it is clear that decreasing the sampling range improves the representation of convection characteristics on the exhaust pipe, however, it introduces the dependency on higher numbers of steady state CFD solutions. The time interval within Figure 6.1, represents the convection behaviour after the warm up phase of the component. The error observed in Figures, 6.1 and 6.2 (right) is calculated based on the area of the net convection heat rates. Here the difference is measured between the simplification scheme and the original transient conditions.

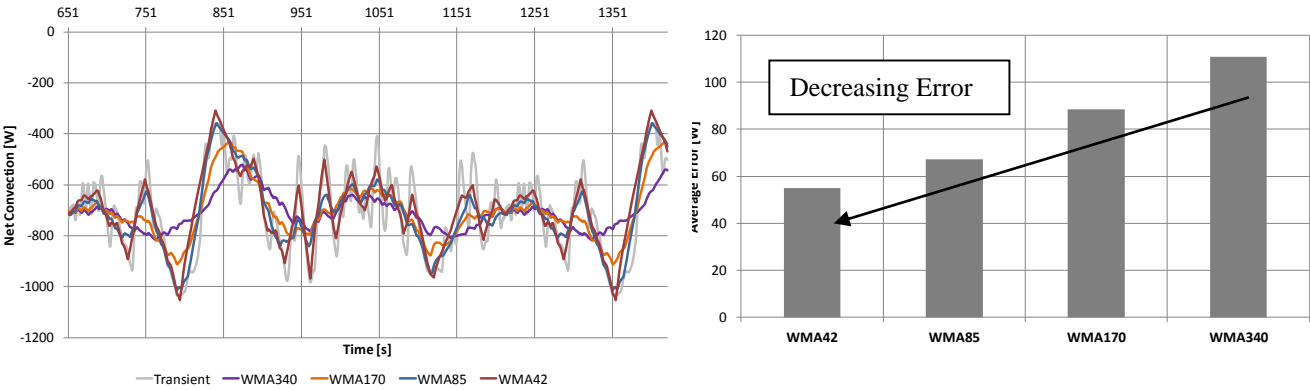


Figure 6.1: Exhaust Convection Comparison (left) with Average Error (right)

Alternatively Figure 6.2 presents the convection characteristics of the heat shield again in both transient (denoted in grey) and quasi-transient utilising the WMA schemes (denoted in colour). Here similar to the temperature behaviour of the component an opposing trend is observed. The larger range WMA's exhibit improved predictability. Therefore the time averaged error (right of Figure 6.2) is also seen to be less than smaller range WMA's.

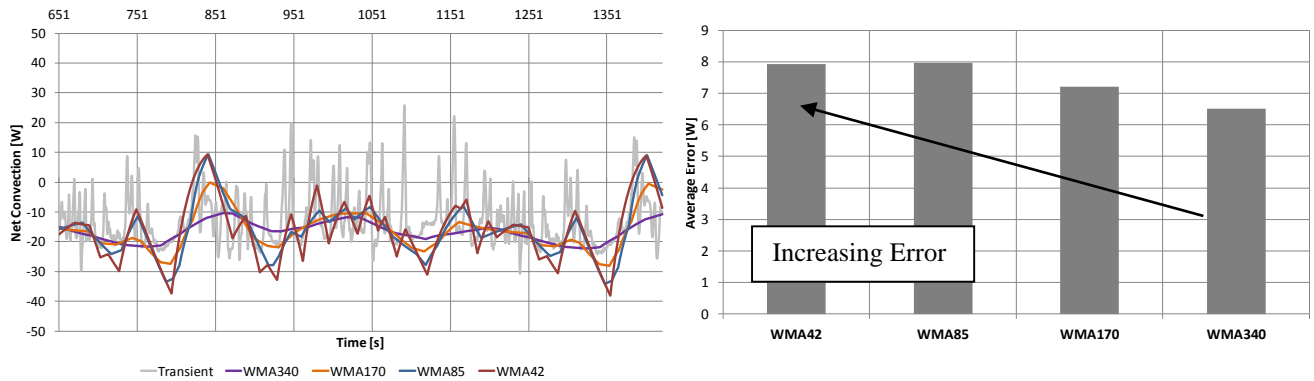


Figure 6.2: Heat Shield Convection Comparison (left) with Average Error (right)

One additional observation that can be made is the transient convection rates oscillating in both positive and negative states. This indicates that the heat shield receives energy (here heat) as well as loses energy from convection. This may explain the opposing accuracy trend of the WMA schemes (seen in Figure 6.1 and 6.2). The larger range WMA tends to average out the overall convective energy balance whereas the smaller ranges oscillate from positive to negative based on the steady state CFD solutions employed in the quasi-transient method. The differences in accuracy between components can also be due to the fact that the exhaust system is a convection dominated component (receiving thermal energy from the inside and losing heat from convection on the outside), where the heat shield primary source of energy comes from radiation and conduction paths.

As the exhaust system is the primary heat source the importance of improving its predictability is of a high priority to this investigation. Additionally due to the minimal variation in overall thermal accuracy on these components (seen in chapter 5) it is assumed that the influences of the alternative WMA schemes are negligible. Therefore the findings from this investigation indicate that a WMA scheme with a series range of 14% to 7.5%, produces an average temperature error under 3K for all exhaust components (Figure 5.5 in chapter 5). This is acceptable considering that the minimum experimental uncertainty induced for full vehicle configuration on climatic tunnels is 3K [Nat14].

The 7.5% WMA range (WMA42) inherently consists of higher quantities of CFD points and interpolation periods compared to the 14% WMA range (WMA85). This however only improves the accuracy of component temperatures by less than 0.5K. In order to improve the simulation efficiency and calculation times the bigger range WMA scheme (14% of series) was selected as the most optimal candidate for the race-track profile. This scheme was later evaluated on a full vehicle configuration which produced promising results and formed the first publication for race-track simulations [Hae13b].

The WMA approach has established that the fundamental boundary conditions can be altered (simplified) without compromising the thermal integrity of the simulation. Via the quasi-transient approach, improvements can be made on the turn-around times simply due to the fact that transient CFD calculation can be avoided. The time required to calculate a VTM type simulation (as well as the resources necessary to do so) is the deciding factor in the global adoption for highly dynamic simulation initiatives within industry. However one major

disadvantage of the WMA schemes was their dependency on the profile series range. Where some worked well for the race-track profile the same series range could not be adapted to alternative dynamic driving profiles as the simplified conditions were not representative of the convectional characteristics. This was further exaggerated when the boundary conditions consisted of alternative time-steps to that of the race-track profile, resulting in the compromised simplified profile. In order to promote transferability and achieve the second objective of this investigation a new signal processing technique was explored, the wavelet transform.

### 6.1.2 Boundary Condition Simplification Using Wavelet Transformation

Deriving the simplified boundary conditions from the wavelet transformation methodology (discussed in chapter 3) established the amount of information that potentially could be removed from the signal. However the application of the simplified signal introduced two process possibilities; a fully transient calculation or a quasi-transient calculation. In order to establish the error of both these process possibilities, simulations were calculated fully transient and also quasi-transient with the simplified signal as the new boundary conditions. The data was then compared to the results from using the original boundary conditions (in transient). In Chapter 5, it was seen that the maximum percentage error induced purely by altering the boundary conditions is under 1% for the exhaust system. Then by employing a quasi-transient approach to simulate the simplified signal a further error is introduced. Depending on component this error ranges from 2% to 9%. Therefore over approximately 50% of the maximum error introduced via the wavelet quasi-transient approach can originate from the steady state solutions utilised in combination to the interpolation between these solutions. The source of this error can be directly identified as the thermal state components under steady state conditions, which consequently affect the fluid temperatures and heat transfer coefficients. This also explains the early warm-up phases of component temperature tendency, where the convectional data (via fluid temperature) can be seen to add energy to a component (Figure 5.11 in chapter 5). Additionally the assumption of steady state time interpolation (here linear) may misrepresent the turbulent nature of the flow, which has an immediate influence on the heat transfer rates. This can be seen in the previous Figures 6.1 and 6.2, where at many times the linear interpolation under-estimates the transient heat rates.

The wavelet transform methodology indicated strong correlations to that of the reference conditions under transient conditions. With approximately 15% of information removed from the signal the corresponding error purely from this simplification was 1% for the primary heat source. This validates the assumption that high frequency components within boundary conditions do not significantly influence the temperature behaviour of components. This naturally is dependent on component thermal mass, and location. When utilising the quasi-transient technique the error increases. However with the potential cost savings in calculation time, the error introduced with quasi-transient techniques are comparable to that experienced with experimental methods. Therefore the quasi-transient approach coupled to the wavelet transformation methodology was utilised for full vehicle configurations which is discussed later on in the chapter.

### 6.1.3 Effects of False Initial Temperature Discussion

In Chapter 5, a further investigation was conducted to isolate the error of false initialisation temperature on components. The duration a component requires through the dynamic simulation to stabilise from an incorrect initialisation temperature can be useful in identifying offset component temperature tendencies. Figure 6.3 examines the small duration differences between each alternative initialisation temperature. Here the 0°C (cvgIT\_00 refers to no error on initialisation) produces the fastest convergence of 435 seconds, whereas 50°C (cvgIT\_50 refers to 50°C error on initialisation) produces a 4.8% increase in time to thermal stabilisation. These results clearly indicates the importance of understanding and implementing the appropriate thermal state of a system prior to a dynamic (or even non-dynamic) test case. The additional error introduced from false temperature conditions coupled to the error of steady-state solutions on a simplified profile can substantially alter the time-dependent behaviour of components. This can be seen later in the chapter with the full vehicle configuration under dynamic loading conditions.

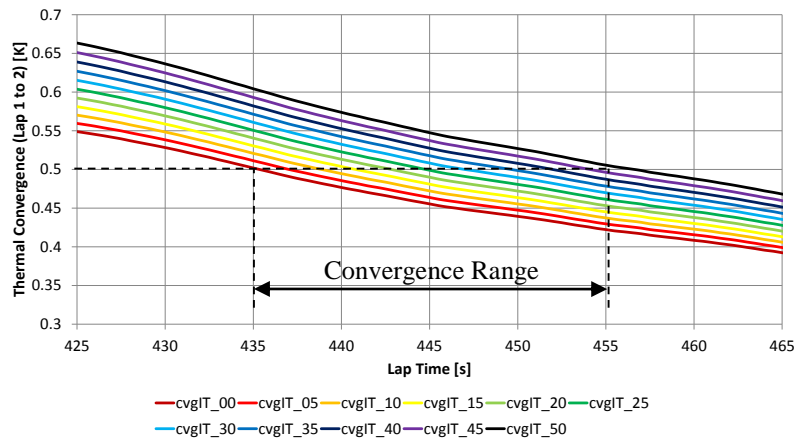


Figure 6.3: Thermal Convergence of False Initial Temperature Condition

### 6.1.4 Sensitivity of CFD Type

In order to evaluate the type of CFD solution necessary in a quasi-transient approach, two alternative CFD solution types were compared. One that was coupled to steady state thermal information (WS) and one that was not (CS). It was found that the CS type drastically improved the prediction of the warm-up phase on all components. Under these conditions the error remained under 2% for the exhaust pipe. However after the warm-up phase was completed the error of CS in the quasi-transient approach fluctuated around 3%, where component temperatures were continually underestimated. The WS type produced opposing results, whereby the error was highest during warm-up phase (approximately 3%) and drastically fell to roughly 0.8% afterwards. This is a clear indication of the influence of thermal state within the CFD solution, generally accelerating the warm-up when using WS and under-predicting the temperatures using CS.

One method to potentially compensate the effect of solution types on time dependent thermal behaviour of components is mixing the convective information between CS and WS. In Chapter 5, the results of a first attempt to mix solutions was presented. Here the warm-up phase

was improved compared to the WS approach however overall the mixing of solutions produced an average error of 1.5%. This was double to that of purely running WS during the simulation. Therefore overall the simulation accuracy deteriorated when mixing arbitrarily. One major observation that was made was the location sensitivity of mixing a solution. Here it was found that in particular time locations mixing solutions improved simulation accuracy with an error under 0.7%. These time areas tended to reside in regions of medium acceleration and deceleration. This indicated a potential to correlate the mixing strategy based on velocity gradients. An example of such a time event can be seen within the convectional data in Figure 6.4. The mixing phases are indicated as boxes in the figure, where the first (denoted by 1) represents the gradual fluctuation of velocity conditions. The convection rates during the mixed solution tend to transition between warm and cold profiles with linear interpolation between them. These can be easily identifiable during driving conditions as WS are used for acceleration (positive velocity gradient) and CS are used in the event of deceleration (negative velocity gradient).

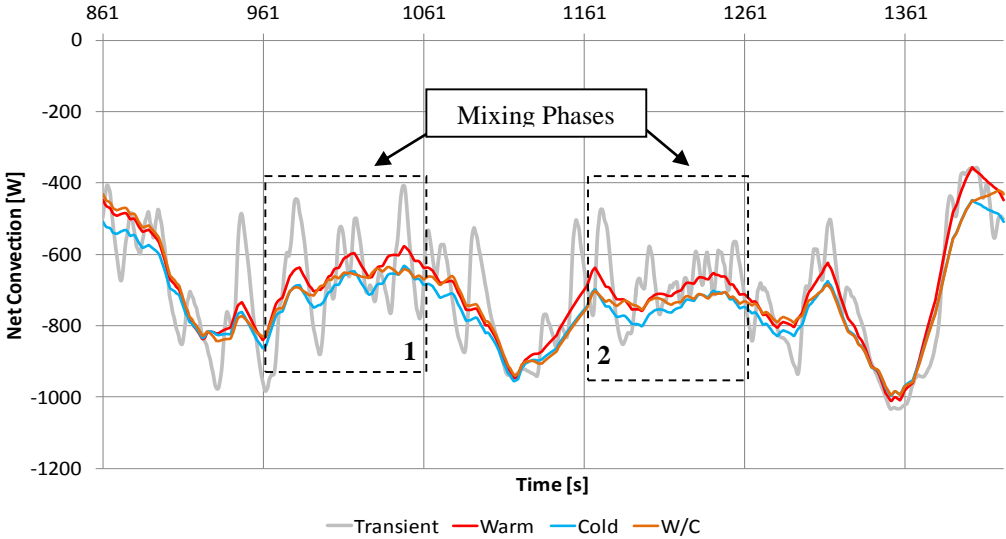


Figure 6.4: Exhaust Convection Characteristics from Solution Type

The second mixing phase (denoted by 2) corresponding to the time period of 1161 to 1261 seconds results in a poor representation of thermal behaviour on the heat shield (Figure 6.4). In this case the warm solution better predicts the temperature behaviour of the component. The primary difference between mixing phase 1 and 2 can only be attributed the frequency of velocity change during driving conditions. Mixing phase 2 corresponds to an aggressive fluctuation of velocity conditions, inducing heavy braking and accelerating in a short period of time. This can be further visualised by the transient reference conditions (denoted in grey) in Figure 6.4. The effect of this is higher component temperatures due to the mere lack of time for components to be exposed to proper convection flow. The components rise in temperature due to the exhaust gas but are cut short of convection from the rapid decelerations. This is a clear example that the mixing regime must also take into account the load conditions of the engine as well as the vehicle velocity.

The potential of mixing steady state CFD solutions as a replacement to either using WS or CS has been introduced. There are clear advantages in mixing solution types not only to improve

moderate driving convection conditions, but also the potential to mix solution (based on fractional percentage) to form new CFD solutions. This can be done via the velocity gradient in combination with the engine load profile. Future work is recommended in this field in which a clear criteria could be derived based on the gradient of velocity and the engine load to produce a fractional mixing strategy between multiple solution types.

### 6.1.5 Sensitivity of CFD Point Quantities

In addition to type of CFD solution, Chapter 5 presented the results of a study on CFD quantities and their effect on convection resolution. Here the error introduced from linear interpolation was examined. The linear interpolation between points compared to the original boundary conditions established the deviation of the quasi-transient profile to that of the simplified signal. The maximum error introduced was 1% with a profile deviation of approximately 9%. This correlated to using 4 CFD points. The minimum boundary condition deviation was 1.62% (utilising 24 CFD points) resulting in an average temperature error of 0.8%. The percentages are derived from the temperature errors (in kelvin) presented in section 5.1.3.

Figure 6.5 provides an example of the convection behavior patterns with corresponding solution quantities. The linear interpolation between points can be observed, whereby when increasing the number of CFD solutions, the convection patterns smooth out. This resembles the reference convection tendency (denoted in grey) of the component. However it can be clearly seen that increasing the quantities of CFD solutions arbitrarily does not equate to improvements in convection characteristics due to the linear nature of point interpolations. Alternatively one may select the directional changes in convection (when velocity gradient is 0) as means of determining the necessary CFD points, this has been seen in other publication [Kau07 and Pry11] available in literature.

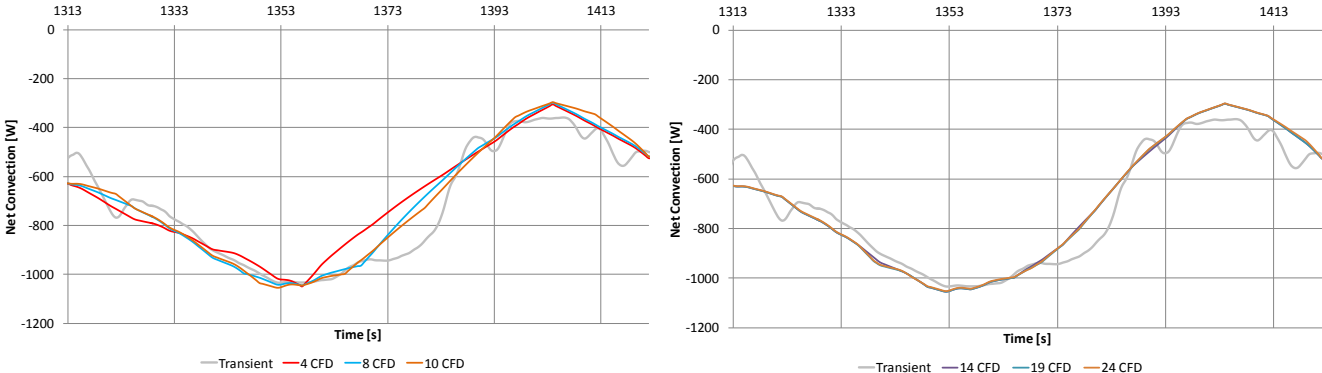


Figure 6.5: Exhaust Convection Characteristics from Solution Quantities

When increasing the number of CFD points it was shown (in section 5.1.3) that no further improvement was made after 14 CFD solutions for the given boundary condition profile. When converting the tail-off error into an average percentage of the different components within the sub-module, 0.8% was derived. This is representative of the error introduced from the CFD type (WS). Therefore for this given boundary condition it can be stated that the quasi-transient error cannot be negated by increasing the number of CFD solution due to the nature of the



steady state assumption made within each of the solutions. Additionally 1% of error can be equated purely from using a quasi-transient approach.

From this investigation certain outcomes can be established. Firstly the optimal quantity of steady state CFD solutions can be derived based on the gradient (or % deviation) of the simplified boundary condition profile to the quasi-transient interpolated profile. Based on this study the optimal deviation condition which corresponds to no further improvement in convection characteristics is approximately 1.8%. Therefore as discussed in section 4.3.3, an algorithm which analyses the profile can be used to determine the CFD points based on this deviation.

#### 6.1.6 Summary of Stage 2 Findings and Errors

There are 5 categories of findings produced within stage 2 of this investigation. These are the following:

- 1) Signal Simplification → It was found that certain degrees of simplification can be made to the fundamental boundary conditions without compromising the component temperature tendencies. The errors associated with the component thermal conditions could be identified based on the type of simplification utilised (WMA or wavelet). The wavelet approach resulted in average deviation ranging from 0.2% to 1% when run under transient modeling conditions.
- 2) Quasi-Transient Approach → The promising wavelet method was then evaluated under quasi-transient conditions in order to evaluate the associated errors of this assumption. It was found that the average error induced purely from quasi-transient approached ranged from 1% to 2.2%. This was primarily due to the utilisation of steady-state CFD solutions at particular time points in combination with the linear interpolation between time intervals.
- 3) Effects of Thermal Initialisation → It was found that the initial part temperatures can influence the thermal behaviors of components by introducing an additional error. Misrepresentation of component initial thermal state can lead to a propagating error throughout the simulation. Coupled to the highly dynamic nature of the boundary conditions, the duration needed to remove this error can range from 77% to 81% of the first lap under race-track conditions. This is a considerable time frame for this type of highly dynamic simulation.
- 4) CFD Solution Type → When implementing a series of steady-state CFD solutions to represent the time dependent convection, there is standard miscalculation of the thermal properties (heat transfer coefficients and fluid temperatures) during the simulation due to the nature of coupled or non-coupled nature of the solutions. It was found that on average the warm solutions (ranging from 0.4% to 1% error) performed better than cold solutions (consisting of 2% to 2.5% error). The cold solutions however improved the component thermal response during the warm-up phase. Therefore an initial mixing scheme was tested. This proved promising in moderate velocity conditions, however

more work needs to be conducted in order to establish a criteria for determining fractional mixing of solutions based on velocity gradient and engine load.

- 5) Quantity of CFD Solutions → The optimal number of CFD solutions (whereby no further improvement of accuracy could be achieved) to represent convective characteristics was found to be of 14 CFD points for the given boundary condition profile. This corresponded to approximately 1.8% deviation.

## 6.2 Stage 3 - Full Vehicle Discussion

The following section explores the integration of full vehicle geometry into the quasi-transient methodology for a variety of highly dynamic driving scenarios. The research outcomes achieved from the prior stage have been implemented into the dynamic driving tool (discussed in chapter 4) to establish the optimal conditions for the quasi-transient. The full vehicle configurations were validated through experimental methods, whereby thermo-couples are placed onto components in order to monitor the time dependent temperature behaviour.

### 6.2.1 Profile Analysis

One major goal throughout the investigation is the ability to have profile independence within the developed methodology. Profile independency not only justifies the validity of the investigated approach but also addresses the applicability of the entire research itself. The following section aims at reviewing the accuracy of each of the investigated component per profile in order to establish conclusions on the transferability potential.

Overall the race-track simulation produced promising results with small localised discrepancies, confirming that the original boundary conditions could be altered in combination with a quasi-transient approach to accelerate the calculation times. The handling course proved to be another successful example of the potential in altering the boundary conditions whereby the temperature tendencies of the majority of components correlated strongly with experimental data. The areas of discrepancies were common to that of the race-track confirming the sources of error. The highway and street profile exhibits the potential transferability of the methodology to less dynamic driving conditions. Amongst all dynamic conditions investigated, the street profile has demonstrated that even quasi-dynamic conditions can be reduced to a simple footprint signal. The quasi-transient approach is most favourable for the street driving profile as the quantity of CFD points employed did not significantly deviate from the original boundary conditions.

The following figures (Figure 6.6 to 6.10) provide an average accuracy of each component under the alternative dynamic driving profiles. It can be seen that differing accuracy tendencies are experienced based on component type, location and material properties. Within the manifold and turbo-charger components similar accuracy tendency are experienced, whereby the maximum error of approximately 7% is experienced under race-track conditions. The range of average component error independent of the dynamic profile, was approximately 4% to 7%. The estimation of error additionally includes the error of convection misrepresentation (via

quasi-transient methods) which can be equated (based on the former study) to approximately 2%. The convection profile follows the simplified signal therefore an additional 1% error can be addressed. The remaining error is a combination of inaccurate internal heat transfer coefficients from the 1-D assumptions and misrepresentation of component mass as discussed in chapter 5.

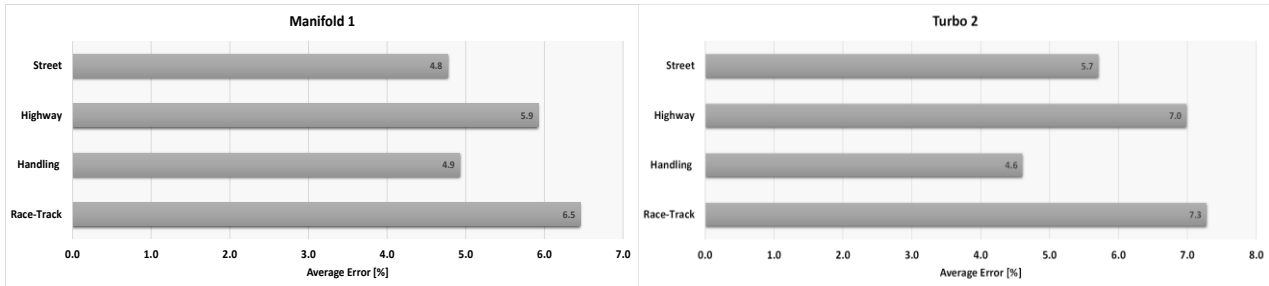


Figure 6.6: Accuracy of Manifold (left) and Turbo-charger (Right)

A linear accuracy pattern can be witnessed in Figure 6.7 for the Pre-CAT and CAT components, with one major anomaly being experienced on the CAT during the highway driving scenario. This decreasing tendency directly correlates to the volatility of each individual dynamic driving profile. Reducing high frequency changes automatically improves overall simulation accuracy. The anomaly experienced in the CAT component of approximately 15% error is due to the transition between 1-D correlations producing the step rise in internal heat transfer rates. This was observed and discussed in chapter 5. Additionally it is important to note that the exothermic reactions during the highway driving profile was not considered in the simulation, however the temperature change within the exhaust gas had been estimated.

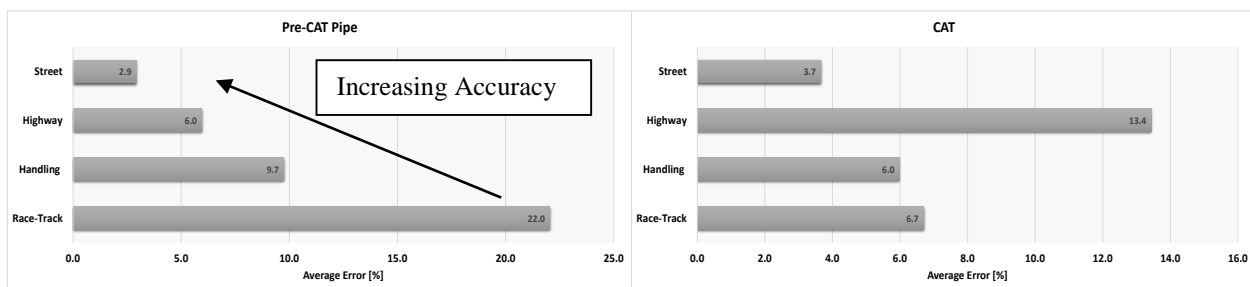


Figure 6.7: Accuracy of Pre-CAT Pipe (left) and CAT (Right)

Within the take-down pipe and middle acoustic silencer, no direct correlation could be established between accuracy potential and dynamic driving profile. This can be seen in Figure 6.8, whereby the Handling and Highway profile consists of the highest discrepancy on the take-down pipe of approximately 12%. Alternatively the middle acoustic silencer error ranges from 2% to 19%. This is primarily due to the modelling assumption of shell elements with virtual thicknesses taking an equivalent multi-layer arrangement to represent internal geometry. In chapter 5, the major discrepancies were during the warm-up phase. This indicates that a portion of the average error described in Figure 6.8 could be a result of inaccurate temperature initialisation conditions. Again removing the 2% error from quasi-transient techniques in

addition to 1% from signal simplification, both the take-down and middle acoustic silencer satisfy the objectives of the investigation.

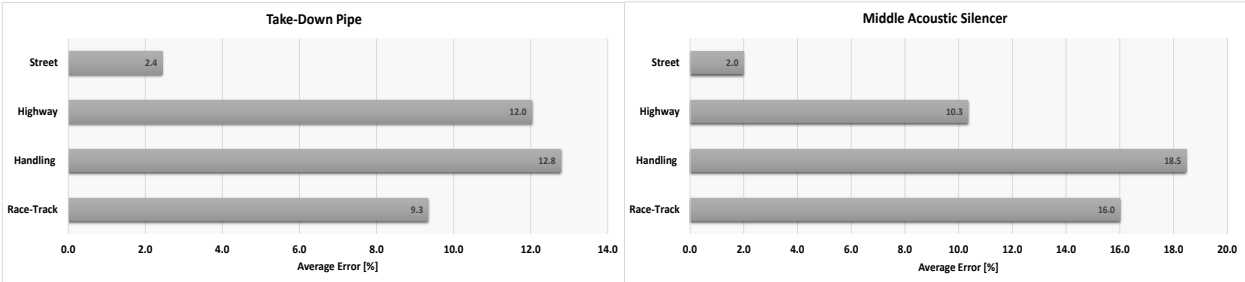


Figure 6.8: Accuracy of Take-Down Pipe (left) and Middle Acoustic Silencer (Right)

The end acoustic silencer accuracy spread (left of Figure 6.9) provides no indication of overall trend. The highway profile consisted of 1% overall error, with the maximum error present in the handling course (approximately 10%). Similar to the middle acoustic silencer the end acoustic silencer experienced the majority of error during the warm up phase. Again this indicates the misrepresentation of thermal mass and internal heat rates within individual chambers. The under-body panel experiences an aggressive decay in accuracy with the reduction of volatile boundary condition. The error ranges from approximately 1% to 10%. The street profile consists of a larger error not conforming to the standard downward trend. This can be a result of removing excessive information from the signal. The street profile itself is a quasi-dynamic profile, which traditionally would need no boundary condition simplification. This can be one indication of the potential limitations of the methodology.

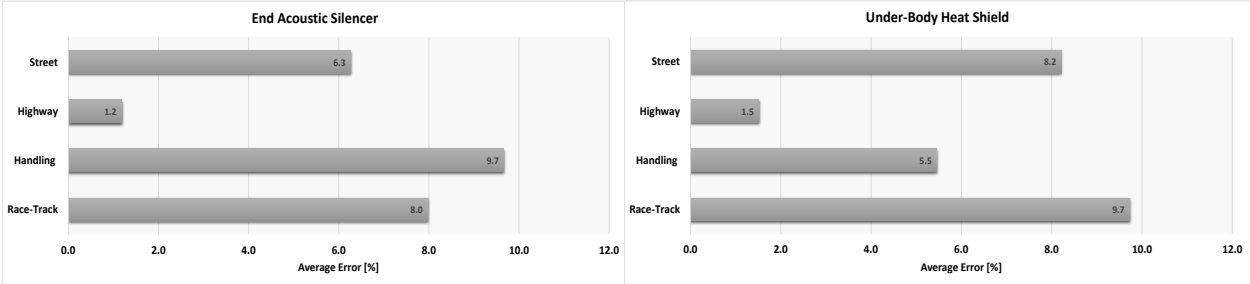


Figure 6.9: Accuracy of End Acoustic Silencer (left) and Under-Body Heat Shield (Right)

Similar to the under-body heat shield both the under-body panel and engine floor panel (Figure 6.10) exhibit a decreasing error trend toward less dynamic driving conditions, excluding the street driving scenario. As seen in chapter 5, all of these components tend to experience small temperature fluctuations. This gives another clear indication of the slow response nature of larger thermal masses under dynamic driving conditions. Again it can be seen that the street profile produces a larger error, not conforming to the overall trend. The maximum error experienced between both components is approximately 11%.

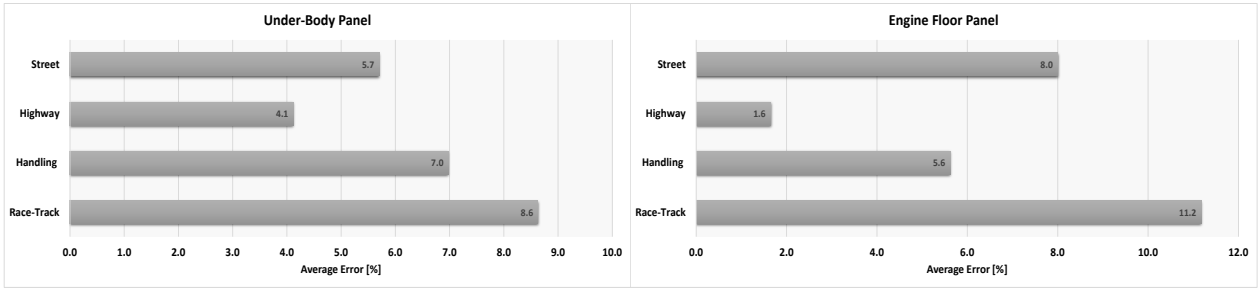


Figure 6.10: Accuracy of Under-Body Panel (left) and Engine Floor Panel (Right)

### 6.2.2 Solution Recycling

13 CFD steady state solutions were calculated prior to the calculation of the alternative dynamic driving profiles. These were recycled within a dynamic driving profile as well as transferred to alternative driving profiles within this investigation. This resulted in the capacity to accelerate the overall calculation time, by reducing the need for independent CFD solutions. Figure 6.16 provides a schematic of the magnitude in solution recycling per profile. Here it can be clearly seen that the handling course reused each steady state solution of 45 times within the total profile. This is a unique occurrence due to the nature of the profile, consisting of shorter lap times. The highway and street driving profiles consist of less recycling opportunities due to the lower frequency dominated boundary conditions. Here it can be seen that the street profile consisted of only 2 recycled positions of the CFD solutions. As discussed previously this could indicate the limits of the signal simplification methodology as the profile is quasi-dynamic.

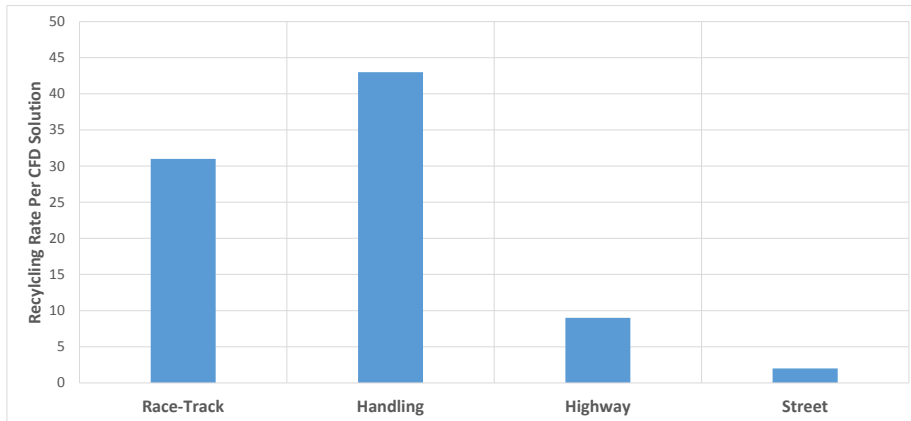


Figure 6.11: Recycling CFD Solutions Statistics

### 6.2.3 Turn-Over Time

Each steady state solution was calculated via 96 CPUs on a distributed network (or cluster). Due to the substantial mesh reduction techniques discussed in chapter 4, the corresponding calculation time was under 5 hours per solution. If the CFD solution was coupled to a steady state thermal model, the calculation time was 8 hours. In total for all the above investigated

profiles, there were 13 unique steady state CFD solutions. The total calculation time for the CFD component of the investigation was approximately 90 hours, as not all CFD solutions were calculated together (due to hardware constraints) rather consecutively. This natural offers the potential for further optimisation whereby the process could be reduced to a single day with 13 parallel calculations on 1,248 CPUs. Figure 6.12 demonstrates the calculation times of the total amount of steady state CFD solution in combination with the individual dynamic driving profiles.

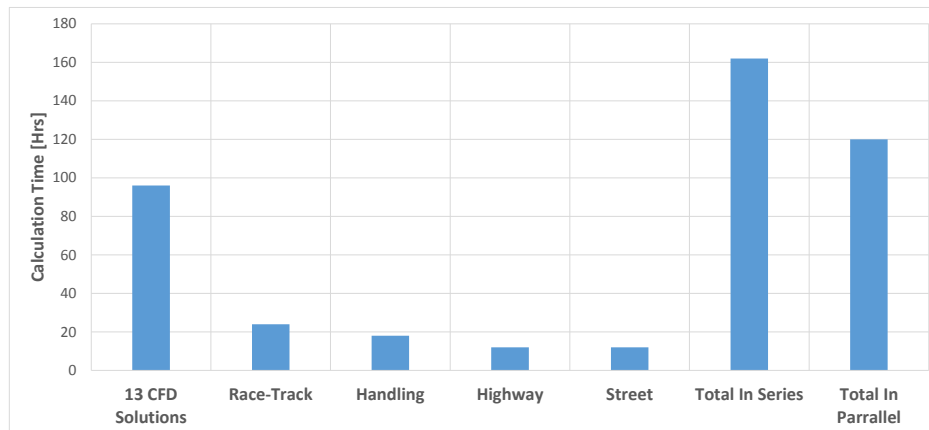


Figure 6.12: Turn-Over Time Statistics

The thermal solver was run as a standalone local calculation with 11 CPUs. The time duration required to map the alternative CFD solutions onto the thermal model at alternative time periods was substantially reduced via the utilisation of customised scripts. For example, the most intensive mapping procedure was the race-track profile consisting of over 405 mapping locations. Utilising the scripts (whilst providing a table of steady state point to time) the mapping duration took approximately 2 hours. The race-track profile calculation time was 24 hours with a time-step of 0.5 seconds. All alternative profiles were also calculated within a 24 hours and run in parallel to the race-track simulation. Therefore two statistics are provided in Figure 6.12, one of which calculates each dynamic profile in series with the additional calculation time of the CFD solutions. This results in a total turn-around time of approximately 160 hours. The alternative statistic is based on parallelising the calculation of the dynamic driving thermal solutions in which the total calculation time is reduced to approximately 120 hours. This correlates to 5 working days of the engineer. In comparison to what has been proposed in literature for a simpler single driving profile [Dis14], this is over an 83% reduction in calculation time, addressing 4 independent profiles, with a fifth of the computational resources. From these outcomes it can be derived that an efficient methodology has been achieved which can address multiple driving profiles without the necessity of high computing resources.

#### 6.2.4 Additional Errors

The following approach demonstrates the ability to alter the original boundary conditions based on the response nature of under-body components. This can only be possible due to the different time-scales within the thermodynamic phenomena compared to that of the fluid domain. From stage 2, the error introduced by removing high frequency information was minimal ( $\leq 1\%$ ). The remaining error was introduced via the quasi-transient approach. Here several sensitivity studies were conducted in order to minimise the error and further refine the quasi-transient methodology. The minimisation of error was conducted via the optimisation of the selection process of steady-state points and representative quantities. As the stage 2 investigation was fundamentally of a numerical type, the full vehicle configuration introduces additional error with the completed methodology. The following section aims at addressing these additional discrepancies for those interested in adopting the research methodology.

There are three additional aspects within real geometrical based models (in this case a full vehicle configuration) which must be considered before adopting the methodology. These are the following:

1. Misrepresentation of Component Thermal Mass → Utilising a shell methodology to represent 3-D solid components relies on the ability to accurately determine the corresponding thickness which is representative of the components thermal mass. Due to the nature of complex vehicle component designs, this can be a challenging task. Therefore it is important to identify the real mass of a component via CAD and then calculate its mass (and average thickness) which should be assigned to the thermal model. An additional factor is the assumptions made on the material property information, which tends to also change over the operational life time of a vehicle. The combination of these two factors can result in a misrepresentation of the component and corresponding inaccurate time dependent thermal behavior. One approach to at least improve the realism of the vehicle is to model components as solids. This introduces larger cell quantities (which exaggerates the calculation time) and complexities surrounding conduction paths via component contact, however addresses the point of misrepresentation.
2. Experimental Thermo-couple Location → any experiment consists of a certain degree of uncertainty. Hence repeated tests are normally conducted in order to validate the temperature patterns experienced with vehicle configurations. The natural experimental deviation between tests is component dependent however ranges from 5K (on a heat shield) to 30K (on a transmission) [Nat14]. The thermo-couples themselves have an uncertainty of  $\pm 3\text{K}$ . If a component surface temperature varies significantly, the position of the thermo-couple compared to the probing location within the simulation becomes an additional discrepancy factor. Therefore careful attention must be paid on identifying the appropriate probe location on the surface of the components. In order to avoid false interpretation of thermo-couple location, pictures of the component with its probing position should be taken during the experiment.

3. Invalid Boundary Conditions → The steady state assumptions utilised in the CFD models need adequate information on the boundary conditions of the heat exchangers, condenser and the rotation on the fan, axles and wheels. Additionally the thermal model requires the appropriate exhaust gas inlet conditions (mass flow rate, temperature) for both steady state conditions and transients. Therefore any assumptions made with the boundary conditions can lead to errors within the individual CFD points, the interpolation between CFD points, and/or the heat flux via the exhaust system. In many cases these boundary conditions are interpolated between known points, or are assumed from fundamental understanding of the vehicle sub-systems. For the given investigation, this data was extracted from the experiment prior to the simulation. However for productive simulations within industry working in early vehicle phases, this information might not be known. Therefore careful consideration on each boundary condition assumption must be taken as many CFD solutions are utilised within the methodology and small errors in boundary conditions can quickly compound to significant discrepancies within the transient driving cases.



## Conclusions & Future Recommendations

The research investigation presented an efficient and innovative methodology in simulating the thermal behavior of a complete vehicle configuration under highly dynamic boundary conditions. To date, there is no material within the literature which has attempted to simulate the highly dynamic driving scenarios for full VTM processes. It was found that this was primarily due to the resources required to simulate these conditions via traditional approaches in combination with the tight time constraints necessary for vehicle development cycles. From these factors the simulation of dynamic driving profiles has been classified as unfeasible for full vehicle geometry with thermal contributing sub-systems. Not only does the presented approach prove that it is possible to conduct such simulations well within the vehicle development time schedules, it also improves on earlier methodologies whereby; the approach utilises substantially less resources with a fraction of the calculation time compared to published attempts on simpler transient cases. These types of revelations not only exist within the performance statistics of the methodology but also in the proposed approach itself. The research has indicated that the fundamental vehicle boundary conditions can be altered or simplified, in which a substantial amount of information can be removed from the input signals without incurring significant error on resulting component time-dependent thermal behavior. Within the simulation field it is unconventional to alter the boundary conditions, rather the simplification is done on the modelling side. The rationale to justify this finding is due to the mass, position and connection of components within the vehicle which dampen the high frequency conditions of the input signals. Therefore the response of underbody components cannot yield major temperature change due to the time scales of the thermal phenomena. The presence of high frequency information in input signals could essentially be removed which consequently accelerates the calculation time without the need to employ more resources. The application potential of this finding extends well beyond the current vehicle investigation, into other fields concerned with time-dependent thermal simulations.

The utilised methodology within this investigation required 3 stages of research. The first was the exploration of 1-D exhaust correlations to represent the energy produced from the major heat source. Even though this stage was developed prior to the research, it deserves attention as no dynamic simulation could be possible without the presence of the time dependent heat source. Stage 1 refined these correlations for the transient application within the current investigation.

Once the rationale was established that the boundary conditions contained irrelevant information, stage 2 was required for the identification of the appropriate simplification technique. A numerical investigation was conducted on simplified geometry in order to establish the optimal simplification approach. Here two particular methods were utilised and compared to the results attained from the original boundary conditions. Firstly averaging schemes were evaluated, whereby the weighted moving average produced promising results for the race-track profile. The averaging schemes however contained one significant flaw. They all carried a dependency on the input series range, therefore a standardized series range for all dynamic driving profiles could not be achieved. The second method of simplification aimed at addressing the limitation of the averaging schemes by identifying the critical frequency which

stimulates thermal change in the system. This critical frequency was then used in a wavelet transformation approach which determined the levels of decomposition necessary on the input signals. Here a simplified signal was derived and utilised as the replacement to the original boundary conditions. This approach achieved excellent results compared to the original conditions. A full transient approach was then compared to a quasi-transient methodology. The quasi-transient parameters of CFD quantities and type were investigated on a sub-module in order to establish the sensitivities and optimal combinations for full vehicle integration. It was found that 1% of error corresponded to the boundary condition simplification. An additional 1-2% of error was introduced due to the quasi-transient approach. Here the steady-state nature of the individual CFD solutions degraded the fluid reference temperature and heat transfer coefficient prediction. The linear interpolation of mapped steady state CFD data contributed to the error experienced within the quasi-transient approach. The finding from stage 2 were then utilised for application to full vehicle geometry within stage 3.

Stage 3 of the investigation consisted of a high performance full vehicle configuration experimentally validated under 4 dynamic driving conditions. The wavelet transformation approach in combination with a new analogy (discussed in chapter 3) was utilised as the signal simplification method whereby the critical frequency was derived from the balanced approach. The balanced approach averages the mass, location, and connectivity over the three critical groups of components (low, medium and high sensitivity) within the vehicle. Here the simplified signal was utilised under quasi-transient conditions in order to accelerate the calculation time. The optimal combination of steady state CFD points were selected from the findings of stage 2, whereby a 1.8 % deviation to the simplified signal was utilised to determine the location of CFD points on the curve. 13 steady-state CFD points were calculated for the full vehicle configurations, whereby the points were recycled within the individual dynamic driving profile as well as transferred to the 3 alternative cases. 10 different probing location on the experiment were selected in order to evaluate to overall accuracy of the proposed methodology. Simulation results for all 4 profiles indicated a strong correlation with the experimental data. The primary area of significant discrepancy was found to be during the warm-up phase of large thermal mass components. The acoustic silencers particularly indicated a misrepresentation of mass and exhaust heat transfer phenomena. Additionally the under-body panels were exposed to a large dependency on CFD points and time interpolation, whereby at some instances discrepancies could be directly linked to the quasi-transient approach. The summation of these errors introduced an addition 1-3% uncertainty compared to the findings found in stage 2. Due to the fact that the CFD solutions themselves were recycled between profiles the overall calculation of 4 alternative driving cases resulted in a 1 week turn-around time. This was approximately 83% reduction in calculation time compared to published material on simpler transient cases. Additionally the methodology was able to achieve such accelerations with one fifth of the resources which were used in published literature. Considering the time to resources advantages of this methodology the consequent discrepancies within the simulations were acceptable.

The research findings have challenged the old simulation paradigm by introducing a simplified version of the highly volatile boundary conditions. Coupled to a quasi-transient methodology

the research has produced considerable time advantages, which could be directly implemented in the current vehicle development time schedules. Overall the research has established that dynamic time-dependent full vehicle simulations are feasible within today's computational resources and that altering the fundamental boundary conditions of the simulation with respect to the systems critical frequency does not incur significant error in the thermal results.

### *Future Work*

The broader applicability of the methodology shall be explored for alternative race-tracks, driving profiles and customer based use cases. The future work consists of the evaluation of all classical driving profiles experimentally validated on climatic wind tunnels. Additionally the limits of transferability should be evaluated on alternative vehicle types and power systems. The solution mixing of alternative steady state points to create new CFD solutions will be further explored. A global correlation to describe the percentage mixing combinations of solutions based on velocity gradient is desired. The application of the philosophy outside the realm of classical vehicle thermal management has already shown promising results. Initial investigations on transient brake-thermal modelling and engine thermal management have been conducted. Here high frequency input signals can be altered in the similar fashion to derive the simplified boundary conditions for the simulation. Additionally the methodology has no conventional limits, therefore the application can spread to any system which contains a mass or thermal inertia. If the simulation boundary conditions can be altered to represent the same thermal state of a vehicle, then the experimental conditions of climatic wind tunnel test could also be altered. Hence work in applying the simplification techniques to experimental strategies are to be further explored in order to reduce energy costs. It is recommended that the response nature of the system be initially analysed in order to establish the critical frequency. From this point any input boundary condition can be simplified using the wavelet transformation.

# References

- [Ahm84] Ahmend, S, Ramm, G. & Faltin, G., “Some Salient Features of Time-Averaged Ground Vehicle Wake”, SAE Technical Paper, **840300**, 1984, *doi:10.4271/840300*.
- [Ban08] Bannister, CD, Brace, CJ. & Lock, GD., “Experimental Characteristics of Heat Transfer in Exhaust Pipe Sections”, SAE Technical Paper, **2008-01-0391**, 2008, *doi:10.4271/2008-01-0391*.
- [Bar92] Barford, L.A., Fazzio, S.R. & Smith, D.R., “An Introduction to Wavelets”, Hewlett Packard, **HPL-92-124**, 1992.
- [Bin00] Binner, T., “Experimentelle und Rechnerische Methoden bei der Entwicklung von Kraftfahrzeugkühlsystemen”, Dissertation, Institut für Strömungsmechanik und Hydraulische Strömungsmaschinen, University of Stuttgart, 2000.
- [Ben11] Bender, T., Hoff, P., Kleemann, R., “The New BMW Climatic Testing Complex – The Energy and Environment Test Centre”, SAE Technical Paper **2011-01-0167**, 2011, *doi:10.4271/2011-01-0167*.
- [Boe48] Boelter, L.M.K, Young, G. & Iversen, H.W., “An Investigation of Aircraft Heaters XXVII – Distribution of Heat Transfer Rates in the Entrance Section of a Circular Tube”, NACA, **TN 1451**, 1948.
- [Bou68] Boussinesq, J., “Memoire sur l’ influence des frottements dans les mouvements reguliers des fluids”, Journal Math Oures Appl., Vol. 13, p.377., 1868.
- [Cen05] Cengel, AY. & Tuner, RH., “Fundamentals of Thermal-Fluid Sceinces”, Second Edition, McGraw-Hill, New York, 2005.
- [Cda14] CD-Adapco, “Technical Manual for StarCCM+”, Volume Meshes Overview, 2014
- [Cha99] Chan, CH & Hoang, DL., “Modeling of Catalytic Coversion of CO/HC in Gasoline Exhaust at Engine Cold-Start”, SAE Technical Paper **1999-01-0452**, 1999, *doi:10.4271/1999-01-0452*.
- [Che12] Cheng, Y, Lian, X, Zhang, X, Xu, C. Xiao, D., “The use of Wavelet Transform and Numerical Algorithn in Application to the Parameter Properties of the Ultrasonic Nondestructive Flaw Detector”, IEEE, **978-1-4577-1415-3/12**, 2012, *doi: 10.1109/CECNet.2012.6201969*.
- [Cog91] Cogotti, A. & Berneburg, H., “Engine Compartment Airflow Invesitgations Using a Laser-Doppler-Velocimeter”, SAE Technical Paper, **910308**, 1991, *doi:10.4271/910308*.
- [Chu02] Chung, T.J., “Computational Fluid Dynamics”, Cambridge University Press, ISBN **978-0-521-59416-5**, New York, 2002.
- [Chr12] Christel, FM., “Full Vehicle Simulations Process at the BMW Group”, Team Leader of CFD Vehicle Simulations, BMW Group, Training Seminar, 2012.
- [Chr14] Christel, FM., “The Current Projects in Transient Aerodynamics at the BMW Group”, Team Leader of CFD Vehicle Simulations, BMW Group, Personal Communication, 2014.
- [Cur09] Curran, A, Peck, S, Schwenn, T. & Hepokoski, M., “Improving Cabin Thermal Comfort by Controlling Equivalent Temperature”, SAE Technical Paper, **2009-01-3265**, 2009, *doi:10.4271/2009-01-3265*.

- [Dep02] Depcik, C & Assanis, D., “A Universal Heat Transfer Correlation for Intake and Exhaust Flows in a Spark-Ignited Internal Combustion Engine”, SAE Technical Paper **2002-01-0372**, 2002, *doi:10.4271/2002-01-0372*.
- [Dis13] Disch, M., Widdecke, N. & Wiedemann, J. “Numerical Simulation of the Transient Heat-Up of a Passenger Vehicle during a Trailer Towing Uphill Drive”, SAE Technical Paper **2013-01-0873**, 2013, *doi:10.4271/2013-01-0873*.
- [Dev14] De Vos, S, Haehndel, K, Frank, T, Christel, F. & Abanteriba, S., “The Development of Turbine Volute Surface Temperature Models for 3D CFD Vehicle Thermal Management Simulations, Part 3: Exhaust Radial Turbine Volute Systems”, SAE Technical Paper **2014-01-0648**, *doi:10.4271/2014-01-0648*.
- [Enr11] Enriquez-Geppert, J, Wiedemann, J, Reister, H. & Binner, T., “Numerical Simulation of Exhaust System Temperatures taking into Account Thermal Interactions with the Vehicle Environment” VTMS, 10<sup>th</sup> Conference, **C1305/055**, 2011.
- [Fra06] Franchetta, M, Bancroft, T.G. & Suen, K. O., “Fast Transient Simulation of Vehicle Underhood in Heat Soak”, SAE Technical Paper **2006-01-1606**, 2006, London, *doi:10.4271/2006-01-1606*.
- [Far06] Farrugia, M, Alkidas, A.C & Sangeorzan, BP., “Cycled-Averaged Heat Flux Measurements in a Straight-Pipe Extension of the Exhaust Port of an SI Engine”, SAE Technical Paper **2006-01-1033**, 2006, *doi:10.4271/2006-01-1033*.
- [Fra09] Frank, T., “Exhaust Modelling Methodologies for Vehicle Simulations”, Project Leader for Vehicle Simulations, BMW Group, Personal Communication, 2009.
- [Fu11] Fu, C. & Dong, F, “Wavelet Packet Entropy Feature Extraction and Characteristics Analysis for Gas/Liquid Two-Phase Flow Regimes”, IEEE, **978-1-4244-7935-1/11**, 2011, *doi:10.1109/IMTC.2011.5944130*.
- [Fis01] Fischer, S. & Cristobal, G, “Minimum Entropy Transform Using Gabor Wavelets for Image Compression”, IEEE, **0-7695-1183-X/01**, 2001, *doi:10.1109/ICIAP.2001.957047*.
- [Guo96] Guo, X. & Sung, HJ., “Analysis of the Nusselt Number in Pulsating Pipe Flow”, Int. J. Heat Mass Transfer, Vol 40, No. 10, pp. 2486-2489, **S0017-9310(96)00317-1**, 1996
- [Ger09] Gerardin, R.C., Hualpa, B.N., Alves, M.A.F. & Arruda, J.R.F., “Analysis of Spark Ignition Engine Knock Signals Using Fourier and Discrete Wavelet Transformation”, SAE Technical Paper **2009-36-0312**, 2009, *doi:10.4271/2009-36-0312*.
- [Hae10] Haehndel, K., “Development of Exhaust Surface Temperature Models through the numerical prediction of 1D/3D CFD Coupling”, Thesis, RMIT, Melbourne, 2010
- [Hae13a] Haehndel, K, Frank, T, Christel, F, Spengler, C, Suck, G. & Abanteriba, S., “The Development of Exhaust Surface Temperature Models for 3D CFD Vehicle Thermal Management Simulations, Part 1: General Exhaust Configurations”, SAE Technical Paper **2013-01-0879**, 2013, *doi:10.4271/2013-01-0879*.
- [Hae13b] Haehndel, K, Frank, T, Christel, F. & Abanteriba, S., “An Innovative Approach to Race Track Simulations for Vehicle Thermal Management”, SAE Technical Paper **2013-01-9121**, 2013, *doi:10.4271/2013-01-9121*.

- [Hae14a] Haehndel, K, Jefferies, A, Schlipf, M, Frank, T, Christel, F. & Abanteriba, S., “The Development of Exhaust Surface Temperature Models for 3D CFD Vehicle Thermal Management Simulations, Part 2: Exhaust Acoustic Silencer Systems”, SAE Technical Paper **2014-01-0646**, 2014, *doi:10.4271/2014-01-0646*.
- [Hae14b] Haehndel, K, Pere, A, Frank, T, Christel, F. & Abanteriba, S., “A Numerical Investigation of Dampening Dynamic Profiles for the Application in Transient Vehicle Thermal Management Simulations”, SAE Technical Paper **2014-01-0642**, 2014, *doi:10.4271/2014-01-0642*.
- [Haw05] Haworth, D., “A Review of Turbulent Combustion Modeling for Multidimensional In-Cylinder CFD”, SAE Technical Paper, **2005-01-0993**, 2005, *doi:10.4271/2005-01-0993*.
- [Hei10] Heinemann, J., “Entwicklung von Teilmodellen zur Berechnung von Oberflächentemperaturen von Abgasanlagenkomponenten”, Wärmeströme im Vorderwagen, Hochschule für Technik und Wirtschaft Berlin, 2010.
- [Her05] Hertel, JE, Suster, J, Hawley, J. & Huang, X., “Finite Difference Heat Transfer Model of a Steel-Clad Aluminium Brake Rotor”, SAE Technical Paper, **2005-01-3943**, 2005, *doi:10.4271/2005-01-3943*.
- [Hua08] Huallpa, B.N, Marano, J. & Arruda, J.R.F., “Time-Frequency Analysis Techniques Applied to Automotive Noise and Vibration Signals”, SAE Technical Paper **2008-36-0350**, 2008, *doi:10.4271/2008-36-0350*.
- [Iee13] IEEE Signal Processing Magazine, “Signal Processing in Large Systems, A New Paradigm”, IEEE, Volume 30, January Edition, ISSN: **1053-5888**, 2013, *doi: 10.1109/MSP.2012.2207490*
- [Joh99] Johnson, FR, Boyland, JE, Meadows, M & Shale, E., “Some properties of a simple moving average when applied to forecasting a time series”, Journal of the Operational Research Society, Palgrave Macmillan, **(1999) 50**, pg. 1267-1271, 1999.
- [Kan99] Kandylas, IP. & Stamatelos, AM., “Engine Exhaust System Design Based on Heat Transfer Computation”, Energy Conversion & Management, Elsevier Science, **40 (1999) 1057-1072**, 1999, *DOI: 10.1016/S0196-8904(99)00008-4*.
- [Kau07] Kaushik, S. “Thermal Management of a Vehicle’s Underhood Using Appropriate Math-Based Analytical Tools and Methodologies”, SAE Technical Paper **2007-01-1395**, 2007, *doi:10.4271/2007-01-1395*.
- [Lau74] Launder, B.E. & Spalding, D.B., “The Numerical Computation of Turbulent Flows”, Comp. Meth. Appl. Mech., Vol. 3, pp.269-289., 1974.
- [Mat14] Mathworks, “Matlab Technical Documentation”, Wavelet Toolbox, Discrete Wavelet Analysis, Signal Analysis, 2014
- [Mes06] Messner, D, Wimer, A, Gerke U. & Gerbig, F., “Application and Validation of the 3D CFD Method for a Hydrogen Fueled IC Engine with Internal Mixture Formation”, SAE Technical Paper, **2006-01-0448**, 2006, *doi:10.4271/2006-01-0448*.
- [Nat14] Nati, A., “BMW Climatic Wind Tunnels - Aerodynamic and Vehicle Thermal Management Experimental Procedures”, Personal Communication, 2014.

- [Oet12] Oettle, N, Mankowski, O, Sims-Williams, D, Dominy, R, Freeman, C. & Gaylard, A., “Assessment of a Vehicle’s Transient Aerodynamic Response”, SAE Technical Paper, **2012-01-0449**, 2012, *doi:10.4271/2012-01-0449*.
- [Pry11] Pryor, J, Pierce, M, Fremond, E, & Michou, Y., “Development of Transient Simulation Methodologies for Underhood Hot Spot Analysis of a Truck”, SAE Technical Paper **2011-01-0651**, 2011, Detroit, *doi:10.4271/2011-01-0651*.
- [Per97] Pervaiz, M, Brewster, R, Ross, F, Bauer, W. & Reister, H., “Numerical Methodology for Automotive Radiator and Condenser Simulations”, SAE Technical Paper, **971840**, 1997, *doi:10.4271/971840*.
- [Pat72] Patankar, S.V. & Spalding, D.B., “A Calculation Procedure for Heat, Mass and Momentum Transfer in Three-Dimensional Parabolic Flows”, Int. J. Heat Mass Transfer, Vol.15, pp. 1787-1806, 1972.
- [Rau14] Rauch, G., “Engine Thermal State under Transient Driving Conditions”, Project Leader, BMW Engine Division, Personal Communication, 2014.
- [Rei97] Reister, H. & Ross, F., “Numerical Simulation of an Axial Colling Fan”, SAE Technical Paper, **971777**, 1997, *doi:10.4271/971777*.
- [Rei12] Reister, H. & Bauer, W., “Simulation Process of the Heat Protection of a Full Vehicle”, SAE Technical Paper **2012-01-0635**, 2012, *doi:10.4271/2012-01-0635*.
- [Rey83] Reynolds, O., “An Experimental Investigation of the Circumstances Which Determine Whether the Motion of Water Shall Be Direct or Sinuous, and of the Law of Resistance in Parallel Channels”, Philosophical Transactions of the Royal Society of London, Vol. 174, pp. 935-982, 1883, *10.1098/rspl.1883.0018*.
- [Rio91] Rioul, O. & Vetterli, M., “Wavelets and Signal Processing” IEEE Signal Processing Magazine, pp. 14-38, ISSN: **1053-5888**, October 1991, *doi: 10.1109/79.91217*.
- [Rug07] Rugh, JP., “Reduction in Vehicle Temperature and Fuel Use from Cabin Ventilation, Solar-Reflective Paint, and a New Solar-Reflective Glazing”, SAE Technical Paper, **2007-01-1194**, 2007, *doi: 10.4271/2007-01-1194*.
- [Rob02] Robb, DJ & Silver, EA., “Using composite moving averages to forecast sales”, Journal of the Operational Research Society, Palgrave Macmillan, **(2002) 53**, pg.1281-1285, 2002, *doi: 0.1057/palgrave.jors.2601440*.
- [Sha08] Shan, X, Burl, J, Jankovic, M. & Cooper S, “Transient Fuel X-Tau Parameter Estimation Using Short Time Fourier Transforms”, SAE Technical Paper **2008-01-1305**, 2008, *doi:10.4271/2008-01-1305*.
- [Sum92] Summa, J., “Steady and Unsteady Computational Aerodynamics Simulations of the Corvette ZR-1”, SAE Technical Paper, **921092**, 1992, *doi:10.4271/921092*.
- [Shm02] Shmaliy, YS., “A Simple Optimally Unbaised MA Filter for Timekeeping”, IEEE Transactions on Ultrasonics, Ferroelectrics, and Frequency Control, IEEE, Vol. 49, No. 6, 2002, *doi: 10.1109/TUFFC.2002.1009337*.

- [Sha84] Shannon, C.E., "A mathematical theory of communication", Bell System Technical Journal, vol. 27, pp. 379-423 and 623-656, July and October, 1948, *doi: 10.1002/j.1538-7305.1948.tb01338.x*.
- [Sch11] Schlipf, M., "Untersuchung der Durchstroemung von Nachschalldaempfern zur Erstellung eines 1D-Modelles fuer die Berechnung der Oberflaechentemperatur", Diplomarbeit, Universitaet Stuttgart, 2011.
- [Sri05] Srinivasan, K, Woronowycz, G, Zabat, M. & Tripp, J., "An Efficient Procedure for Vehicle Thermal Protection Development", SAE Technical Paper, **2005-01-1904**, 2005, *doi:10.4271/2005-01-1904*.
- [Sch09] Schuetz, T., "Cooling Analysis of a Passenger Car Disk Brake", SAE Technical Paper, **2009-01-3049**, 2009, *doi:10.4271/2009-01-3049*.
- [Spi05] Spindler, T., "Numerishe und Experimentelle Untersuchung der Durchströmung von Kraftfahrzeuglüftern", Dissertation, Institut für Strömungsmechanik und Hydraulische Strömungsmaschinen, University of Stuttgart, 2005
- [Tai09] Thermoanalytics Inc., "Technical Manual for Radtherm", Calumet, 2009.
- [Tu08] Tu, Jiyuan, Yeoh, G.H. & Liu, C., "Computational Fluid Dynamics, A Practical Approach", Elsevier, ISBN: 978-0-08-098243-4, 2008.
- [Ten04] Tentner, A, Froehle, P, & Wang, C., "Modeling and Analysis of Transient Vehicle Underhood Thermo-Hydrodynamic Events Using Computational Fluid Dynamics and High Performance Computing", SAE Technical Paper **2004-01-1511**, 2004, Argonne, *doi:10.4271/2004-01-1511*.
- [Tsa09] Tsai, C.S., Hsieh, C.T. & Lew, K. L., "Detection of wind turbine blades damage by spectrum-recognition using gaussian wavelet-entropy", Anti-counterfeiting, Security, and Identification in Communication, 3rd International Conference on , vol., no., pp.108,113, 20-22, ISBN **978-1-4244-3883-9**, 2009, *doi: 10.1109/ICASID.2009.5276949*.
- [Vid91] Vidakovic, B. & Mueller, P., "Wavelets for kids, A Tutorial Introduction", Duke University, NC **27708-0251**, 1991.
- [Woj12] Wojciak, J, Schnepf, B, Indinger, T. & Adams, N., "Study on the Capability of an Open Source CFD Software for Unsteady Vehicle Aerodynamics", SAE Technical Paper, **2012-01-0585**, 2012, *doi:10.4271/2012-01-0585*.
- [Wan05] Wang, X & Zang, N., "Numerical analysis of heat transfer in pulsating turbulent flow in a pipe", International Journal of Heat and Mass Transfer **48(2005)3957-3970**, 2005, Nebraska, *doi: 10.1016/j.ijheatmasstransfer.2005.04.011*.
- [Wei05] Weidmann, E, Wiedermann, J, Binner T. & Reister, H., "Underhood Temperature Analysis in Case of Natural Convection", SAE Technical Paper, **2005-01-2045**, 2005, *doi:10.4271/2005-01-2045*.
- [Wei08] Weidmann, E, Binner, T. & Reister H., "Experimental and Numerical Investigations of Thermal Soak", SAE Technical Paper **2008-01-0396**, 2008, *doi:10.4271/2008-01-0396*.
- [Zhe06] Zheng.you, H, Xiaoqing, C. & Guoming., "Wavelet Entropy Measure Definition and Its Application for Transmission Line Fault Detection and Identification", IEEE, **1-4244-0111-9/06**, 2006, *doi: 10.1109/ICPST.2006.321940*.
- [Zik10] Zikanov, O., "Essential Computational Fluid Dynamics", John Wiley & Sons, Inc., ISBN: **978-0-470-42329-5**, 2010, Canada.



# Appendix 1

In the following appendix, steady state simulations results for the 1-D exhaust methodology are presented. As discussed in chapter 3, the approach to model exhaust dynamics utilising standard Nu number models in combination with CAF factors was developed by the author prior to the current research investigation. However this was only developed for steady state conditions, therefore extensive work needed to be conducted in order to transfer the base methodology to transient conditions. It is important recognise that in dynamic driving scenarios the exhaust system must be modelled as a time dependent heat source in order to achieve the appropriate thermal distribution through the vehicle's underbody environment.

## 2009-2010

The data presented in Figures A1.1 to A1.5 correspond to the research conducted between the years 2009 to 2010. Three vehicle configurations were evaluated at alternative loading conditions under steady state assumptions. Figure A1.1 displays the results of the entire under-body configuration with special focus on the exhaust system. This provides a visual representation of the external environmental conditions of the exhaust system and its potential influence on the induced underbody air flow characteristics. Figure A1.2 to Figure A1.4 consists of the thermal visualisation of each individual exhaust configuration at the respective simulation conditions. Additionally these results contain the experimental data corresponding to each model including the queried temperature location with respect to the exhaust configuration.

Accurately determining the appropriate interrogation element for a corresponding sensor is often difficult, and may be a further source of error. It is not uncommon for adjacent elements to experience a temperature differential of as much as 50°C. Hence, it is essential to determine the exact positioning of the sensor and corresponding element when completing cross-correlation analysis between the numerical and experimental data. Alternatively some sensors may become loose or fall off during an experiment, indicating incorrect thermal results. These may lead the engineer in the wrong validation direction. It is important to always compare experimental results to alternative cases in order to observe the surface temperature trend and in turn trust empirical data. Figure A1.5 indicates an example of the elements which have been probed on the exhaust system and how they correspond to the location of the experimental sensor.

## 2010-2011

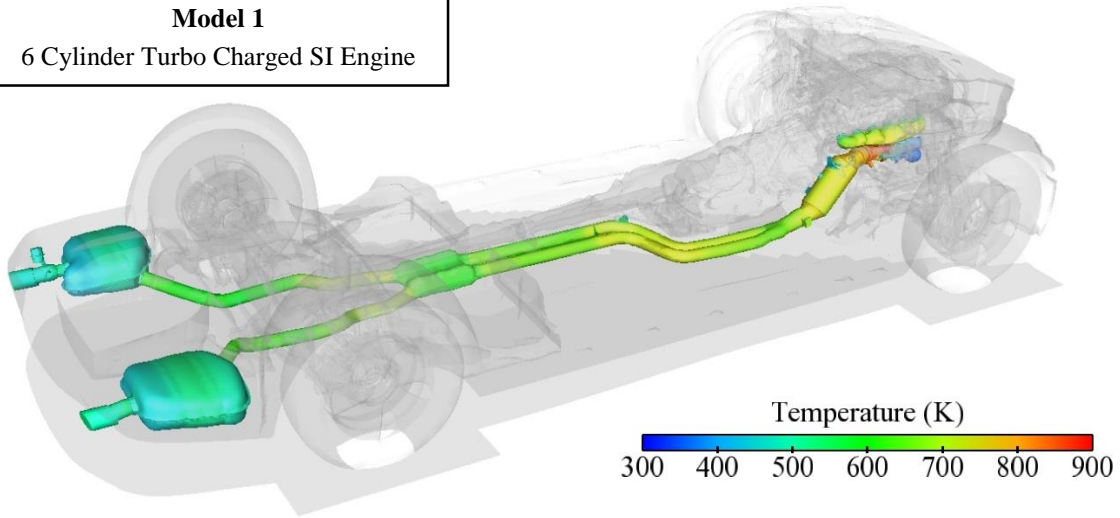
It can be seen in the data presented here that several functional components (e.g. Acoustic silencer) experience significant discrepancies with experimental data. This had initiated several projects that continue the research of the author and built secondary layers on top of the developed exhaust prediction tool. In 2010, Heinemann developed a methodology to predict the increase in thermal energy (and corresponding heat rates) through the catalytic converter due the chemical kinetics [Hei10]. In order to improve the thermal distribution over the acoustic silencers, Schlipf developed

a method of segregated the individual chambers and applying alternative 1-D Nu number models to represent phenomena such as impingement, bifurcation and perforation of internal pipes [Sch11 & Hae14a].

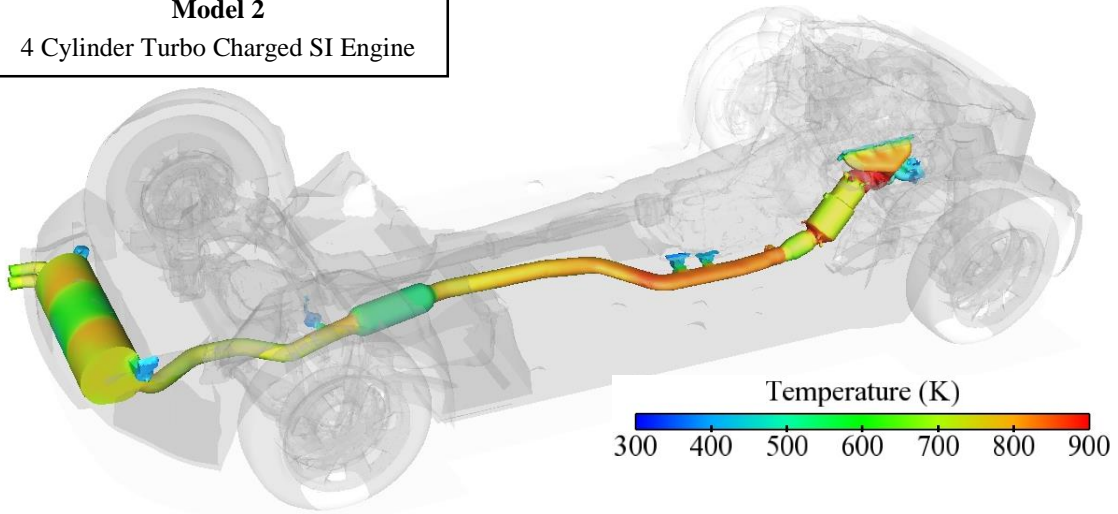
#### 2011-2014

To improve the prediction of heat transfer coefficients within the turbo-charger, Devos implemented a new strategy to segregated the geometry and apply a dean vortices based Nu number model. Additionally the energy extracted from the gas due to the work conducted by the turbine function was implemented via empirically derived correlations [Dev14]. For dynamic driving (time-dependent phenomena) all of the mentioned research was converted into an automatic tool, which conducted a series of calculations per time step to generate time dependent heat transfer coefficients per exhaust component. This new tool interface and corresponding transient functionalities are explored in appendix 2.

**Model 1**  
6 Cylinder Turbo Charged SI Engine



**Model 2**  
4 Cylinder Turbo Charged SI Engine



**Model 3**  
6 Cylinder Turbo Charged CI Engine

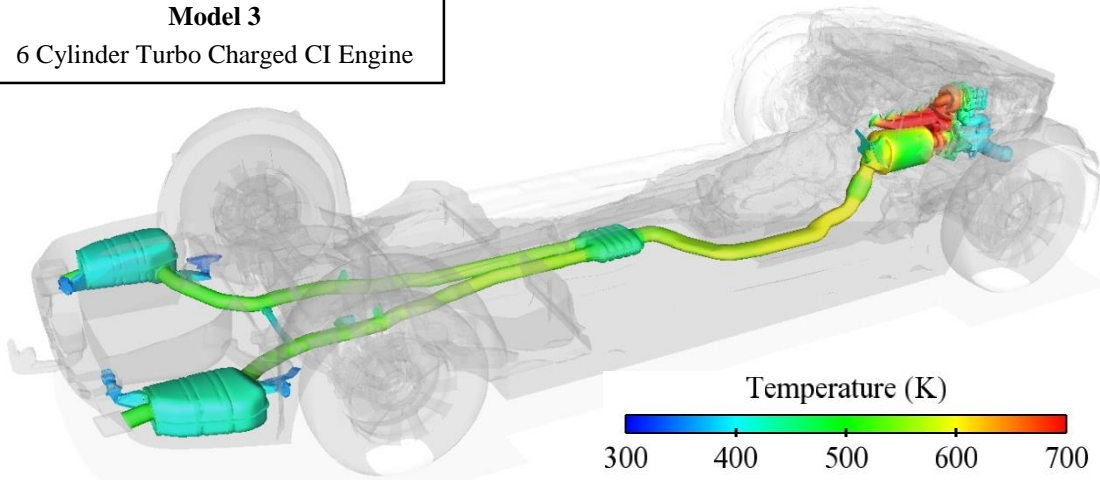


Figure A1.1: Group of Validated Vehicle Models for the 1-D Exhaust Methodology

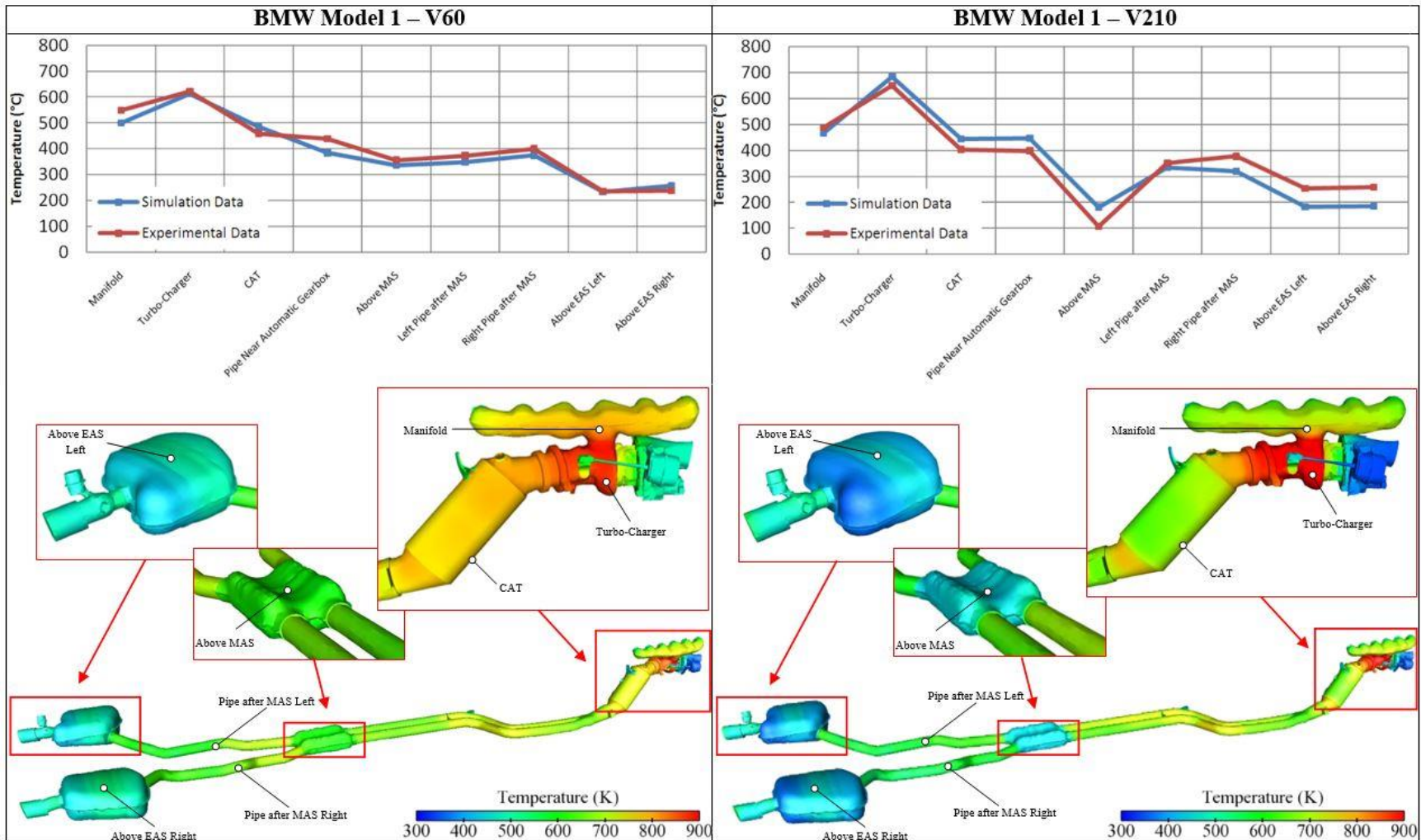


Figure A1.2: BMW Model 1 Result Comparison with Corresponding Probed Positions

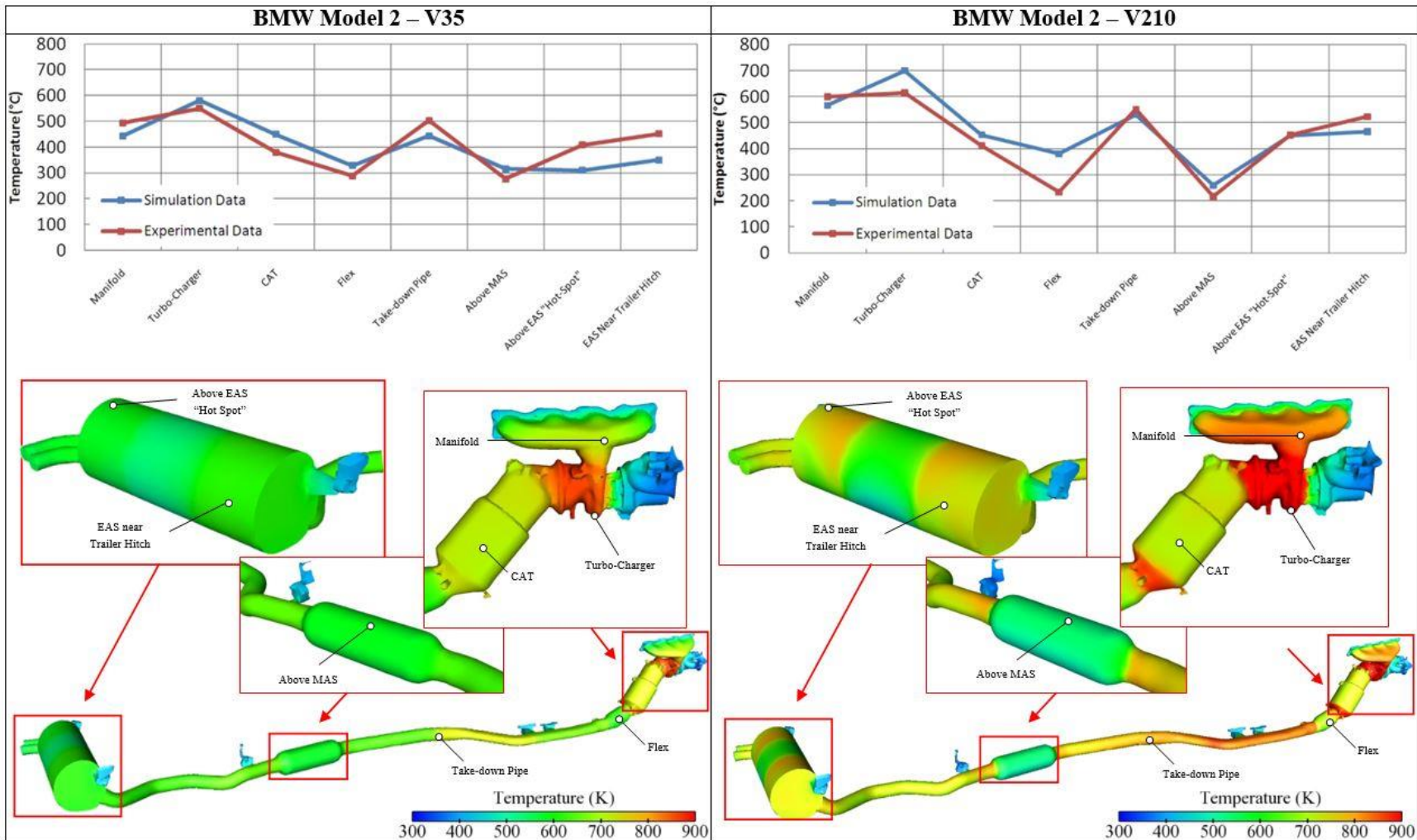


Figure A1.3: BMW Model 2 Result Comparison with Corresponding Probed Positions

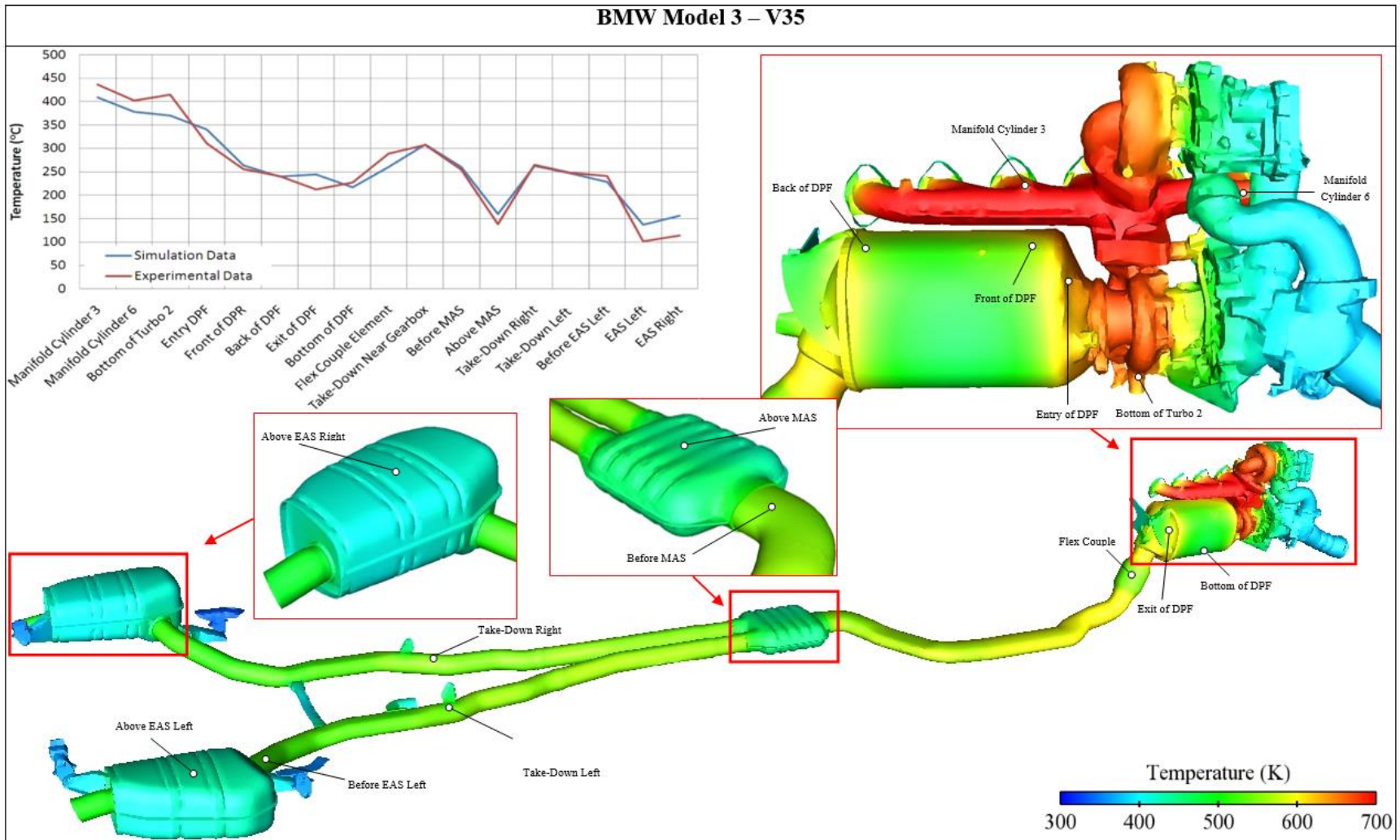


Figure A1.4: BMW Model 3 Result Comparison with Corresponding Probed Positions

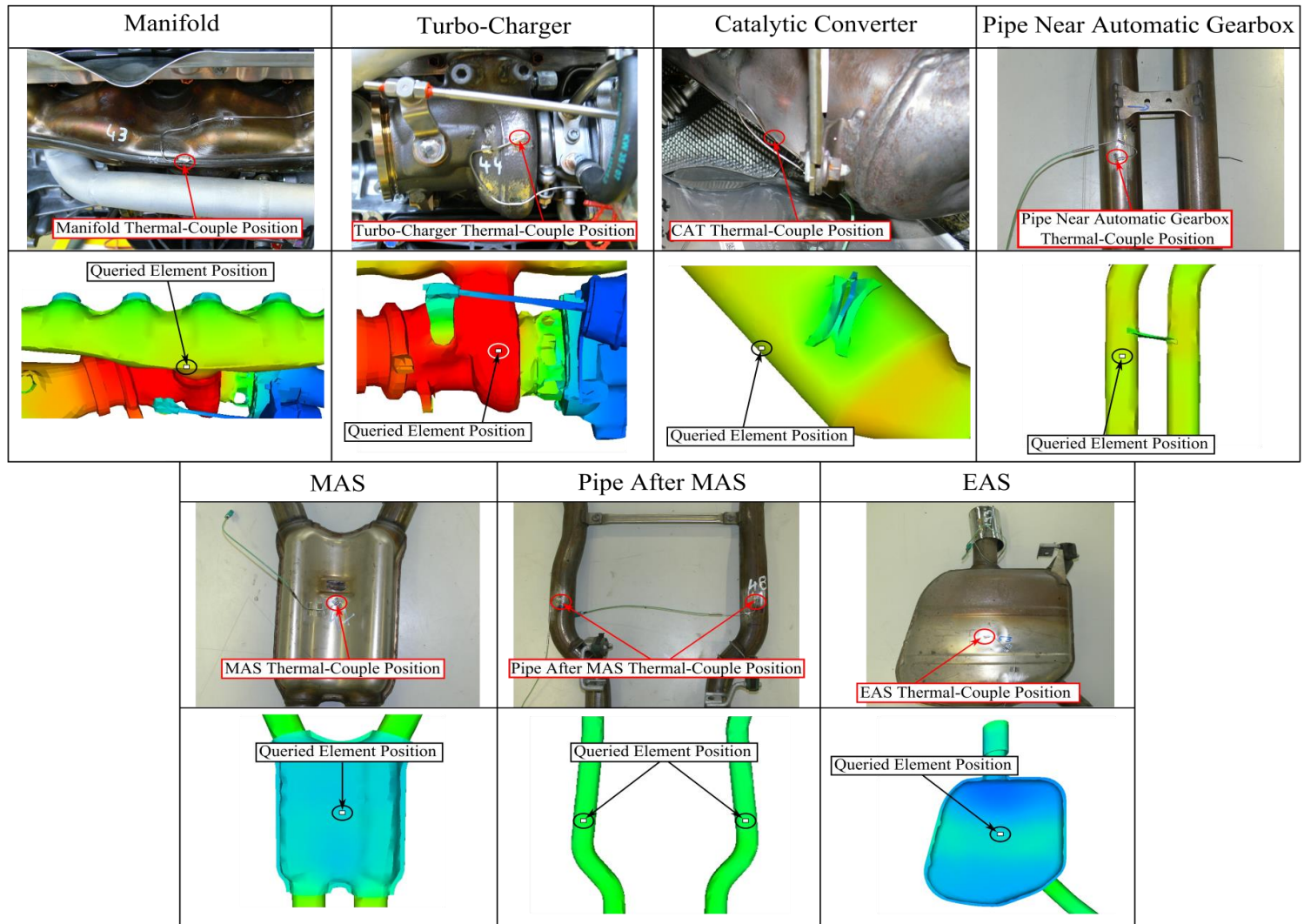


Figure A1.5: Example of Probing Position with Corresponding Experimental Images for Model 1

## Appendix 2

Appendix 2 comprises of the evolutionary stages of the 1-D exhaust prediction tool and corresponding functionalities. The tool was developed in Microsoft excel to allow a wide range of users the ability to alter the fundamental correlations without the need of advanced programming skills. As mentioned previously the inspiration for this type of platform originated from the inherent complexity in selecting the correlations and the means of assembling the proper combinations based on the philosophy described in chapter 3. The platform encompasses all of the available research into internal gas dynamics and exhaust heat transfer, hence aiming to compile and extrapolate this research to suit the conditions of BMW specific exhaust configurations.

Figure A2.1 provides an overview of the platform interface and its available functionalities. The platform is constructed with two interfaces, one which allows the engineer to build the exhaust piping network and generate the corresponding internal 1-D heat rates. The engineer progresses from Hot-End components (e.g. Manifold) to Cold-End components (e.g. Acoustic Silencer), assigning the geometrical input data (diameter, length) to each of the individual sections. The program utilises the boundary condition inputs (gas temperature, mass flow rate and rpm) to select the appropriate correlations and combine them together in order to generate the heat rates per component. The secondary interface is design for an advanced user whereby the individual correlations can be altered or amended based on new information published in literature. The motivations for these two interfaces are the following:

1. **A Basic User** who is not familiar with the platform (or has minimal experience of gas dynamic phenomena and exhaust heat transfer modelling):
  - The user is required to enter the requested parameters and is provided with an estimated HTC value; without additional iterations of the correction settings in the background.
  - Under these circumstances, the program selects which corrections are to be implemented, based on pre-programmed conditions and the user input.
2. **An Advance User** who is familiar with the platform (or who has significant experience in gas dynamic phenomena and exhaust heat transfer modelling):
  - The user has the opportunity to open, unlock and view hidden fold out options and tabs.
  - Alterations can be made to base Nusselt number correlations, correctional models, specific correlations (via check boxes), and also the potential to implement of user defined correlations.



Figure A2.2 provides an overview of the current (post 2011) tool interface and an example of its advance modules. The primary difference between the previous tool and its current version is the ability to add multiple parts per exhaust section. This can be advantageous when having several take-down pipes between Hot-End to Cold-End of the exhaust piping network. Additionally this serves unique exhaust configurations which might consist of multiple turbo-chargers, catalytic converters (upstream and downstream) and also new functional exhaust components. In Figure A2.3 a computational model registry is shown. This database allows the tool to record its predictability performance and stores the data for future use and validation when a physical prototype is experimentally validated. Therefore the tool is continually evaluated and improved over time. Figure A2.4 presents the tools time-dependent functionality and its direct link to the software package *Radtherm*. Here time-dependent heat transfer coefficients are produced in a series of columns corresponding to the exhaust components within the system. This table is then export in a format that is compatible with *Radtherm* import requirement. Each column is converted into a time-dependent curve and associated with the exhaust component of interest. This ultimately saves time and resources for the engineer and allows for a frictionless transfer of boundary conditions for the full vehicle simulation.

+ ————— Basic User Options —————>
+ ————— Advance User Fold-Out Options —————>

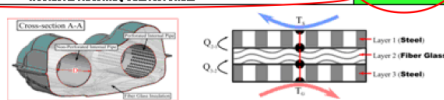
### User Input-Layer 1

**Component Name**

MSD		Entfernung von KAT (m)	1.6
Material	Erhältlich	Temperatur (°C)	603.856244
Durchmesser (m)	0.06	Oberflächenrauigkeit (m)	0.000015
Länge (m)	1.6	Reynold-Zahl	32363.0161
Druck (Bar)	3	Musselt-Zahl	76.43398323

**Calculated Alpha Value**  
Alpha-Wert: 78.80052108

**Radtherm Modelling Considerations**



**Geometrical Scenario Selection**

Take Down Zu NSD

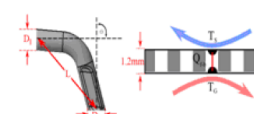
Take Down Zu NSD		Entfernung von KAT (m)	5
Material	Erhältlich	Temperatur (°C)	204.523
Nennweite	0.05	Oberflächenrauigkeit (m)	0.000015
Durchmesser 1 (m)	0.05	Reynold-Zahl	59121.44706
Durchmesser 2 (m)	0.05	Biege-Radius (m)	1.175906668
Länge (m)	0.3	Musselt-Zahl	75.6125285
Biegewinkel (°)	45		

**Alpha-Wert**  
Alpha-Wert: 57.59439106

**Bend Angle**

**Gas Temperature**

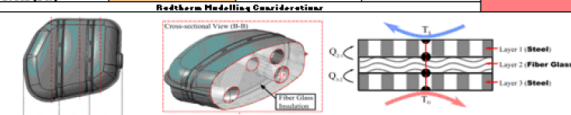
**Distance From CAT**



**Material Selection**

NSD		Entfernung von KAT (m)	3.15
Material	Erhältlich	Temperatur (°C)	428.7283203
Durchmesser (m)	0.05	Oberflächenrauigkeit (m)	0.000015
Länge (m)	0.06	Reynold-Zahl	37671.35008
Druck (Bar)	3	Musselt-Zahl	152.3279171

**Alpha-Wert**  
Alpha-Wert: 131.2889715



### Thermodynamic Properties - Layer 2

**Thermodynamic Properties of Standard Air**

MSD		
Berechnete Eigenschaften		
Charakteristischer Durchmesser (m)	Fläche (m <sup>2</sup> )	Geschwindigkeit (m/s)
He	0.002826	4.1853332
Thermodynamische Eigenschaften von Standard Luft bei 100°C		
Dichte (kg/m <sup>3</sup> )	Wärmeleitfähigkeit (W/m.K)	Dynamische Viskosität (Pa.s)
0.333352905	0.061809192	3.93527E-05
Kinetrischen Viskosität (m <sup>2</sup> /s)	Pr	Reynold-Zahl
0.000000000	0.177625	32363.0161
Basis: Musselt-Zahl Modell-Eigenschaften		
Barid Musselt-Korrelations-Zustand	Rohrwert	Frictional Musselt-Zahl (Gnielinski)
Hydraulisch	0.029477298	76.43398323

**Base Nusselt Number Selection**

Take Down Zu NSD

Take Down Zu NSD		
Berechnete Eigenschaften		
Charakteristischer Durchmesser (m)	Fläche (m <sup>2</sup> )	Geschwindigkeit (m/s)
0.05	0.0019625	42.76246304
Thermodynamische Eigenschaften von Standard Luft bei 100°C		
Dichte (kg/m <sup>3</sup> )	Wärmeleitfähigkeit (W/m.K)	Dynamische Viskosität (Pa.s)
0.725619601	0.038055823	6.62415E-05
Kinetrischen Viskosität (m <sup>2</sup> /s)	Pr	Reynold-Zahl
3.61613E-05	0.705130728	59121.44706
Basis: Musselt-Zahl Modell-Eigenschaften		
Barid Musselt-Korrelations-Zustand	Rohrwert	Frictional Musselt-Zahl (Gnielinski)
Hydraulisch	0.020961211	124.164536

**Base Nusselt Number Value**

NSD		
Berechnete Eigenschaften		
Charakteristischer Durchmesser (m)	Fläche (m <sup>2</sup> )	Geschwindigkeit (m/s)
He	0.002826	43.23544371
Thermodynamische Eigenschaften von Standard Luft bei 100°C		
Dichte (kg/m <sup>3</sup> )	Wärmeleitfähigkeit (W/m.K)	Dynamische Viskosität (Pa.s)
0.438431125	0.051113031	3.4323E-05
Kinetrischen Viskosität (m <sup>2</sup> /s)	Pr	Reynold-Zahl
6.88621E-05	0.115110487	37671.35008
Basis: Musselt-Zahl Modell-Eigenschaften		
Barid Musselt-Korrelations-Zustand	Rohrwert	Frictional Musselt-Zahl (Gnielinski and Shah)
Hydraulisch	0.022132144	105.6214906

### CAF Application - Layer 3

**Activation Function**

CAF von MSD		
Eintrittskorrektur	Eintrittskorrektur	Frictional Eintrittskorrektur (basierend auf KAT-Position)
0	He	He
De-Aktivierung	Manual Override CAF	CAF Gesamt
0	2.5	1

**Manual Over-ride Function**

**Out of Correctional Range Indicator**

**Total CAF**

Take Down Zu NSD CAF		
Eintrittskorrektur	Eintrittskorrektur	Frictional Eintrittskorrektur (basierend auf KAT-Position)
0	He	Yes
De-Aktivierung	Manual Override CAF	CAF Gesamt
0	2.5	0.609453298

**Phenomena Influence Indicator**

CAF von NSD		
Eintrittskorrektur	Eintrittskorrektur	Frictional Eintrittskorrektur (basierend auf KAT-Position)
0	He	Yes
De-Aktivierung	Manual Override CAF	CAF Gesamt
0	2.5	1.442125922

Colour Allocation Index	
User Input	Within Previous Experience Simulation Range
Calculated Parameter	Below Previous Experience Simulation Range
Manual Over-Ride	Above Previous Experience Simulation Range

A2.1: 2009 Exhaust Tool Interface with Corresponding Explanations of Functionalities

**Alpha Approximation Tool v3.0**

Environmental & Operational Scenario Input

Parameter	Input	Units
Mass Flow Rate	0.18668667	kg/s
Velocity	250	km/hr
Engine Speed	5050	RPM
Exhaust Entry Temp	884	(C)
Pressure	1	Bar
Engine Type	5 Cylinder Turbo Charged Diesel	

Update Tool and Output Table Environmental Section

OR

Transient       Steady State

Environmental & Operational Scenario Input ACTIVATE

Advanced Settings					
Parameter	Input	Units	Parameter	Input	Units
Cylinders	n		Injected Fuel		g/cycle
Capacity	L		Fuel Load Fraction		dimensionless
Exhaust Pressure	Bar		Engine Efficiency		%

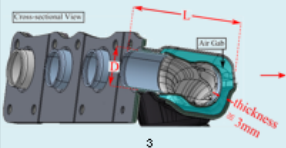
Clear Input tables

Generate Alpha Values

Generate Alpha Values (Advanced NSD)

MANIFOLD

Parameter	Input	Units
Diameter	0.04	m
Length	0.1665	m
Pressure	1	Bar



Create Manifold component

CAF augmentation and Model selection

Zweiflutig?  FALSE

Entrance CAF  TRUE

Pulsation CAF  TRUE

Manual CAF  FALSE

Nusselt Base Correction  TRUE

Material: Edelstahl

Part Name: Manifold

Part Number: 90

Part Identification		Physical Properties			CAF Settings and Model			
Number	Name	Diameter	Length	Pressure	Entrance	Ext. Model	Pulsation	Pulse Mode
90	Manifold	0.04	0.1665	1	TRUE		1	TRUE

TURBO CHARGER

Parameter	Input	Units
Diameter 1	0.08595	m
Diameter 2	0.05475	m
Diameter 3	0.09414	m
Diameter 4	0.043	m

GLOBAL Parameter Input

Parameter	Input	Units
Mass Flow %	50.00	%

Broad range Energy module  TRUE

Volate physics  TRUE

Geometry reference

Part Name: Turbo\_b

Part No. Ab1: 321

Part No. Ab2: 322

Part No. Ab3: 323

Part Identification		Physical Properties			Total components				
Number	Name	Diameter1	Diameter2	Diameter3	UNITS	TYPE	Part ID	Turbo Config	PID2
321	Turbo_b	85.95	54.75	94.14	SI	CONVECTION		0.5	322

Advance Module 1

Advance Module 2

Advance Module 3

**NSD Advanced Component Generator**

This advanced component generator requires internal geometry parameters from CAD. If you do not have access to these parameters, please use the basic component generator.

Global Configuration - Dual Flow (Zweiflutig)?

Ja       Nein

Distance From KAT: \_\_\_\_\_ m

Volume Flow Partition

Manual Volume Flow Assignment

Volume Flow 1: \_\_\_\_\_ %

Volume Flow 2: \_\_\_\_\_ %

Material: \_\_\_\_\_

MSD/NSD Name: \_\_\_\_\_

**Geometrical Parameters**

Trennungswinkel Abzw. 1, Abzw. 2

Abzw1: \_\_\_\_\_ ° Deg

Abzw2: \_\_\_\_\_ ° Deg

Durchmesser / D0, D1, D2

D0: \_\_\_\_\_ m

D1: \_\_\_\_\_ m

D2: \_\_\_\_\_ m

Länge Standard-Rohr Zweig 1,2

LR1: \_\_\_\_\_ m

LR2: \_\_\_\_\_ m

Länge perforierter Teil Zweig 1,2

LRp1: \_\_\_\_\_ m

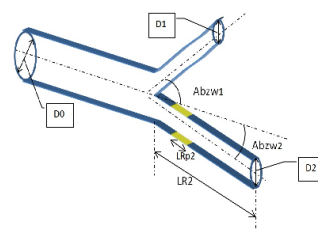
LRp2: \_\_\_\_\_ m

Rohrhaugkeit Perforation

Summe weiterer Zetas Zweig 1,2

ζconst1: \_\_\_\_\_ m

ζconst2: \_\_\_\_\_ m



Add Partition Factors

**Chambers**

Offen Durchströmt

Prallstrahl verwenden

Fluid Source

Abzweigung 1

Abzweigung 2

Austrittsdurchmesser: \_\_\_\_\_ m

Prallstrahl radius: \_\_\_\_\_ m

Part Name: \_\_\_\_\_

Part Number: \_\_\_\_\_

MI Absorptionmaterial

Fluid Source

Abzweigung 1

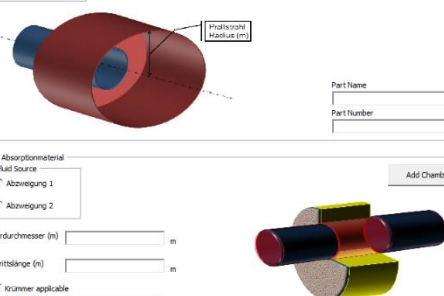
Abzweigung 2

Rohrdurchmesser (m): \_\_\_\_\_ m

Eintrittslänge (m): \_\_\_\_\_ m

Kränner applicable

Begegnungswinkel [°]: \_\_\_\_\_ ° Deg



Add Chamber

Figure A2.2: 2013 Exhaust Tool Interface with Advance Modules

Figure A2.3: Computational Model Registry

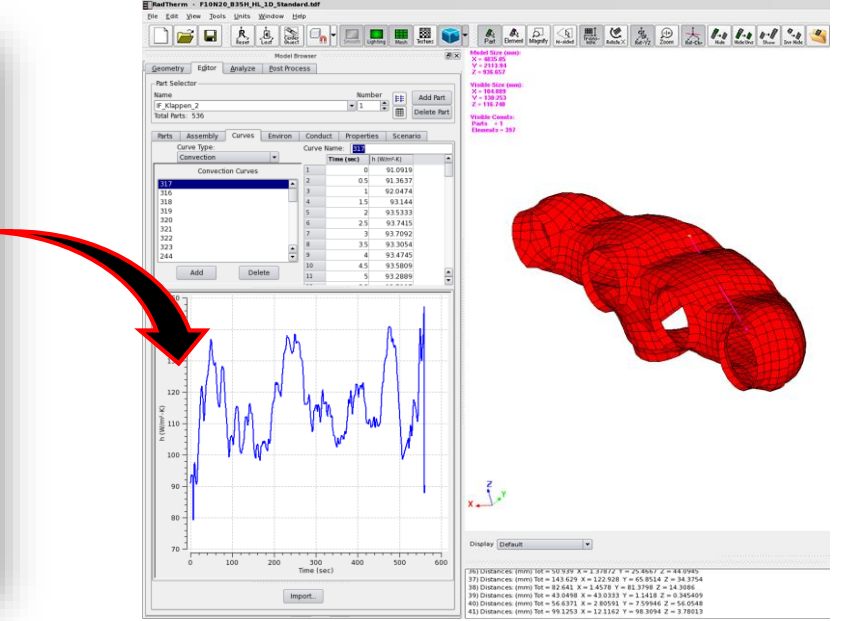


Figure A2.3: Time Dependent Heat Transfer Coefficients for Exhaust Components

## Appendix 3

The following section details the derivation of the formula (Equation 3.9) used in the flat plate analogy described within chapter 3. If one may consider the total energy ( $E_{Total}$ ) being exposed to the flat plate from the boundary conditions as the sum of individual sine functions of alternative frequencies, then Equation A3.1 can be formulated.

$$E_{Total} = \sum_n E^* \cdot \sin(f \cdot n) \quad (A3.1)$$

Here the characteristic energy ( $E^*$ ) acts as a scaling factor for each sine function based up its individual frequency. The characteristic energy (Equation A3.2) itself is a function of the common parameters experienced within vehicle convections, whereby  $T_{Air}$  refers to the fluid temperature,  $v^*$  denotes the near wall velocity,  $A^*$  is there effective area of the plate, with the air properties  $\rho$  and  $C_p$  being dependent on temperature.

$$E^* = T_{Air} \cdot v^* \cdot A^* \cdot \rho_{Air} \cdot C_p(T_{Air}) \quad (A3.2)$$

When examining a sine function of a single cycle ( $2\pi$ ) the net energy introduced is zero. As the frequency changes the cycles are also inversely altered. Therefore a single cycle can be described as  $2\pi/f$ , where  $f$  corresponds to the frequency of the signal. Figure A3.1 displays single cycle sine function based on frequency with energy as the scaling factor.

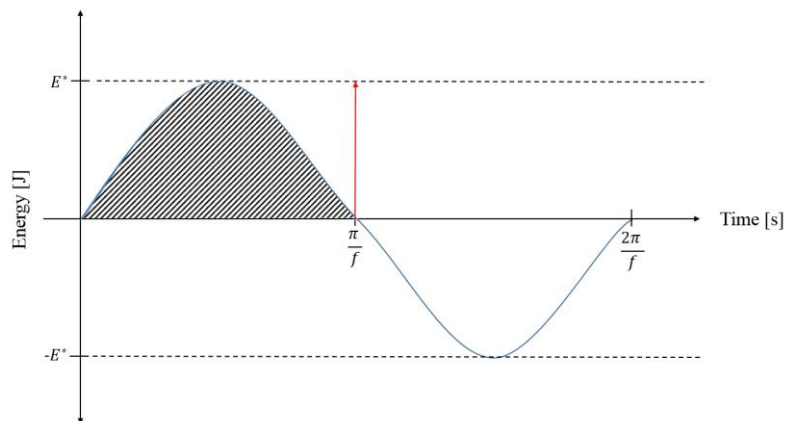


Figure A3.1: Sine Function based on Energy and Frequency

To understand the impact of the introduced energy onto the system a limit of 0 to  $2\pi/f$  is utilised to calculate the integral of the sine function. This can be expressed as the following:

$$E_{In} = \int_0^{\frac{\pi}{f}} E^* \cdot \sin(f \cdot t) dt \quad (\text{A3.3})$$

Hence the integration can be expressed as Equation A3.4

$$\int_0^{\frac{\pi}{f}} E^* \cdot \sin(f \cdot t) dt = \left[ -\frac{E^*}{f} \cos(f \cdot t) \right]_0^{\frac{\pi}{f}} \quad (\text{A3.4})$$

Whereby substituting the limits produces:

$$\left[ -\frac{E^*}{f} \cos(f \cdot t) \right]_0^{\frac{\pi}{f}} = -\frac{E^*}{f} \cos\left(f \cdot \frac{\pi}{f}\right) + \frac{E^*}{f} \cos(f \cdot 0) \quad (\text{A3.5})$$

This can be reduced to Equation A3.6.

$$-\frac{E^*}{f} \cos(f \cdot \pi) + \frac{E^*}{f} \cos(f \cdot 0) = \frac{E^*}{f} + \frac{E^*}{f} = \frac{2 \cdot E^*}{f} \quad (\text{A3.6})$$

The final integration can be express as an inverse relationship of the characteristic energy on frequency, as shown in Equation A3.7.

$$E_{In} = \frac{2 \cdot E^*}{f} \quad (\text{A3.7})$$

When examining the energy required to change the thermal state of the solid (for example the flat plate), Equation A3.8 can be utilised.

$$E_{Solid} = C_p \cdot M \cdot \Delta T \quad (\text{A3.8})$$

If it is assumed that the system is ideal, and no energy losses occur, then the Input energy exposed to the plate must be equivalent to the thermal state of the plate, therefore Equation A3.9 can be formulated.

$$E_{In} = E_{Solid} \quad \therefore \quad C_p \cdot M \cdot \Delta T = \frac{2 \cdot E^*}{f} \quad (A3.9)$$

As mentioned in chapter 3, the common error within experimental methods is approximately 3 K. Therefore the analogy will utilise this uncertainty in order to estimate the critical frequency of the system. This can be expressed as the following:

$$\Delta T = \frac{2 \cdot E^*}{f \cdot C_p \cdot M} \quad \text{hence,} \quad f = \frac{2 \cdot E^*}{\Delta T \cdot C_p \cdot M} \quad (A3.10)$$

Equation A3.10 can be rearrange so that the frequency ( $f$ ) is a function of the energy ( $E^*$ ), temperature tolerance ( $\Delta T$ ) and plate properties ( $C_p$  and  $M$ ). In this form Equation A3.10 can be used as a means of establishing the frequency threshold for the entire vehicle and the corresponding decomposition level necessary for convection conditions.

## Appendix 4

The following appendix explores the derivation of the critical frequency for the full vehicle configuration evaluated in stage 3 of the research investigation. The flat plate analogy is used to describe the exposed energy to a series of components within a sub-system. The components are grouped within the sub-system where parameters used in the flat plate analogy (described in chapter 3) are averaged to form a single flat plate representation of the sub-system. Here a critical frequency can be derived from each sub-system and later used to formulate a general frequency threshold for the vehicle. The sub-systems selected for the research investigation are the following:

1. Engine Bay
2. Underbody
3. Under-Carriage
4. Engine Pipes and Cables
5. Drive Train and axles.

It is to be noted that both major heat sources (Engine and Exhaust system) have not been selected as a sub-system group for the derivation of the general frequency thresholds as the focus of the investigation is on the thermal behavior of surrounding components within the vehicle body architecture.

Table A4.1 to A4.5 present the selected components for each of the sub-systems. In each sub-system there are many components, hence only the most critical components per sub-system were selected. The determination of component importance was based on standard industrial interests in vehicle thermal management processes. The conduction ratio ( $\beta$ ) and coupling strength ( $\alpha$ ) were estimated from visual inspection. Whereas the mass ( $M$ ), area ( $A$ ) and specific heat were determined from CAD geometry and the BMW material database.

The process of deriving the critical frequency for each subsystem is described within Equations A4.1 to A4.20. Once the critical frequency for each sub-system is determined a weighted average is used to produce the general frequency threshold for the vehicle. Here weight is given to systems of higher importance in order to avoid additional errors through the removal of boundary condition information.



Engine Bay						
Part Name	Material Name	Conduction Ration (Connectivity)	Mass (kg)	Coupling Strength	Area (m <sup>2</sup> )	Specific Heat (J/kg.K)
Engine Bay Wall Left- Tunnel Entry	Steel (Mild)	1.00	3.28	0.80	0.14	460.00
Engine Bay Wall Right	Steel (Mild)	1.00	3.28	0.80	0.14	460.00
Engine Bay Side Insulation Left	Absorber	1.00	0.07	0.60	0.27	1895.00
Engine Bay Side Insulation Right	Absorber	1.00	0.07	0.60	0.27	1895.00
Engine Bay Front Insulation	Absorber	1.00	0.08	0.40	0.32	1895.00
Engine Bay Top Insulation	Absorber	1.00	0.25	0.40	0.50	1895.00
<b>Averaged Values</b>		<i>1.00</i>	<i>1.17</i>	<i>0.60</i>	<i>0.27</i>	<i>1416.67</i>

Table A4.1: Engine Bay Group – Flat Plate Analogy

Assuming the average Air temperature in the engine compartment [ $T_{Air}$ ] is 650 K, the density at standard pressure [ $\rho_{Air}$ ] is 0.53 kg/m<sup>3</sup> with a specific heat capacity [ $C_p(T_{Air})$ ] of 1062 J/kg.K the critical frequency for this group can be derived as the following:

$$E^* = T_{Air} \cdot v^* \cdot \overline{A^*} \cdot \rho_{Air} \cdot C_p(T_{Air}) = T_{Air} \cdot (0.01 \cdot v_{Max}) \cdot (\overline{\alpha \cdot A}) \cdot \rho_{Air} \cdot C_p(T_{Air}) \quad (A4.1)$$

$$E^* = 650 \cdot (0.01 \cdot 67) \cdot (0.6 \cdot 0.27) \cdot 0.52 \cdot 1062 = 40.42 \text{ kW} \quad (A4.2)$$

And,

$$\overline{M^*} = \overline{(\beta \cdot M)} = 1.00 \cdot 1.17 = 1.17 \text{ kg} \quad (A4.3)$$

Therefore,

$$f = \frac{2 \cdot E^*}{\Delta T \cdot \overline{C_p} \cdot \overline{M^*}} = \frac{2 \cdot 42421}{1 \cdot 1416.67 \cdot 1.17} = 48.74 \text{ Hz} \quad (A4.4)$$

Under-body						
Part Name	Material Name	Conduction Ration (Connectivity)	Mass (kg)	Coupling Strength	Area (m <sup>2</sup> )	Specific Heat (J/kg.K)
Underbody Panel Left	Multi	1.00	13.28	1.00	0.84	2000.00
Underbody Panel Right	Multi	1.00	13.28	1.00	0.84	2000.00
Front Tunnel	Aluminum	1.50	0.48	0.80	0.18	893.00
Connecting Tunnel Middle	Aluminum	1.50	1.33	0.80	0.50	893.00
Under Back Seat Tank Plate	Polyvinylchloride	1.00	17.69	0.40	0.76	960.00
Floor Plate Back	Polyvinylchloride	1.00	8.09	0.40	0.34	960.00
Trunk Baggage Front Plate	Polyvinylchloride	1.00	6.06	0.40	0.28	960.00
Trunk Baggage Back Plate	Polyvinylchloride	1.00	13.93	0.40	0.57	960.00
<b>Averaged Values</b>		<i>1.13</i>	<i>9.27</i>	<i>0.65</i>	<i>0.54</i>	<i>1203.25</i>

Table A4.2: Underbody Group – Flat Plate Analogy

Assuming the average Air temperature in the engine compartment [ $T_{Air}$ ] is 450 K, the density at standard pressure [ $\rho_{Air}$ ] is 0.78 kg/m<sup>3</sup> with a specific heat capacity [ $C_p(T_{Air})$ ] of 1020 J/kg.K the critical frequency for this group can be derived as the following:

$$E^* = T_{Air} \cdot v^* \cdot \overline{A^*} \cdot \rho_{Air} \cdot C_p(T_{Air}) = T_{Air} \cdot (0.01 \cdot v_{Max}) \cdot (\alpha \cdot A) \cdot \rho_{Air} \cdot C_p(T_{Air}) \quad (A4.5)$$

$$E^* = 450 \cdot (0.01 \cdot 67) \cdot (0.65 \cdot 0.54) \cdot 0.78 \cdot 1020 = 84.16 \text{ kW} \quad (A4.6)$$

And,

$$\overline{M^*} = (\beta \cdot M) = 1.13 \cdot 9.27 = 10.47 \text{ kg} \quad (A4.7)$$

Therefore,

$$f = \frac{2 \cdot E^*}{\Delta T \cdot \overline{C_p} \cdot \overline{M^*}} = \frac{2 \cdot 84156}{1 \cdot 1203.24 \cdot 10.47} = 13.42 \text{ Hz} \quad (A4.8)$$

Under-Carriage						
Part Name	Material Name	Conduction Ration (Connectivity)	Mass (kg)	Coupling Strength	Area (m <sup>2</sup> )	Specific Heat (J/kg.K)
Front Axle Base	Steel (Mild)	1.00	18.65	0.60	0.80	460.00
Back Axle Base	Steel (Mild)	1.00	6.52	0.60	0.28	460.00
Wheel Carrier Front Left	Steel (Mild)	1.00	5.16	0.80	0.13	460.00
Wheel Carrier Front Right	Steel (Mild)	1.00	5.16	0.80	0.13	460.00
Front axle Steering Column	Steel (Mild)	1.00	5.42	0.50	0.23	460.00
Front Tension Strut left	Steel (Mild)	1.00	1.64	0.90	0.05	460.00
Front Tension Strut Right	Steel (Mild)	1.00	1.64	0.90	0.05	460.00
Engine Brace	Steel (Mild)	1.00	16.02	0.70	0.21	460.00
Real Axle Carrier Left	Steel (Mild)	1.00	3.48	0.50	0.15	460.00
Real Axle Carrier Right	Steel (Mild)	1.00	3.48	0.50	0.15	460.00
Real Axle Strut	Steel (Mild)	1.00	6.53	0.40	0.28	460.00
Rear Wishbone left	Steel (Mild)	1.00	1.18	1.00	0.05	460.00
Rear Wishbone Right	Steel (Mild)	1.00	1.18	1.00	0.05	460.00
Rear A-Arm left	Steel (Mild)	1.00	0.65	1.00	0.03	460.00
Rear A-Arm Right	Steel (Mild)	1.00	0.65	1.00	0.03	460.00
<b>Averaged Values</b>		<i>1.00</i>	<i>5.16</i>	<i>0.75</i>	<i>0.18</i>	<i>460.00</i>

Table A4.3: Under-Carriage Group – Flat Plate Analogy

Assuming the average Air temperature in the engine compartment [ $T_{Air}$ ] is 375 K, the density at standard pressure [ $\rho_{Air}$ ] is 1.01 kg/m<sup>3</sup> with a specific heat capacity [ $C_p(T_{Air})$ ] of 1008 J/kg.K the critical frequency for this group can be derived as the following:

$$E^* = T_{Air} \cdot v^* \cdot \overline{A^*} \cdot \rho_{Air} \cdot C_p(T_{Air}) = T_{Air} \cdot (0.01 \cdot v_{Max}) \cdot \overline{(\alpha \cdot A)} \cdot \rho_{Air} \cdot C_p(T_{Air}) \quad (A4.9)$$

$$E^* = 375 \cdot (0.01 \cdot 67) \cdot (0.75 \cdot 0.18) \cdot 1.01 \cdot 1008 = 33.45 \text{ kW} \quad (\text{A4.10})$$

And,

$$\overline{M^*} = \overline{(\beta * M)} = 1.00 \cdot 5.16 = 5.16 \text{ kg} \quad (\text{A4.11})$$

Therefore,

$$f = \frac{2 \cdot E^*}{\Delta T \cdot \overline{C_p} \cdot \overline{M^*}} = \frac{2 \cdot 33449}{1 \cdot 460 \cdot 5.16} = 28.20 \text{ Hz} \quad (\text{A4.12})$$

Engine Pipes and Cables						
Part Name	Material Name	Conduction Ration (Connectivity)	Mass (kg)	Coupling Strength	Area (m <sup>2</sup> )	Specific Heat (J/kg.K)
Inter-Cooler Pipe	Polymer (PA66_GF30)	1.00	0.44	1.00	0.13	1500.00
Condenser Pipe	Polymer (PA66_GF30)	1.00	0.13	0.70	0.04	1500.00
Heat Exchanger Pipe	Polymer (PA66_GF30)	1.00	0.47	0.70	0.17	1500.00
Oil Cooler Pipe	Rubber Hard	1.00	0.14	1.00	0.07	2011.34
Air Intake Pipe	Polyvinylchloride	1.00	0.52	0.90	0.15	960.00
General Cables from ECU	Polymer (PA66_GF30)	1.00	0.14	0.30	0.07	1500.00
<b>Averaged Values</b>		<i>1.00</i>	<i>0.31</i>	<i>0.77</i>	<i>0.10</i>	<i>1495.22</i>

Table A4.4: Engine Pipes and Cables Group – Flat Plate Analogy

Assuming the average Air temperature in the engine compartment [ $T_{Air}$ ] is 500 K, the density at standard pressure [ $\rho_{Air}$ ] is 0.71 kg/m<sup>3</sup> with a specific heat capacity [ $C_p(T_{Air})$ ] of 1030 J/kg.K the critical frequency for this group can be derived as the following:

$$E^* = T_{Air} \cdot v^* \cdot \overline{A^*} \cdot \rho_{Air} \cdot C_p(T_{Air}) = T_{Air} \cdot (0.01 \cdot v_{Max}) \cdot \overline{(\alpha \cdot A)} \cdot \rho_{Air} \cdot C_p(T_{Air}) \quad (A4.13)$$

$$E^* = 500 \cdot (0.01 \cdot 67) \cdot (0.77 \cdot 0.10) \cdot 0.71 \cdot 1030 = 19.41 \text{ kW} \quad (A4.14)$$

And,

$$\overline{M^*} = \overline{(\beta * M)} = 1.00 \cdot 0.31 = 0.31 \text{ kg} \quad (A4.15)$$

Therefore,

$$f = \frac{2 \cdot E^*}{\Delta T \cdot \overline{C_p} \cdot \overline{M^*}} = \frac{2 \cdot 19414}{1 \cdot 1495.22 \cdot 0.31} = 84.96 \text{ Hz} \quad (A4.16)$$

Drive Train and Axles						
Part Name	Material Name	Conduction Ration (Connectivity)	Mass (kg)	Coupling Strength	Area (m <sup>2</sup> )	Specific Heat (J/kg.K)
Gear Box Housing	Special Al_Si_17	1.50	10.00	0.70	0.65	850.00
Connecting Transmission system	Special Al_Si_18	1.50	3.80	0.70	0.28	850.00
Drive Shaft Connection	Aluminum Noppen	1.50	0.50	1.00	0.05	1106.00
Front Axle Gear Box Housing	Special Al_Si_18	1.50	2.09	1.00	0.15	850.00
Rear Axle Transmission Housing	Special Al_Si_18	1.50	4.50	0.70	0.33	850.00
Middle Drive Shaft	Steel (Mild)	1.00	22.42	1.00	0.16	460.00
End Drive Shaft	Steel (Mild)	1.00	20.35	1.00	0.15	460.00
Axle Front Left	Steel (Mild)	1.00	3.98	1.00	0.06	460.00
Axle Front Right	Steel (Mild)	1.00	3.98	1.00	0.06	460.00
Axle Rear Left	Steel (Mild)	1.00	3.80	1.00	0.09	460.00
Axle Rear Right	Steel (Mild)	1.00	3.80	1.00	0.09	460.00
<b>Averaged Values</b>		<i>1.23</i>	<i>7.20</i>	<i>0.92</i>	<i>0.19</i>	<i>660.55</i>

Table A4.5: Drive Train Group – Flat Plate Analogy

Assuming the average Air temperature in the engine compartment [ $T_{Air}$ ] is 400 K, the density at standard pressure [ $\rho_{Air}$ ] is 0.88 kg/m<sup>3</sup> with a specific heat capacity [ $C_p(T_{Air})$ ] of 1013 J/kg.K the critical frequency for this group can be derived as the following:

$$E^* = T_{Air} \cdot v^* \cdot \overline{A^*} \cdot \rho_{Air} \cdot C_p(T_{Air}) = T_{Air} \cdot (0.01 \cdot v_{Max}) \cdot (\overline{\alpha \cdot A}) \cdot \rho_{Air} \cdot C_p(T_{Air}) \quad (A4.17)$$

$$E^* = 400 \cdot (0.01 \cdot 67) \cdot (0.92 \cdot 0.19) \cdot 0.88 \cdot 1013 = 41.36 \text{ kW} \quad (A4.18)$$

And,

$$\overline{M^*} = (\overline{\beta \cdot M}) = 1.23 \cdot 7.20 = 8.84 \text{ kg} \quad (A4.19)$$

Therefore,

$$f = \frac{2 \cdot E^*}{\Delta T \cdot \overline{C_p} \cdot \overline{M}^*} = \frac{2 \cdot 41355}{1 \cdot 660.55 \cdot 8.84} = 14.17 \text{ Hz} \quad (\text{A4.20})$$

Once the critical frequency calculation for each sub-system is conducted, the engineer can then rank each systems importance based on either the motivations of the simulation (engineer is aware of thermally critical problems) or alternatively based on the sensitivity of the system. The sensitivity was previously discussed in chapter 3, whereby three groups were identified; high, medium and low sensitivity. Here a weighting value can be assigned to each of these groups, where a weighted average of all of the groups can be calculated to produce a critical frequency for the entire vehicle. In Table A4.6, high sensitivity is given an importance of 3, whereby medium and low are assigned 2 and 1 consequently. This averaging technique in combination with assigning importance (and therefore weight) is a useful strategy when analysing the whole vehicles thermal response nature to frequency. The simulation should favour sub-systems that are highly sensitivite to change, therefore the averaging would ultimately drive the critical frequency higher for the entire vehicle. This would result in less information being removed from the original boundary conditions and avoid introducing additional simplification errors on sensitive components.

Sub-System	Sensitivity	Importance	Critical Frequency (Hz)
Engine Bay	Medium	2.00	48.74
Underbody	Low	1.00	13.42
Under Carriage	Low	1.00	28.20
Engine Pipes and Cables	High	3.00	84.96
Drive Train and Axles	Low	1.00	14.17
<b>Weighted Average</b>			<b>51.02</b>

Table A4.6: Critical Frequency Group Ranking

In Table A4.6, the weighted average for the whole vehicle system has resulted in a critical frequency of 51 Hz. This then utilised for each of the transient profiles investigated. Alternatively each of these profiles could consist of independent critical frequencies each based on the energy derived from the maximum velocity of the profile. This however would require recalculation of the critical frequency for each of the sub-systems. In current research project the maximum velocity out of all of the investigated profiles was used to derive the energy and the critical frequency. This was held constant for all profiles to represent a worse case scenario.



Once the critical frequency for the vehicle is established the following Equation (A4.21) can be used to determine the decomposition level within the wavelet signal processing methodology. The maximum frequency ( $f_{Max}$ ) for each profile is calculated by a Fourier transformation.

$$f_{critical} > \frac{f_{Max}}{|2n|} \quad (A4.21)$$

Table A4.7 lists both the maximum frequency and the critical frequency. Here the level refers to the absolute theoretical level (n). Since the wavelet decomposition methodology only tolerates whole numbers this number is rounded to produce the utilised level.

<b>Profile</b>	<b>Max Frequency (Hz)</b>	<b>Critical Frequency (Hz)</b>	<b>Level [n]</b>	<b>Used Level</b>
Race-Track	748.00	51	7.33	7.00
Handling Course	570.00	51	5.59	6.00
Highway Driving	467.00	51	4.58	5.00
Street Driving	392.00	51	3.84	4.00

Table A4.7: Deriving level of Decomposition

The used levels described in Table A4.7 are used to derive the simplified signal for each of the driving profiles described in chapter 3. Therefore the simplified signal becomes the boundary conditions for the quasi-transient approach discussed in Chapter 3.

## Appendix 5

The following appendix aims at exploring the influences of cell optimisation/type on consequent convective properties within the vehicle. As discussed in chapter 4, volume control shapes were utilised within the steady-state CFD vehicle models in order to reduce the total quantity of cells and promote faster calculation times. This was necessary due to the inherent dependency of the dynamic driving methodology on a large amounts of steady state CFD solutions. Ultimately these solutions were mapped within the thermal model and interpolated at alternative time periods.

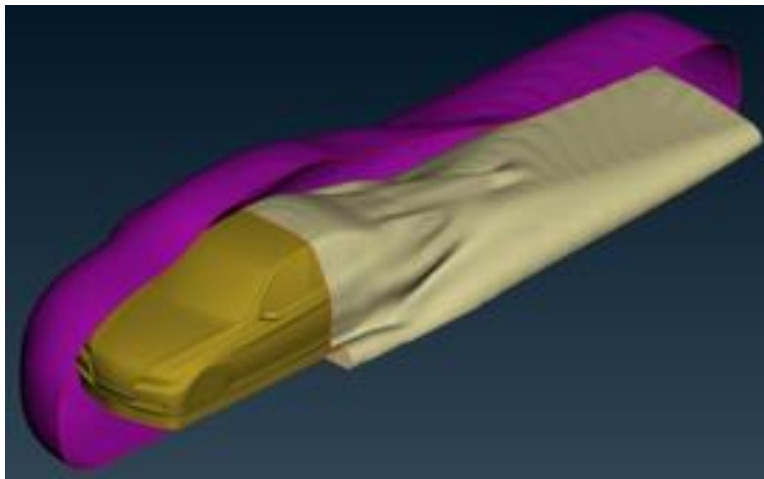


Figure A5.1: Volume Control Shapes for Outer Body Architecture.

Figure A5.1 examines the outer-body volume control shapes used within the steady-state CFD mesh generation. Here iso-surfaces (generated from the maximum velocity conditions) are extracted and used as the volume control shapes. Denoted in purple is the offset of the iso-surface generated from the velocity field and scaled to replace the standard box volume control shape. This can be further seen in Figure A5.2, whereby the mesh arrangement with the iso-surface control volume resulted in a reduction of 4 Mill cells compared to the original mesh setup.

Another example can be seen in Figure A5.2 whereby a polyhedral mesh type was implemented to replace the standard hexahedral setup. Polyhedral cells (due to their increased surfaces and angles of freedom) are thought to better suit complex geometry and therefore promote better simulation convergence with less cell quantities. Polyhedral cell type is applied to both original and optimised meshing arrangements where ‘cuboid’ refers to the standard box and ‘Isosurface’ for the iso-surface derived volume control shape. One immediate observation that can be made is that the cell quantities have increased utilising the polyhedral meshing type compared to the hexahedral. This is due to the specifications given to the meshing algorithm to maintain identical cell sizes (to the hexahedral type) in order to have a comparative study. It is clear that further

improvement could be made if cell sizes were altered in the polyhedral case. Figure A5.3 provides a visualisation of the local heat transfer coefficients (from external convection) mapped onto the Hot-End surfaces of the exhaust system representing a maximum velocity case. Here several difference can be seen with the HTC contours between polyhedral and hexahedral meshing configurations. Firstly on the left hand side of Figure A5.3 it can be seen that there is a higher average HTC value on the exhaust pipe after the catalytic converter, which is not present in the polyhedral case. Additionally on the right hand side of Figure A5.3 a similar phenomenon is seen on the turbo-charger compressor side. Both of these examples can drastically effect the surface temperature distribution of the consequent components.

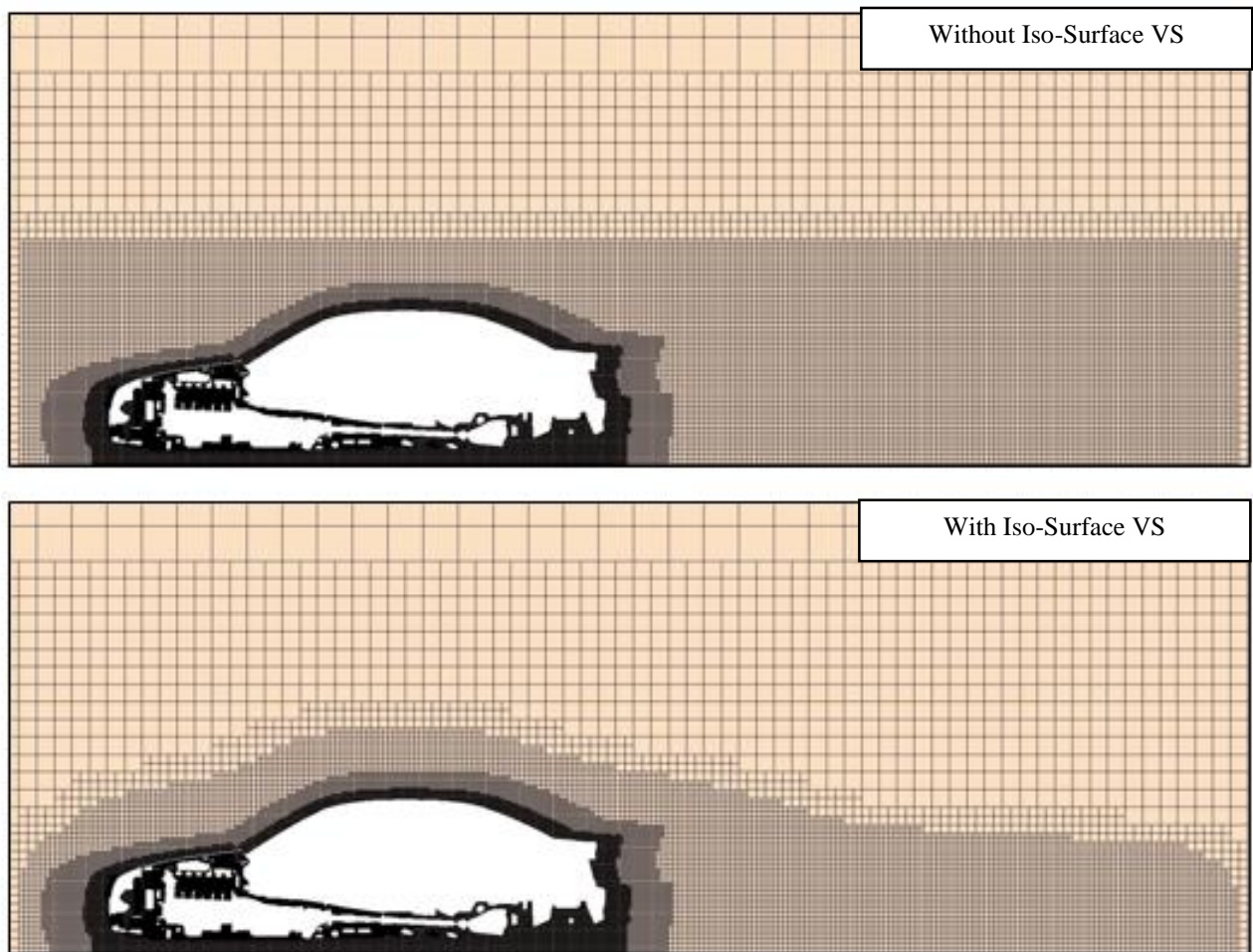


Figure A5.2: Comparison between the CFD mesh with and without outer-body iso-surface volume control shape.

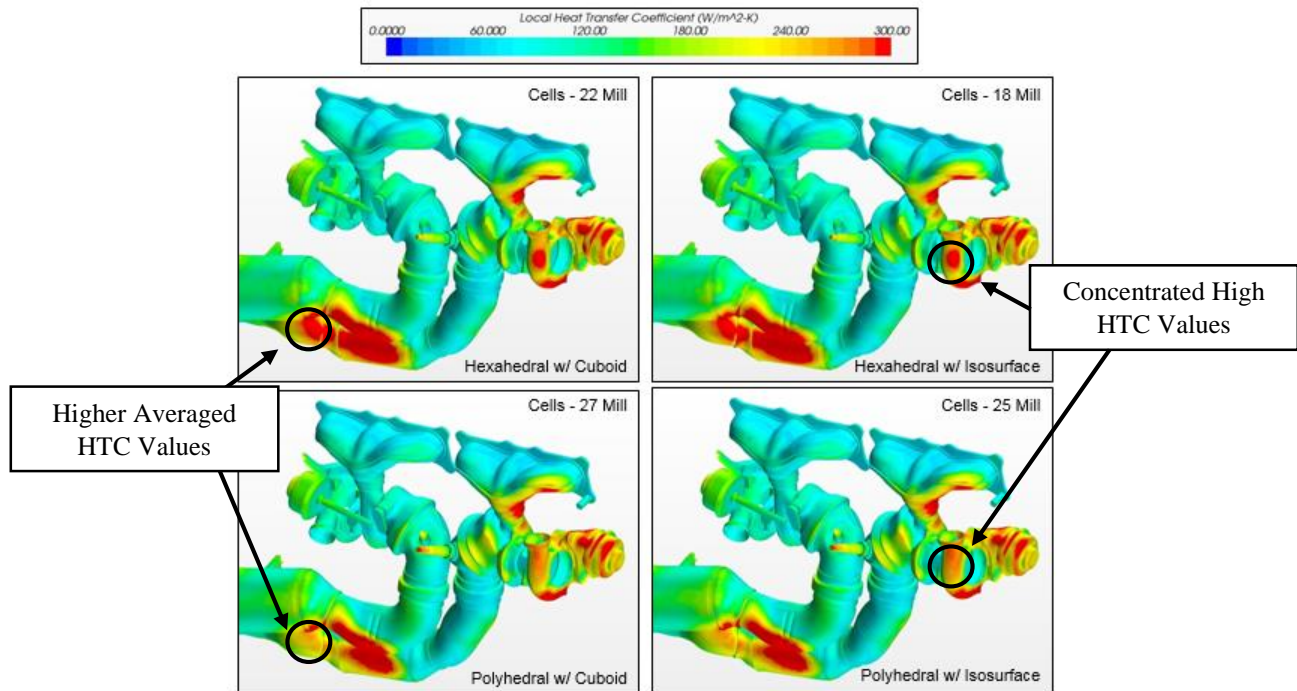


Figure A5.3: Comparison between alternative meshing strategies and the mapped heat transfer coefficients on the Hot End of the exhaust system.

In order to further investigate these differences a full vehicle inspection was conducted. Figure A5.4 displays the under-body of the full vehicle configuration evaluated in the research project. Overall both the hexahedral and polyhedral meshes consist of the same velocity contour tendencies. The hexahedral generally produces higher heat transfer rates over the underbody whereas the polyhedral produces smoother yet lower heat rates. Additionally just underneath the engine, higher HTC concentration is observed in the hexahedral type mesh. This is concurrent with the findings in Figure A5.3. Due to fact that the component temperatures and near wall assumptions (and cell sizes) were identical in all cases the primary difference must be resulting from velocity field.

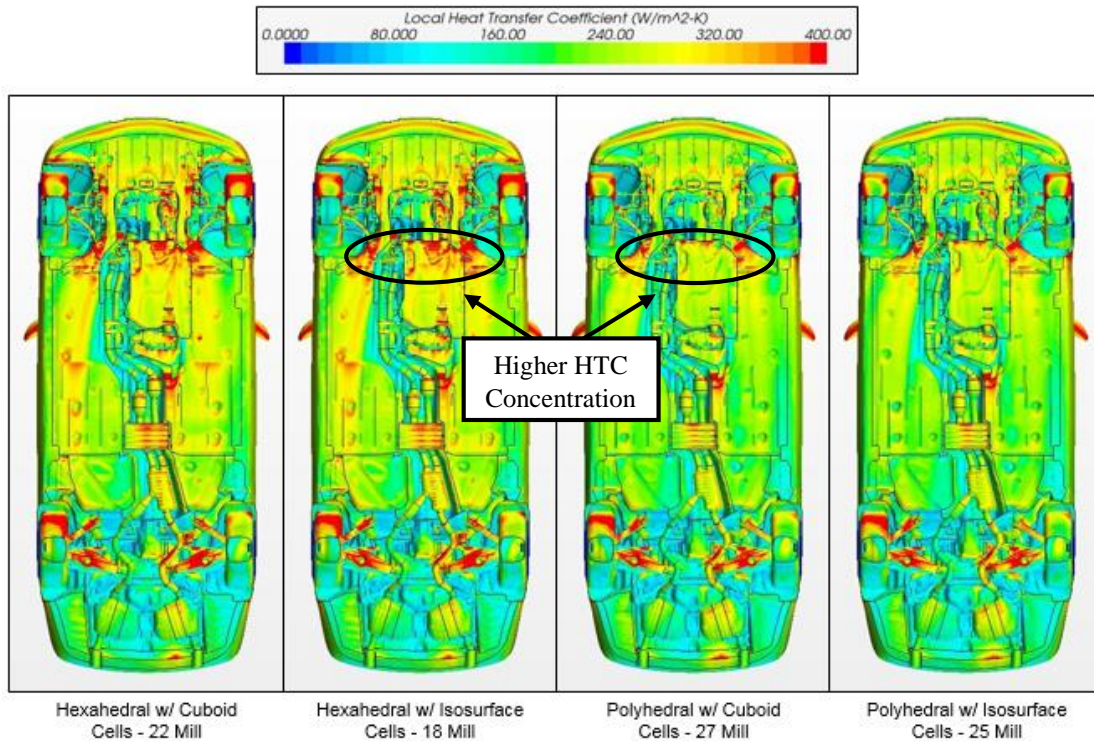


Figure A5.4: Comparison between alternative meshing strategies and the mapped heat transfer coefficients on the underbody of the vehicle.

In Figure A5.5 and A5.6 and plane cut through the center of the vehicle is taken to investigate the differences in the velocity field. Figure A5.5 is focused on the wake region, whereas Figure A5.6 investigates the engine bay flow. It is clear that significant differences are occurring between the velocity fields underneath the vehicle's under-body as well as the engine bay environment. This can lead to significant discrepancies when considering that each individual steady-state CFD model is being time interpolated to fit the simplified boundary conditions.

The potential of using alternative volume control shapes (here optimised based on velocity field iso-surfaces) have shown no detrimental effect on the convective characteristics. This can be seen in Figures A5.3 and A5.4 (with cuboid to isosurface comparisons), where identical HTC contours are achieved over the Hot-End of the exhaust and the vehicle's under-body environment. Since the hexahedral meshing configuration provides the lowest mesh quantities and is the most commonly used cell type for vehicle flow airflow, this type has been used in research project. However the examples provided in Appendix 5, indicate the need to evaluate the impact of alternative meshing types and quantities on flow conditions and potential convection parameters. Here the polyhedral mesh has shown significant differences to the hexahedral type. It is recommended that in future work the differences (in HTC fields) be quantified and each mesh type be compared to experimental data in order to characterise the potential errors introduced to the simulation.

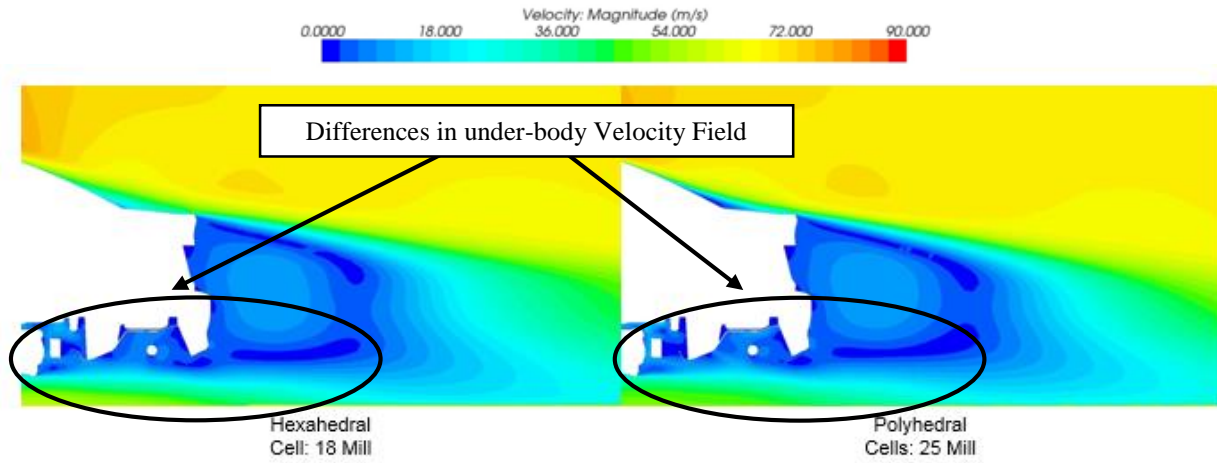


Figure A5.5: Comparison between alternative meshing strategies and the velocity profile in the wake region of the vehicle.

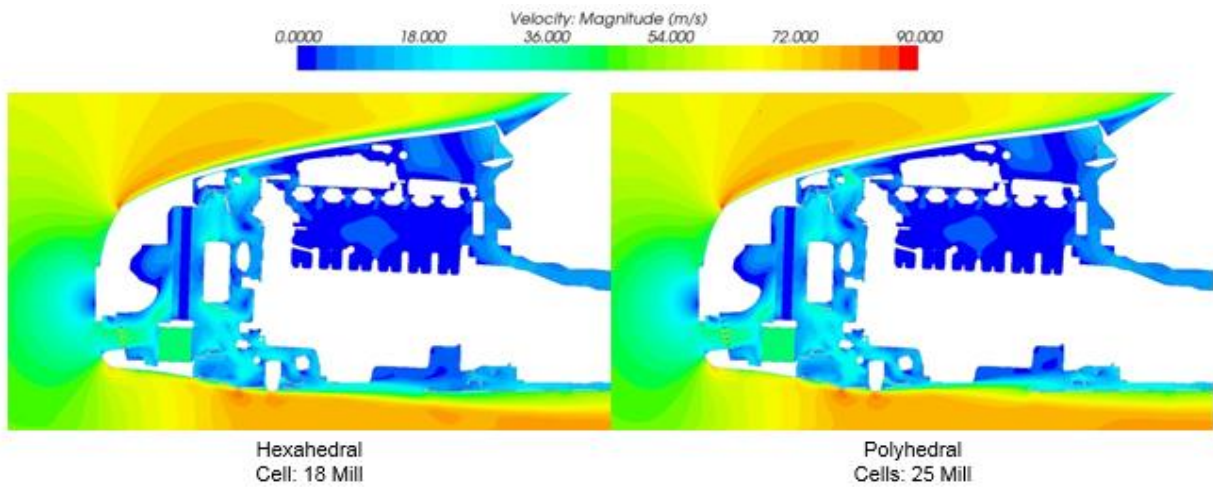


Figure A5.6: Comparison between alternative meshing strategies and the velocity profile in the engine bay of the vehicle.

## Appendix 6

The following appendix presents a series of contour plots from the individual driving profiles examined within the research investigation. Accompanied with the temperature contour plots is the dynamic driving profile simulation (denoted in dotted black line) compared with the original velocity conditions (denoted in blue). Here the time location of each contour plot is indicated in the Figure. The motivation of this appendix is to present the thermal variation of the vehicles under-body during a transient driving conditions. Here it can be seen that not only is the exhaust system experiences a large temperature differential over time, the surrounding geometry is also affected by the radiation influences (which are temperature dependent) and the transportation of warm air. The visualisation of under-body thermal distribution over time is particularly important when optimisation is being conducted, whereby the delegation of protection methods such as heat shielding can be improved. Additionally understanding the time dependent thermal behaviour of the vehicle can lead to savings in weight (from optimising the placement of heat protection mechanisms) and consequent improved vehicle performance with the potential to reduce emissions.

To optimise designs a set thermal thresholds can be defined, to indicate the regions where components exceed their operating conditions. This can be introduced during the visualisation of the time dependent behavior of the vehicle. Thresholds can be also implemented to indicate the locations of high radiation and which components are exposed to the radiation. Here the source can be identified and visualised during the dynamic driving animation. From an automation perspective a series of tables can be exported for the engineer to analyse the performance of the current design. These tables can consist of the major components exposed to high radiation, which components exceed their design temperatures, and the location of unwanted heat sources. Therefore the re-design process can be executed based on the time dependent behavior of a vehicle. This is a major step forward in designing vehicles for the real driving conditions that they are exposed to, not for the theoretical steady state worst cases.

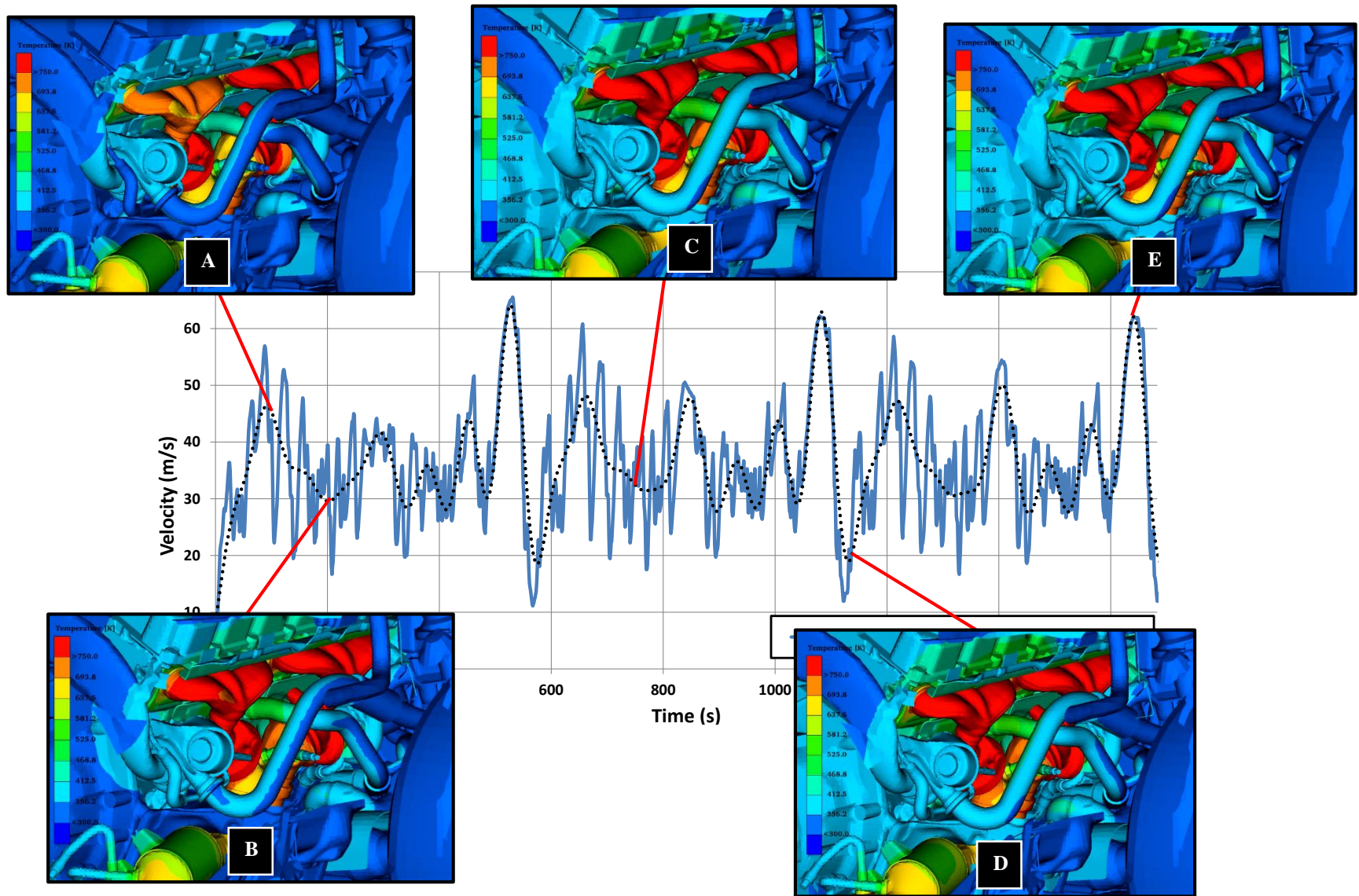


Figure A6.1: Race-Track Simulation, A:T=100 sec, B:T=200 sec, C:T= 700 sec, D:T=1100 sec, E:T=1625 sec.



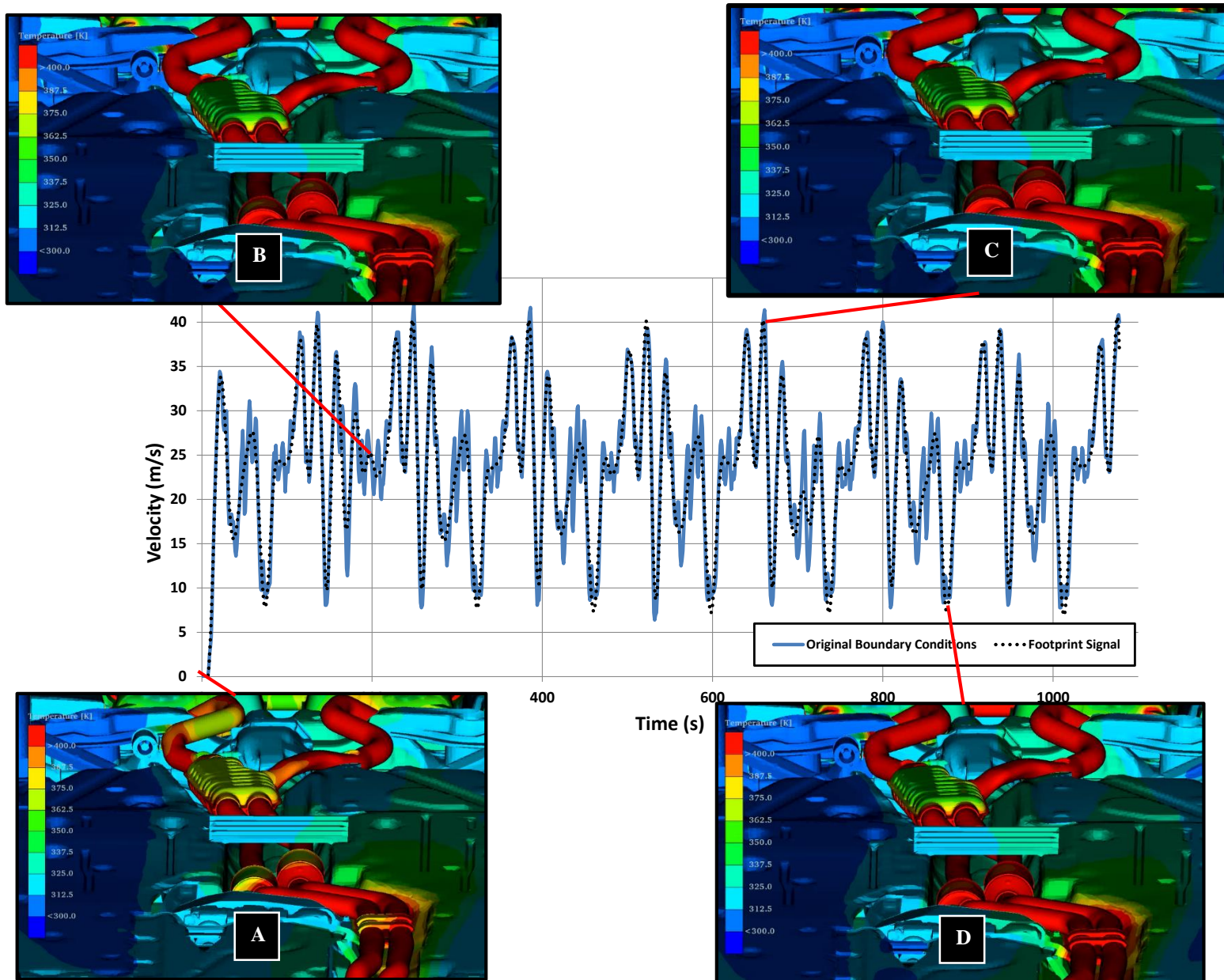


Figure A6.2: Handling Course Simulation, A:T=0 sec, B:T=200 sec, C:T= 650 sec, D:T=900 sec.

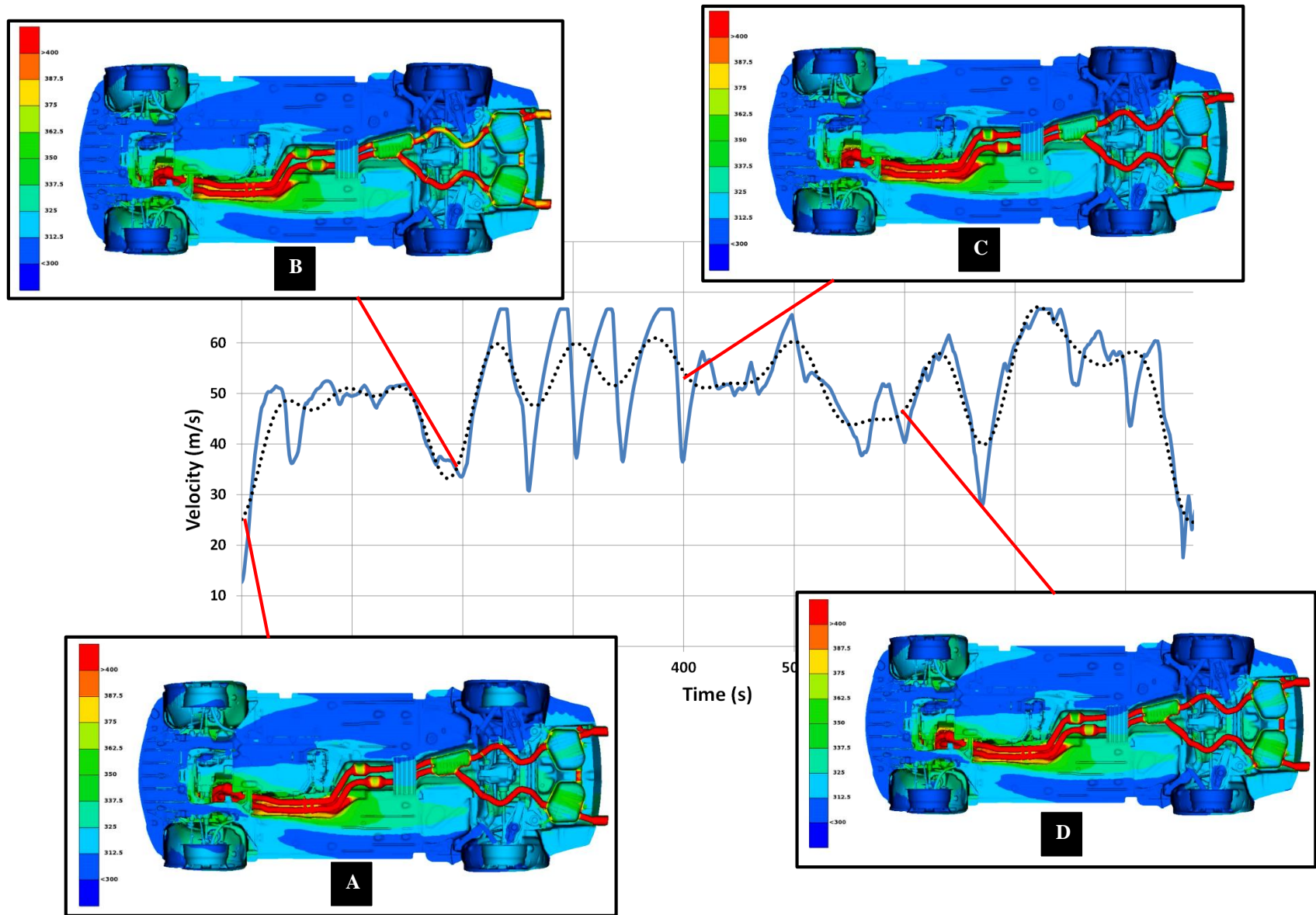


Figure A6.3: Highway Driving Simulation, A:T=0 sec, B:T=200 sec, C:T= 400 sec, D:T=600 sec.

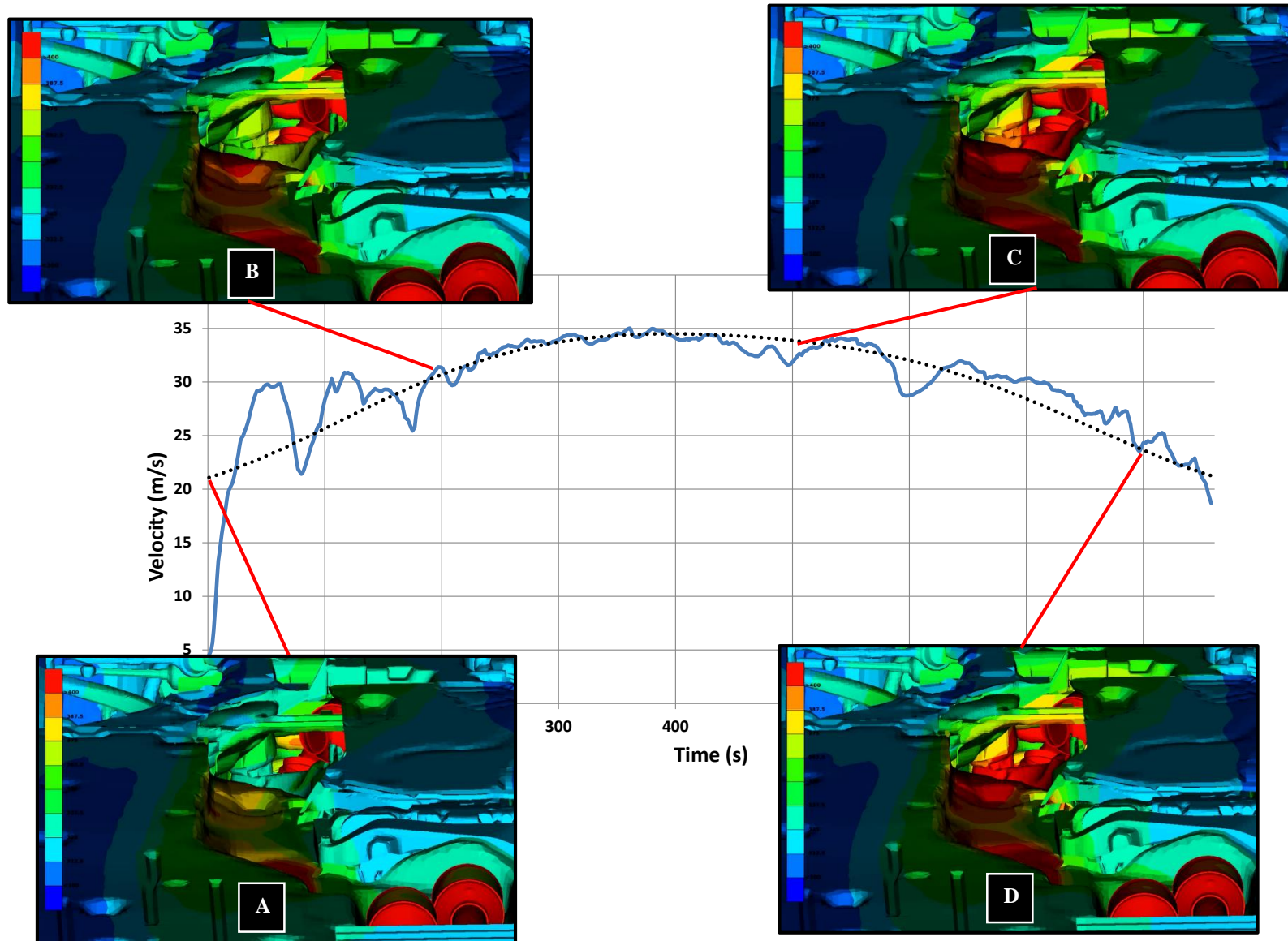


Figure A6.4: Street Driving Simulation, A:T=0 sec, B:T=200 sec, C:T= 500 sec, D:T=800 sec.